

University of Southampton Research Repository ePrints Soton

Copyright © and Moral Rights for this thesis are retained by the author and/or other copyright owners. A copy can be downloaded for personal non-commercial research or study, without prior permission or charge. This thesis cannot be reproduced or quoted extensively from without first obtaining permission in writing from the copyright holder/s. The content must not be changed in any way or sold commercially in any format or medium without the formal permission of the copyright holders.

When referring to this work, full bibliographic details including the author, title, awarding institution and date of the thesis must be given e.g.

AUTHOR (year of submission) "Full thesis title", University of Southampton, name of the University School or Department, PhD Thesis, pagination

UNIVERSITY OF SOUTHAMPTON

School of Electronics and Computer Science

Cooperation and Resource Allocation in Relay and Multicarrier Systems

by

Jia Shi BEng, MSc

A doctoral thesis submitted in partial fulfilment of the requirements for the award of Doctor Philosophy at the University of Southampton

March 2015

SUPERVISOR: Professor Lie-Liang Yang
BEng, MEng, PhD, Senior Member IEEE
Professor of Communications, Southampton Wireless Group
School of Electronics and Computer Science University of Southampton
Southampton SO17 1BJ
United Kingdom

© Jia Shi 2015

 \mathfrak{D} edicated to my family

UNIVERSITY OF SOUTHAMPTON

ABSTRACT

School of Electronics and Computer Science Faculty of Physical Science and Engineering

Doctor of Philosophy

Cooperation and Resource Allocation in Relay and Multicarrier Systems

by Jia Shi

In modern wireless communications, various techniques have been developed in order to exploit the dynamics existing in wireless communications. Diversity has been recognized as one of the key techniques, which has the potential to significantly increase the capacity and reliability of wireless communication systems. Relay communication with possible cooperation among some nodes is capable of achieving spacial diversity by forming a virtual antenna array for receiving and/or transmission. Dynamic resource allocation is capable of taking the advantages of the time-varying characteristics of wireless channels and wireless systems themselves, generating promising increase of energy- and spectrum-efficiency. This thesis focuses on the cooperation and resource allocation in relay and multicarrier systems, via which we motivate to design the low-complexity algorithms that are capable of achieving the spectrum-efficiency and reliability as high as possible.

First, we investigate and compare the error performance of a two-hop communication links (THCL) system with multiple relays, when distributed and cooperative relay processing schemes are respectively employed. Our main objectives include to find some general and relatively simple ways for error performance estimation, and to demonstrate the trade-off of using cooperative relay processing. The error performance of the THCL employing various relay processing schemes is investigated, with the emphasis on the cost of cooperation among relays. In order to analyze the error performance of the THCL systems novel approximation approaches, including two Nakagami approximation methods and one Gamma approximation method, are proposed. With the aid of these approximation approaches, a range of closed-form formulas for the error rate of the THCL systems are derived. Our studies show that cooperation among relays may consume a significant portion of system energy, which should not be ignored in design of cooperative systems.

Second, resource allocation, including both power- and subcarrier-allocation, is investigated in the context of the single-cell downlink orthogonal frequency division multiple-access (OFDMA) and multicarrier direct-sequence code-division multiple-access (MC DS-CDMA) systems. Our resource allocation is motivated to maximize the *system reliability* without making a trade-off with the attainable *spectrum-efficiency* of the system, while demanding the complexity as low as possible. For the sake of achieving low-complexity in implementation, we carry out power- and subcarrier-allocation separately in two stages, which has been proved without much performance loss. On this topic, we propose a range of subcarrier-allocation algorithms and study their performance with

the OFDMA and MC DS-CDMA systems. In general, our proposed algorithms are designed either to avoid assigning users as many as possible the worst subchannels, or to assign users the best possible subchannels. Our studies show that all the proposed algorithms belong to the family of low-complexity subcarrier-allocation algorithms, and they outperform all the other reference sub-optimal algorithms considered, in terms of both the error and spectrum-efficiency performance. Furthermore, some of our proposed subcarrier-allocation algorithms are capable of achieving the performance close to that achieved by the optimum subcarrier-allocation algorithm.

Finally, based on our subcarrier-allocation algorithms, we investigate the resource allocation in multicell downlink OFDMA and MC DS-CDMA systems, with the emphasis on the mitigation of intercell interference (InterCI). Specifically, we extend the subcarrier-allocation algorithms proposed in the single-cell systems to the multicell scenarios, in which each base station (BS) independently carries out the subcarrier-allocation. After the subcarrier-allocation, then minimum BS cooperation is introduced to efficiently mitigate the InterCI. In the multicell downlink OFDMA systems, two novel InterCI mitigation algorithms are proposed, both of which are motivated to set up the space time block coding (STBC) aided cooperative transmissions to the users with poor signal-to-interference ratio (SIR). Our studies show that both the proposed algorithms can significantly increase the spectrum-efficiency of the multicell downlink OFDMA systems. In the multicell MC DS-CDMA systems, after the subcarrier-allocation, we propose two low-complexity code-allocation algorithms, which only require the BSs to share the large-scale fading, including the propagation pathloss and shadowing effect. Our studies show that both the code-allocation algorithms are highly efficient, and they are capable of achieving significantly better error and spectrum-efficiency performance than the random code-allocation (i.e., the case without code-allocation).

Declaration of Authorship

I, <u>Jia Shi</u>, declare that the thesis entitled <u>Cooperation and Resource Allocation in Relay and <u>Multicarrier Systems</u> and the work presented in it are my own and has been generated by me as the result of my own original research. I confirm that:</u>

- This work was done wholly or mainly while in candidature for a research degree at this University;
- Where any part of this thesis has previously been submitted for a degree or any other qualification at this University or any other institution, this has been clearly stated;
- Where I have consulted the published work of others, this is always clearly attributed;
- Where I have quoted from the work of others, the source is always given. With the exception of such quotations, this thesis is entirely my own work;
- I have acknowledged all main sources of help;
- Where the thesis is based on work done by myself jointly with others, I have made clear exactly what was done by others and what I have contributed myself;
- Parts of this work have been published.

Signed:	Date:

Acknowledgements

First of all, I would like to give my sincere gratitude to my supervisor Prof. Lie-Liang Yang for his excellent and careful supervision and support. His guidance and inspiration have greatly benefited me in the past four years of my PhD study.

Secondly, I wish to express my appreciation to Prof. Lajos Hanzo, Prof. Sheng Chen, Dr. Soon Xin Ng, Dr. Rob Mounder, Dr. Rong Zhang and Dr. Mohammed El-Hajjar for their encouragement and engaging for my research work. Furthermore, it is really my pleasure to work with everyone of you in our warming and generous Southampton Wireless group family.

Last but not the least, I would like to express my heartfelt appreciation to my parents, and my parents in law, for their endless love and support forever. I also need to thank my grandparents, and I wish you in good health forever. Finally, I would like to give my deepest appreciation to my wife, wei liang, without whom I would not have finished my PhD study. I love you forever!

List of Publications

Journal Papaers

- Jia Shi, Lie-liang Yang, Novel Subcarrier-allocation Schemes for Downlink MC DS-CDMA systems, *IEEE Transactions on Wireless Communications*, vol.13, pp. 5716-5728, Oct. 2014.
- Jia Shi, Chen Dong, Lie-liang Yang, Performance Comparison of Cooperative Relay Links with Different Relay Processing Stragegies: Nakagami/Gamma-Approximation Approaches, *EURASIP Journal on Wireless Communications and Networking*, 2014:53 doi:10.1186/1687-1499-2014-53, April, 2014.
- Jia Shi, Lie-liang Yang, Worst Subchannel Avoiding versus Best Subchannel Seeking Subcarrier-Allocation in Downlink OFMDA systems, (submitted to *IEEE Transactions on Vehicular Technology*).
- 4. **Jia Shi**, Lie-liang Yang, Novel Resource Allocation Schemes for Multicell Downlink MC DS-CDMA Systems, (submitted to *IEEE Transactions on Wireless Communications*).
- 5. **Jia Shi**, Lie-liang Yang, Subcarrier-Allocation in Multicell Downlink OFMDA Systems with Data Exchange Capability, (Regular Journal Paper, to be submitted).

Conference Papers

- Jia Shi, Lie-liang Yang, Performance of Multiway Relay DS-CDMA Systems over Nakagamim Fading Channels, 2011 IEEE 73rd Vehicular Technology Conference Spring, (VTC 2011-Spring), pp. 15-18, May 2011.
- Jia Shi, Lie-liang Yang, Performance of Two-Hop Communication Links Employing Various Relay Processing Schemes, 2012 IEEE 75th Vehicular Technology Conference Spring, (VTC 2012-Spring), pp. 6-9, May 2012.

- Jia Shi, Lie-liang Yang, Novel Transmission Schemes for Multicell Downlink MC/DS-CDMA Systems Employing Time- and Frequency-Domain Spreading, 2013 IEEE 77th Vehicular Technology Conference Spring, (VTC 2013-Spring), pp. 3-5, June 2013.
- 4. **Jia Shi**, Lie-liang Yang, Subcarrier-Allocation in Downlink Multicarrier DS-CDMA Systems, *2013 IEEE International Conference on Communications in China*, (ICCC 2013), pp. 502-508, Aug. 2013.

Contents

Al	ostrac	t	ii
De	eclara	tion of Authorship	iv
A	cknow	rledgements	v
Gl	ossar	y	xii
Li	st of S	Symbols	xvi
1	Intr	oduction	1
	1.1	Motivation	1
	1.2	Relay Communications	2
	1.3	Multicarrier Schemes and Resource Allocation in Multicarrier Systems	6
		1.3.1 Overview of Multicarrier Communication Schemes	7
		1.3.2 Overview of Resource Allocation in Multicarrier Systems	10
	1.4	Thesis Outline and Contributions	16
2	Perf	formance of Two-Hop Communication Links with Relay Processing	20
	2.1	Introduction	20
	2.2	System Model	23
		2.2.1 System Description and Channel Modeling	23
		2.2.2 Signalling	26
	2.3	Relay Processing Schemes	26

		2.3.1 Distributed Relay Processing			27
			2.3.1.1	TMRC Assisted Distributed Relay Processing	27
			2.3.1.2	TEGC Assisted Distributed Relay Processing	28
		2.3.2	Ideal Coo	operative Relay Processing	28
		2.3.3	Cooperati	ive Relay Processing	30
			2.3.3.1	CMRC Aided Cooperative Relay Processing	30
			2.3.3.2	CMVC Aided Cooperative Relay Processing	32
			2.3.3.3	CMVC/MUD Aided Cooperative Relay Processing	33
	2.4	BER A	Analysis .		36
		2.4.1	BER Ana	alysis of THCL with Distributed Relay Processing	37
		2.4.2	BER Ana	alysis of THCL with Ideal Cooperative Relay Processing	45
		2.4.3	BER Ana	alysis of THCL with Cooperative Relay Processing	47
	2.5	BER P	erformance	e Results	53
	2.6	Conclu	isions		66
3	Reso	ource A	llocation i	n Single-cell Downlink OFDMA Systems	68
3				n Single-cell Downlink OFDMA Systems	68
3	3.1	Introdu	action		68
3	3.1	Introdu	uction		68 71
3	3.1 3.2 3.3	Introdu System Genera	n Model .		68 71 74
3	3.1	Introdu System Genera Power-	uction n Model . nl Theory -Allocation	Algorithms	68 71 74 75
3	3.1 3.2 3.3	Introdu System Genera	n Model . In Model . In Theory -Allocation Channel-	Algorithms	68 71 74 75 75
3	3.1 3.2 3.3	System Genera Power 3.4.1 3.4.2	n Model . In Model . In Theory -Allocation Channel-I Water-Fil	Algorithms	688 711 744 755 75
3	3.1 3.2 3.3 3.4	System Genera Power 3.4.1 3.4.2 Existin	n Model . In Model . In Theory -Allocation Channel- Water-Fil Ing Subcarri	Algorithms	688 711 744 755 75 77
3	3.1 3.2 3.3 3.4	System Genera Power 3.4.1 3.4.2 Existin 3.5.1	n Model . In Model . In Model . In Theory -Allocation Channel-l Water-Fill Ing Subcarri Greedy A	Algorithms	688 711 744 755 777 788 788
3	3.1 3.2 3.3 3.4	Introdu System Genera Power- 3.4.1 3.4.2 Existin 3.5.1 3.5.2	n Model . In Model . In Model . In Theory -Allocation Channel-I Water-Fil Ing Subcarri Greedy A WUF Green	Algorithms	688 711 744 755 775 778 788 799
3	3.1 3.2 3.3 3.4	Introdu System Genera Power- 3.4.1 3.4.2 Existin 3.5.1 3.5.2 3.5.3	n Model . In Model . In Model . In Theory Allocation Channel-I Water-Fil Ing Subcarri Greedy A WUF Gree Maximal	Algorithms	688 711 744 75 75 77 78 78 79 80
3	3.1 3.2 3.3 3.4	Introdu System Genera Power- 3.4.1 3.4.2 Existin 3.5.1 3.5.2 3.5.3 3.5.4	n Model . In Mode	Algorithms	68 71 74 75 75 77 78 78 79 80 81
33	3.1 3.2 3.3 3.4	Introdu System General Power- 3.4.1 3.4.2 Existin 3.5.1 3.5.2 3.5.3 3.5.4 Bidirec	n Model . In Mode	Algorithms	688 711 744 75 75 77 78 78 79 80 81 82
3	3.1 3.2 3.3 3.4	Introdu System Genera Power- 3.4.1 3.4.2 Existin 3.5.1 3.5.2 3.5.3 3.5.4	n Model . In Mode	Algorithms	688 711 744 755 775 778 788 79 80 811 822 822

	5 1	Introdu	ction	142
5	Reso	urce Al	location in Multicell Downlink OFDMA Systems	142
	4.8	Conclu	sions	140
		4.7.2	Spectrum-Efficiency Performance	136
		4.7.1	BER Performance	130
	4.7	Perforn	nance Results	129
	4.6	Comple	exity Analysis of Subcarrier-allocation Algorithms	125
		4.5.2	Characteristics of IWE Algorithms	123
		4.5.1	Principles of IWE Algorithms	121
	4.5	Iterative	e Worst Excluded (IWE) Algorithms	120
		4.4.3	Worst Case First Subcarrier-Allocation Algorithm	118
		4.4.2	Worst Case Avoiding Subcarrier-Allocation Algorithm	116
		4.4.1	Parallel Hungarian Subcarrier-Allocation Algorithm	115
	4.4	Propose	ed Subcarrier-Allocation Algorithms	115
	4.3	Existin	g Subcarrier-Allocation Algorithms	112
	4.2	System	Model	109
	4.1	Introdu	ction	107
4	Reso	urce Al	location in Single-cell Downlink MC DS-CDMA Systems	107
	3.11	Conclu	sions	105
			Spectrum-Efficiency Performance	
		3.10.1	BER Performance	98
	3.10	Perforn	nance Results	98
		3.9.2	Lower-bound BER of Subcarrier-Allocation Algorithms	96
		3.9.1	Upper-bound BER of Subcarrier-Allocation Algorithms	94
	3.9	Upper-	and Lower-Bound BER of Subcarrier-Allocation Algorithms	94
	3.8	Comple	exity Analysis of Subcarrier-Allocation Algorithms	91
		3.7.2	Characteristics of BSS Subcarrier-Allocation Algorithm	89
		3.7.1	Principles of BSS Subcarrier-Allocation Algorithm	86
	3.7	Best Su	bchannel Seeking (BSS) Subcarrier-Allocation Algorithm	86

	5.2	System Model	145
	5.3	General Theory	148
	5.4	On-Off Power InterCI Mitigation	152
	5.5	Distributed Decision Making Assisted Cooperation InterCI Mitigation	154
	5.6	Centralized Decision Making Assisted Cooperation InterCI Mitigation	157
	5.7	Performance Results	166
	5.8	Conclusions	178
6	Reso	ource Allocation in Multicell Downlink MC DS-CDMA Systems	180
	6.1	Introduction	180
	6.2	System Model	182
	6.3	General Theory	185
	6.4	Simplified Strong InterCI Avoiding Code-Allocation	187
	6.5	Enhanced Strong InterCI Avoiding Code-Allocation	192
	6.6	Characteristics of Code-Allocation	195
	6.7	Performance Results	196
	6.8	Conclusions	202
7	Con	clusions and Future Work	204
	7.1	Summary and Conclusions	204
	7.2	Recommendations for Future Research	209
Bibliography			214
Su	Subject Index		
Αι	Author Index		

Glossary

R-QAM R-ary QAM

4G fourth generation5G fifth generation

AF amplify-and-forward

APs access points

AWGN additive white Gaussian noise

BC broadcast
BER bit error rate

BPSK binary phase shift keying

BS base station

BSS best subchannel seeking

BWSA bidirectional worst subchannel avoiding

CDF cumulative distribution function

CDMC centralized decision making assisted cooperation

CF compress-and-forward

CMRC centralized maximal-ratio combining

CMRC-TEGC-RP CMRC- and TEGC-assisted cooperative RPCMRC-TMRC-RP CMRC- and TMRC-assisted cooperative RP

CMVC centralized majority vote combining

CMVC-TEGC-RP CMVC- and TEGC-assisted cooperative RP **CMVC-TMRC-RP** CMVC- and TMRC-assisted cooperative RP

CMVC/MMSE MMSE MUD assisted CMVC

CMVC/MUD MUD aided CMVC

CMVC/RMD RMD/MS-MMSE MUD assisted CMVC

CSI channel state information

DDMC distributed decision making assisted cooperation

DF decode-and-forward

DMT diversity-multiplexing trade-off

DS direct-sequence

DS-CDMA direct-sequence code-division multiple-access

E2E end-to-end

EGC equal gain combining

ESIA enhanced strong InterCI avoiding

F-domain frequency-domain

FFT fast frequency-hopping **FFT** fast Fourier transform

Gamma-Approximation

HetNets heterogeneous wireless networks

ICMRC-TEGC-RP CMRC- and TEGC-assisted ideal cooperative RP
ICMRC-TMRC-RP CMRC- and TMRC-assisted ideal cooperative RP
ICMVC-TEGC-RP CMVC- and TEGC-assisted ideal cooperative RP
ICMVC-TMRC-RP CMVC- and TMRC-assisted ideal cooperative RP

IECU information exchange centra unit

IMD InterCI mitigation decision

IMD InterCI mitigation decision
InterCI intercell interference
IntraCI intracell interference

IS InterCI Scoring

ISI inter-symbol interference
IWE iterative worst excluding

IWE-WCAIWE aided WCAIWE-WCFIWE assisted WCFIWE-WSAIWE aided WSA

LTE long-term evolution

LTE-A long-term evolution advanced

MA multiple access

MAI multiple-access interference

MAP maximum a-posterior

MC DS-CDMA multicarrier direct-sequence CDMA

MC-CDMA multicarrier code-division multiple-access

MGF moment generation function
MIMO multiple input multiple output
MISO multiple input single output

ML maximum likelihood

MLD maximum likelihood detector

MMSE minimum mean-square error

MRC maximal ratio combining

MUD multiuser detection

MUI multiuser interference

MVC majority vote combining

Nakagami-SAp Nakagami Statistical Approximation
Nakagami-TAp Nakagami Theoretical Approximation

OFDM orthogonal frequency division multiplexing
OFDMA orthogonal frequency division multiple-access

OOP on-off power

OPA optimum power-allocation

PAPR peak-to-average power ratio
PDF probability density function
PMF probability mass function

QAM quadrature amplitude modulation

QoS quality-of-service

QPSK quadrature phase-shift keying

R-D relays to destinationRF radio frequency

RMD/MS-MMSE receiver multiuser diversity assisted multi-stage MMSE

RP relay processing

S-R source to relays
SER symbol error rate

SIC successive interference cancellation
SINR signal-to-interference-plus-noise ratio

SIRsignal-to-interference ratioSISOsingle input single output

SNR signal-to-noise ratio

SOPA suboptimal power-allocation

SSIA simplified strong InterCI avoiding

STBC space time block coding

T-domain time-domain

TDD time-division duplex

TEGC equal gain combining assisted transmit preprocessing

TEGC-DRP TEGC-assisted distributed RP
THCL two-hop communication links

TMRC maximal-ratio combining assisted transmit preprocessing

TMRC-DRP TMRC-assisted distributed RP

WCA worst case avoiding

WCF worst case first
WE worst excluding

WSA worst subcarrier avoiding

WUF worst user first

List of Symbols

Special Symbols

x: Transmitted baseband symbol.

x: Transmitted signal vector.

H: Channel state information (CSI) matrix.

y: Received obervation variable.

y: Received observation vector.

n: Complex-valued AWGN vector.

N: Complex-valued AWGN matrix.

 N_0 : Variance of AWGN.

 $\bar{\gamma}_s$: Average SNR per symbol.

 I_N : Identity matrix of $(N \times N)$.

 $diag\{\cdots\} \text{: } Diagonal \ matrix.}$

 P_b , Pe: Bit error rate.

M: Number of subcarriers.

 \mathcal{M} : Set of subcarrier indexes.

K: Number of users in a cell.

 \mathcal{K} : Set of user indexes.

 $\mathcal{K}^{(u)}$: Set of user indexes in cell u.

C: Time(T)-domain DS spreading matrix.

W: Preprocessing matrix.

N: Spreading factor of DS spreading.

 \mathcal{N} : Set of indexes of spreading codes.

 \mathcal{F}_k : Set of indexes of the subcarriers assigned to user k.

 $\tilde{\mathcal{F}}_k$: Set of indexes of the candidate subcarriers for user k.

 $A_{k,m}$: Subchannel quality of subcarrier m of user k.

 \mathcal{F}_m : Set of indexes of the users assigned to subcarrier m.

 $\mathcal{F}_m^{(u)}$: Set of indexes of the users assigned to subcarrier m in cell u.

 $\mathcal{V}_n^{(u)}$: Set of indexes of the users assigned with spreading code n in cell u.

Ø: Empty set.

 L_v : Number of T-domain resolvable paths of the frequency-selective Rayleigh fading

channels.

Special Operations

 $|\cdot|$: Absolute value.

 $\|\cdot\|^2$: Euclidean norm operation.

 $(\cdot)^H$: Hermitian transpose of a matrix.

 $(\cdot)^T$: Transpose of a matrix.

 $(\cdot)^*$: Conjugate of a complex symbol/vector/matrix.

[·]: Rounding a numerical value to the nearest integer higher than the value.

 $\lfloor \cdot \rfloor$: Rounding a numerical value to the nearest integer lower than the value.

 Σ : Summation operation.

☐: Product operation.

 \forall : For all.

 \int : Integration.

 $E[\cdot]$: Expectation operation.

 $\exp(\cdot)$: Exponential function.

 $log(\cdot)$: Logarithm function.

 $ln(\cdot)$: Natural logarithm function.

 $max(\cdot)$: Maximum function.

 $min(\cdot)$: Minimum function.

 $tr(\cdot)$: Trace of a matrix.

 $Var(\cdot)$: Variance of a random variable.

 $diag(\cdot)$: Diagonalizing operation.

 $|\mathcal{F}|$: Cardinality of set \mathcal{F} .

 $\Re\{\cdot\}$: Real part of a complex symbol.

 $\Im\{\cdot\}$: Imaginary part of a complex symbol.

Chapter 1

Introduction

1.1 Motivation

In wireless communications, the communication environments are typically dynamic. First, signals transmitted over wireless channels experience propagation pathloss and shadowing effects, which are usually referred to as the large-scale fading [1]. Simultaneously, due to the reflection, attenuation, deflection, scattering, Doppler effect, etc., wireless signals also experience fast fading. Both the large-scale fading and the small-scale fading are time variant, making the signals received by wireless receiver dynamic. Second, in wireless mobile communication systems, users move around in random ways, making the distribution of users random. Furthermore, different users may have different requirements for their services and corresponding service qualities. All these, plusing the above-mentioned large- and small-scale fading, make the inter-relationship among the communication users highly dynamic, not only the number of users competing the limited resources in a given geographic area is time-varying, but also is the inter-user (or co-channel) interference. Additionally, in wireless communications, the system structures may be different in different areas, the resources for supporting communications can be highly diverse in different areas and at different time, and so on.

Owing to the above-mentioned, in modern advanced wireless communications, techniques have been developed in order to exploit the dynamics existing in wireless communications, instead of trying to avoid them as in the conventional wireless systems. Among these techniques, diversity has been recognized as one of the key techniques, which has the potential to significantly increase the capacity and efficiency of wireless communication systems.

Following the state-of-the-art of wireless communications, in this thesis, we motivate to design and investigate the techniques that can make efficient use of the dynamics of wireless communications. Cooperation and resource allocation are the two themes of the thesis. Specifically, in Chapter 2, we study a two-hop relay link, where one source node communicates with one desti-

nation node with the aid of a number of relay nodes that may cooperate with each other to carry out detection and transmission. In this way, we can mitigate the effect of propagation pathloss and achieve the space diversity provided by the multiple relays. In this chapter, our focuses are on the effect of the power allocated between the source and the relays, and the effect of the energy consumed by relays on the achievable error performance of the two-hop relay link. In Chapters 3-6, our focus is on the resource allocation, which through cooperation implements resource sharing and achieves multiuser diversity. In these chapters, various power- and subcarrier-allocation algorithms are proposed for the single-cell and multicell cellular systems supported by the OFDMA or the MC DS-CDMA. We investigate and compare the spectrum-efficiency and error performance of our proposed algorithms as well as a range of existing algorithms on the topics.

1.2 Relay Communications

In modern wireless communications, relay communication with cooperation among some nodes is capable of achieving spacial diversity by forming a virtual antenna array for each receiving and/or transmission. Relay communication was considered as early as 1971, when Van der Meulen [2] proposed the concept of the relay channel in the context of a three-node communication system. A few of years later, T. M. Cover and EL Gamal [3] studied the capacity of the Guassian relay channel, and proposed some essential relaying protocols. In relay communications, the cooperative diversity can be achieved by the re-transmissions of source signals by relays by exploiting the broadcast nature of wireless channels. In [4,5], Laneman et al. have evaluated and compared the decode-andforward (DF) and amplify-and-forward (AF) relaying protocols in terms of the achievable diversity order and outage probability, as well as characterized the diversity-multiplexing trade-off (DMT) of the two relaying protocols. In [6, 7], the authors have studied the user cooperation, in order to achieve transmit diversity in cellular networks, where a user relays its partner's information in addition to transmitting its own information. The study in [7] has demonstrated that an increase of throughput can be used to trade for an increase of cell coverage. The authors of [8-10] have investigated the achievable DMT of the various cooperative communication systems. Specifically, Azarian et al. of [8] have studied the optimal DMT of both the AF and DF relaying schemes, when both single relay and multiple relay scenarios are considered. For the sake of reducing the implementation complexity without much trade-off the outage and error rate performance, various relay selection schemes have been studied in [11-14]. Specifically, Bletsas et al. in [11] have proposed and studied a relay selection regime, which yields the diversity on the order of the number of relays used. Later in [12], the authors have proposed a simple opportunistic relaying scheme with the DF and AF strategies, which is capable of achieving the optimal outage performance. By introducing a threshold in [13], the authors have investigated the threshold-based opportunistic relaying and relay selection, when the DF relaying protocol is assumed.

The above-mentioned relay communications schemes employ some advantages over the con-

ventional point-to-point communications. However, there is always throughput loss, resulted from the half-duplex operation used by the relay schemes. Therefore, some successive relay protocols [15–18] have been proposed to recover the throughput loss imposed by the conventional relay schemes, using, such as, AF or DF. Specifically, considering a two-path successive relay system, Chunbo Luo *et al.* [17] have proposed a low-complexity network coding scheme to combat the inter-relay interference and provide the simultaneous data transmission from the source and relays with a rate of one. In [18], the same authors have proposed another relay communication scheme, which has a rate one and is capable of fully cancelling the inter-relay interference.

In relay communications, there are various types of relay protocols, which are summarized as follows.

- Amplify-and-forward (AF) [3]: Signals received by a relay within a time slot are forwarded to the destination using another time slot without detection of the information sent by the source. Two time slots are required for using the AF scheme to send a symbol (or frame) from a source node to its destination node.
- Decode-and-forward (DF) [19]: A relay first decodes the signals received from the source, and then re-encodes as well as re-modulates the information, before forwarding it to the destination. Note that, if a relay re-encodes and re-modulates the detected signals in the same way as the source, the scheme is referred to as the "repetition-coded DF" scheme. In DF, two time slots are required to send a symbol (or frame) from a source node to its destination node.
- Compress-and-forward (CF) [19]: In CF scheme, contrary to the AF and DF, a relay first quantizes the signal received from a source and then compresses it, before forwarding it to the destination. The destination combines the quantized and compressed signal received from a relay with the original signal from the source to produce the decision. In CF, two time slots are also required to send a symbol (or frame) from a source node to its destination node.
- Successive relaying [16]: Successive relay schemes usually work with two sets of relays under two phases. In the first phase, the source node and the first set of relay nodes transmit, while the second set of relay nodes and the destination node receive. In the second phase, the source node and the second set of relay nodes transmit, while the first set of relay nodes and the destination node receive. The above two phases work alternatively until the transmission complete. It can be seen that the data rate is approximately one, if sufficiently long data blocks are transmitted.

In relay communications, various topologies have been investigated in diverse cooperative scenarios. Typically, there are the classic three-node topology, two-hop cooperative topologies with multiple sources, multiple relays, and/or multiple destinations, and their extensions of multi-hop cooperative networks.

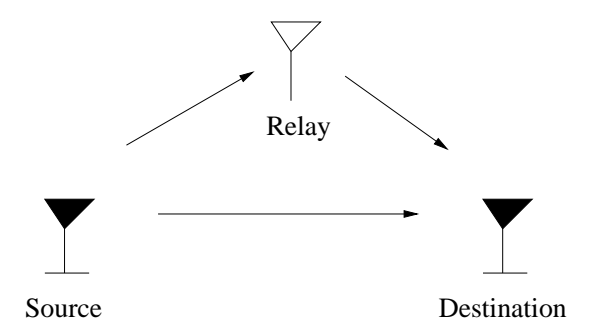


Figure 1.1: System model of the three-node cooperative network, where the source transmits signals to the destination both directly and via the relay.

The three-node network has the conceptual structure shown in Figure 1.1. This cooperative topology has been widely studied. In addition to some of the references mentioned in the previous paragraphs, the authors of [20] have considered the three-node model in cellular network, where subscribers help to relay information for each other to improve the overall network performance. In [21], a relay selection scheme has been designed for a three-node network, with the motivation to minimize the bit error rate (BER) of the network. Onat *et al.* [22] have investigated the SNR-based selective relaying for the three-node network, where the relay either retransmits or retains silent depending on the link quality of the network. Aiming at reducing the outage probability, in [23] an ARQ aided DF relay scheme has been proposed for the three-node cooperative network, where optimum power-allocation between source and relay is addressed. Furthermore, Ropokis *et al.* [24] have investigated the coding issues in the three-node network.

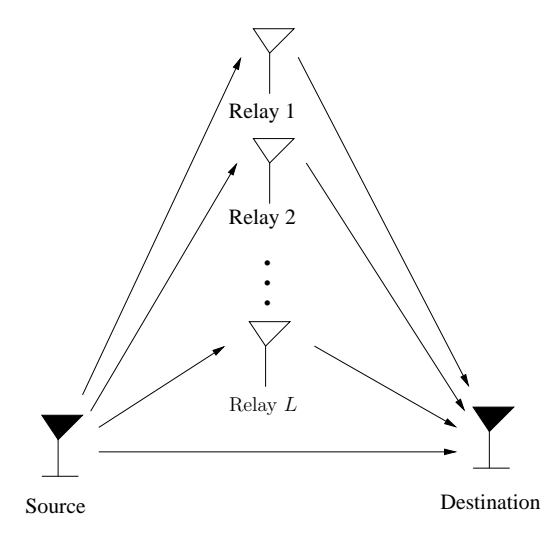


Figure 1.2: System model of a two-hop cooperative network with L relays.

The three-node model system can be extended to a two-hop model [25, 26] having L relays, as shown in Figure 1.2. In this model, all relays may be simultaneously activated to support the

source node to communicate with the destination node [25]. Alternatively, a part of nodes can be selected based on certain criteria to support the communication. The performance of the two-hop multiple-relay model has been widely investigated in the context of various scenarios, including AF/DF, relay selection, different modulation schemes, etc. [25–30].

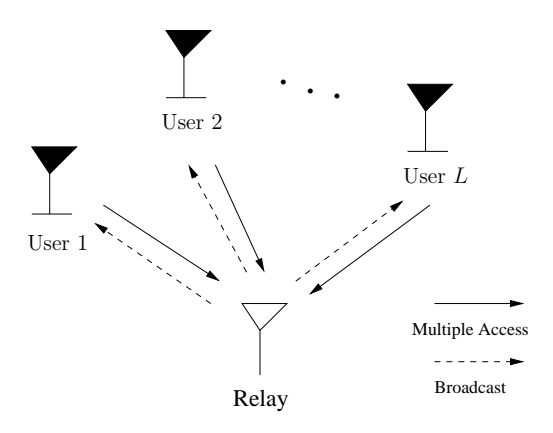


Figure 1.3: System model of a multiway relay cooperative network, where *L* mobile users exchange information via one relay in a two-hop fashion.

Multiway relay cooperative networks can be used for information exchange among a group of distributed mobile users, their system model can be depicted as Figure 1.3. In a multiway relay network, information exchange among the *L* users can be accomplished in two steps, including a multiple access step and a broadcast step. The Multiway relay network was first investigated in [31], as early as in 1977, for the achievable rate region. Recently, multi-way communication has been suggested to be implemented with the aid of relays, forming the multiway relay communication [32–36]. Specifically, in [32], the achievable rate region has been studied, when the AF, DF or CF relay protocol is assumed. In [33,34], the multiway relay communication has been investigated, when assuming that a group of single-antenna users supported by a half-duplex multiantenna relay station are operated under the non-regenerative [33] or regenerative [34] relay strategy. The capacity of the binary multiway relay channels has been studied in [35], where multiple terminals exchange their information with the aid of a relay supported by a so-called functional-decodeforward coding strategy. Furthermore, in [36], the non-coherent fast frequency-hopping (FFH) technique has been proposed for information exchange among a group of users through a relay, which recovers and forwards a time-frequency matrix.

In literature, multi-hop model is another widely studied cooperative topology, which can be simply represented by Figure 1.4 where *L* relays successively forward information from the source to the destination. Concerning this model, Hasna and Alouini [37–39] have analyzed the end-to-end (E2E) equivalent SNR, outage probability, when assuming nonregenerative relays communicating over Nakagami fading channels. Furthermore, they have investigated the power-allocation in multihop networks, when aiming at minimization of outage probability [40]. In [41], Trigui *et*

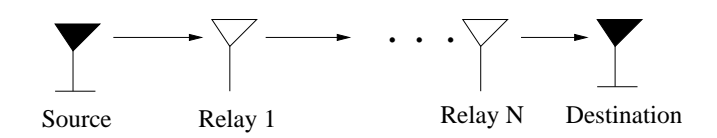


Figure 1.4: System model of a multi-hop network, where the source sends signals to the destination via L intermediate relays.

al. have developed a unified framework for studying the capacity, BER and outage probability of a single input single output (SISO) multihop links operated in AF principles, when communicating over generalized fading channels.

Note that, the multi-hop model of Figure 1.4 can be extended to various and more complex networks, in which each hop may have multiple relays, as well as there are multiple sources and destinations, such as the studies in [12, 42–45].

In cooperative relay communications, a typical assumption widely used is that information exchange among the cooperative relay nodes does not consume energy. In the published references, such as [46–49], on the relay communications employing cooperative relays, the ideal cooperation among relays has been used as a typical assumption. Under this assumption, there is no energy consumption for the information exchange required by cooperation and, furthermore, other overheads required are also often ignored. Against this background, in Chapter 2, we are motivated to study the power-allocation and energy consumption for information exchange among multiple cooperative relays, when we consider a novel relay communication network employing various relay processing schemes. According to our study, we can demonstrate that the ideal cooperation assumptions often result in misleading observations, when practical scenarios are considered.

1.3 Multicarrier Schemes and Resource Allocation in Multicarrier Systems

Multicarrier communication techniques have now played important roles in broadband wireless communications. Without any doubt, in the future generations of wireless communications, multicarrier communication is still one of the promising candidates, due to its capability to support wide range and diverse services, flexibility for implementation, high spectrum-efficiency and capacity, etc. Owing to the above-mentioned, in this thesis, the resource allocation is studied in the context of the multicarrier communications. In this section, we first provide a brief overview for the three most widely employed multicarrier techniques, including the orthogonal frequency division multiplexing (OFDM), multicarrier code-division multiple-access (MC-CDMA), and the multicarrier direct-sequence CDMA (MC DS-CDMA). Then, we provide a literature review of the resource

allocation in multicarrier communications.

1.3.1 Overview of Multicarrier Communication Schemes

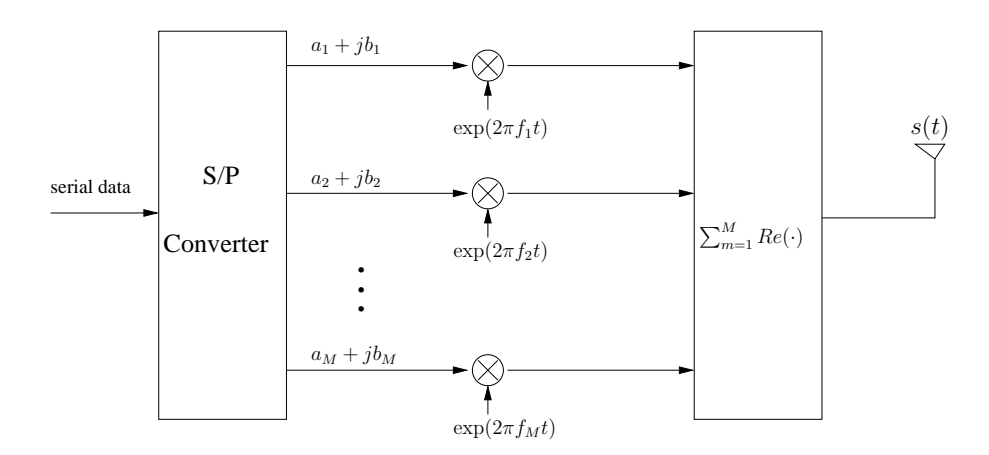


Figure 1.5: The transmitter schematic of the OFDM system employing M number of subcarriers [1].

OFDM and its multiuser extension of orthogonal frequency division multiple-access (OFDMA) belong to the parallel data transmission schemes, which are able to achieve high data rate communications via transmitting data on a number of orthogonal subcarriers [50,51]. Figure 1.5 depicts the transmitter block diagram of the OFDM system, which employs M number of orthogonal subcarriers. In OFDM, data symbols are transmitted in parallel on multiple subcarriers after serial-to-parallel (S/P) conversion. As shown in Figure 1.5, each of the M parallel sub-branches conveys a data symbol, expressed as $a_i + jb_i$ for the ith sub-branch. Then, each of the M symbols modulates one corresponding subcarrier chosen from the M orthogonal subcarriers. In OFDM or OFDMA, this multicarrier modulation is implemented by fast Fourier transform (FFT). As shown in Figure 1.5, after the multicarrier modulation, the final transmitted signal is derived by adding the M sub-branches signals, yielding the composite OFDM signal expressed as

$$s(t) = \sum_{m=1}^{M} \Re \left\{ (a_m + jb_m) \exp(j2\pi f_m t) \right\}$$

=
$$\sum_{m=1}^{M} \left[a_m \cos(2\pi f_m t) - b_m \sin(2\pi f_m t) \right].$$
 (1.1)

OFDM and OFDMA systems are able to achieve high data rate communications benefited from the efficient parallel data transmission. With the aid of cyclic prefixing or zero padding [1], intersymbol interference can be significantly mitigated in OFDM systems. OFDM systems can achieve very high spectrum-efficiency. Furthermore, owing to using FFT techniques for subcarrier modulation and demodulation, OFDM systems have low-complexity. However, OFDM systems suffer from the high peak-to-average power ratio (PAPR) problem [1,50]. When the power of transmitter amplifier is limited, the high PAPR OFDM signals suffer from non-linear distortion, which may

cause significant performance degradation. In order to reduce the non-linear distortion, the average transmit power of OFDM signals may need to be reduced, which however limits the transmission distance. Additionally, due to the limited transmit power of mobile terminals, the PAPR problem in OFDM systems becomes more severe in the uplink transmission. Hence, in order to combat this problem, single-carrier frequency division multiple access (SC-FDMA) schemes employing reduced number of subcarriers have been proposed for the uplink transmission in LTE/LTE-A systems [52,53]. As shown in [1], the localized FDMA (LFDMA) scheme in the SC-FDMA conflicts only slight PAPR problem, since a user only transmits a few of subcarriers. By contrast, the interleaved FDMA (IFDMA) scheme in the SC-FDMA does not have the PAPR problem, as every user only transmits a single subcarrier [1]. Furthermore, with the aid of the *M*-ary pulse-position modulation, time-hopping multicarrier CDMA (TH MC-CDMA) scheme can completely avoid the PAPR problem, as only one of the subcarriers is activated at one time instant [54,55].

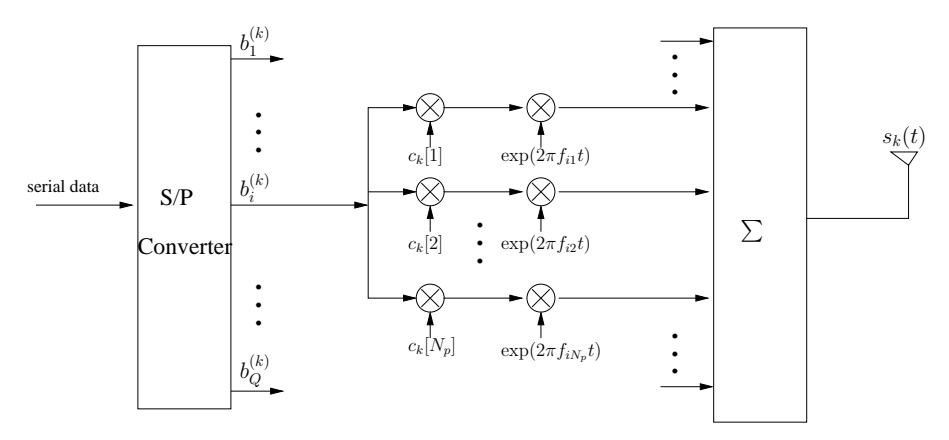


Figure 1.6: The transmitter schematic of the MC-CDMA system with F-domain spreading employing qN_p number of subcarriers [1].

MC-CDMA [56, 57] is another widely used technique in multicarrier systems, which has the general transmitter schematic as shown in Figure 1.6. MC-CDMA uses the frequency-domain (F-domain) spreading. As the figure shows, the serial data is first converted into Q parallel subbranches. Each of the parallel sub-branches is spread over N_p subcarriers using a user specific N-length F-domain spreading code. Finally, after the multicarrier modulation, the composite MC-CDMA signal is obtained by adding the QN_p subcarrier signals, which can be expressed as

$$s_k(t) = \Re\left\{\sqrt{\frac{2P}{N_p}} \sum_{i=1}^{Q} \sum_{j=1}^{N_p} b_i^{(k)}(t) c_k[j] \exp(j2\pi f_{ij}t)\right\}$$
(1.2)

for the kth user. In (1.2), P is the transmission power per sub-branch, $b_i^{(k)}(t)$ represents the ith data stream of user k, $[c_k[1], c_k[2], \ldots, c_k[N_p]]^T$ is the F-domain spreading code of user k. In MC-CDMA, subcarrier modulation can be implemented using FFT techniques, forming the so-called spread OFDM.

MC-CDMA enjoys all the advantages of the OFDMA. Furthermore, MC-CDMA also benefits from the merits of CDMA [58]. In MC-CDMA, one data symbol is spread over multiple subcarri-

ers, which facilitates to achieve frequency diversity, when communicating over frequency selective fading channels [1]. However, as the OFDM, the MC-CDMA also suffers from the PAPR problem.

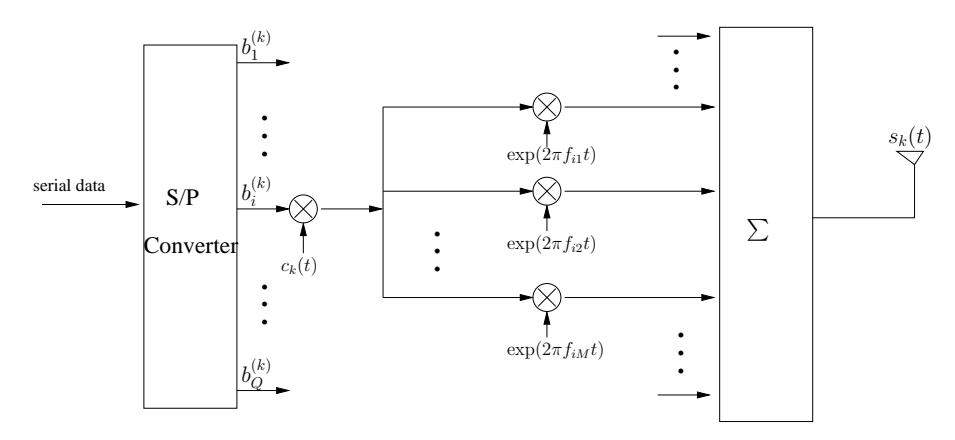


Figure 1.7: Transmitter schematic of the MC DS-CDMA system with time domain spreading, which employs *QM* number of subcarriers [1].

MC DS-CDMA [59, 60] systems use multiple subcarriers to convey parallel data streams with direct-sequence (DS) spreading in time-domain (T-domain) and possibly also F-domain spreading [1]. Figure 1.7 depicts the transmitter schematic of the MC DS-CDMA system using only T-domain spreading. As the figure shows, the serial data stream is converted into Q number of reduced-rate parallel substreams. In order to increase the processing gain of subcarrier signals, MC DS-CDMA system invokes the T-domain spreading on each of the Q substreams. After the DS spreading, each substream is modulated on M number of subcarriers. The composite MC DS-CDMA signal transmitted by user k can be expressed as

$$s_k(t) = \Re\left\{\sqrt{\frac{2P}{QM}} \sum_{i=1}^{Q} \sum_{j=1}^{M} b_i^{(k)}(t) c_k(t) \exp(j2\pi f_{ij}t)\right\}$$
(1.3)

where P and $b_i^{(k)}(t)$ have the same definitions as those in (1.2), $c_k(t)$ is the T-domain spreading sequence of user k.

Owing to the employment of T-domain spreading, MC DS-CDMA system usually requires a significantly lower number of subcarriers than the OFDM and MC-CDMA systems. Therefore, the MC DS-CDMA scheme has less severe PAPR problem suffered by the other two multicarrier schemes. In contrast to the MC-CDMA, the MC DS-CDMA is easy to guarantee independent fading over different subcarriers, since the number of subcarriers in MC DS-CDMA can be significant reduced in comparison with that in MC-CDMA [61]. Furthermore, in the MC DS-CDMA, the number of subcarriers may be reconfigured online according to the communication environments, making the MC DS-CDMA highly-flexibility. In the MC DS-CDMA, if non-orthogonal DS spreading codes are used, multiuser detection may be required to mitigate the multiuser interference. Furthermore, the MC DS-CDMA system may not benefit much from employing the FFT aided multicarrier modulation and demodulation, since the number of subcarriers used is usually not high [1].

1.3.2 Overview of Resource Allocation in Multicarrier Systems

In wireless communications, promising energy- and spectrum-efficiency can be achieved, when taking the advantage of the time-varying characteristics by using, for example, adaptive modulation, dynamically resource allocation, etc. [62]. The studies in references show that dynamic resource allocation is capable of achieving significant gain over fixed resource allocation. So far, various resource allocation algorithms have been proposed for different multicarrier systems [62–74]. In detail, joint bit-, subcarrier- and power-allocation algorithms in have been studied in [62, 63] in order to minimize the total transmission power, while maintaining users' quality-of-service (QoS). Wong et al. [62] have proposed an iterative subcarrier-allocation algorithm, which is operated following bits and power assignment. [63] has considered the joint assignment of the bits, subcarriers and power for each of the users via low-complexity algorithms. Moreover, in [64–68, 75], various sub-optimum joint subcarrier- and power-allocation algorithms have been proposed. Specifically, in [64], the authors have proposed two computationally inexpensive approaches for joint resource allocation, where subcarrier-allocation is carried out in two iterations. Considering the uplink OFDMA systems, the authors in [65,75] have proposed the joint subcarrier- and power-allocation algorithms, with the objectives of maximizing the sum rate and the total utility of resources, respectively. A heuristic non-iterative subcarrier- and power-allocation algorithm has been proposed in [68] for the OFDMA downlink by extending the ordered subcarrier selection algorithm [76] proposed for single user systems. Furthermore, in [69,70], dynamic resource allocation problems have been addressed in the context of cross-layer optimization of OFDMA systems. More recently, the two-part paper [73, 74] has studied the chunk-based subcarrier-allocation and power-allocation in downlink OFDMA systems, in order to reduce the complexity of resource allocation.

Researchers in [77-89] have designed and studied a range of subcarrier-allocation algorithms for the downlink single-cell OFDMA systems. Specifically, Jang and Lee [78] have studied the greedy subcarrier-allocation algorithm without considering the fairness, in order to maximize the sum rate of the downlink OFDMA systems. By contrast, authors in [79] have proposed a fair subcarrier-allocation algorithm of providing equal data rate for all users. The fair greedy algorithm has been introduced in [80, 82] for subcarrier-allocation in the OFDMA systems, where all users are assigned the same number of subcarriers. The fair greedy algorithm has the shortcoming that the users assigned subcarrier later may have poor error performance. For the sake of maximizing the sum rate of downlink OFDMA systems, another two famous greedy-type subcarrier-allocation algorithms have been proposed, which are the worst user first (WUF) greedy algorithm [85] and the maximal greedy algorithm [86]. However, the WUF algorithm is inefficient when operated in highly frequency-selective fading channels, while the maximal greedy algorithm's complexity is dependent on the number of times of applying the above-mentioned fair greedy algorithm, which might be very high. Liu and Yang [83] have proposed a low-complexity worst subcarrier avoiding subcarrier-allocation algorithm, which aims at achieving the best error performance of the frequency-division multiple-access systems including the OFDMA.

A range of references have focused on power-allocation in the downlink OFDMA systems [90–95]. Reference [90] has shown that the water-filling power-allocation is able to maximize the total data rate of the downlink OFDMA systems, which employs with the unfair greedy subcarrier-allocation algorithm. By contrast, Shen *et al.* [92] have proposed an optimal power-allocation scheme performed after the greedy subcarrier-allocation, which aims at maximizing the sum capacity of the OFDMA systems with proportional fairness constraints. In [93], the proposed power-allocation schemes for the OFDMA systems have been designed in the sense of maximizing the sum rate and minimizing the sum power consumption of the systems, respectively. In [94, 95], the authors have investigated the power-allocation in the OFDMA-based cooperative and cognitive radio systems.

A range of researches can be also found in the area of joint resource allocation in the MC-CDMA systems [96–100]. Specifically, the authors in [96] have studied the joint subcarrier- and power-allocation, in order to enhance the power-efficiency and minimize the error rate of the systems. The allocation of transmission rate, subcarrier and power has been considered for MC-CDMA systems in [97], aiming to minimize the total transmission power under certain BER requirement. In [99, 100], the capacity performance of the MIMO-OFDMA and MIMO-MC-CDMA systems has been compared, when only power-allocation is applied. In [101], an iterative resource allocation algorithm implementing bit loading and power-allocation has been developed for the MC-CDMA systems, in order to maximize the throughput, when both transmission power and BER constraints are imposed for all users. In [102, 103] have a special emphasis on subcarrier-allocation in user-group based MC-CDMA systems has been put by the authors, and the algorithm proposed by Huang et al. in [103] aims at maximizing the total throughput, while guaranteeing the fairness among the different user groups. In [104, 105], the authors have studied the subcarrier-allocation in association with linear MUDs in the MC-CDMA systems. Specifically, in [104], the allocation algorithms has been proposed to minimize the uplink power consumptions, when assuming various BER requirements for different users. By contrast, in [105], the authors have demonstrated that the combination of the proposed subcarrier-allocation and linear MUDs is efficient for mitigating multiple-access interference (MAI). The binary power-allocation in single-cell MC-CDMA systems has been addressed in [106, 107], by considering the on-off power control [106], and that power is uniformly distributed over the subcarriers with high relative channel gains, while turning off the power of the subcarriers suffering deep fading [107].

As shown in literature, the MC DS-CDMA scheme employs a range of advantages over the MC-CDMA and OFDMA schemes. It can achieve higher capacity, is more and flexible for design and reconfiguration, and suffers less severe PAPR problem, etc., in comparison with the MC-CDMA and OFDMA. However, very limited researches [108–114] have been devoted to the resource allocation in MC DS-CDMA systems. In a little more detail, in [108], the allocation of subcarrier and non-orthogonal spreading codes have been studied in the generalized MC DS-CDMA systems. It can be shown that the proposed schemes are capable of significantly mitigating the intercarrier

interference without reducing the system's spectrum-efficiency. A joint subcarrier-, power- and code-allocation algorithm has been designed in [110] for the multi-rate MC DS-CDMA systems with both T- and F-domain spreading, with the objectives of maximizing the received signal power as well as eliminating the MAI. In [111, 115], a resource allocation framework has been proposed for cognitive radio-based ad hoc networks with the MC DS-CDMA signalling. A code assignment scheme with interference avoidance has been proposed for the generalized MC DS-CDMA systems in [112–114]. Additionally, for the MC DS-CDMA systems with both T- and F-domain spreading, the authors of [113] have proposed a time slicing code assignment scheme combined with a power-control mechanism, which is shown has much better interference mitigation performance than the scheme proposed in [112].

The resource allocation algorithms considered so far are mainly for the single-cell multicarrier communication systems. The resource allocation in multicell scenarios may be very different from that in single-cell systems. In multicell systems, in order to enhance the aggregate capacity or system reliability, resource allocation in multicell networks is required to effectively capitalize on the spectrum sharing among adjacent cells, in addition to the other considerations in single-cell systems. As a consequence of spectrum sharing among different different cell, intercell interference (InterCI) makes resource allocation in multicell networks more challenging. Usually, the resource allocation schemes proposed for single-cell scenarios cannot be directly used in multicell networks, owing to the InterCI.

In multicell systems, resource allocation schemes can be categorized into the centralized and distributed resource allocation schemes, depending on where and how the allocations take place. Figure 1.8 and Figure 1.9 depict the general schematics of the centralized and distributed resource allocation in multicell systems. In the centralized resource allocation, as shown in Figure 1.8, assume that, via backhaul links, a central control unit is capable of collecting the channel state information (CSI) of all the subcarriers of all the users in all cells. With the CSI, it allocates the resources to all the users in all cells. Such a centralized resource allocation scheme can provide an enormous number of degrees of freedom, which are provided by the number of cells, the number of users, the number of subcarriers, the number of scheduling slots, the number of codes, the power levels, etc., that can be exploited to optimize the network performance [116]. However, implementing such a centralized resource allocation scheme faces a lot of challenges, including an extremely complicated backhaul system, which may consume a lot of resources, huge signalling overhead, for information exchange, etc. By contrast, when the distributed resource allocation is used, as shown in Figure 1.9, each BS is only required to manage its local resources and users independently, based on the CSI between the BS and its users and the interference also measured locally. Evidently, distributed resource allocation scheme can release the burden on backhaul systems and mitigate the signalling overhead. Furthermore, the distributed schemes can quickly response to the dynamic and fast varying environments of mobile communication systems. However, because of the strong coupling between the local resources and the interference from other cells, the performance of distributed resource allocation approaches is in general worse than that of the centralized resource allocation methods [116].

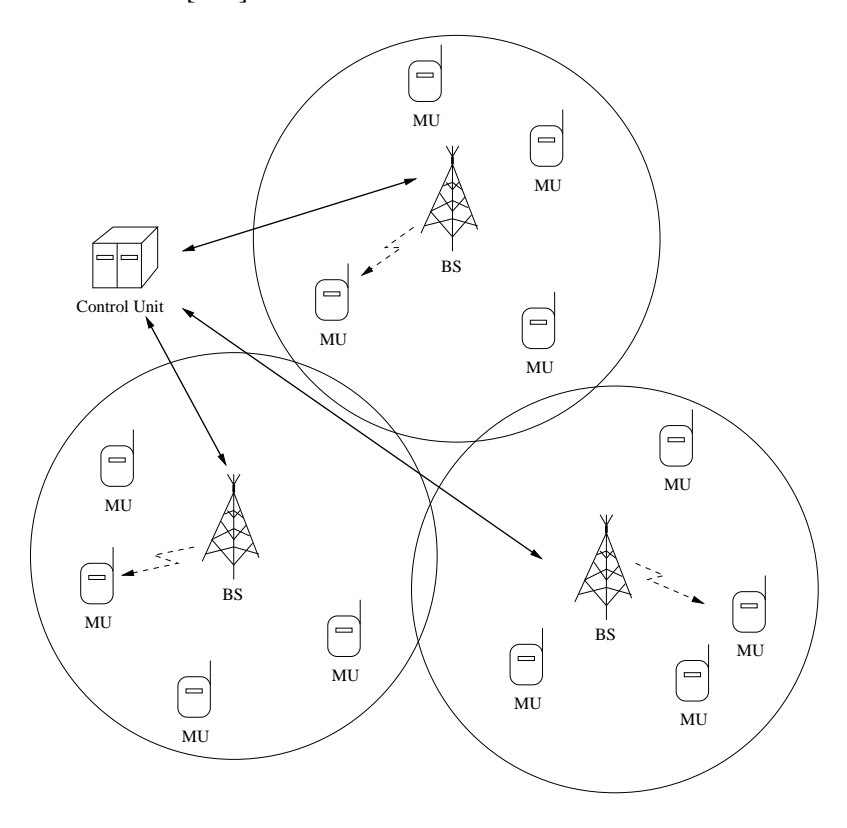


Figure 1.8: Schematic of a multicell system employing centralized resource allocation, where the control unit jointly allocates resources for all the users in all cells.

A range of references, such as, [117–123], have investigated the centralized resource allocation in multicell OFDMA systems. Due to the presence of InterCI, the optimization problem of resource allocation in multicell OFDMA systems is much harder to solve than that in single-cell scenarios. For this sake, the mixed integer nonlinear programming problem of joint resource allocation in the multicell downlink OFDMA systems is usually decoupled into several separate linear programming problems, to allocate subcarrier, bits and power [117]. In [118], a two-stage resource allocation scheme has been proposed, which carries out joint subcarrier-allocation and scheduling in the first stage, followed by an interference-aware power-allocation in the second stage. Considering a two-cell OFDMA system, the authors in [119, 120] have proposed a centralized resource allocation scheme to allocate power and subcarriers. In [120], the NP-hard optimization problem for joint resource allocation is converted to a weighted sum throughput maximization problem, based on which a centralized power- and non-convex subcarrier-allocation algorithm has been proposed. A new cooperative resource allocation scheme for a three-cell OFDMA system has been studied in [122] associated with considering the interference alignment. In [121], the authors have proposed a concept of load matrix, so that the InterCI and intracell interference (IntraCI) of all users in all cells of a wireless cellular network can be jointly managed. The trade-off among energy efficiency, backhaul capacity, and network capacity has been addressed in [123], where the resource allocation problem with limited backhaul capacity has been investigated for the multicell OFDMA systems. In addition to the OFDMA, recently, some research efforts have been made to the centralized resource allocation in the other multicarrier systems. For example, Wang *et al.* have studied the centralized resource allocation in the downlink MC DS-CDMA networks in [124, 125]. Specifically, in [124], the authors have proposed an iterative bisection resource allocation scheme, which aims at maximizing the sum throughput of the system under with transmit power constraints. By contrast, in [125], adaptive allocation of subchannels, power and alphabet size has been considered in a MC DS-CDMA network, in order to maximize its capacity.

The massive growth of various services and the tremendous increase of the number of mobile users demand to install more and more BSs, which causes a lot cost to the mobile operators, and, meanwhile, imposes heavy burden on the environment. Consequently, energy-efficiency motivated resource allocation has become one of the most imperative trends in design of cellular networks [126]. Energy-efficient resource allocation has been investigated in a range of references, such as in [127-134]. Specifically, in [127, 128], the authors have investigated the powerallocation in the AF and DF relay aided cooperative cellular networks. The proposed powerallocation schemes in [128] are shown to be robust against imperfect CSI in slow fading scenarios, while the total uplink transmit power is optimized. In the context of the the cooperative multicell OFDMA systems, Cheung et al. [129] have studied the joint power- and subcarrier-allocation, in order to maximize the energy-efficiency of a multiuser, multi-relay OFDMA cellular system. For the sake of energy-efficiency maximization, in [130], an algorithm has been proposed, which jointly considers the power- and subcarrier-allocation, as well as the relay selection. Furthermore, in [131-134], the authors have investigated the energy-efficiency maximization problem for various multicell multicarrier communication systems. Specifically, Miao et al. [131] have developed the link adaptation and resource allocation algorithms for the uplink communications in multicell OFDMA systems, by emphasizing the energy-efficiency over the peak rate or throughput. Additionally, in [132], the authors have presented a solution to the energy-efficient resource allocation, which maximizes the link capacity of a cognitive radio, under the constraint of the total interference power on of the primary radio.

Distributed resource allocation has also been widely investigated in the context of the various multicell OFDMA systems, such as, in [135–138]. The distributed resource allocation algorithms proposed in [135] consider the joint subcarrier, bit and power-allocation in multicell OFDMA systems, where the proposed algorithms have linear complexity, and the BSs carry out the allocation in a round-robin manner. In [136], the authors have studied the distributed subcarrier- and power-allocation for the multicell OFDMA systems with cognitive radio functionality. By contrast, in [136], a distributed power-allocation scheme has been proposed for multicell multiple input multiple output (MIMO)-based OFDMA systems, when assuming that the CSI of all users is shared among the BSs. Resource allocation in DF relay-assisted multicell OFDMA systems has been considered in [138], and a semi-distributed iterative allocation algorithm has been proposed

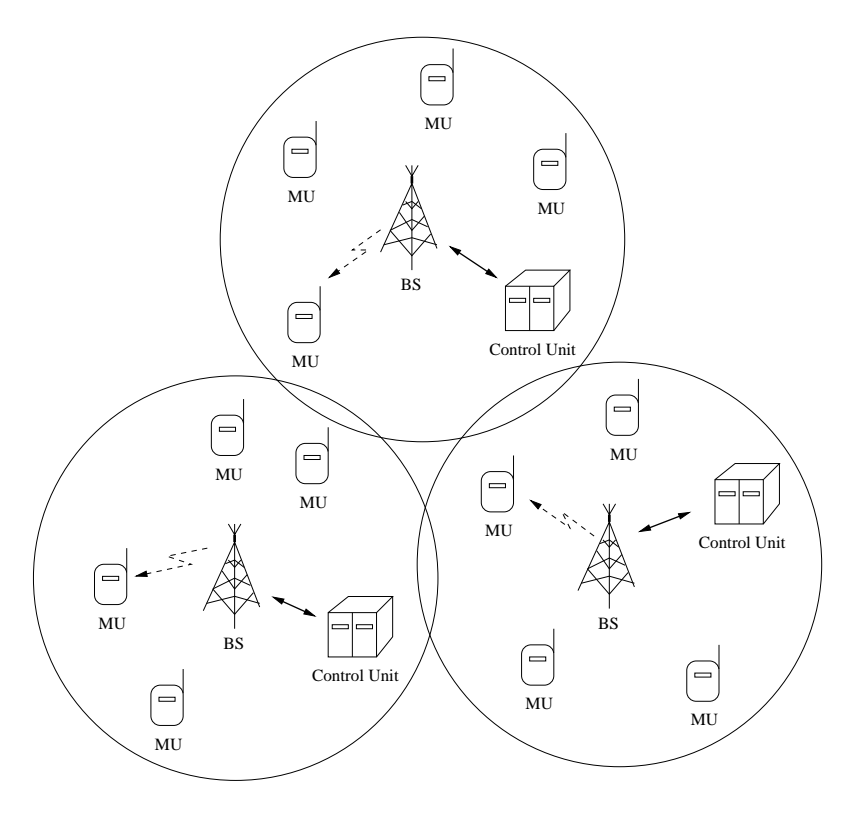


Figure 1.9: Schematic of a multicell system employing distributed resource allocation, in which each BS independently performs resource allocation for the users in its cell.

by constraining the interference temperature. Recently, interference aware resource allocation has drawn more and more research attentions. The authors in [139] have developed a layered architecture, which integrate a packet scheduler with an adaptive resource allocator, in order to avoid strong InterCI. Yu *et al.* [140] have proposed a distributed power-allocation scheme in conjunction with a low-complexity heuristic radio resource allocation scheme, so that the performance of the cell-edge users in the multicell OFDMA systems, can be significantly improved. Furthermore, the studies in [141, 142] have addressed the distributed resource allocation in the uplink multicell OFDMA systems. Specifically, in [141], a distributed low-complexity subcarrier-allocation scheme has been proposed for the uplink OFDMA-based cooperative systems via efficient partition of the allocation into three stages.

Due to the burst effect of traffics and time-varying wireless channels, InterCI becomes a major challenge for resource allocation in multicell systems. For this sake, distributed resource allocation with InterCI coordination has attracted a lot research attentions. As some examples, an efficient distributed resource allocation with InterCI coordination has been proposed in [116] for the multicell TDMA/FDMA systems. Inspired by [143,144], the distributed binary power-allocation scheme in [116] switches off the transmission for the users experiencing strong InterCI. More recently, a range of studies [145–147] have investigated the distributed subcarrier- and power-allocation in the multicell OFDMA systems with InterCI coordination, which typically decompose the optimization problem into several sub-problems that can be distributively processed. Specifically, in [147], the

authors have proposed a scheme, which combines soft frequency reuse with interference limited power-control, in order to avoid severe InterCI to the other cells.

Resource allocation has also been widely investigated in association with game theory. In distributed resource allocation, noncooperative games are operated for users to compete with each other for their resources, with the objective to maximize the utility, which may be capacity, error rate, energy consumed, etc. The game theoretic framework is well suited to the networks of infrastructure-free, such as, peer-to-peer and ad hoc networks [116, 148]. For instance, Goodman et al. in [148] have proposed a noncooperative game assisted power-allocation algorithm for the infrastructure-free wireless data networks, such as, ad hoc networks. In the infrastructure based networks, specifically, in multicarrier cellular systems, distributed resource allocation has been studied based on the noncooperative game models [149-152]. Specifically, Han Zhu et al. in [149, 150] have proposed the distributed noncooperative games for subchannel assignment, adaptive modulation as well as power control in the multicell OFDMA systems. In [151, 152], the noncooperative games have been introduced distributed subcarrier- and power-allocation in multicell OFDMA systems, where interference avoidance is considered in [152], but is not in [151]. Additionally, noncoopertive game framework has been used in [153, 154] for distributed powerallocation in multicell multicarrier systems. More recently, the authors in [155] have studied the distributed resource allocation in the relay-aided multicell OFDMA systems, where all individual relays and BSs independently play a noncooperative game.

In Chapters 3-6, we will design and study various power- and subcarrier-allocation algorithms in both single-cell and multicell scenarios, when both OFDMA and MC DS-CDMA signalling are considered.

1.4 Thesis Outline and Contributions

In this thesis, our focuses are on the cooperation and resource allocation, via which we are motivated to achieve the spectrum-efficiency and the reliability as high as possible. In general, we can see that cooperation and resource allocation are highly related to each other. In order to implement resource allocation in wireless communication systems, base stations (BSs) need to know variety of information of users, including channel state information, data symbols and other control information, etc. BSs may collect these information from users, which can actually be explained as a type of cooperation for information exchange among users. In multicell scenarios, information sharing may happen among BSs by means of cooperation, so that the BSs have the knowledge of the data symbols and channel information of intercell users. In this case, resource allocation can be implemented with the objective to mitigate intercell interference, in addition to achieving multiuser diversity. Therefore, in Chapter 2 of this thesis, we are motivated to investigate the cost of relay cooperation by analyzing the error performance of the system, which gives us a comprehensive understanding on cooperative communication. Based on that, in Chapters 3-6, we are motivated to

study the resource allocation in both the single-cell and multicell downlink multicarrier systems. Our resource allocation algorithms are used to maximize the reliability and spectrum-efficiency by design of the low-complexity algorithms that are practically meaningful. In detail, the main contributions of the thesis can be outlined as follows.

Chapter 2: We investigate and compare the error performance of two-hop communication links (THCL) with multiple relays, when distributed and cooperative relay processing schemes are respectively employed. Our main objectives include finding some general and relatively simple ways for estimating error performance and demonstrating the trade-off of using cooperative relay processing. One distributed relay processing and two cooperative relay processing schemes are compared. In the two cooperative relay processing schemes, one assumes the ideal relay cooperation, in which relays exchange information without consuming energy, while the other one assumes energy consumption for relay cooperation. In this chapter, the error performance of the THCLs employing the considered relay processing schemes is investigated, when the channels from source to relays, the channels for information exchange and that from relays to destination experience various types of fading modeled by the Nakagami-m distributions. In order to derive the formulas for the BER of the THCL employing binary phase-shift keying (BPSK) modulation and various relay processing schemes, we introduce the Nakagami and Gamma approximations for finding the distribution functions of various variables encountered. Our studies show that the proposed approximation approaches are highly effective, which are capable of accurately predicting the BER of the THCLs supported by the different relay processing schemes.

Chapter 3: In this chapter, the resource allocation, including power- and subcarrier-allocation, is investigated in the single-cell downlink OFDMA systems. We design and propose two subcarrierallocation algorithms for the OFDMA systems. One is designed to avoid assigning users as many as possible the worst subchannels, which is referred to as the bidirectional worst subchannel avoiding (BWSA) algorithm. The second one is called the best subchannel seeking (BSS) algorithm, which aims at assigning users the best possible subchannels. When assuming quadrature amplitude modulation (QAM), the BER lower-bound and upper-bound are derived for the OFDMA systems employing dynamic subcarrier-allocation and channel-inverse power-allocation algorithms. We study and compare the error rate and spectrum-efficiency performance, as well as the complexity of the two algorithms. We also compare them with some existing optimum and sub-optimum subcarrier-allocation algorithms. Our studies show that both the BWSA and BSS algorithms belong to the class of low-complexity subcarrier-allocation algorithms. With respect to the error rate and spectrum-efficiency performance, they outperform all the other sub-optimum algorithms considered, especially, when they are operated in relatively large OFDMA systems. If this is the case, we find that both the error performance and the spectrum-efficiency attainable by the BWSA and the BSS algorithms are close to that achieved by the optimum (Hungarian) subcarrier-allocation algorithm.

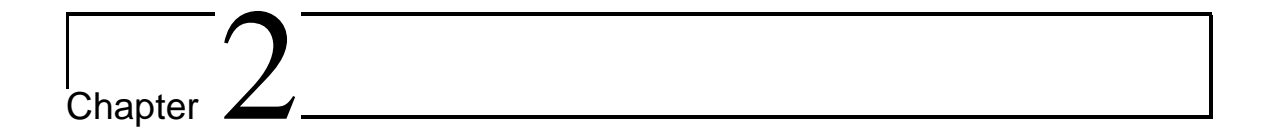
Chapter 4: We investigate the resource allocation in the single-cell downlink MC DS-CDMA sys-

tems, where one subcarrier may be assigned to several users who are then distinguished from each other by their unique DS spreading codes. Our resource allocation is motivated to maximize the system reliability without making a trade-off with the attainable spectrum-efficiency of the system. Without much performance loss, we carry out power- and subcarrier-allocation in a separate approach. In this chapter, we propose a range of subcarrier-allocation algorithms and study them with the MC DS-CDMA systems. We first analyze the advantages and shortcomings of some existing subcarrier-allocation algorithms in the context of the MC DS-CDMA. Then, we generalize the worst subcarrier avoiding (WSA) algorithm to a so-called worst case avoiding (WCA) algorithm, which achieves better performance. Then, the WCA algorithm is further improved by our proposed worst case first (WCF) algorithm. Furthermore, we propose an iterative worst excluding (IWE) algorithm, which can be employed in conjunction with the WSA, WCA and the WCF algorithms, forming the IWE-WSA, IWE-WCA and the IWE-WCF subcarrier-allocation algorithms. The complexities of these algorithms are analyzed, showing that they are all low-complexity subcarrierallocation algorithms. The error and spectrum-efficiency performance are investigated and compared, demonstrating that we can now be very close to the optimum performance attained by the high-complexity Hungarian algorithm.

Chapter 5: In this chapter, we investigate the distributed resource allocation algorithms in multicell downlink OFDMA systems, in which the BSs independently carry out the subcarrier-allocation and then operate the InterCI mitigation with very limited BS cooperation. We propose two novel InterCI mitigation algorithms, one is the distributed decision making assisted cooperation, which is named as the distributed decision making assisted cooperation (DDMC), and the other one is the centralized decision making assisted cooperation, which is referred to as the CDMC. In order to combat the InterCI, both the DDMC and the CDMC algorithms are motivated to set up the space time block coding (STBC) aided cooperative transmissions to the users with poor signal-to-interference ratio (SIR). In the DDMC algorithm, each BS distributively makes the InterCI mitigation decisions. By contrast, the CDMC algorithm makes the centralized InterCI mitigation decisions, based on limited InterCI information. While the DDMC algorithm aims at maximizing the sum rate of the users sharing a subcarrier, the CCMC algorithm motivates to maximize the sum rate of the users sharing a subcarrier, and also improve the frequency reuse factor of the subcarriers. Our studies show that, both the DDMC and the CDMC algorithms can achieve better spectrum-efficiency performance than the existing well-known on-off power (OOP) algorithm, which switches off the subchannels experiencing strong InterCI. Furthermore, the CDMC algorithm is demonstrated to achieve the highest frequency reuse factor among all the InterCI mitigation algorithms considered.

Chapter 6: The resource allocation, including the allocation of both subcarriers and spreading codes in the multicell MC DS-CDMA systems is investigated. Specifically, we extend the subcarrier-allocation algorithms proposed in the single-cell MC DS-CDMA systems in Chapter 4 to the multicell scenarios, while focusing our attention on the code-allocation to mitigate the InterCI. For the sake of achieving low-complexity code-allocation, we assume that the BSs only share

the information about large-scale fading, which includes both the propagation pathloss and shadowing effect. Based on the information shared among the BSs, two code-allocation algorithms are proposed, namely, the simplified strong InterCI avoiding (SSIA) algorithm and the enhanced strong InterCI avoiding (ESIA) algorithm. Both the SSIA and the ESIA algorithms are motivated to minimize the average InterCI of the users sharing the same subcarrier and the same code. Specifically, in our considered three-cell MC DS-CDMA systems, we can form three InterCI factor matrices by considering two cells at a time. In the context of the SSIA algorithm, the code-allocation considers only one of the InterCI factor matrices at a time. By contrast, the ESIA algorithm considers the code-allocation by making use of all the three InterCI factor matrices simultaneously. Therefore, the ESIA algorithm is capable of achieving higher diversity and better performance than the SSIA algorithm, but at the cost of slight increased complexity. Furthermore, our studies show that both the proposed SSIA and ESIA algorithms are highly-efficiency and low-complexity. They are capable of achieving significantly better BER and spectrum-efficiency performance than the random code-allocation (or, in other word, the case without code-allocation).



Performance of Two-Hop Communication Links with Relay Processing

2.1 Introduction

It has widely been recognised that cooperative wireless communications will play more and more important roles in the future generations of wireless communications systems [5–7,156]. One type of cooperative communication systems is the relay-assisted wireless communications, where distributed mobile nodes, often referred to as relay nodes, are exploited for attaining cooperative diversity, in order to enhance the reliability of wireless communications [157–159]. The relay-assisted wireless communication systems have been investigated in the context of various relay protocols, which include amplify-and-forward (AF), decode-and-forward (DF), compress-and-forward (CF), etc. [19, 31, 157–159]. The concept of cooperative communication has been proposed and studied in [160, 161]. Specifically, in [160], the authors have shown that a cooperative system can achieve a capacity improvement in comparison with the conventional non-cooperative system. In [162], the authors have discussed the basic concept of a three-node cooperative network with the focus on the various relaying schemes. A novel cooperative paradigm, referred to as user cooperation diversity, has been proposed in [6, 7], where two users in the same cell cooperate with each other to transmit information to a destination, so that space diversity can be achieved.

Along with the relay-assisted wireless communications, a lot of researchers have addressed the bit error rate (BER) or symbol error rate (SER) analysis, when assuming communications over, such as, Rayleigh fading, Rician fading and Nakagami-*m* fading channels [46,163–169]. In the analyses, various cooperative relaying scenarios have been considered, which include the classic three-node relaying network [46,168], serial or parallel multihop cooperative relaying networks [164,167,169],

2.1. Introduction 21

etc. A lot of exact or approximate closed-form formulas have been derived for evaluating the BER/SER of considered scenarios. In [165], the exact average SER formulas have been obtained for the cooperative network, where a source sends messages to a destination with the aid of multiple AF relays, when assuming communications over flat Rayleigh fading channels. In [166], the SER analysis has been done in the context of the multihop cooperative relaying networks over various types of fading channels, when both the number of relays and the number of hops may take arbitrary values.

In addition to BER/SER, the outage probability of cooperative networks has been investigated in [47, 170–172]. To be in a little more detail, lower and asymptotic bounds of outage probability have been derived in [170] for the dual-hop relaying networks experiencing Rayleigh fading channels. In [171, 172], extended analytical results of outage probability have been derived, when communicating over independent and non-identically distributed Nakagami-*m* fading channels. Furthermore, the achievable capacity bound and rate region of two-hop relaying networks have been studied in [173–175]. Traditional three-node relaying network has been considered in [174], upper and lower bounds on the ergodic capacity have been derived for various relaying schemes. In [175], capacity bounds have been analyzed for the multinode ad hoc networks.

From the published references, such as [46–49], on the relaying communications employing cooperative relays, a typical assumption often used is the ideal cooperation among relays, which does not consume any energy for the information exchange required by cooperation. Against this background, in this chapter, we study and compare three types of relay processing (RP) schemes in association with two-hop communication links (THCL). We assume that a THCL consists of one source and one destination, which cannot communicate directly. Instead, the source sends information to the destination via a cluster of relays that are close to each other. Therefore, sending signals from the source to the destination requires two hops, the source to relays (S-R) and the relays to destination (R-D). At the relays, signals received from the source may be processed in a distributed way or jointly via relay cooperation. Specifically, in this chapter, three main types of RP schemes are considered, including a) distributed RP, which does not require information exchange among relays; b) ideal cooperative RP, which carries out information exchange without error and also without energy consumption; c) cooperative RP, which carries out information exchange among relays via a local network governed by one information exchange centra unit (IECU), and in this local network, the communications are based on the principles of direct-sequence code-division multiple-access (DS-CDMA). In the context of the cooperative RP, the IECU needs to recover the information transmitted from the relays or source, with the aid of two processing schemes. The first one is called the centralized maximal-ratio combining (CMRC), which requires exchange of both the channel information as well as the data information of all the relays. The second one is termed as the centralized majority vote combining (CMVC), which requires to exchange the data information, but not the channel information, of all the relays. Finally, information is transmitted by the relays to the destination with the aid of transmit preprocessing schemes. In this chapter,

2.1. Introduction 22

two preprocessing schemes are considered, one is the maximal-ratio combining assisted transmit preprocessing (TMRC), and the other one is the equal gain combining assisted transmit preprocessing (TEGC). In summary, the RP schemes are classified according to the processing schemes used at the IECU and the transmit preprocessing schemes employed by the relays, as shown in Figure 2.1.

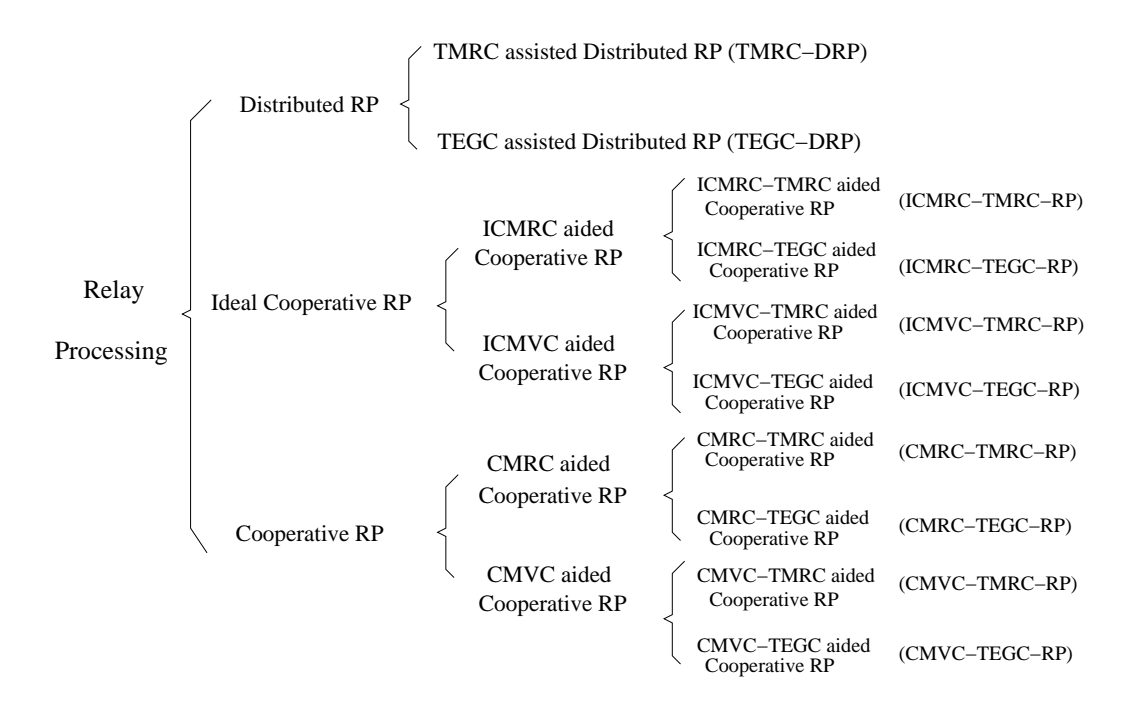


Figure 2.1: Classifications of the relay processing schemes for the THCL systems.

In this chapter, the average BER expressions of the THCL systems with different types of RP schemes are analyzed and derived, where the binary phase shift keying (BPSK) baseband modulation scheme is assumed, and when the first and second hops experience flat Nakagami-*m* fading. The BER performance of the THCL systems employing the various RP schemes is investigated and compared, when different communication scenarios are considered. Our performance results imply that cooperation among relays imposes a big trade-off between the complexity required and the BER performance achievable. Specifically, when employing the ideal cooperative RP, which is explicitly not practical, the THCL systems achieve the best BER performance. However, when energy consumption for relays' cooperation is taken into account, the distributed RP may achieve better BER performance than the cooperative RP, even under the assumption that the communications for local information exchange are highly reliable.

The rest of this chapter is organized as follows. Section 2.2 details the system model of the THCL and gives the main assumptions for channels. In Section 2.3, various RP schemes are described in detail. Section 2.4 analyzes the average BER of the THCL systems associated with various RP schemes and derives the BER expressions, when the BPSK baseband modulation is assumed. Section 2.5 demonstrates and evaluates the BER performance of the THCL systems, and

2.2. System Model 23

provides some insightful discussions. Finally, in Section 2.6, conclusions are summarized.

2.2 System Model

In this section, we describe the system model of the THCL, and state the main assumptions about the channels, power-allocation amongst the nodes involved. Furthermore, the signalling schemes used in the THCL are detailed.

2.2.1 System Description and Channel Modeling

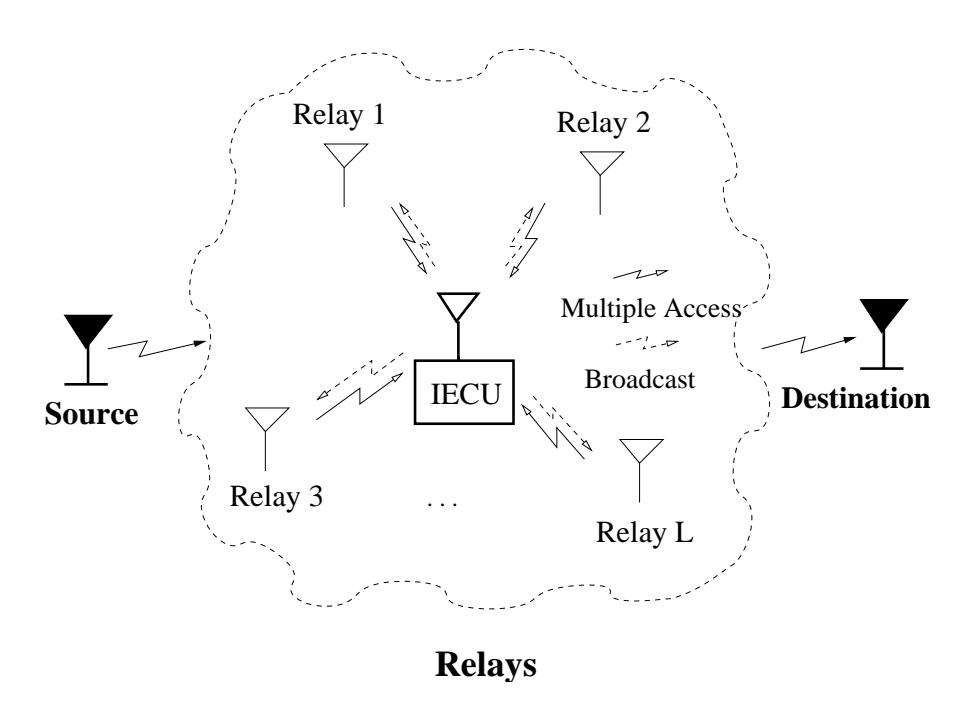


Figure 2.2: Schematic diagram for the two-hop communication links

Figure 2.2 is the schematic diagram for the THCL system considered. The system consists of one source, one destination and L relays. Information is transmitted from the source to the destination with the aid of a cluster of L number of relays, which either cooperate with each other or independently process their signals. As seen in Figure 2.2, when the cooperative RP is employed, the information exchange among the relays are accomplished via an IECU. By contrast, when the distributed RP is employed, the relays independently process their signals without the aid of the IECU for information exchange.

We assume that each of the communication terminals, including the source, destination, relays as well as IECU, is equipped with one antenna for receiving and transmission. The source and destination are separated by a long distance, making their direct communication unavailable. Hence, information is transmitted from source to destination in two hops under the support of relays. We assume that the L relays are close to each other and, when they are in cooperation, the IECU seats in the middle of the L relays and has a small distance from all the relays. We also assume that the

relays do not communicate with each other. They can only receive signals from the source, share their information with the aid of the IECU and independently process and transmit their signals to the destination. By contrast, the IECU is assumed to communicate only with the relays, it does not receive signals from the source or transmit signals to the destination. Note that, the IECU may be viewed as a signal processing unit, which implements multi-way relay [32,176] to aid information exchange among the relays. As shown in Figure 2.2, the relays forward their signal to the IECU based on the principle of DS-CDMA and, then the IECU broadcasts the processed signal back to the relays. Additionally, we assume that all the communication terminals work in the half duplex model, i.e., they cannot receive and transmit signals at the same time. Moreover, we assume that a relay employs the channel state information (CSI) of the S-R and R-D channels related to this relay, and the IECU has the required receiving CSI for carrying out the MRC. When the cooperative RP is considered, a relay also has the CSI of its outgoing channel.

When the distributed RP is used, signal transmission from the source to destination is completed in two phases:

Phase 1 S-R transmission: the source transmits signal to the L number of relays.

Phase 2 R-D transmission: each of the relays decodes and processes the received signal and then, sends the processed signal to the destination, where the information sent by the source is finally detected.

When the THCL employs the cooperative RP, signal transmission from the source to the destination requires four phases:

- **Phase 1** S-R transmission, which is the same as the above described for the distributed RP.
- **Phase 2** Multiple access transmission: the relays decode their received signals and transmit them to the IECU, respectively.
- **Phase 3** Broadcast transmission: the IECU detects based on the signals received from the relays, and then, broadcasts the decision back to the relays.
- **Phase 4** R-D transmission, which is the same as the described for the distributed RP.

In the THCL system, we assume that the channels during the S-R transmission, multiple access (MA) transmission, broadcast (BC) transmission as well as the R-D transmission experience Nakagami-*m* fading with the probability density function (PDF) given by [177]

$$f(r) = \frac{2m^m r^{2m-1}}{\Gamma(m)\Omega^m} e^{-(m/\Omega)r^2}, \ r \ge 0$$
 (2.1)

where $\Omega = E[r^2]$ denotes the average power of a channel, and m ($m \ge 0.5$) is the Nakagami-m fading parameter characterizing the severity of fading. The fading becomes less severe, as the value

of m decreases. Specifically, when m=1, the corresponding channel experiences the Rayleigh fading. By contrast, m>1 corresponds to the Rician fading. Furthermore, when $m\to\infty$, the channel becomes a non-fading channel. In addition to fading, we assume that, in the THCL systems, all the signals received at the L relays, at the IECU, and at the destination conflict additive white Gaussian noise (AWGN), which obeys the Gaussian distribution associated with zero mean and a variance of $\epsilon/(2\bar{\gamma}_s)$, where $\bar{\gamma}_s$ denotes the average signal-to-noise ratio (SNR) per symbol, while ϵ is a parameter related to the allocated power, which will become explicit during our forthcoming discourses.

The signals at the relays are operated in the following ways. First, when the distributed RP is used, we assume that the DF relaying scheme is employed. In this case, the received signal at each relay is firstly decoded and then is forwarded to the destination after the preprocessing. In this chapter, two types of preprocessing schemes are considered, which are the maximal ratio combining (MRC) assisted transmit preprocessing, denoted as TMRC, and the equal gain combining (EGC) transmit preprocessing, denoted as TEGC. By contrast, when the cooperative RP is employed, the relays can either employ a DF or a AF relaying scheme for the MA transmission. In this chapter, we assume that the DS-CDMA scheme is used for the MA transmission. Both random spreading codes and orthogonal spreading codes are considered for spreading. At the IECU, the MRC-based detection, which is referred to as the CMRC, is employed, if the AF relaying scheme is used at the relays for MA transmission. By contrast, the majority vote combining (MVC) scheme is implemented at the IECU, which is referred to as the CMVC, if the relays use the DF relaying scheme for the MA transmission.

It is well-known that, when the DS-CDMA uses random spreading codes, the signals received from the relays conflict with multiuser interference (MUI). In this case, multiuser detection (MUD) is exploited to suppress the MUI. In this chapter, two types of relative low-complexity MUD are employed by the IECU, which are the minimum mean-square error (MMSE) MUD [1], and the receiver multiuser diversity assisted multi-stage MMSE (RMD/MS-MMSE) MUD [178,179]. Correspondingly, the MUD aided CMVC (CMVC/MUD) schemes can be further classified into two types, which are the MMSE MUD assisted CMVC (CMVC/MMSE) and the RMD/MS-MMSE MUD assisted CMVC (CMVC/RMD).

Note that, for the sake of comparison, in this chapter the total transmission power of a symbol is constraint to P, regardless of the RP schemes used. Specifically, the total transmission power per symbol is normalized to be P=1. If the distributed RP is employed, the power used by the first and the second hops are expressed as α_1 and α_2 , respectively, with $\alpha_1 + \alpha_2 = 1$. By contrast, if the systems employ the cooperative RP, a portion of power expressed as α_r for information exchange among relays is allocated, in addition to α_1 and α_2 . Furthermore, according to our above discussion, the relay cooperation includes the MA and BC transmissions, and their power are expressed as α_{ma} and α_{bc} , respectively. Consequently, when given total P=1, we have $\alpha_r=\alpha_{ma}+\alpha_{bc}$ and furthermore, $\alpha_1+\alpha_2+\alpha_r=1$. Additionally, when the ideal cooperative RP is employed, it is

2.2.2. Signalling 26

assumed that no energy is consumed for the relay cooperation. Hence, we have $\alpha_1 + \alpha_2 = 1$ which means that the power is only allocated to the first and second hops. In this chapter, the effect of power-allocation on the BER performance of the THCL systems will be investigated in Section 2.5.

2.2.2 Signalling

With the aid of the above assumptions, below we describe the operations of the THCL system in detail. First, after the source transmits a symbol x, which is assumed to satisfy E[x] = 0 and $E[|x|^2] = 1$, the received signals by the L relays can be expressed in vector form as

$$\mathbf{y}_r = \sqrt{\alpha_1} \mathbf{h}_{sr} x + \mathbf{n}_r. \tag{2.2}$$

In (2.2), we define $\mathbf{y}_r = [y_{r_1}, y_{r_2}, \dots, y_{r_L}]^T$ as the observations obtained by the L relays, and $\mathbf{h}_{sr} = [h_{sr_1}, h_{sr_2}, \dots, h_{sr_L}]^T$ contains the corresponding gains of the channels from the source to the L relays, where $\{|h_{sr_i}|\}$ obey the Nakagami-m distribution in the form of (2.1). In (2.2), $\mathbf{n}_r = [n_{r_1}, n_{r_2}, \dots, n_{r_L}]^T$ is an L-length AWGN noise vector, each element of which obeys the Gaussian distribution with zero mean and a variance of $2\sigma^2$, where $\sigma^2 = 1/(2\bar{\gamma}_s)$ with $\bar{\gamma}_s$ denoting the average SNR per symbol. Explicitly, from (2.2) we can know that the average SNR of the first hop is $\gamma_{sr} = \alpha_1 \bar{\gamma}_s$ per relay.

Based on (2.2), the relays carry out the relay processing, which will be detailed in Section 2.3. Let us express $\tilde{\boldsymbol{y}}_r = [\tilde{y}_{r_1}, \tilde{y}_{r_2}, \dots, \tilde{y}_{r_L}]$ the results after the RP. Then, the relays forward $\tilde{\boldsymbol{y}}_r$ to the destination. Correspondingly, the received signals at the destination can be written as

$$y_d = \sum_{i=1}^{L} \sqrt{\alpha_2} h_{r_i d} \, \tilde{y}_{r_i} + n_d \tag{2.3}$$

where h_{r_id} represents the channel gain between the *i*th relay and the destination, the magnitude $|h_{r_id}|$ obeys the Nakagami-*m* distribution with the PDF expressed in the form of (2.1), while n_d is the Gaussian noise distributed with zero mean and a variance of $2\sigma^2$. Based on (2.3), we can know that the average SNR from the *i*th relay to the destination is $\gamma_{r_id} = \alpha_2 |h_{r_id}|^2 E[|\tilde{y}_{r_i}|^2]\bar{\gamma}_s$, where i = 1, 2, ..., L. Let us now consider in detail the processing at the relays.

2.3 Relay Processing Schemes

In this section, we discuss the different types of RP schemes for the THCL system. Three main RP schemes are considered, which are the distributed RP, ideal cooperative RP and the cooperative RP. According to the different processing schemes used by the IECU and various transmitter preprocessing schemes, , as mentioned in Section 2.2.1 , we may further classify the RP schemes into a range of sub-types RP schemes. In this section, we detail respectively theses RP in the context of the three main scenarios, which are the distributed, ideal and non-ideal cooperative.

2.3.1 Distributed Relay Processing

When the THCL system employs the distributed RP, the relays use the DF relaying scheme, and simply forward their decisions about the symbol received from the source to the destination, after carrying out the transmit preprocessing. As mentioned in Section 2.2, two transmit preprocessing schemes are studied, which are the TMRC and TEGC. Correspondingly, they are referred to as the TMRC-assisted distributed RP (TMRC-DRP) and the TEGC-assisted distributed RP (TEGC-DRP).

2.3.1.1 TMRC Assisted Distributed Relay Processing

For both the TMRC-DRP and TEGC-DRP, the relays first decode the received symbols $\{y_{r_i}\}$, which are given in (2.2). Let the symbols detected by the relays be expressed as $\{x_{r_i}\}$. Then, for the TMRC-DRP, the *i*th relay forwards the destination the signal

$$\tilde{y}_{r_i} = \frac{h_{r_i d}^*}{\sqrt{\sum_{i=1}^L |h_{r_i d}|^2}} x_{r_i}, \quad i = 1, 2, \dots, L.$$
(2.4)

Explicitly, in order to implement the TMRC-DRP, each relay needs to have the knowledge about the channels from the L relays to the destination. Consequently, when substituting (2.4) into (2.3), the decision variable formed at the destination is given by

$$y_d = \sum_{i=1}^{L} \sqrt{\alpha_2} \frac{|h_{r_i d}|^2}{\sqrt{\sum_{i=1}^{L} |h_{r_i d}|^2}} x_{r_i} + n_d.$$
 (2.5)

As the relays may make erroneous detections, in the above equations, we have $x_{r_i} = x$, when the detection of the *i*th relay is correct. Otherwise, $x_{r_i} \neq x$, if the detection of the *i*th relay is incorrect. In other words, $\{x_{r_i}\}$ in (2.5) may take different values. As a result, directly analyzing the error performance of the THCL is very difficult, as will be discussed in detail in Section 2.4. Specifically, let us below analyze the average SNR when assuming that the BPSK is employed by the THCL. Let us assume that there are l number of relays achieving correct detection, while the remaining q = L - l number of relays make erroneous detection. Then, for the TMRC-DRP, (2.5) can be expressed as

$$y_d^{(l,q)} = \frac{\sqrt{\alpha_2}}{\sqrt{\sum_{i=1}^L |h_{r_id}|^2}} \left[\sum_{i \in I\{1,\dots,L\}} |h_{r_id}|^2 - \sum_{j \in I_q\{1,\dots,L\}} |h_{r_jd}|^2 \right] x + n_d$$
 (2.6)

where $\in \{1,\ldots,L\}$ represents selecting l random numbers from the collection of $\{1,\ldots,L\}$, while, $\hat{\in}_q\{1,\ldots,L\}$ means selecting the remaining q numbers. Based on (2.6), the SNR for the TMRC-DRP at the destination can be formulated as

$$\gamma_d^{(l,q)} = \frac{\alpha_2}{\sum_{i=1}^L |h_{r_i d}|^2} \left[\sum_{i \in I\{1,\dots,L\}} |h_{r_i d}|^2 - \sum_{j \in I\{1,\dots,L\}} |h_{r_j d}|^2 \right]^2 \bar{\gamma}_s.$$
 (2.7)

2.3.1.2 TEGC Assisted Distributed Relay Processing

When the TEGC-DRP is employed, we employ the DF relaying scheme, and obtain the decisions as given in (2.4). In contrast to the TMRC-DRP, in TEGC-DRP, every relay only requires the channel knowledge from itself to the destination, in order to carry out the TEGC. In this case, the signal forwarded by the ith relay can be expressed as

$$\tilde{y}_{r_i} = \frac{1}{\sqrt{L}} \frac{h_{r_i d}^*}{\sqrt{|h_{r_i d}|^2}} x_{r_i}, \quad i = 1, 2, \dots, L.$$
(2.8)

By substituting (2.8) into (2.3), the decision variable obtained by the destination can be expressed as

$$y_{d} = \sum_{i=1}^{L} \sqrt{\alpha_{2}} h_{r_{i}d} \frac{1}{\sqrt{L}} \frac{h_{r_{i}d}^{*}}{\sqrt{|h_{r_{i}d}|^{2}}} x_{r_{i}} + n_{d}$$

$$= \sum_{i=1}^{L} \frac{\sqrt{\alpha_{2}} |h_{r_{i}d}|}{\sqrt{L}} x_{r_{i}} + n_{d}.$$
(2.9)

For the TEGC-DRP, when assuming the BPSK baseband modulation and considering the correctly and erroneously detected symbols at the relays, (2.9) can be written as

$$y_{d}^{(l,q)} = \sqrt{\frac{\alpha_{2}}{L}} \left[\sum_{i \in I\{1,...,L\}} |h_{r_{i}d}| - \sum_{j \in I\{1,...,L\}} |h_{r_{j}d}| \right] x + n_{d}$$

$$= \sqrt{\frac{\alpha_{2}}{L}} \left[h_{\Sigma l} - h_{\Sigma q} \right] x + n_{d}$$

$$= \sqrt{\frac{\alpha_{2}}{L}} h_{l,q} x + n_{d}$$
(2.10)

where, for convenience of BER analysis, we defined $h_{\sum l} = \sum_{i \in l} |h_{r_i d}|$, $h_{\sum q} = \sum_{j \in q} |h_{r_j d}|$ and $h_{l,q} = h_{\sum l} - h_{\sum q}$.

Correspondingly, the SNR for the TEGC-DRP case can be expressed as

$$\gamma_d^{(l,q)} = \frac{\alpha_2}{L} \left[\sum_{i \in I\{1,...,L\}} |h_{r_i d}| - \sum_{j \in I_q\{1,...,L\}} |h_{r_j d}| \right]^2 \bar{\gamma}_s
= \frac{\alpha_2}{L} h_{l,q}^2 \bar{\gamma}_s.$$
(2.11)

Let us now consider the ideal cooperative RP.

2.3.2 Ideal Cooperative Relay Processing

When the ideal cooperative RP is employed, we assume that information exchange among the L relays is error free and does not consume energy. These are typical assumptions used in many references considering cooperative relays [46–49]. In this case, the total power P=1 is only

consumed by the first (S-R) and second (R-D) hops. Therefore, we have $\alpha_1 + \alpha_2 = 1$. At the IECU, the symbol transmitted by the source is detected with the aid of the MRC or the MVC. Then, the IECU returns the detected symbol to the relays without consuming energy. Finally, after the TMRC- or TEGC-assisted preprocessing, the relays forward the symbol received from the IECU to the destination. According to the different processing schemes employed by the IECU and various preprocessing schemes used by the relays, we can classify the ideal cooperative RP into four subtypes: a) CMRC- and TMRC-assisted ideal cooperative RP (ICMRC-TMRC-RP), b) CMRC- and TEGC-assisted ideal cooperative RP (ICMRC-TEGC-RP), c) CMVC- and TMRC-assisted ideal cooperative RP (ICMVC-TMRC-RP), d) CMVC- and TEGC-assisted ideal cooperative RP (ICMVC-TEGC-RP).

Since information exchange is ideal, the signals received by the IECU are given by $y_{cu} = y_r$, where y_r is given by (2.2). Hence, when the MRC is employed, it is assumed that the CSI of all the S-R channels are known to the IECU. Therefore, the decision variable is given by

$$z_{cu} = \boldsymbol{h}_{sr}^{H} \boldsymbol{y}_{cu} = \sum_{i=1}^{L} \left(\sqrt{\alpha_1} |h_{sr_i}|^2 x + h_{sr_i}^* n_{r_i} \right).$$
 (2.12)

From (2.12) we can know that the instantaneous SNR can be expressed as

$$\gamma_{cu} = \left(\alpha_1 \sum_{i=1}^{L} |h_{sr_i}|^2\right) \bar{\gamma}_s \tag{2.13}$$

implying that the IECU is capable of obtaining L-order of diversity for detection of the symbol transmitted by the source.

When the IECU employs the MVC, the IECU first makes a hard-decision based on the signals s_r received by the IECU y_r , obtaining the estimations. The IECU then carries out the MVC-based detection and the symbol presented in $s_r = \{s_{r_1}, s_{r_2}, \dots, s_{r_L}\}$ the most times is taken as the estimate of the symbol transmitted by the source.

Let us express the symbol detected by the IECU as \hat{x} , based on either the MRC or the MVC. Then, \hat{x} is sent back to the L relays without error, as the transmission from the IECU to relays is assumed ideal. Finally, every relay transmits \hat{x} to the destination with the aid of the TMRC-assisted transmitter preprocessing, the final decision variable formed at the destination is given by

$$y_d = \sqrt{\alpha_2 \sum_{i=1}^{L} |h_{r_i d}|^2 \hat{x} + n_d}.$$
 (2.14)

By contrast, when the relays employ the TEGC-assisted transmitter preprocessing, which can be described as (2.9) by setting $x_{r_i} = \hat{x}$. Correspondingly, the final decision variable formed at the destination can be expressed as (2.10) with $x_{r_i} = \hat{x}$, i.e.,

$$y_d = \sum_{i=1}^{L} \sqrt{\frac{\alpha_2}{L}} |h_{r_i d}| \hat{x} + n_d.$$
 (2.15)

2.3.3 Cooperative Relay Processing

When the cooperative RP is employed, information exchange among the *L* relays is carried out in two phases: MA and BC transmissions. According to the different processing schemes employed by the IECU and various transmitter preprocessing schemes used by the relays, we have four types of cooperative RP schemes: a) CMRC- and TMRC-assisted cooperative RP (CMRC-TMRC-RP), b) CMRC- and TEGC-assisted cooperative RP (CMRC-TEGC-RP), c) CMVC- and TMRC-assisted cooperative RP (CMVC-TMRC-RP), d) CMVC- and TEGC-assisted cooperative RP (CMVC-TEGC-RP). In this section, we will introduce the cooperative RP in association with different processing schemes used at the IECU.

2.3.3.1 CMRC Aided Cooperative Relay Processing

The CMRC aided RP is used by the THCL supported by a cluster of cooperative relays, which exchange information with the aid of the IECU, as seen in Figure 2.2. Specifically, with this scheme, the L number of relays first employ the AF relaying scheme to transmit the signals received from the source to the IECU. Then, at the IECU, signals received from the L relays are combined based on the MRC principles and a decision is made for the symbol transmitted by the source. Then, the IECU sends the detected symbol back to the L relays, which finally utilize the DF relaying scheme to transmit the detected symbols to the destination. Like the distributed RP, the signals transmitted by the relays to the destination can also be preprocessed based on the MRC or the EGC principles. Hence, according to the different preprocessing methods, we can further classify the CMRC assisted RP into two types: (a) CMRC-TMRC-RP, and (b) CMRC-TEGC-RP. In more detail, the above steps can be analyzed as follows.

Once the L relays obtain the observations of \mathbf{y}_r , as shown in (2.2), each of the relays firstly normalizes its observation, forming $s_{r_i} = y_{r_i} / \sqrt{|h_{sr_i}|^2 + 2\sigma^2}$, based on the knowledge about the channel from the source to this relay, where $i = 1, 2, \ldots, L$. Then, the relays forward their normalized observations to the IECU based on the principles of DS-CDMA. Correspondingly, the observations obtained by the IECU can be represented as

$$\mathbf{y}_{cu} = \sqrt{\frac{\alpha_{ma}}{L}} \mathbf{C} \mathbf{A}_{ma} \mathbf{s}_r + \mathbf{n}_{cu}$$

$$= \sqrt{\frac{\alpha_{ma}}{L}} \mathbf{C} \mathbf{A}_{ma} \mathbf{G}_r \mathbf{y}_r + \mathbf{n}_{cu}$$

$$= \sqrt{\frac{\alpha_{ma}}{L}} \mathbf{H}_{ma} \mathbf{s}_r + \mathbf{n}_{cu}$$
(2.16)

where $\mathbf{s}_r = [s_{r_1}, s_{r_2}, \dots, s_{r_L}]^T$ with s_{r_i} denoting the normalized observation of the *i*th relay as abovementioned, and \mathbf{y}_{cu} is an *N*-length vector, when a spreading factor of *N* is assumed for the DS-CDMA. In (2.16), $\mathbf{H}_{ma} = \mathbf{C}\mathbf{A}_{ma}$, $\mathbf{C} = [\mathbf{c}_1, \mathbf{c}_2, \dots, \mathbf{c}_L]$ is an $(N \times L)$ matrix containing the spreading sequences assigned to the *L* relays to communicate with the IECU, where \mathbf{c}_i satisfies $||\mathbf{c}_i||^2 = 1$, while $A_{ma} = \text{diag}\{a_1, a_2, \dots, a_L\}$, where a_i is the fading gain of the channel from the ith relay to the IECU. We assume that $|a_i|$ obeys the Nakagami-m distribution with the PDF expressed as $f_{|a_i|}(r)$, as shown in (2.1). In (2.16), $G_r = \text{diag}\{g_1, g_2, \dots, g_L\}$, where $g_i = 1/\sqrt{|h_{sr_i}|^2 + 2\sigma^2}$ $(i = 1, 2, \dots, L)$. Finally, in (2.16), $n_{cu} = [n_{cu_1}, n_{cu_2}, \dots, n_{cu_N}]^T$, the element n_{cu_i} obeys the Gaussian distribution with zero mean and a variance of $2\sigma_{cu}^2$ with $\sigma_{cu}^2 = 1/(2\bar{\gamma}_s\beta_1)$, where β_1 depends on the noise variance at the IECU, in comparison with that at the relays and destination. Note that, it can be shown that the SNR of each of the DS-CDMA channels is $\gamma_{ma} = \alpha_{ma}\bar{\gamma}_s\beta_1/L$.

When substituting (2.2) into (2.16), we can obtain another expression for the observation y_{cu} of the IECU, which explicitly relates to the symbol transmitted by the source, and can be expressed as

$$\mathbf{y}_{cu} = \sqrt{\frac{\alpha_1 \alpha_{ma}}{L}} \mathbf{H}_{ma} \mathbf{G}_r \mathbf{h}_{sr} x + \sqrt{\frac{\alpha_{ma}}{L}} \mathbf{H}_{ma} \mathbf{G}_r \mathbf{n}_r + \mathbf{n}_{cu}$$

$$= \sqrt{\frac{\alpha_1 \alpha_{ma}}{L}} \mathbf{h}_T x + \mathbf{n}_T$$
(2.17)

where, for simplicity, we express $h_T = H_{ma}G_rh_{sr}$, which is an N-length vector and can be interpreted as the equivalent source-to-IECU channel matrix. Similarly, in (2.17), the N-length noise vector $\mathbf{n}_T = \sqrt{\frac{\alpha_{ma}}{L}}H_{ma}G_r\mathbf{n}_r + \mathbf{n}_{cu}$ is the combined noise conflicted at both the relays and the IECU. Additionally, it can be shown that the jth (j = 1, 2, ..., N) element of \mathbf{n}_T has zero mean and a variance $2\sigma_{T_i}^2$, with $\sigma_{T_i}^2$ expressed as

$$\sigma_{T_j}^2 = \frac{\alpha_{ma}\sigma_r^2}{L} \left[\sum_{i=1}^L |h_{ji}|^2 |g_i|^2 \right] + \sigma_{cu}^2$$

$$= \frac{\alpha_{ma}}{2\bar{\gamma}_s L} \left[\sum_{i=1}^L |h_{ji}|^2 |g_i|^2 \right] + \frac{1}{2\bar{\gamma}_s \beta_1}.$$
(2.18)

Note that, for the sake of simplicity, in (2.18), the variable h_{ji} stands for the (j,i)th element of matrix \mathbf{H}_{ma} .

Having obtained y_{cu} as shown in (2.16) or (2.17), with the aid of the channel knowledge matrix of h_T , the IECU can carry out the detection based on the MRC principle, yielding the decision variable

$$z_{cu} = \boldsymbol{h}_{T}^{H} \boldsymbol{y}_{cu}$$

$$= \sqrt{\frac{\alpha_{1} \alpha_{ma}}{L}} \boldsymbol{h}_{sr}^{H} \boldsymbol{G}_{r}^{T} \boldsymbol{H}_{ma}^{H} \boldsymbol{H}_{ma} \boldsymbol{G}_{r} \boldsymbol{h}_{sr} x$$

$$+ \sqrt{\frac{\alpha_{ma}}{L}} \boldsymbol{h}_{sr}^{H} \boldsymbol{G}_{r}^{T} \boldsymbol{H}_{ma}^{H} \boldsymbol{H}_{ma} \boldsymbol{G}_{r} \boldsymbol{n}_{r} + \boldsymbol{h}_{sr}^{H} \boldsymbol{G}_{r}^{T} \boldsymbol{H}_{ma}^{H} \boldsymbol{n}_{cu}. \tag{2.19}$$

From (2.19), we can express the instantaneous SNR for detecting symbol x as

$$\gamma_{cu} = \sum_{j=1}^{N} \gamma_{cu_{j}} = \frac{\alpha_{1} \alpha_{ma}}{L} \sum_{j=1}^{N} |h_{T_{j}}|^{2} / (2\sigma_{T_{j}}^{2})$$

$$= \frac{\alpha_{1} \alpha_{ma}}{L} \sum_{j=1}^{N} \frac{\sum_{i=1}^{L} |h_{ji}|^{2} |g_{i}|^{2} |h_{sr_{i}}|^{2}}{\frac{\alpha_{ma}}{\bar{\gamma}_{s}L} \sum_{i=1}^{L} |h_{ji}|^{2} |g_{i}|^{2} + \frac{1}{\bar{\gamma}_{s}\beta_{1}}}.$$
(2.20)

Note that, after the expansion, (2.19) can also be expressed as

$$z_{cu} = \sum_{i=1}^{L} |h_{sr_i}|^2 g_i^2 \sum_{j=1}^{N} |h_{ji}|^2 x + \sum_{i=1}^{L} |h_{sr_i}|^2 g_i^2 \sum_{q=1, q \neq i}^{L} \sum_{j=1}^{N} h_{ji}^* h_{jq} x + \sum_{i=1}^{L} h_{sr_i}^* g_i^2 \sum_{q=1}^{L} \sum_{j=1}^{N} h_{ji}^* h_{jq} n_{r_q} + \sum_{j=1}^{N} \sum_{i=1}^{L} h_{sr_i}^* g_i h_{ji}^* n_{cu_j}$$

$$(2.21)$$

which shows that there exists MUI among the relays, when the DS-CDMA employs non-orthogonal spreading codes. However, when orthogonal spreading codes are employed, we can obtain a free-MUI decision varible, expressed as

$$z_{cu} = \sqrt{\frac{\alpha_1 \alpha_{ma}}{L}} \left(\sum_{i=1}^{L} |h_{sr_i}|^2 g_i^2 \sum_{j=1}^{L} |a_j|^2 \right) x + \sqrt{\frac{\alpha_{ma}}{L}} \sum_{i=1}^{L} h_{sr_i}^* g_i^2 \sum_{j=1}^{L} |a_j|^2 n_{r_j}$$

$$+ \sum_{j=1}^{N} \sum_{i=1}^{L} h_{sr_i}^* g_i h_{ji}^* n_{cu_j}.$$
(2.22)

Based on z_{cu} , the IECU can detect for the symbol transmitted by the source. Let the detected symbol be expressed as \hat{x} . Then, the IECU broadcasts it to the L relays. The received signals by the relays can be expressed as

$$\hat{y}_{r_i} = \sqrt{\alpha_{bc}} h_{bc_i} \hat{x} + \hat{n}_{r_i}, \quad i = 1, 2, \dots, L$$
 (2.23)

where \hat{n}_{r_i} denotes the Gaussian noise of the *i*th BC channel, which has zero mean and a variance of $\sigma_r^2 = 1/(2\bar{\gamma}_s\beta_2)$ per dimension, here β_2 is related to the noise variance of the BC channels. We assume that the signals experience Nakagami-*m* fading over the BC channels, where $|h_{bc_i}|$ obeys the Nakagami-*m* distribution in the form of (2.1). Furthermore, from (2.23) we can readily know that the SNR of the BC channels is given by $\gamma_{bc} = \alpha_{bc}\bar{\gamma}_s\beta_2$. From $\{\hat{y}_{r_i}\}$, the relays can make their decisions about the symbol transmitted by the IECU. Let the symbol detected by the *i*th relay be expressed as x_{r_i} .

Once the relays obtain the detected symbols, they carry out the preprocessing based on the TMRC or TEGC, in the same way as that discussed in Section 2.3.1. After the preprocessing, the signals are transmitted to the destination. Finally, the decision variables formed at the destination are given as (2.5) and (2.9) respectively, for the TMRC and TEGC schemes used.

2.3.3.2 CMVC Aided Cooperative Relay Processing

Instead of the CMRC aided cooperative RP, the CMVC aided cooperative RP can be employed. In comparison with the CMRC aided RP, the CMVC aided RP has much lower complexity, as the IECU does not require the knowledge of the L channels from the source to the relays. The IECU makes a decision based on the MVC principles for the symbol transmitted by the source. Then, the

IECU sends its detected symbol back to the relays and the following operations are the same as that with the CMRC aided cooperative RP.

In more detail, for the CMVC aided cooperative RP, after the *i*th relay receives y_{r_i} , which is given in (2.2), it carries out the hard-decision with the aid of the knowledge about the channel from the source to the *i*th relay. Let the estimates of the *L* relays be expressed as s_{r_i} (i = 1, 2, ..., L). Then, the relays transmit their estimates to the IECU based on the principles of the DS-CDMA, as discussed in Section 2.3.1. Correspondingly, the observations received at the IECU can be written as

$$\mathbf{y}_{cu} = \sqrt{\frac{\alpha_{ma}}{L}} \mathbf{C} \mathbf{A}_{ma} \mathbf{s}_r + \mathbf{n}_{cu}$$

$$= \sqrt{\frac{\alpha_{ma}}{L}} \mathbf{H}_{ma} \mathbf{s}_r + \mathbf{n}_{cu}$$
(2.24)

where the spreading matrix C, channel matrix A_{ma} and the noise vector \mathbf{n}_{cu} have the same explanation as those in (2.16). However, in (2.24), $\mathbf{s}_r = [s_{r_1}, s_{r_2}, \cdots, s_{r_L}]^T$ with $\{s_{r_i}\}$ being the hard-decision symbols.

The IECU detects \mathbf{s}_r based on (2.24), and let the detected symbols be expressed as $\{\hat{s}_{r_i}\}$. Then, the IECU carries out the MVC-based detection and the symbol presented in $\{\hat{s}_{r_i}\}$ the most times is taken as the estimate of the symbol transmitted by the source. Let this symbol be expressed by \hat{x} . It is then sent back to the L relays by the IECU via the broadcast channels using the same principles as that described in Section 2.3.3.1, yielding the decision variables for the relays, which can be expressed as (2.23). Finally, the relays can detect the symbol \hat{x} transmitted by the IECU and send their detected symbols to the destination in the same way as that discussed in Section 2.3.1.

2.3.3.3 CMVC/MUD Aided Cooperative Relay Processing

In the context of the CMVC/MUD aided RP, the relays use the DF relaying scheme to transmit the information received from the source to the IECU. Once the IECU receives the signals from the relays, it carries out multiuser detection (MUD) to detect the symbols transmitted by the relay, when the non-orthogonal spreading codes are used for the DS-CDMA. In this chapter, two types of MUD are considered, which are the (a) minimum mean-square error (MMSE) MUD and (b) receiver multiuser diversity assisted multi-stage MMSE MUD (RMD/MS-MMSE MUD). In this section, we will briefly describe the two MUDs.

Let us below first consider the MMSE MUD operated at the IECU. In order to simplify our description and discussion, we ignore the subscripts of the matrices and vectors, as well as the power term in (2.24). Hence, it can be written as

$$\mathbf{y} = \mathbf{H}\mathbf{s}_r + \mathbf{n}. \tag{2.25}$$

When the MMSE MUD is employed, the decision variable vector for \mathbf{s} is given by [1],

$$z = W^{H}y$$
, or $z_{k} = w_{k}^{H}y$, $k = 1, 2, ..., L$ (2.26)

where $\mathbf{z} = [z_1, z_2, \dots, z_L]^T$ is an L-length decision variable vector, $\mathbf{W} = [\mathbf{w}_1, \mathbf{w}_2, \dots, \mathbf{w}_L]$ is an $(N \times L)$ weight matrix, while \mathbf{w}_k is an N-length weight vector, \mathbf{W} and \mathbf{w}_k are expressed as [1]

$$\mathbf{W} = \mathbf{R}_{y}^{-1} \mathbf{H}, \ \mathbf{w}_{k} = \frac{\mathbf{R}_{k}^{-1} \mathbf{h}_{k}}{1 + \mathbf{h}_{k}^{H} \mathbf{R}_{k}^{-1} \mathbf{h}_{k}}$$
 (2.27)

where \mathbf{R}_y and \mathbf{R}_k denote, respectively, the autocorrelation matrix of \mathbf{y} and the autocorrelation matrix of the interference-plus-noise, which are given by

$$\mathbf{R}_{y} = \mathbf{H}\mathbf{H}^{H} + 2\sigma^{2}\mathbf{I}_{N} = \sum_{k=1}^{L} \mathbf{h}_{k}\mathbf{h}_{k}^{H} + 2\sigma^{2}\mathbf{I}_{N}$$

$$\mathbf{R}_{k} = \sum_{i \neq k}^{L} \mathbf{h}_{i}\mathbf{h}_{i}^{H} + 2\sigma^{2}\mathbf{I}_{N} = \mathbf{R}_{y} - \mathbf{h}_{k}\mathbf{h}_{k}^{H}$$
(2.28)

where $2\sigma^2$ is the variance of the noise samples in n, h_k is kth column of H, while I_N is the $(N \times N)$ identity matrix.

By contrast, the RMD/MS-MMSE MUD originally proposed in [178, 179] belongs to the class of successive interference cancellation (SIC) assisted MUDs, it uses the MMSE MUD analyzed above as its basic detection scheme at each stage.

As discussed in [179], when the RMD/MS-MMSE MUD is applied to the systems with I-Q type baseband modulation, such as, *R*-ary quadrature amplitude modulation (*R*-QAM), it is desirable that the real and imaginary parts of a transmitted symbol are separately detected based on an equivalent real-domain MIMO equation formed from (2.25). This equivalent real-domain MIMO equation can be expressed as

$$\boldsymbol{y}_R = \boldsymbol{H}_R \boldsymbol{s}_R + \boldsymbol{n}_R \tag{2.29}$$

where

$$\mathbf{y}_{R} = \begin{bmatrix} \Re{\{\mathbf{y}^{T}\}}, \Im{\{\mathbf{y}^{T}\}} \end{bmatrix}^{T}, \mathbf{s}_{R} = \begin{bmatrix} (\mathbf{s}_{r}^{(I)})^{T}, (\mathbf{s}_{r}^{(Q)})^{T} \end{bmatrix}^{T}$$

$$\mathbf{H}_{R} = \begin{bmatrix} \Re{\{\mathbf{H}\}} & -\Im{\{\mathbf{H}\}} \\ \Im{\{\mathbf{H}\}} & \Re{\{\mathbf{H}\}} \end{bmatrix}, \mathbf{n}_{R} = \begin{bmatrix} \Re{\{\mathbf{n}\}} \\ \Im{\{\mathbf{n}\}} \end{bmatrix}.$$
(2.30)

Then, when the MMSE MUD is derived based on (2.29), the decision variable vector \mathbf{z} for the symbol vector \mathbf{s} or, specifically, the decision variable $z_k^{(I)}$ (or $z_k^{(Q)}$) for $s_{r_k}^{(I)}$ ($s_{r_k}^{(Q)}$) can be expressed as

$$\boldsymbol{z} = \tilde{\boldsymbol{W}}^T \boldsymbol{y}_R, \ z_k^{(\cdot)} = \tilde{\boldsymbol{w}}_k^{(\cdot)T} \boldsymbol{y}_R, \ k = 1, 2, \dots, L$$
 (2.31)

where $\tilde{\boldsymbol{W}}$ and $\tilde{\boldsymbol{w}}_{k}^{(\cdot)}$ optimized in MMSE sense are given by

$$\tilde{\mathbf{W}} = (\tilde{\mathbf{R}}_y)^{-1} \mathbf{H}_R$$

$$= (\mathbf{H}_R \mathbf{H}_R^T + 2\sigma^2 \mathbf{I}_{2N})^{-1} \mathbf{H}_R,$$

$$\tilde{\mathbf{w}}_k^{(\cdot)} = \frac{\mathbf{R}_k^{-1} \mathbf{h}_k^{(\cdot)}}{1 + \mathbf{h}_k^{(\cdot)T} \mathbf{R}_k^{-1} \mathbf{h}_k^{(\cdot)}}, k = 1, 2, \dots, L$$
(2.32)

with \mathbf{R}_k being the autocorrelation matrix of interference-plus-noise, which is expressed as $\mathbf{R}_k = \mathbf{H}_R \mathbf{H}_R^T + \sigma^2 \mathbf{I}_{2N} - \mathbf{h}_k^{(\cdot)} \mathbf{h}_k^{(\cdot)T} = \tilde{\mathbf{R}}_y - \mathbf{h}_k^{(\cdot)} \mathbf{h}_k(\cdot) T$, where $\tilde{\mathbf{R}}_y = \mathbf{H}_R \mathbf{H}_R^T + \sigma^2 \mathbf{I}_{2N}$.

The detailed procedures for implementing RMD/MS-MMSE MUD can be summarized as follows [178, 179].

Algorithm 1. (RMD/MS - MMSE Multiuser Detection)

Step 1 Initialization: When one-dimensional modulation, such as BPSK, is employed, the initializations are

$$\mathbf{y}^{(0)} = \mathbf{y}, \, \mathbf{R}_{y}^{(0)} = \mathbf{R}_{y}, \, \mathbf{H}^{(0)} = \mathbf{H}, \, \mathbf{W}^{(0)} = \mathbf{W}$$
 (2.33)

where \mathbf{R}_y and \mathbf{W} are given by (2.27) and (2.28), respectively. When two-dimensional modulation, such as R-QAM, is employed, the initializations are

$$\mathbf{y}^{(0)} = \mathbf{y}_R, \ \mathbf{R}_y^{(0)} = \tilde{\mathbf{R}}_y, \ \mathbf{H}^{(0)} = \mathbf{H}_R, \ \mathbf{W}^{(0)} = \tilde{\mathbf{W}}$$
 (2.34)

where \mathbf{y}_R , \mathbf{H}_R , $\tilde{\mathbf{R}}_{\psi}$ and $\tilde{\mathbf{W}}$ are given in (2.32).

- **Step 2** Let s denote the detection stage. Then, for $s=1,2,\ldots,L$, if one-dimensional modulation is employed, or $s=1,2,\ldots,2L$, if two-dimensional modulation is employed, the following operations are executed:
 - 1. **MMSE MUD**: Forming the decision variable vector $\mathbf{z}^{(s)} = \Re\{(\mathbf{W}^{(s-1)})^H \mathbf{y}^{(s-1)}\}$ in the one-dimensional modulation case, or $\mathbf{z}^{(s)} = (\mathbf{W}^{(s-1)})^H \mathbf{y}^{(s-1)}$ in the two-dimensional modulation case.
 - 2. Finding the most reliable symbol among the L-s+1 or 2L-s+1 symbols that have not been detected according to their reliabilities measured based on a scheme that will be given later. Let the index of the most reliable user is $k^{(s)}$.
 - 3. Detecting the most reliable symbol, which is expressed as $\hat{x}^{(s)}$.
 - 4. Cancelling the component related to the detected symbol from the observation equation (2.25) or (2.29), forming the updated observation equation $\mathbf{y}^{(s)} = \mathbf{y}^{(s-1)} \mathbf{h}_{k^{(s)}}^{(s-1)} \hat{x}^{(s)}$, where $\mathbf{h}_{k^{(s)}}^{(s-1)}$ is a N- or 2N- length vector and is the $k^{(s)}$ th $\mathbf{H}^{(s-1)}$.
 - 5. Updating matrices:

$$H^{(s-1)} \to H^{(s)}, R^{(s-1)} \to R^{(s)}, W^{(s-1)} \to W^{(s)}.$$
 (2.35)

6. Setting s = s + 1 and returning to 1) until all the symbols are detected.

2.4. BER Analysis 36

In the above algorithm for the RMD/MS-MMSE MUD, when BPSK is employed and assuming that the source data bits obey independent identical distribution (iid), the reliabilities measured in the maximum a-posterior (MAP) principles is given by

$$L_{k} = \left| \ln \left[\frac{f(x_{k} = +1|z_{k}^{(I)})}{f(x_{k} = -1|z_{k}^{(I)})} \right] \right|$$

$$= \left| \ln \left[\frac{f(z_{k}^{(I)}|x_{k} = +1)}{f(z_{k}^{(I)}|x_{k} = -1)} \right] \right|, k = 1, 2, \dots, L.$$
(2.36)

Upon applying the PDF of $f(z_k^{(I)}|s_{r_k})$ associated with $s_{r_k} = +1$ or -1 into the above equation, we obtain [178]

$$L_k = (1 + \bar{\gamma}_k)|z_k^{(I)}|, k = 1, 2, \dots, L.$$
 (2.37)

By contrast, when I-Q modulation, such as R-QAM, is employed, given the decision variable $z_k^{(I)}$ (or $s_{r_k}^{(Q)}$) for $s_{r_k}^{(I)}$ (or $s_{r_k}^{(Q)}$), where $s_{r_k}^{(I)}$ (or $s_{r_k}^{(Q)}$) $\in \mathcal{E}' = \{e_0, \dots, e_{\sqrt{M}-1}\}$, then the reliability of detecting $s_{r_k}^{(I)}$ (or $s_{r_k}^{(Q)}$) can be evaluated in MAP sense by the formula [179]

$$L_{k}^{(\cdot)} = \frac{\max_{e_{i} \in \mathcal{E}'} \left\{ \exp\left[-\left(\frac{1 + \bar{\gamma}_{k}^{(\cdot)}}{\sqrt{\bar{\gamma}_{k}^{(\cdot)}}} z_{k}^{(\cdot)} - \sqrt{\bar{\gamma}_{k}^{(\cdot)}} e_{i}\right)^{2} \right] \right\}}{\sum_{e_{j} \in \mathcal{E}'} \exp\left[-\left(\frac{1 + \bar{\gamma}_{k}^{(\cdot)}}{\sqrt{\bar{\gamma}_{k}^{(\cdot)}}} z_{k}^{(\cdot)} - \sqrt{\bar{\gamma}_{k}^{(\cdot)}} y e_{j}\right)^{2} \right]},$$

$$k = 1, 2, \dots, 2L - 1. \tag{2.38}$$

In (2.38), e_i is given by [179].

Additionally, in the RMD/MS-MMSE MUD, the weight matrix needs to be updated at the end of every stage until the last stage. The details for updating weight matrix can be found in [179].

2.4 Bit Error Rate Analysis

In this section, we carry out the numerical analysis of the BER of the THCL systems employing various types of RP schemes. Our analysis is based on the assumptions that the S-R channels, the MA channels and BC channels for information exchange, and the R-D channels experience independent fading. Specifically, the S-R channels experience the independent and identically distributed (iid) Nakagami-*m* fading, the same occurs with the MA/BC channels and the R-D channels. However, the fading parameters characterizing the S-R channels, MA/BC channels and the R-D channels may be different. In this section, some exact closed-form BER expressions are derived. For some cases, where the exact closed-form expressions are unavailable, approximate approaches are proposed to derive the closed-form expressions for computing the approximate BER. In this section, only the BER of the THCL systems employing BPSK baseband modulation is considered for the sake of simplicity.

Before considering the specific scheme, we first note that the average BER of the BPSK communicating over flat Nakagami-*m* fading channels can be formulated as [1,180]

$$P_{b}(m,\gamma_{c}) = \sqrt{\frac{\gamma_{c}}{\gamma_{c} + m}} \frac{(1 + \gamma_{c}/m)^{-m} \Gamma(m + 1/2)}{2\sqrt{\pi} \Gamma(m + 1)} \times {}_{2}F_{1}\left(1, m + 1/2; m + 1; \frac{m}{m + \gamma_{c}}\right)$$
(2.39)

where ${}_{2}F_{1}(a,b;c;z)$ is the hypergeometric function that is defined as [181], [182]

$${}_{2}F_{1}(a,b;c;z) = \sum_{k=0}^{\infty} \frac{(a)_{k}(b)_{k}z^{k}}{(c)_{k}k!}$$
(2.40)

associated with $(a)_k = a(a+1)...(a+k-1), (a)_0 = 1.$

Note that, as shown in [181], when $m \ge 1$ is an integer, the BER expression in (2.39) can be simplified to

$$P_b(m,\gamma_c) = \left[\frac{1-\mu}{2}\right]^m \sum_{v=0}^{m-1} \binom{m-1+v}{v} \left[\frac{1+\mu}{2}\right]^v$$
 (2.41)

where $\mu = \sqrt{\gamma_c/(\gamma_c + m)}$.

Furthermore, when m=1, corresponding to the Rayleigh fading channels, the average BER above can be expressed as

$$P_b(m, \gamma_c) = \frac{1}{2} \left[1 - \sqrt{\frac{\gamma_c}{\gamma_c + 1}} \right]. \tag{2.42}$$

2.4.1 Bit Error Rate Analysis of Two-Hop Communication Links with Distributed Relay Processing

When the THCL systems employ the distributed RP, the received signals of the L relays experience non-identical independent distributed (nid) fading, the errors of the L S-R channels occur independently. Therefore, the average BER of the THCL system can be expressed as

$$P_{b}^{(\text{THCL-DRP})}\left(\gamma_{d}^{(l,q)}\right) = \sum_{l=0}^{L} \sum_{k=0}^{\binom{L}{l}-1} \left[\prod_{i \in I\{1,\dots,L\}} (1 - P_{b}^{(\text{S-R}_{i})}) \prod_{j \in I\{1,\dots,L\}} P_{b}^{(\text{S-R}_{j})} \right]^{(k)} P_{b}^{(\text{R-D})}(l) \quad (2.43)$$

where $i \in {l}\{1,\ldots,L\}$ represents one option of selecting l numbers from the total L available numbers $\{1,2,\ldots,L\}$, there are in total ${l \choose l}$ different options, while $j \in {q}\{1,\ldots,L\}$ represents the remaining q = L - l numbers in $\{1,2,\ldots,L\}$, after choosing the l numbers. The superscript (k) stands for the kth option. To be in a little more detail, the term in the bracket of $[\cdot]$ represents the probability of one option that there are l relays which correctly detect the signals received from the source, while the other q relays detect theirs in error. In (2.43), $P_b^{(S-R_i)}$ is the average BER of the S-R $_i$ channel, while $P_b^{(R-D)}(l)$ is the BER of detection at the destination on the condition that the corresponding l relays correctly detect the symbols and the q relays erroneously detect the symbols

received respectively from the source. Given the S-R_i channel experiences the Nakagami-m fading, the average BER of $P_b^{(S-R_i)}$ in (2.43) can be expressed as

$$P_b^{(S-R_i)} = P_b(m = m_{sr_i}, \gamma_c = \alpha_1 \Omega_{sr_i} \bar{\gamma}_s)$$
(2.44)

where $P_b(m, \gamma_c)$ is given by (2.39).

Note that, if all the S-R channels experience i.i.d. fading, resulting in the same error rate for the detection at the L relays, then (2.43) can be simplified to

$$P_b^{\text{(THCL-DRP)}}\left(\gamma_d^{(l,q)}\right) = \sum_{l=0}^{L} \binom{L}{l} \left(1 - P_b^{\text{(S-R)}}\right)^l \left(P_b^{\text{(S-R)}}\right)^q P_b^{\text{(R-D)}}(l). \tag{2.45}$$

As discussed in Section 2.3.1, it is extremely hard to derive a closed-form formula for the THCL employing the TMRC-DRP. However, we may derive relatively simple expressions for the approximate average BER of the THCL system with TEGC-DRP. Specifically, when the TEGC-DRP is considered, the average BER of the R-D channels $P_b^{(\text{R-D})}(l)$ in (2.45) can be expressed as

$$P_{b}^{(\text{R-D})}(l) = P_{b}^{(\text{TEGC})}(l) = \begin{cases} \int_{-\infty}^{\infty} Q\left(x\sqrt{\frac{2\alpha_{2}\bar{\gamma}_{s}}{L}}\right) f_{h_{l,q}}(x)dx, & \text{if } 0 < l < L\\ \int_{0}^{\infty} Q\left(x\sqrt{\frac{2\alpha_{2}\bar{\gamma}_{s}}{L}}\right) f_{h_{\Sigma L}}(x)dx, & \text{if } l = L\\ 1 - \int_{0}^{\infty} Q\left(x\sqrt{\frac{2\alpha_{2}\bar{\gamma}_{s}}{L}}\right) f_{h_{\Sigma L}}(x)dx, & \text{if } l = 0. \end{cases}$$
 (2.46)

In (2.46), $f_{h_{l,q}}(x)$ is the PDF of $h_{l,q}$, which is given by $h_{l,q}=h_{\sum l}-h_{\sum q}$, as shown in (2.11). Moreover, $h_{\sum L}=\sum_{i=1}^L|h_{r_id}|$, which corresponds to the case that all the L relays correctly detect the symbols received from the source. In order to derive $P_b^{(\mathrm{TEGC})}(l)$, we need first derive $f_{h_{l,q}}(x)$ and $f_{h_{\sum L}}(x)$. As $h_{l,q}=h_{\sum l}-h_{\sum q}$, we can express $f_{h_{l,q}}(x)$ as [183]

$$f_{h_{l,q}}(x) = \int_{u}^{\infty} f_{h_{\Sigma l}}(y) f_{h_{\Sigma q}}(z) \, \mathrm{d}y$$

$$= \int_{u}^{\infty} f_{h_{\Sigma l}}(y) f_{h_{\Sigma q}}(y - x) \, dy \qquad (2.47)$$

where $u = \max\{0, x\}$ and, by definition, z = y - x.

In order to derive the BER expression, we need to derive the PDF of $h_{l,q}$ and, therefore, need to obtain the PDFs of $h_{\sum l}$ and $h_{\sum q}$, according to (2.47). Hence, below we derive their PDFs by first introducing the *Nakagami-Approximation*. Two types of Nakagami-approximation approaches are employed, which are the Nakagami Statistical Approximation (Nakagami-SAp) and the Nakagami Theoretical Approximation (Nakagami-TAp) (or modified Nakagami-TAp).

In the context of the Nakagami-SAp, we approximate $h_{\Sigma l}$ (and $h_{\Sigma q}$) as the Nakagami-m distributions with their PDFs $f_{h_{\Sigma l}}(y|m_l,\Omega_l)$ (and $f_{h_{\Sigma q}}(y|m_q,\Omega_q)$) in the form of (2.1). The corresponding fading parameters m_l and Ω_l (m_q and Ω_q) are derived via simulations. Note that, the Nakagami-m PDF is not very sensitive to the values of m and Ω , especially, when these values are

Table 2.1: Parameters (m_L, Ω_L) for the PDF of $h_{\sum L} = \sum_{l=1}^L |h_l|$ obtained by the Nakagami-SAp, where the L components are iid Nakagami-m random variables with parameters (m_0, Ω_0) .

L	n_0 Ω_0	0.5	1	1.5	2	2.5	3
	0.125	0.929, 0.424	1.908, 0.443	2.929, 0.46	3,948, 0.469	4.918, 0.474	5.869, 0.477
2	0.25	0.929, 0.808	1.908, 0.886	2.929, 0.919	3,948, 0.938	4.918, 0.948	5.869, 0.958
	0.5	0.929, 1.617	1.908, 1.771	2.929, 1.838	3,948, 1.875	4.918, 1.895	5.869, 1.904
	1	0.929, 3.234	1.908, 3.542	2.929, 3.676	3,948, 3.751	4.918, 3.791	5.869, 3.819
3	0.125	1.36, 0.843	2.851, 0.957	4.314, 1.007	5.872, 1.038	7.303, 1.052	8.809, 1.061
	0.25	1.36, 1.687	2.851, 1.913	4.314, 2.015	5.872, 2.077	7.303, 2.105	8.809, 2.122
	0.5	1.36, 3.373	2.851, 3.826	4.314, 4.029	5.872, 4.154	7.303, 4.21	8.809, 4.244
	1	1.36, 6.746	2.851, 7.652	4.314, 8.059	5.872, 8.307	7.303, 8.419	8.809, 8.487
4	0.125	1.776, 1.443	3.758, 1.67	5.731, 1.77	7.737, 1.828	9.693, 1.858	11.842, 1.871
	0.25	1.776, 2.885	3.758, 3.34	5.731, 3.541	7.737, 3.656	9.693, 3.715	11.842, 3.742
	0.5	1.776, 5.77	3.758, 6.68	5.731, 7.082	7.737, 7.312	9.693, 7.431	11.842, 7.485
	1	1.776, 11.54	3.758, 13.36	5.731, 14.163	7.737, 14.624	9.693, 14.861	11.842, 14.97
	0.125	2.226, 2.207	4.656, 2.58	7.082, 2.746	9.696, 2.835	12.12, 2.891	14.66, 2.916
5	0.25	2.226, 4.414	4.656, 5.161	7.082, 5.491	9.696, 5.67	12.12, 5.782	14.66, 5.831
	0.5	2.226, 8.829	4.656, 10.322	7.082, 10.982	9.696, 11.34	12.12, 11.564	14.66, 11.662
	1	2.226, 17.658	4.656, 20.645	7.082, 21.964	9.696, 22.68	12.12, 23.128	14.66, 23.324
	0.125	2.647, 3.13	5.636, 3.688	8.538, 3.932	11.6, 4.067	14.511, 4.149	17.685, 4.189
6	0.25	2.647, 6.26	5.636, 7.376	8.538, 7.864	11.6, 8.314	14.511, 8.299	17.685, 8.378
	0.5	2.647, 12.519	5.636, 14.752	8.538, 15.728	11.6, 16.268	14.511, 16.597	17.685, 16.756
	1	2.647, 25.038	5.636, 29.505	8.538, 31.456	11.6, 32.536	14.511, 33.195	17.685, 33.512

relatively large. For example, the PDFs of $f_{|h_{ij}|}(y|m,\Omega)$ do not have any noticeable differences, when $\Omega \pm 0.01\Omega$ and $m \pm 0.01m$ are applied. Hence, it is usually sufficient for us to derive m and Ω based on about 10^3 - 10^4 realizations of h_{ij} . Hence, the time spent for using the Nakagami-SAp to obtain BER results can be significantly less than that required by using direct simulations. When using direct simulations, we know that at least 10^7 (independent) realizations are required for a BER of about 10^{-5} , in order to generate sufficient accuracy.

Note furthermore that, the Nakagami-SAp is very general and robust, as it does not need to understand the components' distributions. However, if the parameters of the components' distributions are known, the approximation is in fact an 'once for all' thing. For instance, we can make a table, like Table 2.1, showing the parameters, (m_L, Ω_L) , for the resultant Nakagami-m distributions of $\sum_{l=1}^{L} |h_l|$, when L takes different values and the components, $\{|h_l|\}$, obey the iid Nakagami-m distributions with different values for the parameters (m_0, Ω_0) . The values of (m_L, Ω_L) shown in the table were generated based on 10^4 realizations. Our performance results in Section 2.5 show that they can generate very accurate approximation. Furthermore, this table can be repeatedly used and, possibly, for different applications.

In the context of the Nakagami-TAp, first, according to [184], when the l components in $h_{\sum l}$ are independent and obey the same Nakagami-m distribution with the parameters m_0 and Ω_0 , $h_{\sum l}$

Table 2.2: Parameters κ for the PDF of $h_{\sum l}$ obtained by the Nakagami-TAp, where the component distributions have the parameter $\Omega_0 = 1$.

m_0	1.0	1.5	3.0	4.0
2	0.842	0.879	0.914	0.924
3	0.825	0.867	0.914	0.929
4	0.812	0.862	0.915	0.930
5	0.807	0.859	0.918	0.931
6	0.803	0.857	0.919	0.933

can be approximated as a Nakagami-m distributed random variable with the PDF $f_{h_{\Sigma l}}(y|m_l,\Omega_l)$ in the form of (2.1) and

$$m_l = l \times m_0, \ \Omega_l = l^2 \times \Omega_0. \tag{2.48}$$

However, as the results in [184] show, the Nakagami-TAp approximation may be very inaccurate. Based on our careful studies and numerous simulation verifications, we find that the PDF $f_{h_{\Sigma l}}(y|m_l,\Omega_l)$ can be slightly modified to make it very accurate, yielding the modified Nakagami-TAp, with the PDF given by

$$f_{h_{\Sigma l}}^{\text{Mod}}(y|m_l, \Omega_l) = f_{h_{\Sigma l}}(y|m_l, \kappa \Omega_l)$$
(2.49)

where κ is a coefficient that is dependent on the distribution of the components in $h_{\sum l}$ and the value of l. For instance, when $\Omega_0=1$, a range of values for κ have been found, which are summarized in Table 2.2. From the table we see that $\kappa<1$ is always the case. This implies that the approximation using the parameters in (2.48) overestimates Ω_l .

Figures 2.3 and 2.4, 2.5 show the PDFs of $f_{h_{\Sigma l}}$ obtained by the Nakagami-SAp, the Nakagami-TAp and the modified Nakagami-TAp. In the figures, the curves labeled as "simu." were derived by simulation using 10^6 realizations, acting as the accurate reference PDFs. By contrast, the curves labeled as "approx." were obtained from the approximate formulas of the Nakagami-TAp. In all figures, we considered various scenarios including l=4,6 and m=1,1.5,3, respectively. In Figure 2.3, the PDFs obtained by the Nakagami-SAp can match with the simulated PDFs, revealing that the Nakagami-SAp is very efficient in terms of approximating the PDF of the sum of Nakagami-m variables. However, as shown in Figure 2.4, we can clearly observe that the approximated PDFs obtained via theoretical approximation are not aligned with the corresponding PDFs obtained by simulations. Moreover, the deviation becomes larger as the value of l gets bigger or as the m value becomes smaller. With the aid of the modified Nakagami-TAp, as expressed in (2.49) in association with Table 2.2, the approximate PDFs shown in Figure 2.5 agree with the simulated PDFs very well.

Having obtained the PDFs of $f_{h_{\Sigma l}}(y)$ and $f_{h_{\Sigma g}}(z)$ for the case of using the Nakagami-SAp or

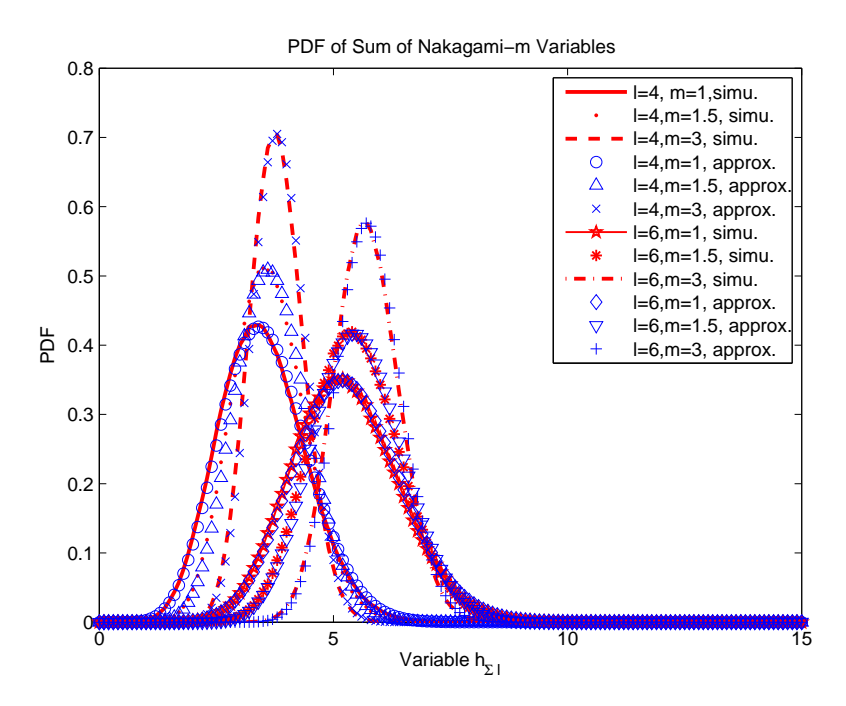


Figure 2.3: The PDF $f_{h_{\Sigma l}}$ obtained by Nakagami-SAp, where all the l Nakagami-m variables have the same parameters.

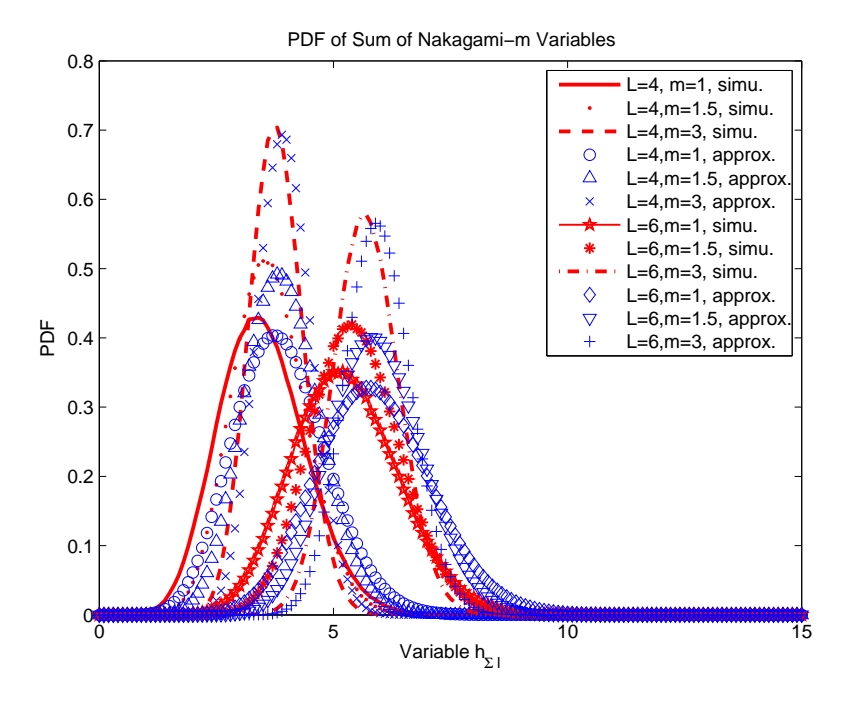


Figure 2.4: The PDF $f_{h_{\Sigma l}}$ obtained by Nakagami-TAp, where all the l Nakagami-m variables have the same parameters.

Nakagami-TAp, let us below derive the PDF of $f_{h_{l,q}}(x)$ by using (2.47). When substitute $f_{h_{\sum l}}(y)$ and $f_{h_{\sum q}}(z)$ in the form of (2.1) associated with the parameters m_l , m_q , Ω_l and Ω_q , into (2.47), we

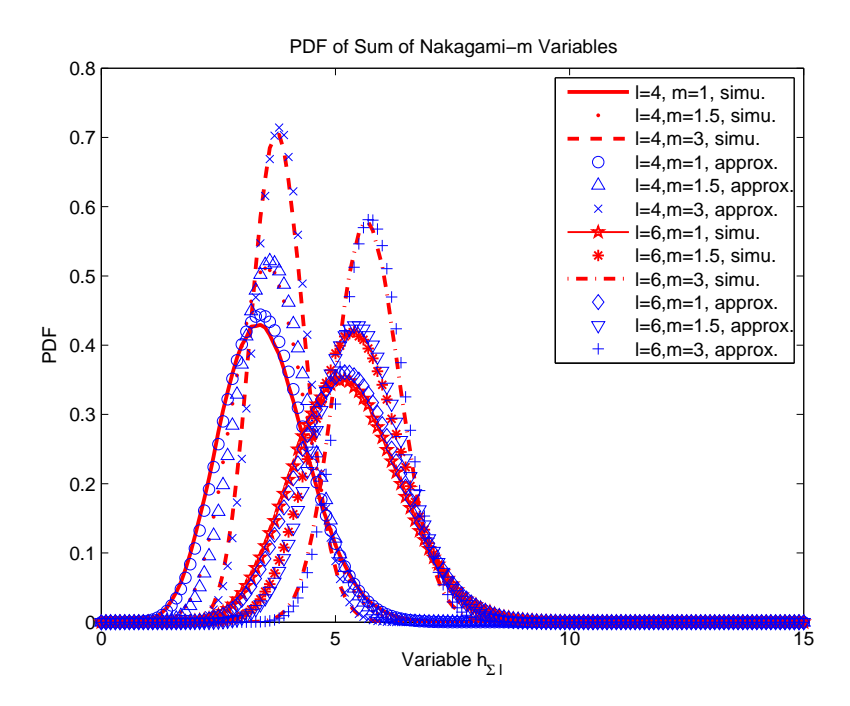


Figure 2.5: The PDF $f_{h_{\sum l}}$ obtained by modified Nakagami-TAp, where all the l Nakagami-m variables have the same parameters.

obtain

$$f_{h_{l,q}}(x) = \int_{u}^{\infty} f_{h_{\Sigma l}}(y) f_{h_{\Sigma q}}(y - x) \, dy$$

$$= \frac{4m_{l}^{m_{l}} m_{q}^{m_{q}}}{\Omega_{l}^{m_{l}} \Omega_{q}^{m_{q}} \Gamma(m_{l}) \Gamma(m_{q})} \int_{u}^{\infty} y^{2m_{l}-1} (y - x)^{2m_{q}-1} \exp\left[-\frac{m_{l}}{\Omega_{l}} y^{2} - \frac{m_{q}}{\Omega_{q}} (y - x)^{2}\right] \, dy$$

$$= \frac{4m_{l}^{m_{l}} m_{q}^{m_{q}}}{\Omega_{l}^{m_{l}} \Omega_{q}^{m_{q}} \Gamma(m_{l}) \Gamma(m_{q})} \, \varphi(x)$$
(2.50)

where

$$\varphi(x) = \int_{u}^{\infty} y^{2m_{l}-1} (y-x)^{2m_{q}-1} \exp\left[-\frac{m_{l}}{\Omega_{l}} y^{2} - \frac{m_{q}}{\Omega_{q}} (y-x)^{2}\right] dy$$

$$= \exp\left(\frac{m_{q}^{2} - m_{q} \Omega_{q} \varsigma^{2}}{\Omega_{q}^{2} \varsigma^{2}} x^{2}\right) \int_{u \varsigma - \frac{m_{q} x}{\Omega_{q} \varsigma}}^{\infty} \frac{1}{\varsigma} \left(\frac{s}{\varsigma} + \frac{m_{q} x}{\Omega_{q} \varsigma^{2}}\right)^{2m_{l}-1}$$

$$\left(\frac{s}{\varsigma} + \frac{m_{q} x}{\Omega_{q} \varsigma^{2}} - x\right)^{2m_{q}-1} e^{-s^{2}} ds$$
(2.51)

after defining

$$\varsigma = \sqrt{\frac{m_l}{\Omega_l} + \frac{m_q}{\Omega_q}}, \qquad s = \varsigma y - \frac{m_q x}{\Omega_q \varsigma}.$$
(2.52)

In the general cases, (2.51) is hard to be further simplified to the best of our knowledge. However, when $2m_l - 1$ and $2m_q - 1$ are integers, $\varphi(x)$ can be expressed in a sequence of limited terms

as

$$\varphi(x) = \exp\left(\frac{-m_{l}m_{q}x^{2}}{m_{l}\Omega_{q} + m_{q}\Omega_{l}}\right) \int_{u_{\zeta} - \frac{m_{q}x}{\Omega_{q}\zeta}}^{\infty} \frac{1}{\zeta} \left[\sum_{l_{1}=0}^{2m_{l}-1} {2m_{l}-1} \left(\frac{s}{\zeta}\right)^{l_{1}} \left(\frac{m_{q}x}{\Omega_{q}\zeta^{2}}\right)^{2m_{l}-1-l_{1}}\right] \\
\times \left[\sum_{q_{1}=0}^{2m_{q}-1} {2m_{q}-1} \left(\frac{s}{\zeta}\right)^{q_{1}} \left(\frac{m_{q}x}{\Omega_{q}\zeta^{2}} - x\right)^{2m_{q}-1-q_{1}}\right] e^{-s^{2}} ds \\
= \exp\left(\frac{-m_{l}m_{q}x^{2}}{m_{l}\Omega_{q} + m_{q}\Omega_{l}}\right) \sum_{l_{1}=0}^{2m_{l}-1} \sum_{q_{1}=0}^{2m_{q}-1} {2m_{l}-1} \left(\frac{2m_{l}-1}{q_{1}}\right) \left(\frac{m_{q}x}{\Omega_{q}\zeta^{2}}\right)^{2m_{l}-1-l_{1}} \\
\times \left(\frac{m_{q}x}{\Omega_{q}\zeta^{2}} - x\right)^{2m_{q}-1-q_{1}} \left(\frac{1}{\zeta}\right)^{l_{1}+q_{1}+1} \int_{u_{\zeta} - \frac{m_{q}x}{\Omega_{q}\zeta}}^{\infty} s^{l_{1}+q_{1}} e^{-s^{2}} ds \\
= \frac{1}{2} \exp\left(\frac{-m_{l}m_{q}x^{2}}{m_{l}\Omega_{q} + m_{q}\Omega_{l}}\right) \sum_{l_{1}=0}^{2m_{l}-1} \sum_{q_{1}=0}^{2m_{q}-1} \left(2m_{l}-1\right) \left(2m_{q}-1\right) \left(\frac{m_{q}}{\Omega_{q}\zeta^{2}}\right)^{2m_{l}-1-l_{1}} \\
\times \left(\frac{m_{q}}{\Omega_{q}\zeta^{2}} - 1\right)^{2m_{q}-1-q_{1}} \left(\frac{1}{\zeta}\right)^{l_{1}+q_{1}+1} \\
\times \left(\frac{m_{q}}{\Omega_{q}\zeta^{2}} - 1\right)^{2m_{q}-1-q_{1}} \left(\frac{1}{\zeta}\right)^{l_{1}+q_{1}+1} \\
\times \Gamma\left(\frac{l_{1}+q_{1}+1}{2}, \left(u_{\zeta} - \frac{m_{q}x}{\Omega_{q}\zeta}\right)^{2}\right) x^{2m_{l}+2m_{q}-l_{1}-q_{1}-2} \tag{2.53}$$

where $\Gamma(a, x)$ represents the incomplete gamma function defined as [182]

$$\Gamma(a,x) = \int_{x}^{\infty} t^{a-1}e^{-t} dt.$$
 (2.54)

Finally, when substituting (2.53) into (2.50), the PDF of $f_{h_{l,q}}(x)$ can be written as

$$f_{h_{l,q}}(x) = \frac{2m_{l}^{m_{l}}m_{q}^{m_{q}}}{\Omega_{l}^{m_{l}}\Omega_{q}^{m_{q}}\Gamma(m_{l})\Gamma(m_{q})} \exp\left(\frac{-m_{l}m_{q}x^{2}}{m_{l}\Omega_{q} + m_{q}\Omega_{l}}\right)$$

$$\times \sum_{l_{1}=0}^{2m_{l}-1}\sum_{q_{1}=0}^{2m_{q}-1} \binom{2m_{l}-1}{l_{1}} \binom{2m_{q}-1}{q_{1}} \left(\frac{m_{q}}{\Omega_{q}\varsigma^{2}}\right)^{2m_{l}-1-l_{1}} \left(\frac{m_{q}}{\Omega_{q}\varsigma^{2}} - 1\right)^{2m_{q}-1-q_{1}}$$

$$\times \left(\frac{1}{\varsigma}\right)^{l_{1}+q_{1}+1} \Gamma\left(\frac{l_{1}+q_{1}+1}{2}, \left(u\varsigma - \frac{m_{q}x}{\Omega_{q}\varsigma}\right)^{2}\right) x^{2m_{l}+2m_{q}-l_{1}-q_{1}-2}. \tag{2.55}$$

When given the PDF $f_{h_{l,q}}(x)$, the average BER of the R-D transmission employing TEGC-DRP can be derived from (2.46) by invoking (2.53) or (2.55). Specifically, when $2m_l - 1$ and $2m_q - 1$ are integers, it can be shown that

$$P_{b}^{(\text{TEGC})}(l) = \frac{m_{l}^{m_{l}} m_{q}^{m_{q}}}{\Omega_{l}^{m_{l}} \Omega_{q}^{m_{q}} \Gamma(m_{l}) \Gamma(m_{q})} \sum_{l_{1}=0}^{2m_{l}-1} \sum_{q_{1}=0}^{2m_{q}-1} {2m_{l}-1 \choose l_{1}} {2m_{q}-1 \choose q_{1}}$$

$$\times \left(\frac{m_{q}}{\Omega_{q} \zeta^{2}}\right)^{2m_{l}-1-l_{1}} \left(\frac{m_{q}}{\Omega_{q} \zeta^{2}}-1\right)^{2m_{q}-1-q_{1}} \left(\frac{1}{\zeta}\right)^{l_{1}+q_{1}+1}$$

$$\times \int_{-\infty}^{\infty} Q\left(x\sqrt{2\alpha_{2}/L}\right) \exp\left(\frac{-m_{l} m_{q} x^{2}}{m_{l} \Omega_{q}+m_{q} \Omega_{l}}\right)$$

$$\times \Gamma\left(\frac{l_{1}+q_{1}+1}{2}, \left(u_{\zeta}-\frac{m_{q} x}{\Omega_{q} \zeta}\right)^{2}\right) x^{2m_{l}+2m_{q}-l_{1}-q_{1}-2} dx \tag{2.56}$$

when 0 < l < L.

In (2.56) m_l , Ω_l and m_q , Ω_q are the parameters of the PDFs $f_{h_{\Sigma l}}(y)$ and $f_{h_{\Sigma q}}(z)$, respectively, which are the Nakagami-m distributed PDFs. Note that, when the parameters m_l , m_q derived by the Nakagami-SAp or Nakagami-TAp are relatively large, such as m_l , $m_q > 1.5$, we may further approximate them to their nearest values, so that $2m_l - 1$ and $2m_q - 1$ are integers, in order to apply (2.56). This is because, when the value of m is relatively large, the Nakagami-m distribution is not sensitive to m.

Furthermore, when the Nakagami-TAp is employed, we have that $m_L = Lm_2$, $\Omega_L = L^2$ and $m_l = lm_2$, $m_q = qm_2$, $\Omega_l = l^2$ and $\Omega_q = q^2$. In this case, if m_2 is an integer, then (2.56) can be simplified to

$$P_{b}^{(\text{TEGC})}(l) = \frac{1}{2} \int_{-\infty}^{\infty} \operatorname{erfc}\left(x\sqrt{\frac{\alpha_{2}}{L}}\right) \frac{2m_{2}^{lm_{2}+qm_{2}}}{l^{lm_{2}}q^{qm_{2}}\Gamma(lm_{2})\Gamma(qm_{2})} \times \exp\left[x^{2}\left(\frac{lm_{2}}{ql+q^{2}} - \frac{m_{2}}{q}\right)\right] \sum_{l_{1}=0}^{2lm_{2}-1} \sum_{q_{1}=0}^{2qm_{2}-1} \binom{2lm_{2}-1}{l_{1}} \binom{2qm_{2}-1}{q_{1}} \times \left(\frac{m_{2}}{q\varsigma^{2}}\right)^{2lm_{2}-1-l_{1}} \left(\frac{m_{2}}{q\varsigma^{2}} - 1\right)^{2qm_{2}-1-q_{1}} \left(\frac{1}{\varsigma}\right)^{l_{1}+q_{1}+1} \times \Gamma\left(\frac{l_{1}+q_{1}+1}{2}, \left(u\varsigma - \frac{m_{2}x}{q\varsigma}\right)^{2}\right) x^{2lm_{2}+2qm_{2}-l_{1}-q_{1}-2} dx$$

$$(2.57)$$

where $\zeta = \sqrt{\frac{m_2}{l} + \frac{m_2}{q}}$ and $u = \max\{0, x\}$.

Additionally, when the L S-R channels as well as the L R-D channels experience Rayleigh fading, making $m_1 = m_2 = 1$. Then, we have

$$\begin{split} P_{b}^{(\text{TEGC})}(l) = & \frac{1}{2} \int_{-\infty}^{\infty} \text{erfc} \left(x \sqrt{\frac{\alpha_{2}}{L}} \right) \frac{2}{l^{l} q^{q} \Gamma(l) \Gamma(q)} \text{exp} \left[x^{2} \left(\frac{l}{ql + q^{2}} - \frac{1}{q} \right) \right] \\ & \times \sum_{l_{1}=0}^{2l-1} \sum_{q_{1}=0}^{2q-1} \binom{2l-1}{l_{1}} \binom{2q-1}{q_{1}} \left(\frac{1}{q\varsigma^{2}} \right)^{2l-1-l_{1}} \left(\frac{1}{q\varsigma^{2}} - 1 \right)^{2q-1-q_{1}} \\ & \times \left(\frac{1}{\varsigma} \right)^{l_{1}+q_{1}+1} \Gamma \left(\frac{l_{1}+q_{1}+1}{2}, \left(u\varsigma - \frac{x}{q\varsigma} \right)^{2} \right) (x)^{2l-2q-l_{1}-q_{1}-2} \, \mathrm{d}x, \ 0 < l < L \end{split}$$

$$(2.58)$$

where, correspondingly, $\zeta = \sqrt{\frac{1}{l} + \frac{1}{q}}$ and $u = \max\{0, x\}$.

When l=L, meaning that all the L relays correctly detect the symbols transmitted by the source, then, using the Nakagami-SAp or Nakagami-TAp, we can express the PDF $f_{h_{\Sigma L}}(y)$ as (2.1) associated with the parameters m_L , Ω_L . Consequently, when substituting the PDF into (2.46), the average BER of the R-D transmission is

$$P_b^{(\text{TEGC})}(l) = P_b(m = m_L, \gamma_c = \alpha_2 \Omega_L \bar{\gamma}_s / L)$$
(2.59)

when l = L, and P_b is given in (2.39). Furthermore, when l = 0, we have

$$P_b^{(\text{TEGC})}(l) = 1 - P_b(m = m_L, \gamma_c = \alpha_2 \Omega_L \bar{\gamma}_s / L).$$
 (2.60)

Finally, the average BER of the THCL employing the TEGC-DRP can be obtained by substituting (2.56) or (2.57) or (2.58), and (2.59), (2.60) into (2.43) or (2.45).

2.4.2 Bit Error Rate Analysis of Two-Hop Communication Links with Ideal Cooperative Relay Processing

In this section, we analyze the error probability of the THCL systems with ideal cooperative RP. As in Section 2.4.1, we assume that the first and second hops experience the flat Nakagami-m fading. As mentioned before, when the ideal cooperative RP is assumed, information exchange among the L relays do not consume power. Therefore, we have the power allocation $\alpha_1 + \alpha_2 = 1$. As discussed in Section 2.3.2, we classify the ideal cooperative RP into four sub-types: (a) ICMRC-TMRC-RP, (b) ICMRC-TEGC-RP, (c) ICMVC-TMRC-RP, (d) ICMVC-TEGC-RP. In this section, we drive the closed-form average BER expressions for the THCL systems employing these four RP schemes.

When the ideal cooperative RP scheme is considered, as shown in Section 2.3.2, the bits transmitted by the L relays to the destination are the same bit detected by the IECU. The average BER of the THCL systems using the ideal cooperative RP scheme can be written as

$$P_b^{(\text{THCL-ICRP})} = P_b^{(\text{IECU})} \left(1 - P_b^{(\text{R-D})} \right) + \left(1 - P_b^{(\text{IECU})} \right) P_b^{(\text{R-D})}. \tag{2.61}$$

In (2.61), the first (second) term at the right hand side denotes the probability that the detection at the IECU is incorrect (correct), while the detection at the destination is correct (incorrect).

The received signals by the IECU can be expressed as $y_{cu} = y_r$, where y_r is given in (2.2). When the IECU emoploys the ICMRC, the decision variable z_{cu} was given in (2.12), as the IECU perfectly knows the signals received by the relays. Therefore, the instantaneous SNR of the IECU was expressed as (2.13). According to [181], it can be shown that, when communicating over Nakagami-m fading channels, the average BER of the IECU detection can be expressed as

$$P_b^{(\text{IECU})} = \frac{1}{\pi} \int_0^{\pi/2} \prod_{i=1}^L \left(\frac{m_{sr_i} \sin^2 \theta}{\alpha_1 \Omega_{sr_i} \bar{\gamma}_s + m_{sr_i} \sin^2 \theta} \right)^{m_{sr_i}} d\theta$$
 (2.62)

if the IECU employs the ICMRC. In (2.62), m_{sr_i} is the fading parameter of the channel from the source to the *i*th relay. In (2.62), if $m_{sr_i} = m$, i = 1, ..., L, we can have

$$P_b^{(\text{IECU})} = \sqrt{\frac{\alpha_1 \Omega_{sr_i} \bar{\gamma}_s}{\alpha_1 \Omega_{sr_i} \bar{\gamma}_s + m}} \frac{(1 + \alpha_1 \Omega_{sr_i} \bar{\gamma}_s / m)^{-mL} \Gamma(mL + 1/2)}{2\sqrt{\pi} \Gamma(mL + 1)} \times {}_{2}F_{1}\left(1, mL + 1/2; mL + 1; \frac{m}{m + \alpha_1 \Omega_{sr_i} \bar{\gamma}_s}\right). \tag{2.63}$$

Furthermore, when mL is a positive integer, (2.63) can be reduced to

$$P_b^{\text{(IECU)}} = \left[\frac{1-\mu}{2}\right]^{mL} \sum_{v=0}^{mL-1} {mL-1+v \choose v} \left[\frac{1+\mu}{2}\right]^v$$
 (2.64)

where
$$\mu = \sqrt{\alpha_1 \Omega_{sr_i} \bar{\gamma}_s / (\alpha_1 \Omega_{sr_i} \bar{\gamma}_s + m)}$$
.

By contrast, in the context of the ICMVC employed by the IECU, the relays first decode the signals received from the source. The IECU is assumed to have perfect knowledge about the detected symbols by the relays and uses the MVC to make a decision of the symbol transmitted by the source. The average BER of the detection at the ith relay is $P_b^{(S-R_i)}$, $i=1,2,\ldots,L$, when communicating over Nakagami-m fading channels, which is given in (2.44). Therefore, the average BER measured at the IECU after the CMVC can be expressed as

$$P_b^{(\text{IECU})} = \sum_{l=0}^{\lceil \frac{L}{2} \rceil - 1} \sum_{k=0}^{\binom{L}{l} - 1} \left[\prod_{i \in {}_{l} \{1, \dots, L\}} (1 - P_b^{(\text{S-R}_i)}) \prod_{j \in {}_{q} \{1, \dots, L\}} P_b^{(\text{S-R}_j)} \right]^{(k)}$$
(2.65)

when $\lceil \frac{L}{2} \rceil \neq \frac{L}{2}$, where $\lceil A \rceil$ means that rounding A to a nearest integer greater than or equal to A. However, if $\lceil \frac{L}{2} \rceil = \frac{L}{2}$, we have

$$P_{b}^{(\text{IECU})} = \sum_{l=0}^{\lceil \frac{L}{2} \rceil - 1} \sum_{k=0}^{\binom{L}{l} - 1} \left[\prod_{i \in I\{1, \dots, L\}} (1 - P_{b}^{(\text{S-R}_{i})}) \prod_{j \in q\{1, \dots, L\}} P_{b}^{(\text{S-R}_{j})} \right]^{(k)} + \frac{1}{2} \sum_{k=0}^{\binom{L}{L/2} - 1} \left[\prod_{i \in L/2\{1, \dots, L\}} (1 - P_{b}^{(\text{S-R}_{i})}) \prod_{j \in L/2\{1, \dots, L\}} P_{b}^{(\text{S-R}_{j})} \right]^{(k)}.$$
(2.66)

Let the symbol detected by the IECU be expressed as \hat{x} . Then all the relays know \hat{x} , as the transmission from IECU to relays is assumed ideal. Then, \hat{x} is transmitted from the relays to the destination with the aid of either the TMRC or TEGC, which is described in (2.4) or (2.8). In (2.61), $P_b^{(\text{R-D})}$ is the average BER of the R-D transmission. Specifically, when the TMRC is employed, the average BER of the R-D transmission can be expressed as

$$P_b^{(\text{R-D})} = \frac{1}{\pi} \int_0^{\pi/2} \prod_{i=1}^L \left(\frac{m_{r_i d} \sin^2 \theta}{\alpha_2 \Omega_{r_i d} \bar{\gamma}_s + m_{r_i d} \sin^2 \theta} \right)^{m_{r_i d}} d\theta$$
 (2.67)

where m_{r_id} and $\Omega_{r_id} = E[|h_{r_id}|^2]$, i = 1, ..., L, are the parameters for the Nakagami-m fading of the ith R-D channel. Hence, by substituting (2.62) and (2.67) into (2.61), the overall average BER of the THCL system employing the ICMRC-TMRC-RP can be expressed as

$$P_{b}^{(\text{THCL-ICRP})} = \frac{1}{\pi} \int_{0}^{\pi/2} \prod_{i=1}^{L} \left(\frac{m_{sr_{i}} \sin^{2} \theta}{\alpha_{1} \Omega_{sr_{i}} \bar{\gamma}_{s} + m_{sr_{i}} \sin^{2} \theta} \right)^{m_{sr_{i}}} d\theta$$

$$+ \frac{1}{\pi} \int_{0}^{\pi/2} \prod_{i=1}^{L} \left(\frac{m_{r_{i}d} \sin^{2} \theta}{\alpha_{2} \Omega_{r_{i}d} \bar{\gamma}_{s} + m_{r_{i}d} \sin^{2} \theta} \right)^{m_{r_{i}d}} d\theta$$

$$- \frac{2}{\pi^{2}} \int_{0}^{\pi/2} \prod_{i=1}^{L} \left(\frac{m_{r_{i}d} \sin^{2} \theta}{\alpha_{2} \Omega_{r_{i}d} \bar{\gamma}_{s} + m_{r_{i}d} \sin^{2} \theta} \right)^{m_{r_{i}d}} d\theta$$

$$\times \int_{0}^{\pi/2} \prod_{i=1}^{L} \left(\frac{m_{sr_{i}} \sin^{2} \theta}{\alpha_{1} \Omega_{sr_{i}} \bar{\gamma}_{s} + m_{sr_{i}} \sin^{2} \theta} \right)^{m_{sr_{i}}} d\theta. \tag{2.68}$$

By contrast, when the relays employ TEGC, the instantaneous SNR at the destination is $\gamma_d = \alpha_2 \bar{\gamma}_s \left(\sum_{i=1}^L |h_{r_id}|\right)^2$, where $|h_{r_id}|$ obeys the Nakagami-m distribution. Then, when the Nakagami-SAp or Nakagami-TAp, as discussed in Section 2.4.1, is employed, the average BER of the R-D transmission can be expressed as

$$P_{b}^{(\text{R-D})} = \sqrt{\frac{\bar{\gamma}_{r_{i}}}{\alpha_{2}\Omega_{sL}\bar{\gamma}_{s} + m_{sL}}} \frac{(1 + \alpha_{2}\Omega_{sL}\bar{\gamma}_{s}/m_{sL})^{-m_{sL}}\Gamma(m_{sL} + 1/2)}{2\sqrt{\pi}\Gamma(m_{sL} + 1)} \times {}_{2}F_{1}\left(1, m_{sL} + 1/2; m_{sL} + 1; \frac{m_{sL}}{m_{sL} + \alpha_{2}\Omega_{sL}\bar{\gamma}_{s}}\right)$$
(2.69)

where m_{sL} and Ω_{sL} can be derived by the Nakagami-SAp or Nakagami-TAp. Consequently, when applying (2.69) into (2.61), we obtain the average BER of the THCL system with the ICMRC-TEGC-RP, which can be expressed as

$$P_{b}^{(\text{THCL-ICRP})} = \frac{1}{\pi} \int_{0}^{\pi/2} \prod_{i=1}^{L} \left(\frac{m_{sr_{i}} \sin^{2} \theta}{\alpha_{1} \Omega_{sr_{i}} \bar{\gamma}_{s} + m_{sr_{i}} \sin^{2} \theta} \right)^{m_{sr_{i}}} d\theta$$

$$+ \sqrt{\frac{\alpha_{2} \Omega_{sL} \bar{\gamma}_{s}}{\alpha_{2} \Omega_{sL} \bar{\gamma}_{s} + m_{sL}}} \frac{(1 + \alpha_{2} \Omega_{sL} \bar{\gamma}_{s} / m_{sL})^{-m_{sL}} \Gamma(m_{sL} + 1/2)}{2\sqrt{\pi} \Gamma(m_{sL} + 1)}$$

$$\times {}_{2}F_{1} \left(1, m_{sL} + 1/2; m_{sL} + 1; \frac{m_{sL}}{m_{sL} + \alpha_{2} \Omega_{sL} \bar{\gamma}_{s}} \right)$$

$$- \sqrt{\frac{\alpha_{2} \Omega_{sL} \bar{\gamma}_{s}}{\alpha_{2} \Omega_{sL} \bar{\gamma}_{s} + m_{sL}}} \frac{(1 + \alpha_{2} \Omega_{sL} \bar{\gamma}_{s} / m_{sL})^{-m_{sL}} \Gamma(m_{sL} + 1/2)}{\pi \sqrt{\pi} \Gamma(m_{sL} + 1)}$$

$$\times {}_{2}F_{1} \left(1, m_{sL} + 1/2; m_{sL} + 1; \frac{m_{sL}}{m_{sL} + \alpha_{2} \Omega_{sL} \bar{\gamma}_{s}} \right)$$

$$\times \int_{0}^{\pi/2} \prod_{i=1}^{L} \left(\frac{m_{sr_{i}} \sin^{2} \theta}{\alpha_{1} \Omega_{sr_{i}} \bar{\gamma}_{s} + m_{sr_{i}} \sin^{2} \theta} \right)^{m_{sr_{i}}} d\theta.$$

$$(2.70)$$

Similarly, when the THCL employing the ICMVC-TMRC-RP, the average BER of the system is obtained by substituting (2.67), (2.65) or (2.66) into (2.61). Furthermore, the average BER of the system employing the ICMVC-TEGC-RP can be derived by substituting (2.69), (2.65) or (2.66) into (2.61).

2.4.3 Bit Error Rate Analysis of Two-Hop Communication Link with Cooperative Relay Processing

In this section, we analyze the average BER of the THCL employing the cooperative RP schemes. In this context, we assume that the total energy for conveying one bit from the source to the destination is one unit. Then, we have $\alpha_1 + \alpha_r + \alpha_2 = 1$, where α_1 , α_2 and α_r denote respectively the transmit power for the first hop, the second hop and the information exchange among the relays. Furthermore, as information exchange includes both the MA and BC transmission, whose transmit power is assumed to be α_{ma} and α_{bc} . Hence, we also have $\alpha_{ma} + \alpha_{bc} = \alpha_r$. Additionally, we assume that the MA transmission for information exchange among RNs is implemented in the principles of DS-CDMA, which, for the sake of simplicity, employs orthogonal spreading codes.

In general, when the THCL employs the cooperative RP, the average BER of the THCL system can be written as

$$P_b^{(\text{THCL-CRP})} = P_b^{(\text{IECU})} \left(1 - P_b^{(\text{IECU-D})} \right) + \left(1 - P_b^{(\text{IECU})} \right) P_b^{(\text{IECU-D})} \tag{2.71}$$

where $P_b^{(\mathrm{IECU})}$ is the average BER measured at the IECU, and $P_b^{(\mathrm{IECU}-\mathrm{D})}$ is the average BER of the transmissions from the IECU to the relays and finally, to the destination.

Let us first consider the BER at the IECU. When the IECU employs the MRC on its received signals, the decision variable z_{cu} can be expressed in (2.19), and the instantaneous SNR of the IECU after carrying out the CMRC can be expressed as

$$\gamma_{cu} = \frac{\mathrm{E}^{2}[z_{cu}]}{\mathrm{Var}[z_{cu}]}
= \frac{\alpha_{1}\alpha_{ma}}{L} \frac{(\boldsymbol{h}_{T}^{H}\boldsymbol{h}_{T})^{2}}{\frac{\alpha_{ma}}{L} \sum_{i=1}^{L} |h_{D_{i}}|^{2} + \sum_{i=1}^{N} |h_{T_{i}}|^{2}} \bar{\gamma}_{s}$$
(2.72)

when we used the definitions that $H_D = [h_{D_1}, h_{D_2}, \dots, h_{D_L}] = H_T^H H_{ma} G_r$ and $H_T = H_{ma} G_r h_{sr}$, where $G_r = \text{diag}\{g_1, g_2, \dots, g_L\}$ and $g_i = \frac{1}{\sqrt{|h_{sr_i}|^2 + 1/\bar{\gamma}_s}}$. Based on (2.72), it is very difficult to derive the PDF of γ_{cu} . In this case, we are unable to derive the exact average BER of $P_b^{\text{(IECU)}}$. In this chapter, we propose the Gamma-Approximation (Gamma-Ap) to evaluate the PDF of γ_{cu} , which will be verified by our simulation results and found in general very accurate.

Note that, in performance analysis, the Gaussian-Ap is typically employed. However, for some scenarios, such as for the PDF of (2.72), where the concerned variables are always positive, the Gamma-Ap has the advantages over the Gaussian-Ap. First, the Gamma distribution [180], which can be obtained by the square of a Nakagami-m distributed variable, is defined in $[0,\infty)$, while the Gaussian distribution is defined in $(-\infty,\infty)$. Second, for applying the Gaussian-Ap, usually a high number of component variables is required, so that their sum yields a symmetric distribution. By contrast, the Gamma-Ap does not impose this constraint, and can be applied for the sum of any number of component variables. Furthermore, as the number of components increases, the resultant Gamma-distribution appears the Gaussian-like shape, but, in the range $[0,\infty)$. Hence, the Gamma-Ap (also including the Nakagami-approximation, as they belong to the same family) represents a versatile approximation approach, which may find applications for a lot of problems in practice, including a lot of performance analysis problems in wireless communications.

Specifically, for the current case, let us rewrite (2.72) as

$$\gamma_{cu} = \frac{\alpha_1 \alpha_{ma} \bar{\gamma}_s}{L} \zeta_{cu} \tag{2.73}$$

where

$$\zeta_{cu} = \frac{(\boldsymbol{h}_{T}^{H}\boldsymbol{h}_{T})^{2}}{\frac{\alpha_{ma}}{L}\sum_{i=1}^{L}|h_{D_{i}}|^{2} + \sum_{j=1}^{N}|h_{T_{j}}|^{2}}.$$
(2.74)

L	$\bar{\gamma}_s(\mathrm{dB})$	m_{sr}	m_{ma}	m_{cu}	Ω_{cu}
	1	1.0	1.0	2.573	18.121
	4	2.0	3.0	7.347	27.007
4	9	1.0	4.0	5.332	29.775
	14	3.0	1.5	7.730	33.445
	20	2.5	1.5	6.401	33.150
	3	1.5	1.0	4.872	37.363
	7	1.0	1.0	4.506	43.158
6	13	3.0	3.0	13.320	64.612
	18	1.0	4.0	5.189	49.028
	22	1.5	3.0	6.199	55.084

Table 2.3: Parameters for the Gamma PDF $f_{\zeta_{cu}}(\zeta)$ obtained based on simulations.

With the aid of the Gamma-Ap, we can approximate ζ_{cu} as a Gamma distributed random variable with the PDF [180]

$$f_{\zeta_{cu}}(y) = \left(\frac{m_{cu}}{\Omega_{cu}}\right)^{m_{cu}} \frac{y^{m_{cu}-1}}{\Gamma(m_{cu})} \exp\left(-\frac{m_{cu}y}{\Omega_{cu}}\right)$$
(2.75)

where
$$\Omega_{cu} = E[\zeta_{cu}]$$
, and $m_{cu} = \Omega_{cu}^2 / E[(\zeta_{cu} - \Omega_{cu})^2]$.

From (2.74), we can see that the parameters m_{cu} and Ω_{cu} determining the PDF of ζ_{cu} depend on the average SNR $\bar{\gamma}_s$ of the S-R channels through the matrix G_r in h_D , the fading of the L S-R channels, the fading of the MA channels and the spreading factor N_t of the DS-CDMA signalling. Hence, it is usually extremely hard (if it is not impossible) derive the parameters m_{cu} and Ω_{cu} by mathematical analysis. However, they can be readily found by simulations based on about 10^4 realizations. For instance, in Table 2.3, a range of cases are considered, where the spreading factor N_t is 16, the L S-R channels experience the same Nakagami-m fading with the parameters m_{sr} and $\Omega_{sr} = 1$, and the MA channels also experience the same Nakagami-m fading with the parameters m_{ma} and $\Omega_{ma} = 1$. As our results in this section show, the Gamma-Ap in general yields very accurate approximation.

Figures 2.6- 2.9 show the approximated PDFs of ζ_{cu} when first hop and the MA links experience various of fading conditions, in comparison with the corresponding accurate PDFs of ζ_{cu} , which are labelled as "simu.", which were obtained by using 10^6 realizations of ζ_{cu} . In Figures 2.6 and 2.7, we observe that the approximated PDFs have deviations from the accurate ones at the top part of the curves, when the average SNR $\bar{\gamma}_s$ equals to 1 dB and 20 dB. However, we see that the deviations become smaller as the number of relays increases. Furthermore, we find that the approximated PDFs agree well with the accurate PDFs, when $\bar{\gamma}_s = 10$ dB. According to our simulation results, we can deduce that the approximated PDFs have a very good similarity as the accurate PDFs within the the average SNR region of 8-12 dB.

In Figures 2.8 and 2.9, we give the PDF $f_{\gamma_{cu}}(y)$ plots when the average SNR is fixed at 20 dB.

Both plots show that a deviation always presents between the approximated PDF and the accurate one at top part of the curves. However, from Figure 2.8, it knows that the difference at the top of the curves increases, when the fading of MA links become less severe while the fading of S-R links stay constant. By contrast, in Figure 2.9, we observe that the similarity between the approximated PDF and the accurate one increases, as the first hop has a better channel fading condition.

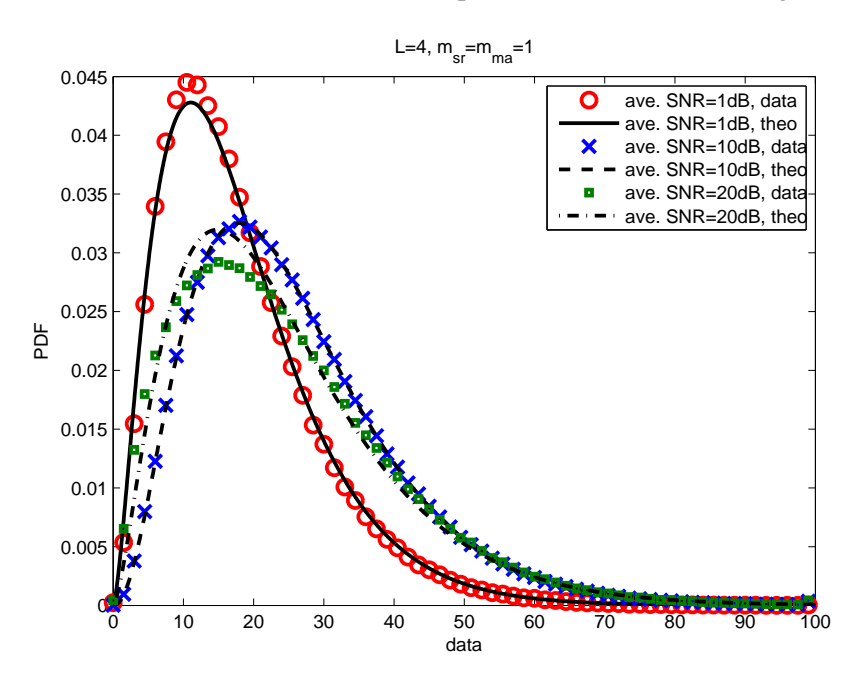


Figure 2.6: Approximated PDFs of the decision variable of the IECU, when the CMRC is employed, and when the S-R links and the MA links in the cooperative RP scenario experience Rayleigh fading.

With the aid of the Gamma-Ap for finding the PDF of ζ_{cu} , which is (2.75), we can now easily obtain the average BER of the detection at the IECU, which can be expressed as

$$P_b^{\text{(IECU)}} = P_b \left(m = m_{cu}, \gamma_c = \alpha_1 \alpha_{ma} \Omega_{cu} \bar{\gamma}_s / L \right). \tag{2.76}$$

In (2.71), $P_b^{(\mathrm{IECU-D})}$ is the average BER of the transmission from the IECU to the relays and, finally, to the destination. Note that, as we mentioned in Section 2.3.1, it is hard to derive the BER of the R-D transmissions, when the relays use the TMRC. Hence, below we only consider the case that the relays employ the TEGC. Therefore, when the relays employs the TEGC, the average BER of the transmission from the IECU to the relays can be expressed as

$$P_{b}^{(\text{IECU-D})} = \sum_{l=0}^{L} \sum_{k=0}^{\binom{L}{l}-1} \left[\prod_{i \in l \{1,\dots,L\}} (1 - P_{b}^{(\text{IECU-R}_{i})}) \prod_{j \in q \{1,\dots,L\}} P_{b}^{(\text{IECU-R}_{j})} \right]^{(k)} \times P_{b}^{(\text{TEGC})}(l)$$
(2.77)

where $P_b^{(\mathrm{IECU-R}_i)}$ denotes the average BER of the BC link from the IECU to the ith relay, $P_b^{(\mathrm{TEGC})}(l)$ is the average BER of the R-D transmission, when l relays correctly detect the symbol transmitted by the IECU, while the other q(=L-l) relays make erroneous detection. As the analysis

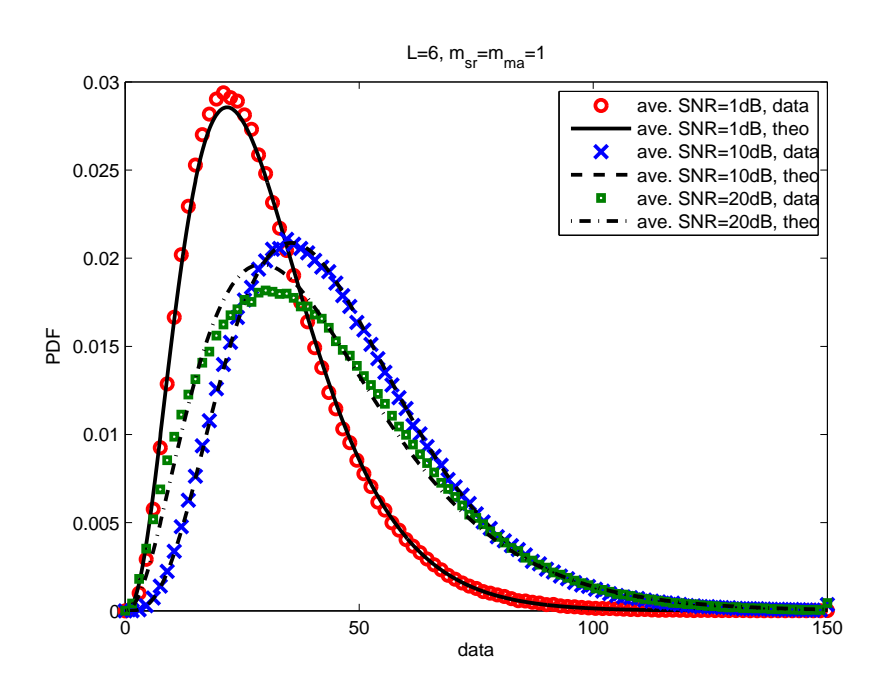


Figure 2.7: Approximated PDFs of the decision variable of the IECU, when the CMRC is employed, and when the S-R links and the MA links in the cooperative RP scenario experience Rayleigh fading.

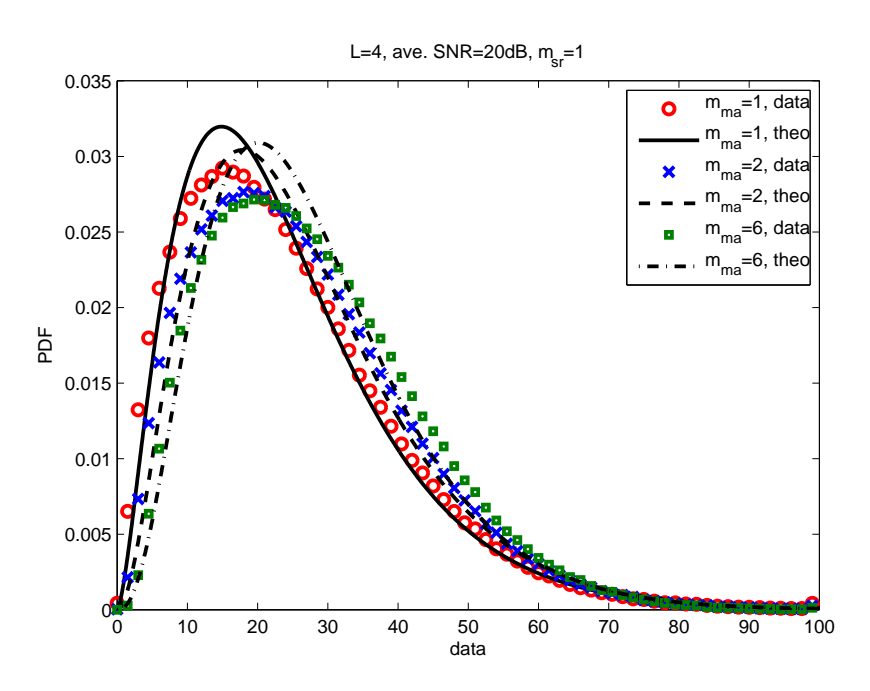


Figure 2.8: Approximated PDFs of the decision variable formed by the IECU, when the CMRC associated with L=4 relays is employed by the cooperative RP.

in Section 2.4.1 shows, when the channels between the L relays and the destination experience Nakagami-m fading, $P_b^{({\rm TEGC})}(l)$ can be evaluated by (2.56)-(2.60). When the BC channels experience flat Nakagami-m fading, we have $P_b^{({\rm IECU-R}_i)} = P_b(m = m_{bc_i}, \gamma_c = \alpha_{bc}\beta_2\Omega_{bc_i}\bar{\gamma}_s)$, where the parameters have been defined in Section 2.3.3.1. By contrast, when the BC channels are AWGN,

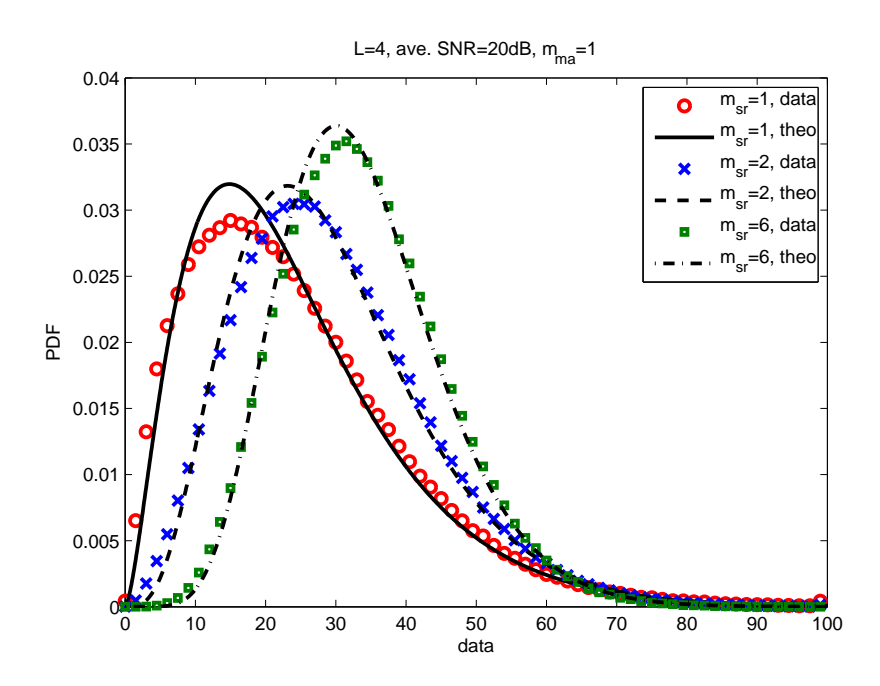


Figure 2.9: Approximated PDFs of the decision variable formed by the IECU, when the CMRC associated with L=4 relays is employed by the cooperative RP.

we have
$$P_b^{(\text{IECU-R}_i)} = Q\left(\sqrt{2\alpha_{bc}\beta_2\bar{\gamma}_s}\right)$$
.

Finally, the average BER of the THCL employing the CMRC-TEGC-RP can be evaluated by (2.71) associated with (2.76) and (2.77).

When the THCL employs the CMVC-TEGC-RP, the average BER of the system can also be expressed as (2.71), where the average BER measured at the IECU can be written as

$$P_b^{(\text{IECU})} = P_b^{(\text{IECU})}|_{P_b^{(\text{S-R}_i)} = P_b^{(\text{S-R}_i - \text{IECU})}}$$
(2.78)

with $P_b^{(\mathrm{IECU})}$ at the left-side of the equation denoting the BER at the IECU, when the ICMVC is employed, which is given in (2.65) and (2.66). In (2.78), $P_b^{(\mathrm{S-R}_i\mathrm{-IECU})}$ represents the average BER of the signals transmitted from the source to the ith ($i=1,\ldots,L$) relay and then to the IECU, which can be expressed as

$$P_b^{(S-R_i-IECU)} = P_b^{(S-R_i)} (1 - P_b^{(R_i-IECU)}) + (1 - P_b^{(S-R_i)}) P_b^{(R_i-IECU)}$$
(2.79)

where $P_b^{(R_i\text{-IECU})}$ is the average BER of the link from the *i*th Relay to the IECU, which is

$$P_b^{(R_i\text{-IECU})} = P_b(m = m_{ma_i}, \gamma_c = \alpha_{ma}\beta_1\Omega_{ma_i}\bar{\gamma}_s/L)$$
 (2.80)

with $P_b(m, \gamma_c)$ was defined in (2.39).

Specifically, when the MA links are assumed the AWGN channels, the BER of the R_i-IECU links is $P_b^{(R_i\text{-IECU})} = Q\left(\sqrt{2\alpha_{ma}\beta_1\bar{\gamma}_s/L}\right)$. In this case, (2.79) can be expressed as

$$P_b^{(\text{S-R}_i\text{-IECU})} = P_b^{(r_i)} \left(1 - Q \left(\sqrt{2\alpha_{ma}\beta_1 \bar{\gamma}_s/L} \right) \right) + \left(1 - P_b^{(r_i)} \right) Q \left(\sqrt{2\alpha_{ma}\beta_1 \bar{\gamma}_s/L} \right). \quad (2.81)$$

Finally, the average BER of the THCL employing the CMVC-TEGC-RP can be obtained by substituting (2.78) and (2.77) into (2.71).

2.5 Bit Error Rate Performance Results

In this section, we demonstrate a range of performance results for characterizing the achievable performance of the THCL systems with the various RP schemes as considered. Both numerical results evaluated from the formulas derived in the previous sections and simulation results are provided. Note that, for obtaining the results, we assume that all channels of the first and second hops experience independent but identical Nakagami-m fading. The MA/BC channels are either Gaussian channels or iid Nakagami-m fading channels. When the cooperative RP is employed, we assume that the parameters β_1 and β_2 take a value of 10, which results in that the average SNR of the MA/BC channels is typically 10 dB higher than that of the S-R and R-D channels, when equal power of 1/3 is allocated respectively to the S-R, MA/BC and R-D transmissions. Furthermore, when the DS-CDMA is used for the MA transmission, the spreading codes are assumed to be the random sequences with a spreading factor $N_t = 16$.

First, let us compare the BER performance of the THCL systems employing various RP schemes. Both analytical results and simulation results are demonstrated, so as to verify the accuracy of our analytical BER results.

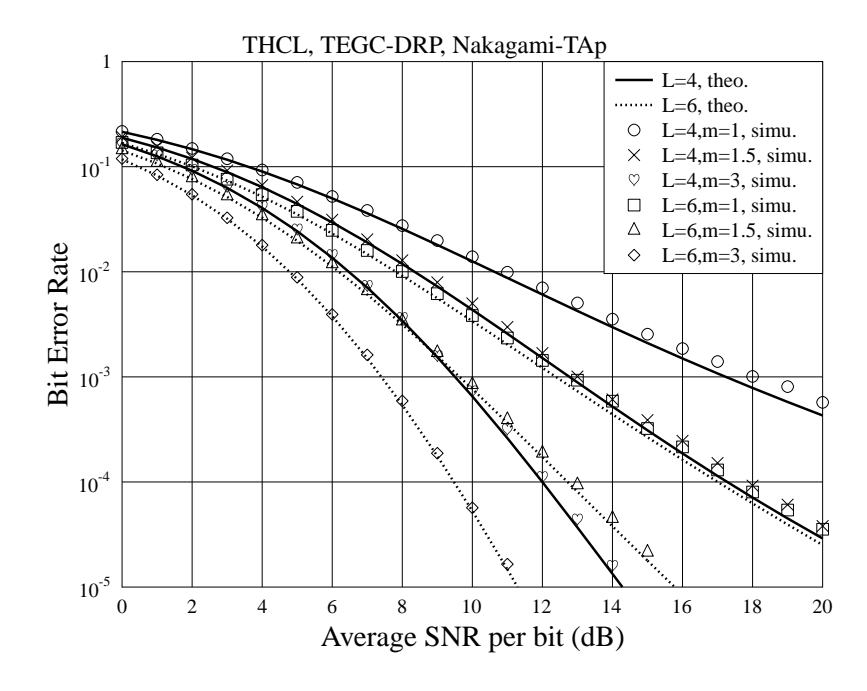


Figure 2.10: BER of the TEGC-DRP assisted THCL employing BPSK baseband modulation and power allocation factors $\alpha_1 = \alpha_2 = 0.5$, when communicating over iid Nakagami-m fading channels.

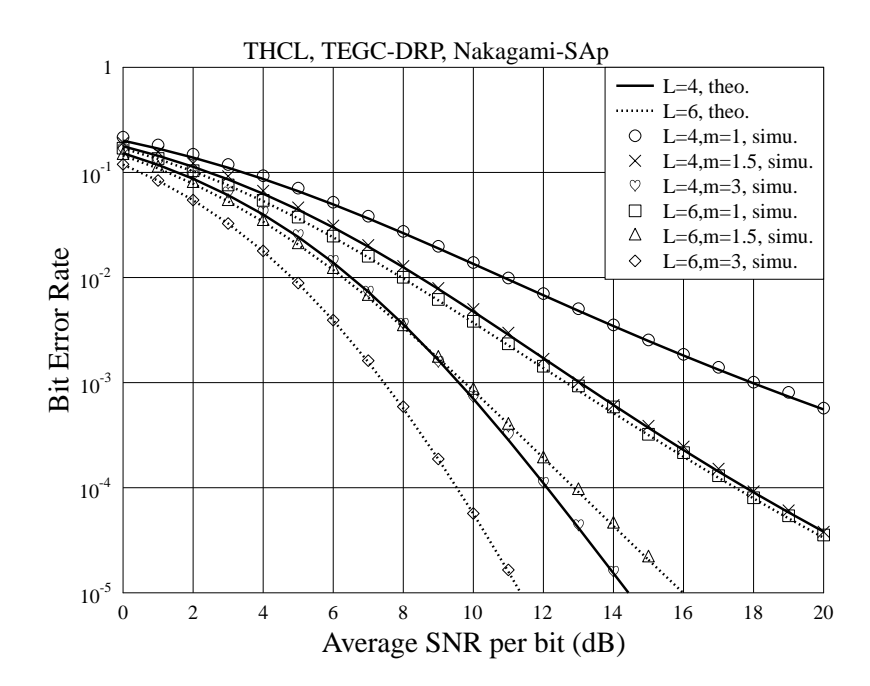


Figure 2.11: BER of the TEGC-DRP assisted THCL employing BPSK baseband modulation and power allocation factors $\alpha_1 = \alpha_2 = 0.5$, when communicating over iid Nakagami-m fading channels.

In Figures 2.10 and 2.11, we compare the approximate BER of the TEGC-DRP assisted THCL with the corresponding BER obtained by simulations. Furthermore, Figures 2.10 and 2.11 illustrate the impacts of the number of relays and the fading parameter m on the achievable BER performance. Note that, the approximate BER was evaluated based on (2.45), when either the Nakagami-TAp or the Nakagami-SAp was employed. From Figure 2.10, we can observe that there is a slight deviation between the approximate BER and the simulated BER, when the Nakagami-TAp is applied. However, the difference becomes smaller as the Nakagami-m fading becomes less severe, i.e., as m increases. The difference also becomes smaller, as the number of relays increases. Nevertheless, for all the scenarios considered, the analytical BER and simulated BER are close to each other. When the Nakagami-SAp is employed, as shown in Figure 2.11, the analytical BER and the simulated BER always agree with each other. Therefore, we are confident that both the Nakagami-TAp and Nakagami-SAp are highly effective, while the Nakagami-SAp is more accurate than the Nakagami-TAp.

Additionally, as shown in Figures 2.10 and 2.11, the BER performance improves as the fading becomes less severe. It also improves as the number of relays increases, owing to the increased spatial diversity.

The BER performance of the ICRP-assisted THCL is shown in Figure 2.12, when assuming that both the S-R and R-D channels experience iid Nakagami-*m* fading. The BER results demonstrated in the figure were evaluated based on the Nakagami-TAp in the context of the ICMRC-TEGC-RP

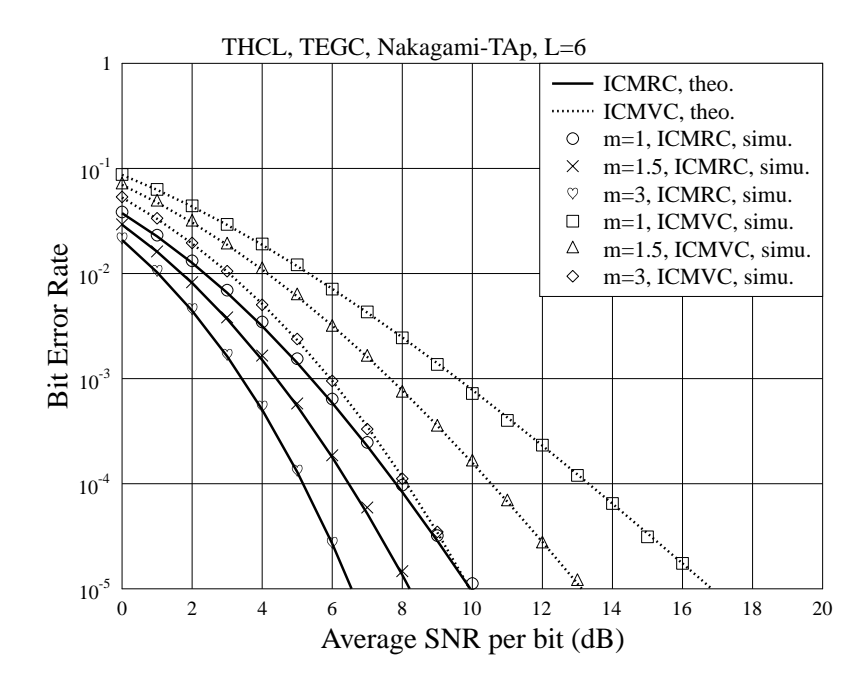


Figure 2.12: BER of the ICMRC-TEGC-RP and ICMVC-TEGC-RP assisted THCL employing BPSK baseband modulation and power allocation factors $\alpha_1 = \alpha_2 = 0.5$, when using L = 6 relays and communicating over iid Nakagami-m fading channels.

or ICMVC-TEGC-RP. Again, from the results of Figure 2.12, we can observe that the approximate BER of all the considered cases closely matches the corresponding BER obtained by simulations. Explicitly, the ICMRC-TEGC-RP always outperforms the ICMVC-TEGC-RP, although the difference becomes smaller as the channel fading becomes less severe.

Figure 2.13 gives the BER performance of the ICRP-TMRC assisted THCL systems, when assuming that both the S-R and R-D channels experience iid Nakagami-*m* fading. We can see that the analytical BER of all cases are nearly the same as the corresponding BER obtained by simulations. As we discussed in Section 2.4.2, the closed-form BER expressions of the ICRP-TMRC assisted THCL systems are given in (2.68) and (2.65). By comparing Figure 2.12 with Figure 2.13, we can observe that the TMRC aided systems have slight better BER performance than the TEGC assisted systems.

Furthermore, in comparison with the BER results shown in Figure 2.10 and Figure 2.11, we can see that in Figure 2.13 remarkable SNR gain is observed, when the ideal cooperative RP is employed by the systems, instead of using the distributed RP. Note that, this performance gain achieved by the ideal cooperative RP is mainly due to the cooperative detection of the first hop, which generates the symbols having much higher reliability than that detected by the relays operated under the distributed RP. However, the ideal cooperative RP scheme assumes no energy consumption for the relays' cooperation, which is impractical.

When non-ideal cooperation is assumed, Figures 2.14 and 2.15 show the BER performance of

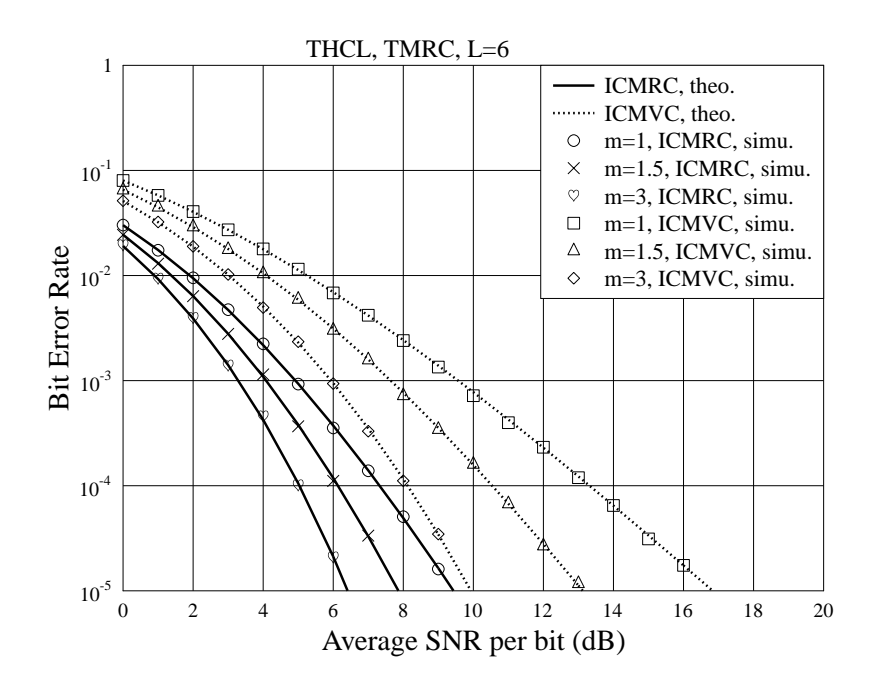


Figure 2.13: BER of the ICMRC-TEGC-RP and ICMVC-TEGC-RP assisted THCL employing BPSK baseband modulation and power allocation factors $\alpha_1 = \alpha_2 = 0.5$, when using L = 6 relays and communicating over iid Nakagami-m fading channels.

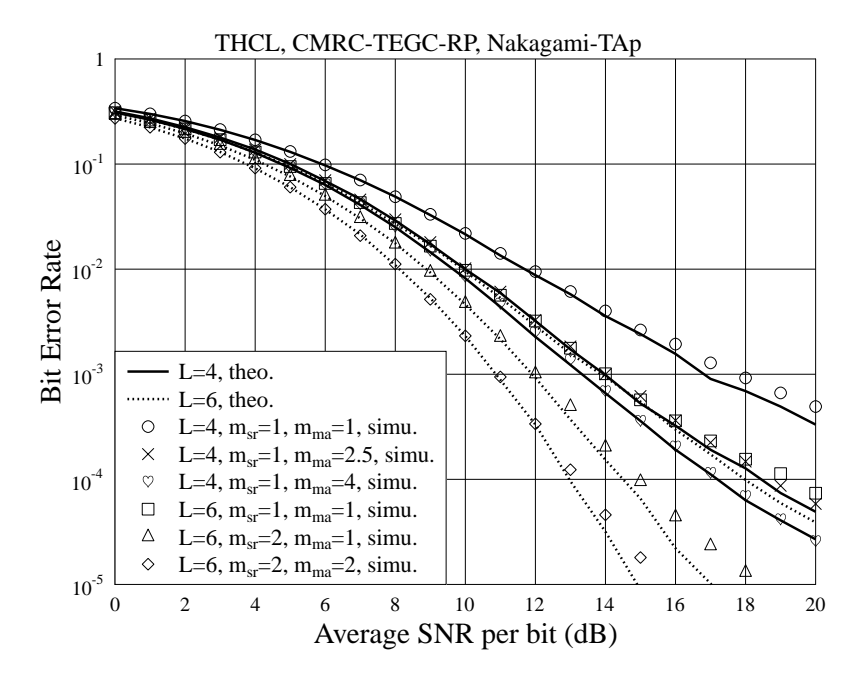


Figure 2.14: BER of the CMRC-TEGC-RP assisted THCL employing BPSK baseband modulation and power allocation factors $\alpha_1 = \alpha_2 = \alpha_r = 1/3$, when all the S-R and R-D channels are assumed iid Nakagami-m fading channels with a fading parameter m_{Sr} , while the MA/BC channels are assumed iid Nakagami-m fading channels with a fading parameter m_{ma} .

the cooperative RP assisted THCL, when 1/3 of the total transmission power is allocated for S-R, MA/BC and R-D transmissions, respectively. Let us first have a look of Figure 2.14, where the CMRC-TEGC-RP scheme was employed by the THCL, and the approximate BER was obtained based on the Gamma-Ap for the detection at the IECU and the Nakagami-TAp for the detection at the destination. From the figure, we can have the following observations. First, the approximate BER agrees with the corresponding BER obtained by simulations in the relatively low SNR region, but there appear some deviations in the high SNR region. Second, the approximate BER becomes more accurate, as the channel condition becomes less severe. Third, the approximate BER also becomes more accurate, as the first and/or second hops become more reliable. Additionally, when comparing the BER results shown in Figure 2.14 with that shown in Figure 2.12, we are implied that, due to the energy consumed for relays' cooperation, the achievable BER performance of the THCL using the cooperative RP scheme of practically reasonable is much worse than that of the THCL employing the ideal cooperative RP. Note that, as shown at the beginning of this section, the MA/BC channels are assumed more reliable than the S-R and R-D channels. This issues will be further discussed later associated with the other figures.

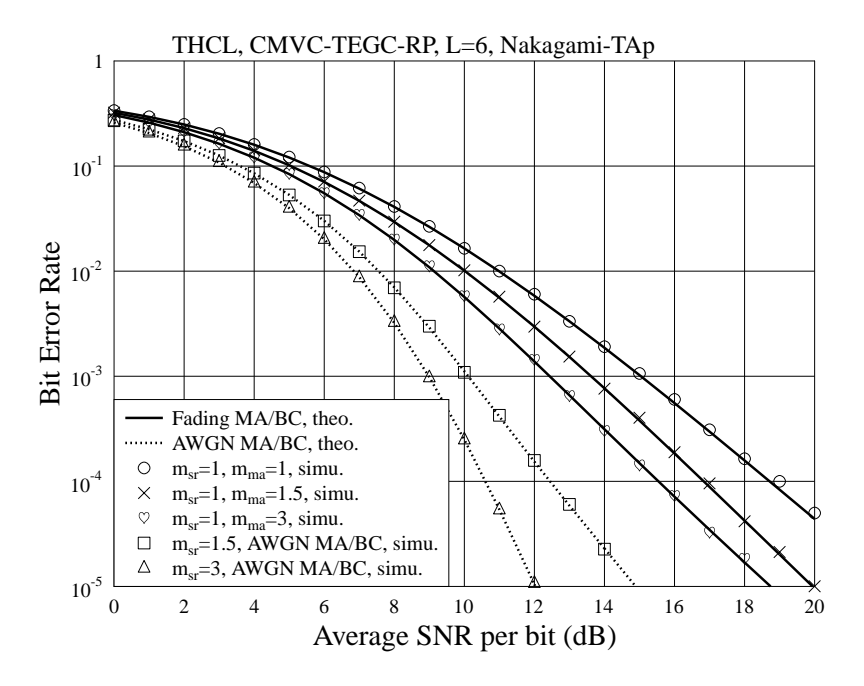


Figure 2.15: BER of the CMVC-TEGC-RP assisted THCL employing BPSK baseband modulation and power allocation factors $\alpha_1 = \alpha_2 = \alpha_r = 1/3$, when all the S-R and R-D channels are assumed iid Nakagami-m fading channels with a fading parameter m_{Sr} , while the MA/BC channels are assumed either iid Gaussian channels or iid Nakagami-m fading channels with a fading parameter m_{ma} .

In Figure 2.15, we investigate the BER performance of the CMVC-TEGC-RP assisted THCL, where, again, the analytical BER was obtained based on the Gamma-Ap for the detection at the IECU and the Nakagami-TAp for the detection at the destination. In addition, in Figure 2.15, we

considered the cases that the MA/BC channels are either Nakagami-*m* fading channels or AWGN channels. From the figure we observe that, for all the cases, the analytical BER agrees well with the simulated BER. The other observations are similar as that obtained from Figure 2.14.

Having verified the accuracy of our proposed approximation approaches, we investigate the effect of power-allocation on the BER performance of the THCL systems employing various RP schemes. When the distributed and the ideal cooperative RP schemes are used, we show the performance change, when different portions of power are respectively allocated to the first and second hops. When the cooperative RP is employed, we demonstrate the cost of energy for the cooperation among relays, as well as evaluate the BER performance of the THCL systems under different power-allocation.

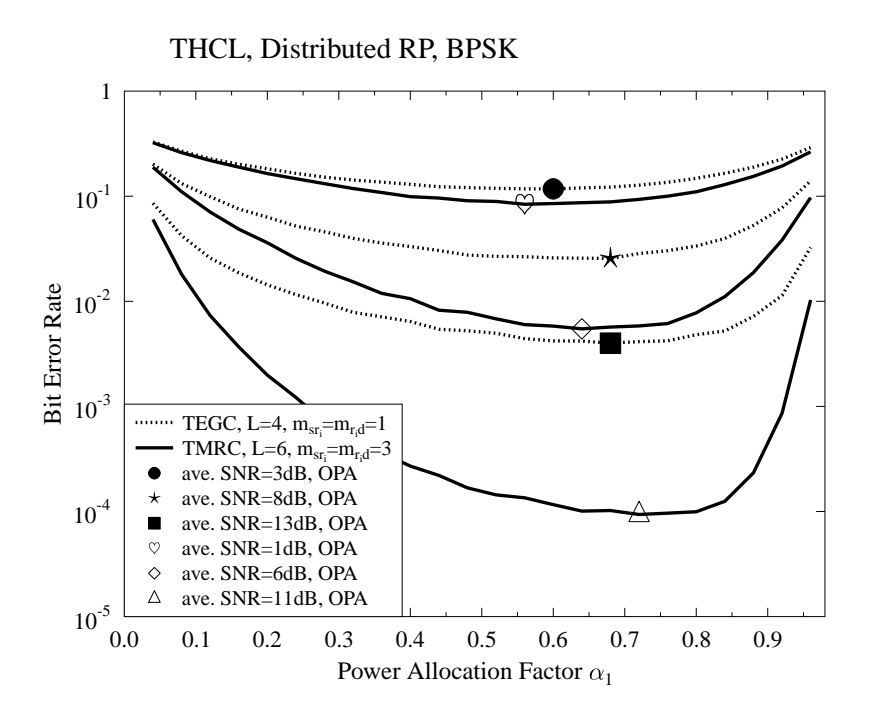


Figure 2.16: Effect of power-allocation factors on the BER performance of the distributed RP assisted THCL employing BPSK baseband modulation, when both the first and second hop channels experience flat iid Nakagami-*m* fading.

Figure 2.16 investigate the BER performance of the THCL system employing the distributed RP, when different transmit power is allocated to the first and second hops. For every case considered in the figure, there is an optimum power-allocation (OPA), which corresponds to the lowest BER achieved. From the figure, we observe that, in order to achieve the best BER performance, the first hop always demand higher power than the second hop does. The reason behind is that the DF relaying scheme used by the relays is highly dependent on the channel condition of the first hop. When the fading of the S-R channels becomes less severe, more reliable signals are forwarded to the destination and, hence, the error performance of the system improves. Furthermore, from the figure we also see that the first hop requires relatively more power to achieve the optimum power-allocation, when the average SNR or the number of the relays increases.

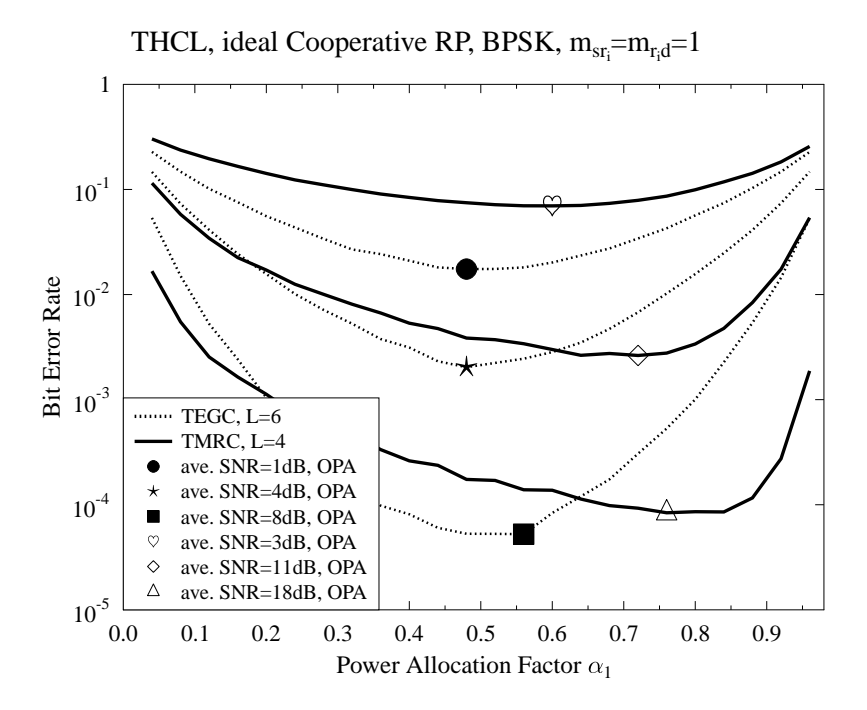


Figure 2.17: Effect of power-allocation factors on the BER performance of the ideal cooperative RP assisted THCL employing BPSK baseband modulation, when both the first and second hop channels experience flat iid Nakagami-*m* fading.

In Figure 2.17, we study the effect of power-allocation on the BER performance, when the system employs the ideal cooperative RP. As we know, there is no power required for the cooperation among relays, when the ideal cooperative RP is used. Similarly to the observations in Figure 2.16 for the distributed RP, more power is usually required by the first hop in order to obtain the OPA, when the average SNR increases. However, in contrast to the observations shown in Figure 2.16, the first hop requires less power for reaching the OPA, when the number of relays increases. This is because information exchange among the relays becomes more reliable, as the number of relays increases. Therefore, more power is required by the second hop, so that the error performance of the THCL system can be enhanced.

In Figures 2.18 and 2.19, we demonstrate the impact of power-allocation on the achievable BER performance of the THCL employing the CMRC-TEGC-RP, when both the S-R and the R-D links experience iid flat Rayleigh fading. For the MA/BC transmission, AWGN channels are assumed for Figure 2.18, while flat Rayleigh fading channels are assumed for Figure 2.19. In the figures, the OPA indicates the power-allocation and the corresponding lowest BER achievable. As seen in Figure 2.18 for the AWGN MA/BC scenario, the optimum power-allocation is $\alpha_1 = 0.44$, $\alpha_2 = 0.28$, $\alpha_r = 0.28$. Hence, the main portion of power is allocated to the first hop to improve the reliability of the first hop to a sufficient level.

By contrast, when the MA/BC channels are also Rayleigh fading channels, as seen in Figure 2.19, the power-allocation for the THCL system to achieve the best BER performance is

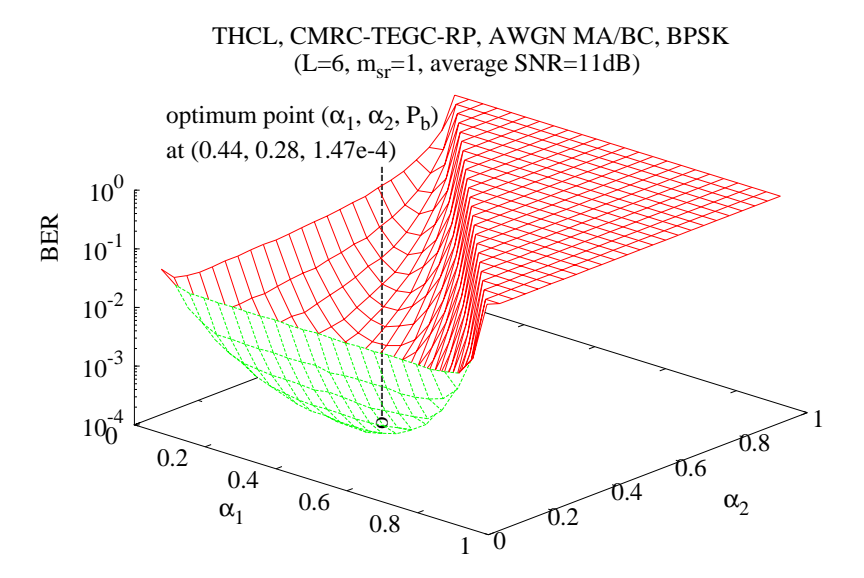


Figure 2.18: Effect of power-allocation factors on the BER performance of the CMRC-TEGC-RP assisted THCL employing BPSK baseband modulation, when both the first and second hop experience flat iid Rayleigh fading, while the MA/BC channels are AWGN channels.

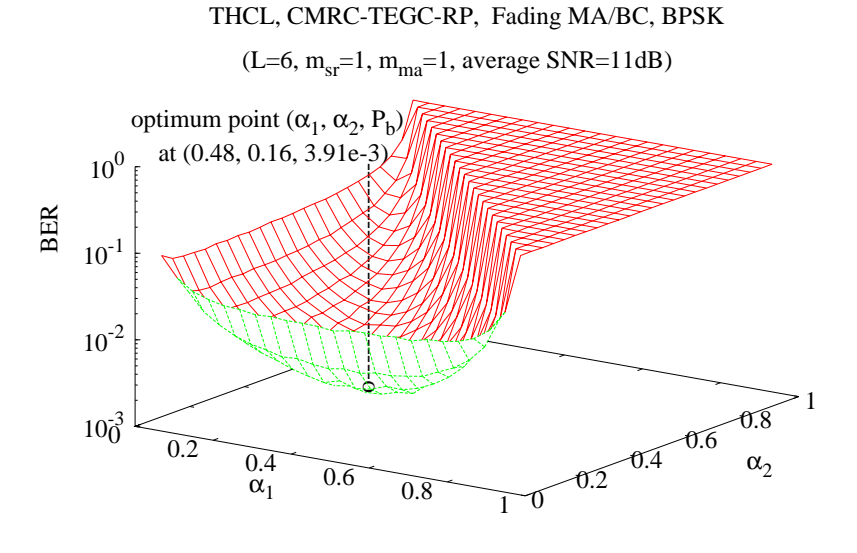


Figure 2.19: Effect of power-allocation factors on the BER performance of the CMRC-TEGC-RP assisted THCL employing BPSK baseband modulation, when all the S-R, MA/BC and R-D links experience flat iid Rayleigh fading.

 $\alpha_1 = 0.48$, $\alpha_2 = 0.16$, $\alpha_r = 0.36$. More portion of the total power is required for information exchange among the relays, when compared with the AWGN MA/BC case. From Figures 2.18 and 2.19, we are informed that a big portion of energy is required for implementing cooperation

among relays. Hence, in wireless networks, using cooperative relays is in fact highly challenging. Not only is a substantial amount of energy is required for cooperation, the accompanied increase of complexity may be substantial as well. This is because, first, extra channel estimation is required. Second, power-allocation will become more difficult, as four hops need to be considered in a network employing cooperative relays, instead of two hops in a network using distributed relays.

Additionally, we may compare the best BER achieved in Figure 2.18, which we assumed the AWGN MA/BC channels, with Figure 2.12. In Figure 2.12, the curve corresponding to the parameters of m=1, L=6 shows that the BER at 11 dB is well below 10^{-5} . This BER is much lower than the best BER of 1.47×10^{-4} shown in Figure 2.18. From this comparison we are implied that the BER predicted by applying ideal assumptions is far overoptimistic.

In Figure 2.20, we consider another example of power-allocation for the CMVC-TEGC-RP assisted THCL system, when the S-R and R-D transmissions experience Nakagami-m fading with $m_{sr} = m_{rd} = 3$, and the average SNR is 15 dB. As we can see, the OPA for the RP is achieved, when $\alpha_r = 0.48$. Hence, for the RP process demands a large portion of the total power to achieve the OPA, when the S-R and R-D channels become better, in comparison with Figure 2.18.

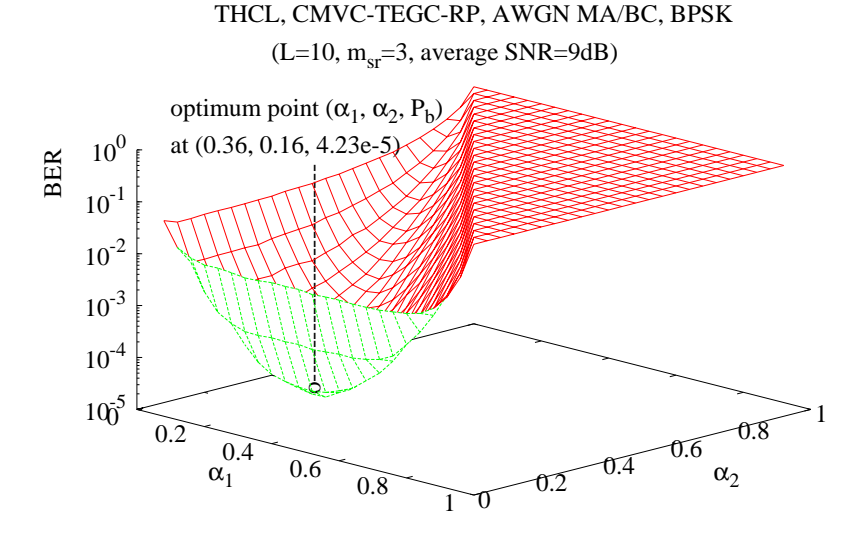


Figure 2.20: Effect of power-allocation factors on the BER performance of the CMVC-TEGC-RP assisted THCL employing BPSK baseband modulation, when both the first and second hop channels experience flat iid Nakagami-*m* fading, while the MA/BC channels are AWGN channels.

Having shown the impact of power-allocation on the BER performance, below we further investigate the BER performance of the THCL systems employing various of RP schemes, when the first and second hops as well as the MA/BC transmission experience independent Nakagami-*m* fading. Note that, the results below were obtained by applying our proposed suboptimal power-allocation (SOPA) scheme. In the context of the SOPA, the OPA is first found for a certain average

SNR. Then, this OPA is used for a specified region of average SNR, instead of using a specific OPA for each given average SNR, which demands high complexity. By this way, the SOPA scheme provides a relatively low complexity of implementation, but does not cause noticeable error performance loss.

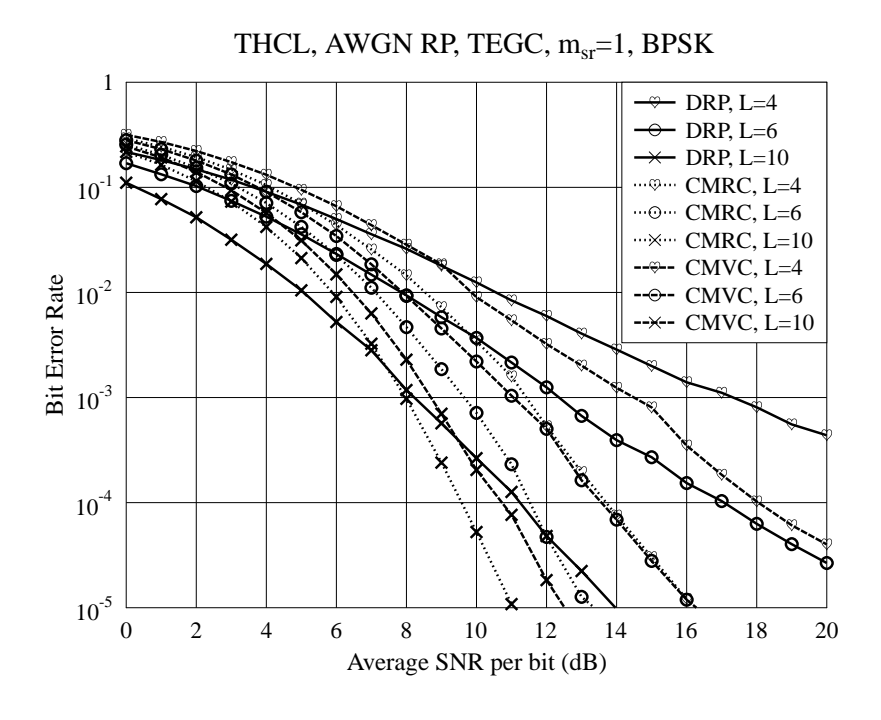


Figure 2.21: Comparison of BER performance of the THCL systems employing the TEGC-DRP, CMRC-TEGC-RP and the CMVC-TEGC-RP, when the S-R and R-D channels are all flat Rayleigh fading channels, while the MA/BC channels are AWGN channel.

Figures 2.21 and 2.22 demonstrate the BER performance of the THCL systems using the cooperative RP, when the TEGC is employed (Figure 2.21) or the TMRC is employed (Figure 2.22). For these figures, we assumed the AWGN channels for information exchange, and the first and second hop channels experience iid Rayleigh fading. From these two figures, we can obtain the following observations. First, in both figures, when considering the same number of relays and the identical transmit preprocessing scheme, the CMRC aided cooperative RP always has the best BER performance, and the CMVC aided cooperative RP outperforms the distributed RP scheme, when the SNR is sufficiently high. However, as shown in both figures, the BER curves of the distributed RP intersect with the corresponding BER curves for the CMRC and CMVC aided cooperative RP. Before the intersections, the distributed RP outperforms the CMRC or CMVC aided cooperative RP. Second, for any of the RP schemes employed, the BER performance of the THCL systems becomes better, as the number of relays increases. Third, when comparing these two figures, we can see when the same number of relays is employed, the BER performance of the THCL with the TEGC-DRP is better than that of the THCL with the TMRC-DRP, and the difference becomes larger, as the number of relays increases. By contrast, for any given number of relays, the BER performance of the THCL with the CMRC-TMRC-RP is slightly better than that of the THCL with the

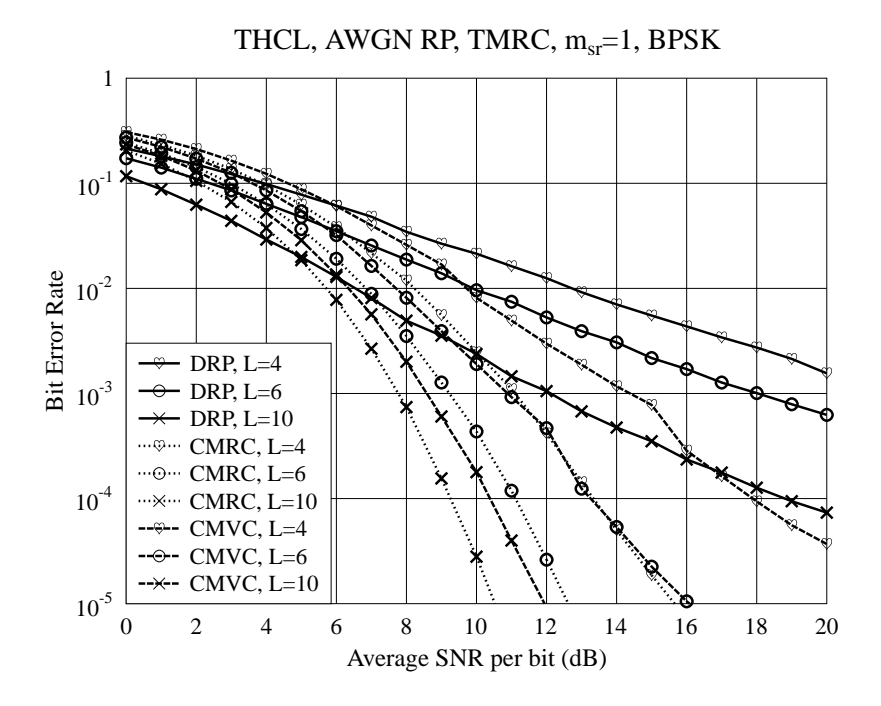


Figure 2.22: Comparison of BER performance of the THCL systems employing the TMRC-DRP, CMRC-TMRC-RP and the CMVC-TMRC-RP, when the S-R and R-D channels are all flat Rayleigh fading channels, while the MA/BC channels are AWGN channel.

CMRC-TEGC-RP. Similarly, for a given value of L, the CMVC-TMRC-RP slightly outperforms the CMVC-TEGC-RP in terms of BER performance.

From the above observations, we may conclude that the BER performance of the THCL systems employing the distributed RP is dominated by the transmit preprocessing scheme employed. By contrast, when the cooperative RP schemes are employed, the processing schemes used by the IECU and by the relays impose impact on the BER performance of the THCL systems.

In Figures 2.23 and 2.24, we compare the BER performance of the THCL systems employing the TEGC-DRP, CMRC-TEGC-RP and the CMVC-TEGC-RP, in order to illustrate the cost for the cooperation among relays. Specifically, in Figure 2.23, all the S-R, MA/BC and R-D channels are assumed flat Rayleigh fading channels, while in Figure 2.24, the S-R and R-D channels are assumed flat Rayleigh fading channels, while the MA/BC channels are assumed Nakagami-m fading channels with a fading parameter $m_{ma} = 3$. From the results of these two figures, we can explicitly see that, for all the cases considered, the TEGC-DRP outperforms the CMVC-TEGC-RP. Hence, for all these cases, no CMVC aided cooperation is desirable, as implementing the CMVC requires extra complexity. By contrast, when comparing the TEGC-DRP with the CMRC-TEGC-RP, we do see that, in the cases of L = 4 and 6, the CMRC-TEGC-RP may outperform the TEGC-DRP, when the average SNR is sufficiently high. However, for the case of L = 10, the TEGC-DRP always outperforms the CMRC-TEGC-RP. As the CMRC-TEGC-RP requires extra channel estimation and centralized detection, its achievable BER performance will be sensitive to the channel esti-

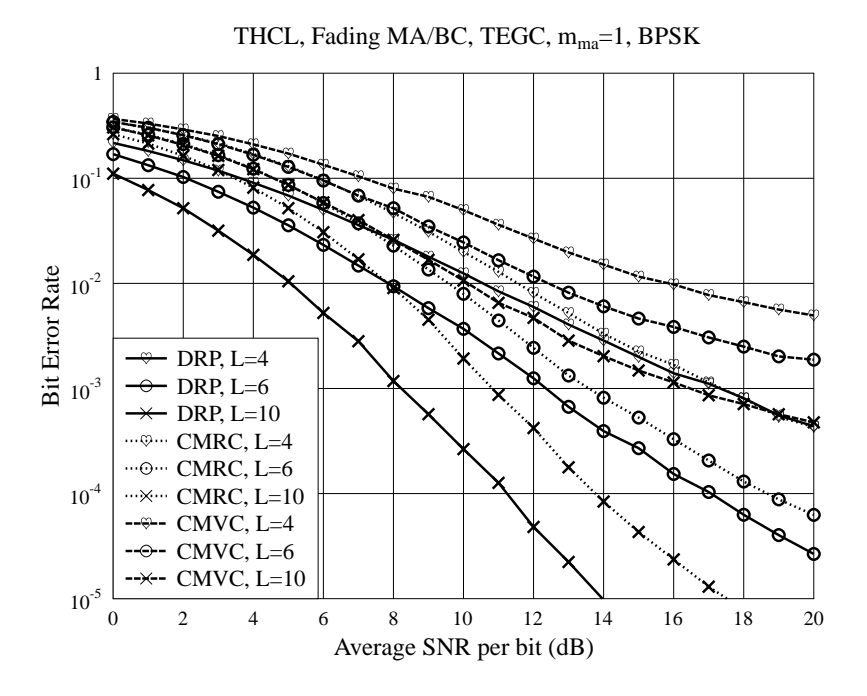


Figure 2.23: Comparison of BER performance of the THCL systems employing the TEGC-DRP, CMRC-TEGC-RP and the CMVC-TEGC-RP, when the S-R, MA/BC and R-D channels are all flat Rayleigh fading channels.

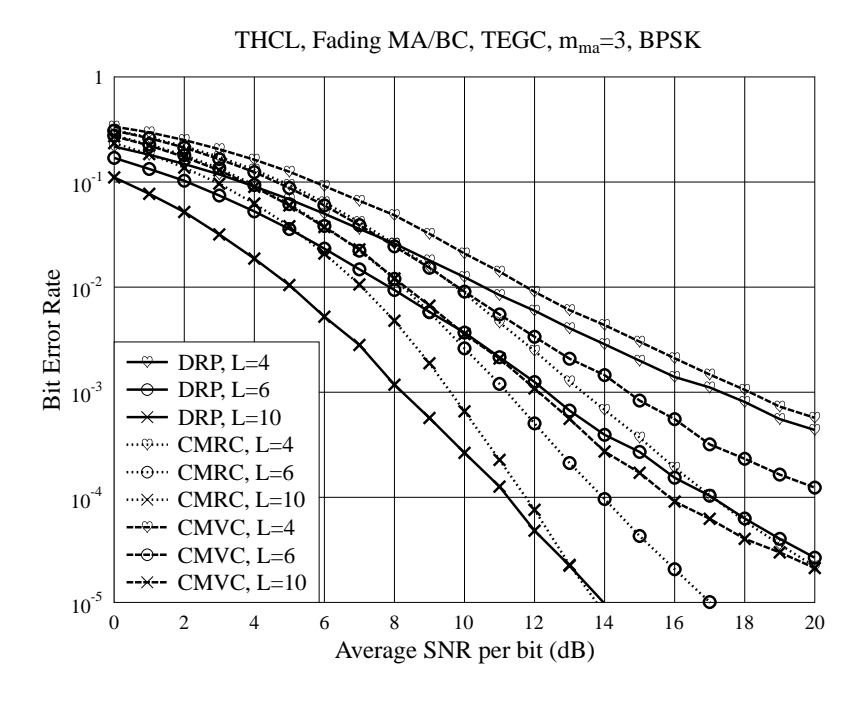


Figure 2.24: Comparison of BER performance of the THCL systems employing the TEGC-DRP, CMRC-TEGC-RP and the CMVC-TEGC-RP, when the S-R and R-D channels are flat Rayleigh fading channels, while the MA/BC channels are flat Nakagami-m fading channels associated with a fading parameter $m_{ma} = 3$.

mation's accuracy, in addition to the added complexity for the channel estimation and centralized signal detection. When taking into account of all the above, we may conclude that the TEGC-DRP constitutes a desirable and practical RP scheme. It has the relatively low-complexity for implementation, achieves diversity from the TEGC and yields less processing delay owing to no information exchange required among relays.

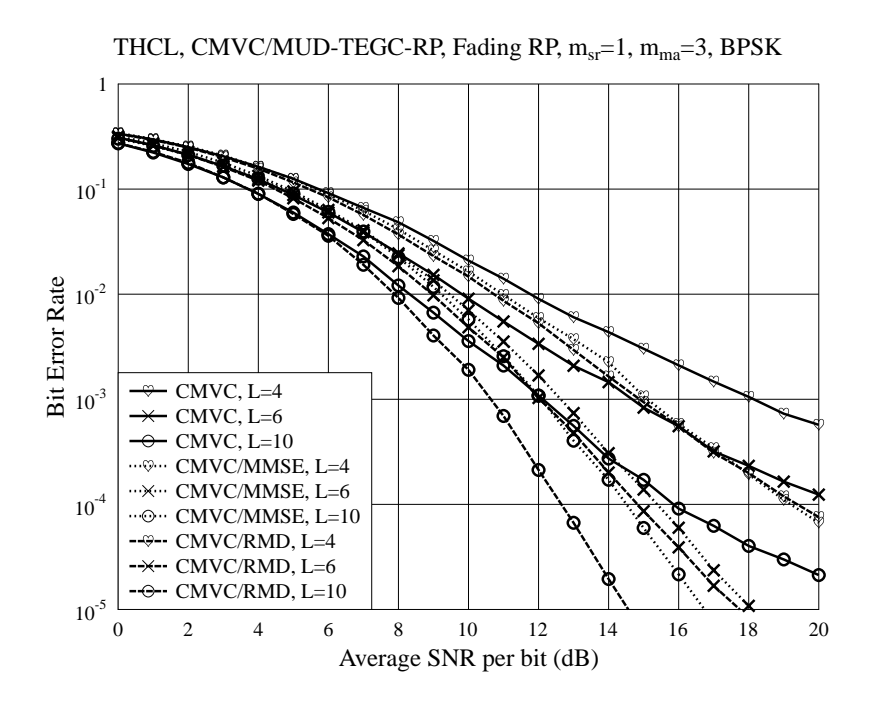


Figure 2.25: Comparison of BER performance of the THCL systems employing the CMVC/MUD-TEGC-RP, when the S-R and R-D channels are flat Rayleigh fading channels, while the MA/BC channels are flat Nakagami-m fading channels associated with a fading parameter $m_{ma} = 3$.

Figure 2.25 shows the BER performance of the THCL systems with the CMVC/MUD-TEGC aided cooperative RP for L=4,6,10, when the MA/BC channels experience the flat Nakagami-m fading with m=3. From Figure 2.25 we can observe that, for all cases considered, the THCL system with the CMVC/MUDs-TEGC-RP outperforms the THCL system with the CMVC-TEGC-RP scheme. The BER performance gain of using the CMVC/MUD at the IECU over that of employing the CMVC at the IECU becomes larger, as the number of relays increases. Furthermore, we can observe that the RMD/MS-MMSE MUD always achieves better BER performance than the MMSE MUD, at the cost of slightly higher complexity. The performance advantage of the RMD/MS-MMSE MUD over that of the MMSE MUD becomes bigger, as the number of relays increases. For example, a 2 dB of SNR gain can be obtained, when L=10. However, for L=10 the CMVC/MMSE-TEGC-RP results in would have a high error rate than the CMVC-TEGC-RP, when the average SNR is smaller than 12 dB.

2.6. Conclusions 66

2.6 Conclusions

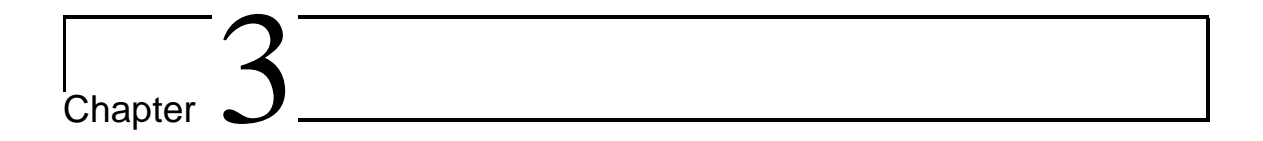
In this chapter, we have introduced a so-called THCL system, which aims to accomplish a communication between a source node and a destination node with the aid of a cluster of relays, in order to demonstrate the cost for relay cooperation and the challenges for performance analysis of this type of systems. Three RP schemes have been investigated in association with the THCL system, which are the distributed RP, ideal cooperative RP and the cooperative RP. When the distributed RP is employed, the relays employ the DF relaying scheme, and the signals are forwarded to the destination with the aid of the MRC- or EGC-assisted transmit preprocessing scheme, which are hence termed as the TMRC and TEGC, respectively. In the context of the ideal cooperative RP, we assume that information exchange among relays can be accomplished without energy consumption, which is also a typical assumption used in many existing references [46–49]. For the sake of investigating the cost of cooperation among relays, we have considered the cooperative RP scheme, which assumes energy consumption for the information exchange among relays via the MA and BC transmissions by invoking an IECU.

We have provided detailed analyses for the BER of the THCL systems employing various RP schemes, when BPSK baseband modulation is assumed. We have derived the closed-form formulas for the average BER of the THCL systems with some of the considered ideal cooperative RP schemes. In this chapter, we have proposed the novel approaches for obtaining the PDF of the sum of Nakagami-*m* variables. Two approaches for obtaining the approximate PDF have been proposed. The first one is called the Nakagami-TAp, and the second one is referred to as the Nakagami-SAp. With the aid of these two approaches, we have obtained the approximate average BER expressions of the THCL systems employing the TEGC-DRP or the CMVC-TEGC-RP, when the first and second hops are assumed to experience flat Nakagami-*m* fading, while the communications for information exchange among relays suffers from flat Nakagami-*m* fading or only AWGN. Furthermore, when the CMRC scheme is used at the IECU, we have proposed the Gamma-AP approach for finding the approximate PDF of the instantaneous SNR of the detection at the IECU. Furthermore, we have derived the average BER of the THCL systems employing the CMRC-TEGC-RP scheme.

By comparing the numerical results with our simulation results, we have found that, when the distributed RP or the cooperative RP is employed, the approximated average BER of the THCL systems has some small deviations from that obtained by simulations, when the fading of communication channels is severe, whereas, they agree with each other, as the channel conditions become better. When the ideal cooperative RP is employed, our results show that the average BER obtained from analytical formulas agrees well with the BER obtained from simulations. Furthermore, we have found that the first hop always requires a higher transmission power than the second hop, in order to achieve the best BER performance, when the distributed RP is employed. When the cooperative RP is employed, we have observed that, the cooperation among the relays for infor-

2.6. Conclusions 67

mation exchange requires $30\% \sim 70\%$ of the total system transmission power, in order to achieve the best BER performance. Specifically, the cooperative RP aided THCL systems can outperform the distributed PR aided THCL systems, when AWGN MA/BC channels are assumed. When the same transmit preprocessing scheme is employed by the relays for the second hop transmission, the CMRC aided cooperative RP achieves better BER performance than the CMVC aided cooperative RP, but at the cost of higher complexity. However, the cooperative RP scheme may achieve worse BER performance than the distributed RP, when the MA/BC links for information exchange experience flat Rayleigh fading. By considering the BER performance and complexity, we may conclude that the TEGC-DRP constitutes a desirable and practical RP scheme, which demands the lowest complexity for implementation, but is capable of achieving the required BER performance, especially, when the number of relays is relatively high.



Resource Allocation in Single-cell Downlink OFDMA Systems

3.1 Introduction

Multicarrier communication techniques, including the orthogonal frequency division multiplexing (OFDM) and its multiuser extension of orthogonal frequency division multiple access (OFDMA) [61], have been widely accepted as the key techniques for high-speed and broadband wireless communications. Multicarrier and OFDM techniques employ a range of merits, including the capability of combating inter-symbol interference (ISI), low-complexity modulation/demodulation implemented based on fast Fourier transform (FFT), dynamic resource allocation, etc. As wireless communication systems are usually operated in time-varying fading environments, taking the advantage of the time-varying characteristics by dynamically allocating the communication resources, which may include power, subcarrier, etc., is capable of providing promising energy and spectrum-efficiency [62].

References show that dynamic resource allocation is capable of achieving significant gain over fixed resource allocation, and various of resource allocation schemes have been proposed for different multicarrier systems [62–70]. In more detail, bit-, subcarrier- and power-allocation algorithms in [62, 63] have been designed in order to minimize the total transmission power, while the users' transmission qualities are maintained, i.e., under certain error rates. Wong *et al.* [62] proposed an iterative subcarrier-allocation algorithm followed by bits and power assignments. Whereas, in [63] it considered jointly assignment of the bits, subcarriers and power for each user in a novel fast way with low complexity. Moreover, in [64–68, 75], various sub-optimum joint subcarrier- and power-allocation algorithms were proposed. Specifically, in [64] they proposed two computationally inexpensive approaches for joint resource allocation where subcarrier-allocation was carried out in two iterations. Considering the uplink OFDMA systems, the authors in [65, 75] have pro-

3.1. Introduction 69

posed the joint subcarrier- and power-allocation algorithms, which respectively aim at maximizing the sum rate and the total utility of resources. A heuristic non-iterative subcarrier- and power-allocation scheme has been proposed in [68] for the OFDMA by extending the order subcarrier selection algorithm [76] for single user systems. Furthermore, in [69, 70], dynamic resource allocation problems have been addressed with respect to the cross-layer optimization of OFDMA systems. In more recently, some significant researches, such as [71–74] have also been dedicated to the resource allocation in OFDMA systems. Specifically, in [71], multiple BSs are coordinated to carry out the iterative subcarrier- and power-allocation to maximize the weighted sum of minimal user rates. For the sake of reducing the complexity of allocation, the two-part papers [73, 74] have studied the chunk-based subcarrier-allocation in downlink OFDMA systems. The first part [73] has proposed the average SNR- and BER-based chunk allocation schemes in order to maximize the system throughput when considering the average BER constraint over a chunk transmission. While the part two [74] has proposed a joint chunk-, power- and bit-allocation, in which, a range of system parameters including power constraint, number of users, coherent bandwidth, number of subcarriers and chunks are introduced and their impacts on the average throughput are studied.

A range of researches in [77-89], have designed and studied subcarrier-allocation algorithms for the downlink OFDMA systems. Specifically, in relation to our studies in this chapter, the greedy algorithm without considering the fairness has been applied for subcarrier-allocation in [78], in order to maximize the sum rate of OFDMA systems. Furthermore, in [78], the water-filling powerallocation has been employed. By contrast, authors in [79] addressed a fair subcarrier-allocation algorithm, providing equal data rate for all users. The fair greedy algorithm has been introduced by [80, 82] for subcarrier-allocation, however, its error performance is usually poor. For this sake, its extensions have been proposed, which include the worst user first (WUF) greedy algorithm [85] and the maximal greedy algorithm [86]. In more detail, under the WUF greedy algorithm, subcarriers are allocated in an order from the user with the worst average subchannel quality to the user with the best subchannel quality. This algorithm may be inefficient when operated in highly frequency-selective fading channels, as, in this case, the average channel qualities of all users may be similar. When the maximal greedy algorithm is employed, the above-mentioned fair greedy algorithm is repeatedly applied in the context of different user orders. Finally, the allocation giving the highest reliability, such as SNR, is chosen as the allocation results. While the WUF algorithm is inefficient in highly frequency-selective fading channels, the maximal greedy algorithm's complexity is dependent on the number of iterations of applying the greedy algorithm, which might be very high. In [83], a so-called worst subcarrier avoiding (WSA) algorithm has been proposed, which allocates the subcarriers based on the greedy algorithm in an order from the subcarrier holding the lowest subchannel quality. In this way, the (M-1) worst subcarriers can always be avoided assigning to users, if a multicarrier system with M subcarriers is considered. The WSA algorithm can be viewed another extension of the fair greedy algorithm. However, the error performance of the WSA algorithm usually significantly outperforms that of the greedy, WUF greedy and maximal 3.1. Introduction 70

greedy algorithms. It has been shown that the performance achieved by the WSA algorithm is close to that of the Hungarian algorithm [185], which is recognized as the optimum subcarrier-allocation algorithm, but of high-complexity.

Except the maximal greedy algorithm, the other greedy-based subcarrier-allocation algorithms employ the merit of low-complexity. However, when fair subcarrier-allocation is considered, the greedy and WUF algorithms often force the users of choosing their subcarriers at the latest stages to accept the subcarriers possibly with very poor qualities. Although the WSA algorithm is able to avoid assigning users a number of worst subchannels, it does not care about whether the allocated subcarriers are the best subchannels. Furthermore, in the WSA algorithm [83], the subcarrier-allocation order identified at the start of the algorithm is fixed during the whole allocation process, regardless of whether the situation might be changed after some subcarriers are allocated.

Based on the above observations, in this chapter, we design and compare two novel lowcomplexity subcarrier-allocation algorithms, and compare them with some other related subcarrierallocation algorithms proposed in literature. In addition to low-complexity, our algorithms motivate to assign users the sets of subchannels with the best possible qualities, in order to maximize the attainable reliability (throughput) but without making a trade-off with the achievable throughput (reliability), which, however, exists in some existing subcarrier-allocation algorithms, such as, the fair greedy subcarrier-allocation algorithm. In order to achieve our objectives, our subcarrier-allocation algorithms are operated either by identifying the worst subchannels or by seeking the best subchannels at the start of the algorithms, forming the so-called bidirectional worst subchannel avoiding (BWSA) and best subchannel seeking (BSS) algorithms. Our BWSA algorithm represents an extension of the WSA algorithm. In the WSA algorithm [83], according to the fixed allocation order identified at the start of the algorithm, a subcarrier is assigned to the best user, while avoiding the worst subchannel. Hence, the WSA algorithm is an one-dimensional worst subchannel avoiding algorithm. By contrast, in our BWSA algorithm, first, the worst subchannel, which has the lowest subchannel quality, of the remaining subchannels is found at each of the allocation iterations. Then, for an identified worst subchannel at an allocation iteration, the best subchannel is assigned by considering both the subcarrier direction and the user direction, while also with the objective to avoid the other poorest subchannels for the following allocations. Therefore, our BWSA algorithm is a two-dimensional worst subchannel avoiding algorithm, which has a higher diversity order than the WSA algorithm [83], and, hence, has the merit to further improve the WSA algorithm. The BSS algorithm aims at allocating all users the subchannels with the best qualities. In a little more detail, the BSS algorithm first finds a subchannel subset containing a number of best subchannels. Then, subcarrier-allocation is carried out in the greedy principles based on the subchannel subset obtained.

After the subcarrier-allocation, power-allocation is either based on the principles of channel-inverse [84] in order to maximize the reliability for a given baseband modulation scheme, or based on the principles of water-filling [78] to maximize system's sum rate. In this chapter, the error

3.2. System Model 71

and spectrum-efficiency performance of the BWSA and BSS algorithm are investigated and compared, which are also compared with that of a range of greedy-based algorithms as well as that of the optimal Hungarian algorithm. Our studies and performance results show that, both the BWSA and BSS algorithms have the merits to provide promising performance. While the BWSA algorithm outperforms the WSA and other greedy-based sub-optimum algorithms, the BSS algorithm may outperform as well the BWSA algorithm, especially, when it is operated in the relative large OFDMA systems of using a large number of subcarriers to support a range of users, which are true in practical systems. Furthermore, we demonstrate that the both the BWSA and BSS algorithms can attain their promising reliability without making trade-off with the achievable throughput.

In this chapter and the following three chapters, we focus on the resource allocation in the downlink multicarrier systems, both power- and subcarrier-allocation are addressed. Note that, our proposed subcarrier-allocation algorithms can be directly employed for the uplink communications via some information exchange between the BS carrying out the allocation and the mobile terminals controlled by the BS. By contrast, the power-allocation in the uplink communications need to be modified according to the transmitting power constraints on each individual users.

The rest of this chapter is organized as follows. Section 3.2 introduces the system model and gives the main assumptions. Section 3.3 discusses the general principle of the power- and subcarrier-allocation algorithms. Section 3.4 introduces two famous power-allocation schemes including the channel-inverse and the water-filling algorithms. Section 3.5 overviews some existing subcarrier-allocation algorithms and discusses their strengths and weaknesses. Sections 3.6 and 3.7 introduce the proposed subcarrier-allocation algorithms, and analyze their characteristics. Section 3.8 analyzes the complexity with the subcarrier-allocation algorithms considered. Section 3.10 shows and evaluates the BER and spectrum-efficiency simulation results. At last, conclusions are made in Section 3.11.

3.2 System Model

The considered downlink OFDMA system consists of one base station (BS) supporting *K* mobile users. We assume that each of the communication terminals, including the BS and *K* mobile users, employs one antenna for receiving and transmission. For the sake of clarity, the main variables and notations used in this chapter are summarized as follows:

K number of mobile users;

 \mathcal{K} set of user indexes, defined as $\mathcal{K} = \{0, 1, \dots, K-1\}$;

M number of subcarriers of OFDMA system;

 \mathcal{M} set of subcarrier indexes, defined as $\mathcal{M} = \{0, 1, \dots, M-1\}$;

3.2. System Model 72

Q set of numbers of subcarriers allocated to the K users, $Q = \{q_0, q_1, \dots, q_{K-1}\}$, where q_k is the number of subcarriers assigned to user k;

 Q_k set of data stream indexes of user k, defined as $Q_k = \{0, 1, \dots, q_k - 1\}$;

 $h_{k,m}$ fading channel gain of subcarrier m of user k;

 \mathcal{F}_k set of indexes of the q_k subcarriers assigned to user k;

 $\tilde{\mathcal{F}}_k$ set of indexes of the candidate subcarriers for user k;

 $|\mathcal{F}|$ cardinality of the set \mathcal{F} , i.e., the number of elements in the set $|\mathcal{F}|$;

 $A_{k,m}$ subchannel quality of subcarrier m of user k, $A_{k,m} = |h_{k,m}|^2/N_k$, where N_k is the noise variance for user k;

 $P_{k,m}$ transmission power for subcarrier m of user k, where $i \in \mathcal{F}_k$;

P total transmission power of BS, $P = \sum_{k \in \mathcal{K}} \sum_{m \in \mathcal{F}_k} P_{k,m}$.

In this chapter, we consider the fair subcarrier-allocation, which assigns all the users the same number of subcarriers, and assume that each subcarrier can only be assigned to one user. Therefore, we have the expressions of

$$\sum_{k \in \mathcal{K}} \mathcal{F}_k = \mathcal{M} \tag{3.1}$$

$$|\mathcal{F}_k| = Q, \quad \forall k \in \mathcal{K}$$
 (3.2)

$$\mathcal{F}_k \cap \mathcal{F}_l = \emptyset, \quad \text{if } k \neq l, \, \forall k, l \in \mathcal{K}$$
 (3.3)

where \emptyset means an empty set. The channels between the BS and mobile users are assumed to experience frequency-selective Rayleigh fading with L_p number of resolvable paths in the time-domain.

In Figure 3.1, it shows the schematic for resource allocation in the downlink OFDMA systems. In the considered OFDMA systems, we assume that the uplinks and downlinks are operated in the time-division duplex (TDD) mode. Hence, an uplink channel and its corresponding downlink channel can be assumed to be reciprocal. In this way, the BS is capable of obtaining the knowledge of all the KM downlink subchannels $\{h_{k,m}\}$, and all the subchannel qualities $\{A_{k,m}\}$ for $\forall k \in \mathcal{K}$, and $\forall i \in \mathcal{M}$. Therefore, given the transmission power of $P_{k,m}$, the instantaneous SNR of subcarrier m of user k can be expressed as

$$\gamma_{k,m} = \frac{P_{k,m}|h_{k,m}|^2}{N_k} = P_{k,m}A_{k,m}, \qquad k \in \mathcal{K}, \ m \in \mathcal{M}$$
 (3.4)

where N_k is the noise power of AWGN at mobile user k. For simplicity, we assume all the users have the same noise power, and we have $N_k = 1/\bar{\gamma}_s$, $\forall k \in \mathcal{K}$ where $\bar{\gamma}_s$ denotes the average SNR per symbol.

3.2. System Model 73

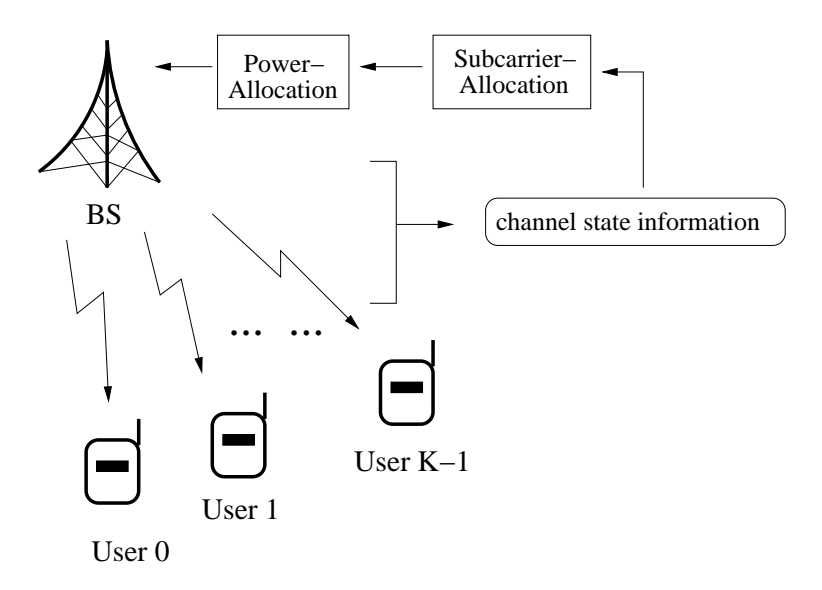


Figure 3.1: Schematic for resource allocation in the downlink OFDMA systems

Note that in this chapter we consider the most difficult scenario in the downlink OFDMA systems, all the M subcarriers have to allocate to users, as described in (3.1). It is straightforward that we can relax the constraint to the case that part of subcarriers are assigned to users, i.e. $\sum_{k \in \mathcal{K}} q_k \leq M$, in which case, all the considered allocation algorithms can also be used in the considered systems, and the system's performance can be significantly improved. Furthermore, for the considered power- and subcarrier-allocation algorithms, we also have the conventional fairness constraint that each user is assigned the same number of subcarriers, as shown in (3.2). Interestingly, these algorithms can be extended to the scenarios that the proportional fairness is assumed, which is given by

$$R_0: R_1: \dots: R_{K-1} = v_0: v_1: v_{K-1}$$
 (3.5)

where R_k is the achievable data rate of user k, and v_k is the corresponding rate proportion.

For the sake of simplicity, the subcarrier- and power-allocation are carried out seperately, which will be respectively detailed in the following sections. Note that, as the studies in [84] show, the power- and subcarrier-allocation can be carried out independently without performance loss, when optimum power-allocation is employed. Furthermore, it was shown in [68, 84] that the channel-inverse power-allocation is optimum in terms of maximizing the minimum SNR of users, as a result, minimizing the average BER of the systems. Therefore, we use the channel-inverse power-allocation scheme in this chapter. The water-filling power-allocation is also a widely used scheme, and can be employed to optimize the sum rate of the systems [186, 187].

3.3 General Theory

In an OFDMA system having M subcarriers, when the power- and subcarrier-allocation aim to maximize the system reliability, the ultimate objective is to minimize the average BER. Hence, the optimization problem for power- and subcarrier-allocation can be described as

$$\bigcup \{\mathcal{F}_{k}, P_{k}\}^{*} = \arg \min_{\bigcup \{\mathcal{F}_{k}, P_{k}\}} \{\bar{P}_{e}\}
= \arg \min_{\bigcup \{\mathcal{F}_{k}, P_{k}\}} \left\{ \frac{1}{M} \sum_{k \in \mathcal{K}} \sum_{q \in \mathcal{Q}_{k}} \bar{P}_{e}^{(k,q)} \right\}
\text{s.t. (3.1), (3.2), (3.3), and}
\sum_{k \in \mathcal{K}} \sum_{q \in \mathcal{Q}_{k}} P_{k,q} = P$$
(3.7)

where "s.t." stands for subject to, and \bar{P}_e denotes the system's average BER and $\bar{P}_e^{(k,q)}$ denotes the average BER of the qth data stream of user k. In (3.8), $\cup \{\mathcal{F}_k, P_k\}$ stands for testing all the possible candidates for all users, while $\cup \{\mathcal{F}_k, P_k\}^*$ contain the final results for subcarrier- and power-allocation of all the users. In practice, however, it is often very hard to solve the optimization problem of (3.8). Nevertheless, in OFDMA and other multicarrier communications employing the same data modulation schemes, the average BER \bar{P}_e is usually dominated by the subcarrier with the lowest SNR [84]. In this thesis, we assume the same baseband modulation scheme when reliability is concerned. In this case, as shown in [75,83,188], the power- and subcarrier-allocation schemes can be designed to maximize the minimum SNR of subcarriers, which can be expressed as

$$\bigcup \{\mathcal{F}_{k}, P_{k}\}^{*} = \arg \max_{\bigcup \{\mathcal{F}_{k}, P_{k}\}} \left\{ \min_{k \in \mathcal{K}, q \in \mathcal{Q}_{k}} \{\gamma_{k, q}\} \right\}$$
s.t. (3.1), (3.2), (3.3) and (3.7).

In this chapter, we aim to maximize the SNR of all subcarriers, in contrast to maximizing only the minimum SNR of the subcarriers as done in [75,83,188], so that the sub-optimum solution can be found in terms of minimizing the average BER of the system. Correspondingly, our optimization problem can be described as

$$\bigcup \{\mathcal{F}_{k}, P_{k}\}^{*} = \arg \max_{\bigcup \{\mathcal{F}_{k}, P_{k}\}} \{\gamma_{k,q}, \ k \in \mathcal{K}, \ q \in \mathcal{Q}_{k}\}$$
s.t. (3.1), (3.2), (3.3) and (3.7).

The philosophy behind can be explained as follows.

It has been demonstrated in [83, 84] that power- and subcarrier-allocation can be carried out separately without loss of much performance but having much lower complexity. Therefore, we assume that the power- and subcarrier-allocation are executed separately in two steps. Following the implementation of subcarrier-allocation, the power-allocation is carried out, according to the channels of the subcarriers allocated to different users. Therefore, our subcarrier-allocation algorithm is

designed for optimizing

In this chapter, the channel-inverse power-allocation is employed in order to minimize the average BER of the system, and it has been proved to be optimum in terms of maximizing the reliability [84]. Our proposed subcarrier-allocation will be designed in conjunction with the channel-inverse power-allocation algorithm, which aims at minimizing the average BER of the system. The water-filling power-allocation algorithm was designed for maximizing the system throughput [189, 190]. Hence, we will also compare the throughput (spectrum-efficiency) of the system employing various subcarrier-allocation algorithms, when the water-filling power-allocation algorithm is used. In the next section, we will briefly discuss the channel-inverse and the water-filling power-allocation algorithms.

3.4 Power-Allocation Algorithms

In this section, we will introduce the channel-inverse and the water-filling power-allocation algorithms. Furthermore, along with the considered power-allocation algorithms, we will continue to discuss the general theory for the resource allocation in the downlink OFDMA systems, and focus on the issue of designing the subcarrier-allocation.

3.4.1 Channel-Inverse Power-Allocation Algorithm

In the context of the channel-inverse assisted power-allocation, the power allocated to a subcarrier of a user is inversely proportional to the corresponding subchannel quality. The more power allocates to the one with less reliable subchannel quality, and vice versa. In that case, it guarantees that all the subchannels have a similar quality of service. Consequently, according to [84], given the subchannel qualities $\{A_{k,j}\}$ of the subcarriers allocated to the K users, the power is allocated as

$$P_{k,q} = P\left(\sum_{l \in \mathcal{K}} \sum_{i \in \mathcal{Q}_l} A_{l,i}^{-1}\right)^{-1} A_{k,q}^{-1}, \ q \in \mathcal{Q}_k, k \in \mathcal{K}.$$
(3.11)

Furthermore, as shown in [83], after the above power-allocation, the qth sub-stream of user k obtains the SNR of

$$\gamma_{k,q} = \gamma_c = P\left(\sum_{l \in \mathcal{K}} \sum_{i \in \mathcal{Q}_l} A_{l,i}^{-1}\right)^{-1}, \ q \in \mathcal{Q}_k, k \in \mathcal{K}.$$
(3.12)

Note that, (3.12) shows that the SNR is independent of the indexes k and q, implying that all the sub-streams of all the users attain the same SNR and, hence, they have the same error probability.

Furthermore, as shown in (3.10), our subcarrier-allocation algorithm aims to maximize the SNR of all the subcarriers of all the users. Therefore, when the channel-inverse assisted power-allocation is employed, from (3.12) we can be implied that, in order to maximize the SNR γ_c , we need to solve the subcarrier-allocation optimization problem of

$$\bigcup \{\mathcal{F}_k\}^* = \arg \max_{\bigcup \{\mathcal{F}_k\}} \left\{ \left(\sum_{l \in \mathcal{K}} \sum_{i \in \mathcal{Q}_l} A_{l,i}^{-1} \right)^{-1} \right\}$$
s.t. (3.1), (3.2), and (3.3).

In order to solve the above optimization problem, we may need to execute exhaustive search or implement the optimum Hungarian algorithm [185]. The principles of the Hungarian algorithm can be found in many references, such as in [185, 191], and we will also detail its principles in Section 4.3. However, these algorithms have high complexity, preventing them from practical implementation, when the number of subcarriers is relatively high, which is usually the case in the LTE/LTE-A systems.

In this chapter, we aim for designing the relatively low-complexity sub-optimum algorithms, which are capable of achieving the performance close to that obtained by solving the optimum problem of (3.13). Specifically, from (3.12) we can be implied that, in order for the SNR to achieve the maximum, it is expected that the allocated subcarriers should the ones with the largest possible values in $\{A_{k,q}\}$ of containing the KM candidates. Therefore, our optimization problem for subcarrier-allocation can be stated as

$$\bigcup \{\mathcal{F}_k\}^* = \arg \max_{\bigcup \{\mathcal{F}_k\}} \left\{ A_{k,q}, \ k \in \mathcal{K}, \ q \in \mathcal{Q}_k \right\},$$

$$\triangleq \arg \min_{\bigcup \{\mathcal{F}_k\}} \left\{ A_{k,q}^{-1}, \ k \in \mathcal{K}, \ q \in \mathcal{Q}_k \right\},$$
s.t. (3.1) (3.2) and (3.3).

In order to find a solution approximately solving (3.14), we may either start from the worst subchannel side, motivating to avoid a maximum number of worst subchannels of the *KM* subchannels, or start from the best subchannel side to directly allocate the subcarriers corresponding to the best possible subchannels. These are the motivations for us to design the proposed subcarrier-allocation algorithms, as detailed in our forthcoming discourses.

Explicitly, the optimization problem of (3.14) also fulfills the objective to maximize the sum rate of an OFDMA system, when subcarrier and power are allocated separately. This is because, for a given total transmission power and water-filling assisted power-allocation, the best subset of subchannels also yields the highest sum rate. When given the best set of subcarriers having the subchannel qualities $\{A_{k,q}^*\}$, the sum rate can be expressed as

$$C = \sum_{k \in \mathcal{K}} \sum_{q \in \mathcal{Q}_k} \log_2 \left(1 + P_{k,q}^* A_{k,q}^* \right). \tag{3.15}$$

3.4.2 Water-Filling Power-Allocation Algorithm

The water-filling assisted power-allocation was found as the optimum solution for maximizing the sum rate of system [190]. For a given subcarrier-allocation, the optimization problem for maximizing the system's throughput can be expressed as

$$\bigcup \{P_k\}^* = \arg \max_{\bigcup \{P_k\}} \sum_{k \in \mathcal{K}, q \in \mathcal{Q}_k} \log \left(1 + P_{k,q} A_{k,q}\right)$$
s.t. (3.7).

The above objective function is jointly concave in powers, and the optimization problem can be solved by the Lagrangian method, resulting in the water-filling power-allocation. Let Φ be the water-filling level, according to the algorithm, the power allocated to data-stream q of user k can be given by

$$P_{k,q} = \left[\Phi - \frac{1}{A_{k,q}}\right]^{+} \tag{3.17}$$

where $[x]^+ = \max\{0, x\}$, and the water-filling level Φ is set to satisfy the requirement of

$$\sum_{k \in \mathcal{K}} \sum_{q \in \mathcal{Q}_k} P_{k,q} \le P. \tag{3.18}$$

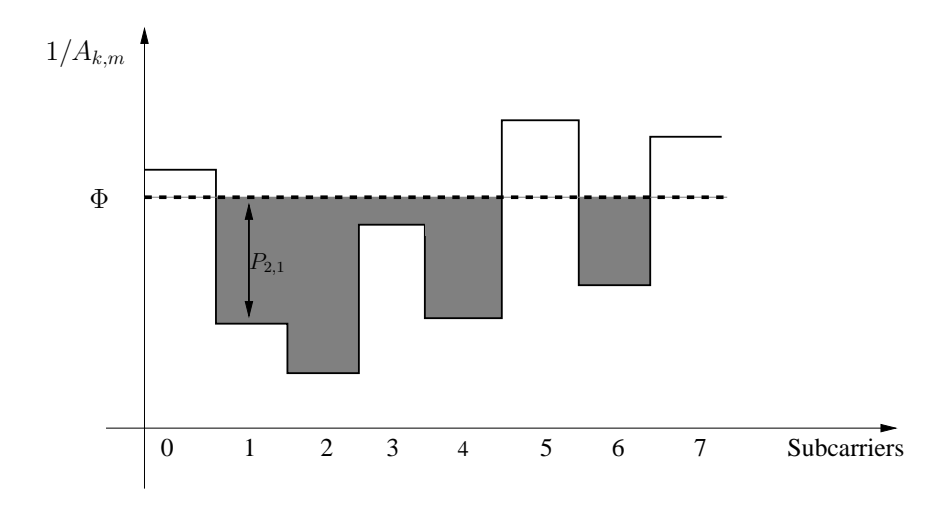


Figure 3.2: An example for water-filling power-allocation in the downlink OFDMA system with M=8 subcarriers

According to (3.17), we know that more power is allocated for the subchannel with better quality, and no power is assigned when the subchannel quality is lower than the inverse of water level, i.e., $A_{k,q} \leq 1/\Phi$. We can readily find that the water-filling algorithm has a counter-operation of the channel-inverse power-allocation algorithm. Furthermore, Figure 3.2 shows a pictorial view of the water-filling algorithm employed by an OFDMA systems, where M=8 subcarriers are

Scrs	0	1	2	3	4	5	6	7
0	0.45	5.19	1.94	3.24	5.27	1.59	0.16	4.24
1	4.95	14.92	0.50	0.79	2.04	16.91	0.48	0.36
2	1.78	2.78	0.92	6.58	3.14	5.23	0.54	0.99
3	2.91	0.33	5.97	0.41	0.49	2.20	8.87	1.64
4	2.11	1.22	3.12	1.72	4.37	1.82	5.17	0.23
5	9.53	1.34	1.27	3.90	3.36	3.07	0.63	5.15
6	4.83	2.58	4.26	0.56	2.14	8.15	1.16	1.87
7	5.49	0.48	5.38	3.74	1.68	2.01	0.84	0.15

Table 3.1: An Example for Channel Qualities of M=8 Subcarriers of the K=8 Users.

considered. Seen from the figure, the power is allocated to the subcarriers of users with the inverse of subchannel qualities under the water level Φ , which is as pouring water to a vessel.

3.5 Existing Subcarrier-Allocation Algorithms

In this section, we review the principles of some representative subcarrier-allocation algorithms, including the greedy algorithm, the WSA algorithm, and the maximal greedy algorithm. For clarity, we discuss the three schemes using an example, which employs M=8 subcarriers to support K=8 mobile users. Therefore, each subcarrier can only be allocated to one user and, correspondingly, we have $q_k=1$, $\forall k\in\mathcal{K}$. Let us assume that the subchannel qualities of the eight subcarriers of the eight users are given in Table 3.1, where the first row and first column denote the subcarrier indexes and user indexes, respectively. With the aid of this example, we now discuss the advantages and disadvantages of the existing algorithms considered. In the next section, the proposed subcarrier-allocation algorithm will be described. Note that, our proposed algorithm aims to minimize the average BER of the system, and hence, we assume that the channel-inverse power-allocation is used for the example considered. Let us now consider the greedy algorithm.

3.5.1 Greedy Algorithm

The greedy algorithm has been designed to maximize the sum rate of the system, and aims to solve the optimization problem that can be expressed as

$$\bigcup \{\mathcal{F}_k\}^* = \arg \max_{\bigcup \{\mathcal{F}_k\}} \left\{ \sum_{l \in \mathcal{K}} \sum_{i \in \mathcal{Q}_l} A_{l,i} \right\}$$
s.t. (3.1) (3.2) and (3.3).

Note that, unless specifically notified, in this chapter, the greedy algorithm considered is *fair* greedy algorithm, which allocates all the users the same number of subcarriers.

In the context of the greedy algorithm [80], subcarriers are allocated one-by-one from the first to the last, and a subcarrier is simply allocated to the user with the best subchannel quality among the users having not obtained their required number of subcarriers. After a user obtains its required number of subcarriers, it is then removed from the list of users for further subcarrier-allocation. For the example of Table 3.1, the subcarrier-allocation is carried out one-by-one from subcarrier 0 to 7. The operation of the Greedy algorithm can be described as the allocation matrix shown below

Explicitly, in (3.20), the underlined subchannel qualities indicate the allocation result. For subcarrier 0, since $A_{5,0}=9.53$ is the best subchannel quality among $\{A_{1,0},\ldots,A_{7,0}\}$, subcarrier 0 is allocated to user 5. Likewise, subcarrier 1 selects the best from the available users, $\{0,1,2,3,4,6,7\}$, and obtains user 1. Similarly, as shown in (3.20), subcarriers 2 to 7 choose respectively their best users from their available options, according to the subchannel qualities. Finally, we can obtain the subcarrier-allocation results: $\mathcal{F}_0=\{4\}$, $\mathcal{F}_1=\{1\}$, $\mathcal{F}_2=\{3\}$, $\mathcal{F}_3=\{2\}$, $\mathcal{F}_4=\{6\}$, $\mathcal{F}_5=\{0\}$, $\mathcal{F}_6=\{5\}$, $\mathcal{F}_7=\{7\}$. The corresponding subchannel qualities are $\{5.27,14.92,6.58,5.97,5.17,9.53,8.15,0.15\}$. It can be seen that the minimum subchannel quality of the subcarriers allocated is $\min_{k\in\mathcal{K},j\in\mathcal{F}_k}\{A_{k,j}\}=0.15$. Let us assume that the total transmit power P is 1. When the channel-inverse power-allocation is employed, it can be shown that the achieved SNR given by (3.12) is $\gamma_c=0.13$.

The main drawback of the greedy algorithm is that the subcarriers assigned later are left with fewer options. In this case, they might have to choose the users of poor subchannel qualities. In the above example, subcarrier 7 is forced to allocate to user 7 having the poor subchannel quality of 0.15, as there are no other options. As the result, the overall attainable SNR becomes relatively low, which may significantly degrade the error performance of the system.

3.5.2 Worst User First Greedy Subcarrier-Allocation Algorithm

The worst user first (WUF) greedy algorithm motivates to improve the greedy algorithm's performance, and it arranges the users in ascending order according to their average subchannel qualities [85]. In that case, the users with worst average subchannel qualities choose their subcarriers first in the principle of the greedy algorithm.

For the example considered, the WUF greedy algorithm first orders the eight users according to their average subchannel qualities. Then, we have the user order {4,7,2,0,3,6,5,1}, since user 4 has the worst average subchannel quality while user 7 has the best one. The allocation process can be seen as the matrix below

After the user ordering, the subcarrier-allocation for each user is the same as that for the greedy algorithm. Explicitly, for user 4, as shown in (3.21), subcarrier 6 has the best subchannel quality among all subcarriers, therefore, user 4 is assigned with subcarrier 6. Similarly, the remaining users select their subcarriers. Finally, we can obtain the subcarrier-allocation results: $\mathcal{F}_0 = \{1\}$, $\mathcal{F}_1 = \{4\}$, $\mathcal{F}_2 = \{3\}$, $\mathcal{F}_3 = \{2\}$, $\mathcal{F}_4 = \{6\}$, $\mathcal{F}_5 = \{7\}$, $\mathcal{F}_6 = \{5\}$, $\mathcal{F}_7 = \{0\}$. It can be seen that the minimum subchannel quality of the subcarriers allocated is $\min_{k \in \mathcal{K}, j \in \mathcal{F}_k} \{A_{k,j}\} = 2.04$. Then, it can be shown that the achieved SNR is $\gamma_c = 0.59$ according to (3.12), when assuming the total transmit power P is 1.

From the allocation results, we can clearly observe that the WUF greedy algorithm can outperform the greedy algorithm. By ordering the users, it avoids assigning subcarrier 7 to user 7, which happened under the greedy algorithm and this significantly degrades the BER performance of the system. However, the average subchannel qualities of the users cannot reflect the worst subchannel qualities of the users. In some cases, the WUF greedy algorithm still cannot avoid assigning the worst subchannel qualities to the users. Therefore, the WUF greedy algorithm is not an efficient way of subcarrier-allocation in terms of maximizing the system reliability.

3.5.3 Maximal Greedy Subcarrier-Allocation Algorithm

The maximal greedy algorithm [86] aims to maximize the sum of subchannel qualities, i.e., to maximize $\sum_{k \in \mathcal{K}} \sum_{j \in \mathcal{F}_k} A_{k,j}$ in this chapter. Under this algorithm, the conventional greedy algorithm [80] is iteratively operated by ordering the subcarriers involved in different ways to obtain the various sets of allocation results. At the end, the set of allocation results achieving the maximum of the total subchannel quality is chosen as the final allocation result. Considering the example of Table 3.1, the principles of the maximal greedy algorithm can be explained as follows.

Let us assume that, during the first iteration, the greedy algorithm is operated with the subcarrier

order of $\{0,1,2,3,4,5,6,7\}$. Then, the allocation results are the same results as that described in Section 3.5.1. Correspondingly, the sum of subchannel qualities of the allocated subcarriers is $\sum_{k \in \mathcal{K}} \sum_{j \in \mathcal{F}_k} A_{k,j} = 55.74$. During the second iteration, let us assume that the subcarrier order is $\{0,1,2,3,7,6,5,4\}$. Then, using the greedy algorithm again, we obtain the subcarrier-allocation results: $\mathcal{F}_0 = \{7\}$, $\mathcal{F}_1 = \{1\}$, $\mathcal{F}_2 = \{3\}$, $\mathcal{F}_3 = \{2\}$, $\mathcal{F}_4 = \{6\}$, $\mathcal{F}_5 = \{0\}$, $\mathcal{F}_6 = \{5\}$, $\mathcal{F}_7 = \{4\}$. It can be shown that the sum of subchannel qualities becomes $\sum_{k \in \mathcal{K}} \sum_{j \in \mathcal{F}_k} A_{k,j} = 56.24$, which is larger than that obtained from the first iteration. Therefore, the allocation results obtained from the second iteration are taken as the final subcarrier-allocation results, if only two iterations are used. Straightforwardly, more than two iterations may be used. Furthermore, subcarriers can be ordered either randomly or in a pre-specified way.

Although the maximal greedy algorithm is capable of improving the error performance of the multicarrier system, it is however a search algorithm, the achievable performance of which depends on the size of the searching space, i.e., the number of iterations. In order to reach a target of the total subchannel quality, sometimes, many iterations might be required, which demands a high complexity. Additionally, the maximal greedy algorithm does not motivate to maximize the achievable SNR, as given in (3.12), of the system. Hence, the attained SNR is not necessary close to the maximum SNR possible. Specifically, for the above considered example, when the channel-inverse power-allocation is employed, the SNR obtained after two iterations is $\gamma_c = 0.61$, which is significantly higher than that obtained by the greedy algorithm.

3.5.4 Worst Subcarrier Avoiding Subcarrier-Allocation Algorithm

The WSA algorithm is designed to avoid assigning users the subcarriers having the worst subchannel qualities [83]. The principles of the WSA algorithm can also be illustrated with the aid of the example shown in Table 3.1. The allocation process can be described as follows in association with the matrix

$$\begin{bmatrix} & S_7 & S_6 & S_1 & S_3 & S_0 & S_4 & S_2 & S_5 \\ U_0 & 4.24 & \textbf{0.16} & 5.19 & 3.24 & \textbf{0.45} & \underline{5.27} & 1.94 & \textbf{1.59} \\ U_1 & 0.36 & 0.48 & \underline{14.92} & 0.79 & 4.95 & 2.04 & \textbf{0.50} & 16.91 \\ U_2 & 0.99 & 0.54 & 2.78 & \underline{6.58} & 1.78 & 3.14 & 0.92 & 5.23 \\ U_3 & 1.64 & \underline{8.87} & \textbf{0.33} & \textbf{0.41} & 2.91 & \textbf{0.49} & 5.97 & 2.20 \\ U_4 & 0.23 & 5.17 & 1.22 & 1.72 & 2.11 & 4.37 & \underline{3.12} & 1.82 \\ U_5 & \underline{5.15} & 0.63 & 1.34 & 3.90 & 9.53 & 3.36 & 1.27 & 3.07 \\ U_6 & 1.87 & 1.16 & 2.58 & 0.56 & 4.83 & 2.14 & 4.26 & \underline{8.15} \\ U_7 & \textbf{0.15} & 0.84 & 0.48 & 3.74 & 5.49 & 1.68 & 5.38 & 2.01 \\ \end{bmatrix}$$

where the boldfaced values represent the worst subchannel qualities of the subcarriers, while the underlined values corresponds to the subcarriers assigned to users.

In detail, under the WSA algorithm, for each of the subcarriers, the worst subchannel quality of

the users is first identified, which are represented by boldface values in (3.22). Then, the subcarriers are arranged in ascent order according to the worst channel qualities as $\{7,6,1,3,0,4,2,5\}$, as shown in (3.22), where the elements are the subcarrier indexes. Then, subcarriers are allocated to users one-by-one in the above-derived order, by following the principles of the greedy algorithm, as described in Section 3.5.1. As shown in (3.22), the algorithm starts the allocation of subcarrier 7, which is assigned to user 5, as user 5 has the best subchannel quality. Similarly, the remaining subcarriers are assigned to the remaining users in the derived order. Finally, it can be shown that the subcarrier-allocation results are $\mathcal{F}_1 = \{1\}$, $\mathcal{F}_2 = \{3\}$, $\mathcal{F}_3 = \{6\}$, $\mathcal{F}_4 = \{2\}$, $\mathcal{F}_5 = \{7\}$, $\mathcal{F}_6 = \{5\}$, $\mathcal{F}_7 = \{0\}$. The corresponding subchannel qualities of the subcarriers allocated are $\{5.27, 14.92, 6.58, 8.87, 3.12, 5.15, 8.15, 5.49\}$. Hence, the minimum subchannel quality of the allocated subcarriers is $\min_{k \in \mathcal{K}, j \in \mathcal{F}_k} \{A_{k,j}\} = 3.12$, which is significantly higher than that obtained by the greedy algorithm of Section 3.5.1. Furthermore, according to (3.12) and assuming P = 1, the achieved SNR is $\gamma_c = 0.75$, which is also much larger than that obtained by the greedy algorithm.

The WSA algorithm can avoid assigning users the subcarriers having the worst subchannel qualities. Hence, in comparison with the greedy algorithm, the minimum subchannel quality of the subcarriers allocated by the WSA algorithm may be significantly improved, ensuring a better error performance of the system, as demonstrated in [83]. However, while avoiding the worst subcarriers, the WSA algorithm does not motivate to maximize the subchannel quality of every subcarrier allocated, which leaves some space for further improving the achievable error performance of the system.

3.6 Bidirectional Worst Subchannel Avoiding Subcarrier-Allocation Algorithm

In this section, we first describe the principles of the proposed bidirectional worst subchannel avoiding (BWSA) algorithm and then discuss its characteristics.

3.6.1 Principles of Bidirectional Worst Subchannel Avoiding Subcarrier-Allocation Algorithm

The BWSA algorithm aims at maximizing the SNR of subcarriers, as shown in (3.10), by avoiding the worst subchannels as many as possible. As discussed in Section 3.5.4, the WSA algorithm has been designed to avoid the worst subchannels. However, it has the potential to be improved by our proposed BWSA algorithm, as detailed below. First, let us use an example to illustrate the principles of the BWSA algorithm. In the example, we assume M=8 and K=8, the one shot of 64 subchannel qualities are given in Table 3.1.

As our discussion in Section 3.5.4 shows, when the WSA algorithm is operated, subcarriers 1 and 3 are allocated at iteration 3 and iteration 4, since $A_{3,1}$ and $A_{3,3}$, both belong to user 3, are the third and fourth minimum worst subchannel qualities. However, user 3 cannot be the option for either subcarrier 1 or subcarrier 3, as user 3 has already been assigned subcarrier 6 during the second iteration. In this case, further considering user 3 after the second iteration makes the subcarrier-allocation less profitable. Instead, it is more profitable to carry out the remaining subcarrier-allocation without invoking user 3. Consequently, at iteration 3, allocation of subcarrier 0 should be considered, as the worst subchannel quality of 0.45 held by subcarrier 0 is the minimum of the remaining 6 subcarriers for the remaining users. Furthermore, the WSA algorithm can be viewed as a subcarrier-oriented algorithm, where subcarrier-by-subcarrier is allocated by finding the best user among the available ones for a subcarrier. Explicitly, subcarriers can also be allocated in a user-oriented way, where user-by-user is allocated a subcarrier with the best subchannel quality among the remaining subcarriers. Furthermore, the above-mentioned subcarrier-oriented and user-oriented ways may be jointly operated to maximize the diversity by avoiding the worst subchannels as many as possible. Our BWSA algorithm is designed based on the above-mentioned observations, which is described with the aid of the example shown in Table 3.1 associated with the operations shown in Figure 3.3. In Figure 3.3, the circled numbers indicate the allocation iterations, the triangles represent the worst subchannel qualities that are avoided at the corresponding iterations identified by the associated numbers, while the squares represent the second worst subchannel qualities that are avoided at the corresponding iterations explained by the attached numbers. Finally, the locations with the mark ' $\sqrt{\ }$ ' give the allocation results.

As Table 3.1 shows, $A_{7,7}=0.15$ is the lowest subchannel quality in the table. Hence, the BWSA algorithm will first avoid this worst subchannel quality during iteration 1. Furthermore, while avoiding this worst subchannel quality, the BWSA algorithm also aims to avoid the second worst one related to this worst subchannel quality. Specifically, considering the worst subchannel quality $A_{7,7}=0.15$, if the subcarrier is allocated in the subcarrier-oriented way based on the greedy principles, subcarrier 7 will be assigned to user 5. Since in this case subcarrier 7 and user 5 will not be further considered during the following iterations, the second worst subchannel quality of $A_{4,7}=0.23^1$ can be avoided for further iterations. By contrast, if the user-oriented subcarrier-allocation is applied, subcarrier 0 will be assigned to user 7, as $A_{7,0}=5.49$ is the largest in row 7. If this is supposed to be the allocation, as subcarrier 0 and user 7 will not be further considered during the following iterations, the second worst subchannel quality avoided is $A_{0,0}=0.45$. Comparing the above two cases, we find $A_{4,7}(=0.23) < A_{0,0}(=0.45)$. Hence, the BWSA algorithm finally chooses the subcarrier-oriented allocation result and allocates subcarrier 7 to user 5, in order to avoid $A_{4,7}=0.23$ for the following iterations.

After iteration 1, $A_{0,6} = 0.16$ is the smallest one among the remaining elements. During the second iteration, the BWSA algorithm works in the same way as iteration 1, and the subcarrier-

 $^{^{1}}A_{4,7}=0.23$ is the smallest among the elements in row 5 and column 7, after excluding $A_{7,7}=0.15$.

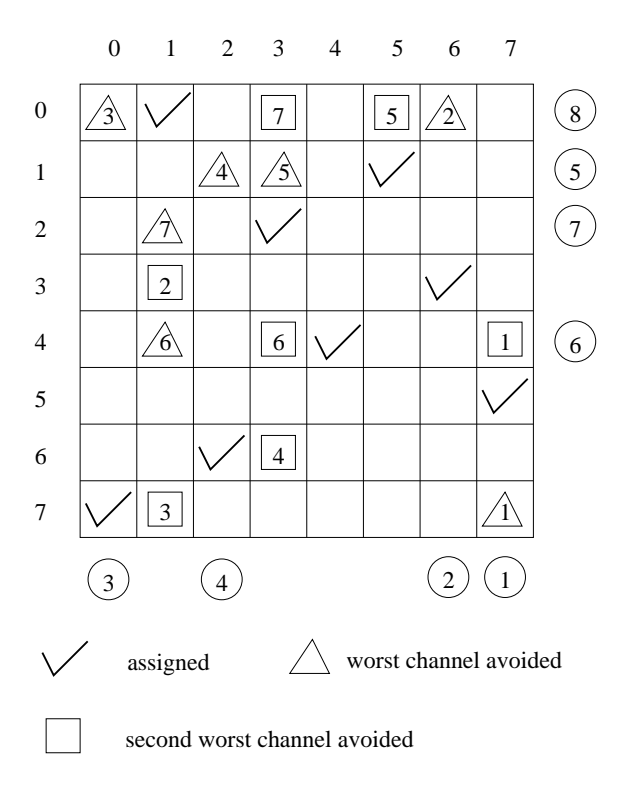


Figure 3.3: Schematic showing the operations of the BWSA algorithm having the subchannel qualities as shown in Table 3.1.

oriented mode is chosen to allocate subcarrier 6 to user 3, so as to remove $A_{3,1}=0.33$ from the following possible allocations, in addition to avoiding $A_{0,6}=0.16$. Similarly, during iteration 3, subcarrier 0 is assigned to user 7, which can exclude both $A_{0,0}=0.45$ and $A_{7,1}=0.48$ from the following possible allocations. Note that, if the WSA algorithm is employed, iteration 3 will consider subcarrier 1, as $A_{3,1}=0.33$ is the third largest in Table 3.1. After the above three iterations, now $A_{1,2}=0.5$ becomes the smallest in the remaining subchannel qualities. Again, the subcarrier-oriented mode is chosen to assign subcarrier 2 to user 6, which removes both $A_{1,2}=0.5$ and $A_{6,3}=0.56$. During iterations 5-8, the situations can be similarly considered. It can be found that the user-oriented mode is chosen during all these iterations and the allocation results are shown in Figure 3.3.

Finally, as shown in Figure 3.3, the BWSA algorithm yields the allocation results: $\mathcal{F}_0 = \{7\}$, $\mathcal{F}_1 = \{0\}$, $\mathcal{F}_2 = \{6\}$, $\mathcal{F}_3 = \{2\}$, $\mathcal{F}_4 = \{4\}$, $\mathcal{F}_5 = \{1\}$, $\mathcal{F}_6 = \{3\}$, $\mathcal{F}_7 = \{5\}$. The minimum subchannel quality of the subcarriers allocated is $\min_{k \in \mathcal{K}, j \in \mathcal{F}_k} \{A_{k,j}\} = 4.26$, which is higher than that obtained by the WSA algorithm as well as by the other algorithms discussed in Section 3.5.4. Furthermore, when the channel-inverse power-allocation is employed and assuming P = 1, from (3.12) we obtain the SNR $\gamma_c = 0.74$, which is also larger than $\gamma_c = 0.65$ obtained by the WSA algorithm.

For the general cases where one user may require several subcarriers, the BWSA algorithm can

be operated as follows.

Algorithm 2. (Bidirectional Worst Subchannel Avoiding)

Initialization: *Set* $\mathcal{F}_k = \emptyset$, $\forall k \in \mathcal{K}$; $\tilde{\mathcal{K}} = \mathcal{K}$, $\tilde{\mathcal{M}} = \mathcal{M}$.

Execute:

Step 1 Find the worst subchannel quality among the available ones: $A_{k^*,j^*} = \arg\min_{k \in \tilde{\mathcal{K}}, j \in \tilde{\mathcal{M}}} \{A_{k,j}\}.$

Step 2 Select the allocation mode based on two conditions:

Condition (a): avoiding the worst subchannel quality of A_{k^*,i^*} .

Condition (b): avoiding the second smallest subchannel quality, while (a).

Step 3 Allocate a subcarrier having the best available subchannel quality to a user in the selected mode.

Subcarrier-oriented mode - allocate subcarrier j^* to the user with the best subchannel quality:

$$\mathcal{F}_{k'} \leftarrow \mathcal{F}_{k'} \cup \{j^*\}, \text{ where } k' = \arg\min_{k \in \mathcal{K}} \{A_{k,j^*}\}.$$

User-oriented mode - allocate user k^* the subcarrier with the best subchannel quality:

$$\mathcal{F}_{k^*} \leftarrow \mathcal{F}_{k^*} \cup \{j'\}, \text{ where } j' = \arg\min_{j \in \tilde{\mathcal{M}}} \{A_{k^*,j}\}.$$

Step 4 Update:

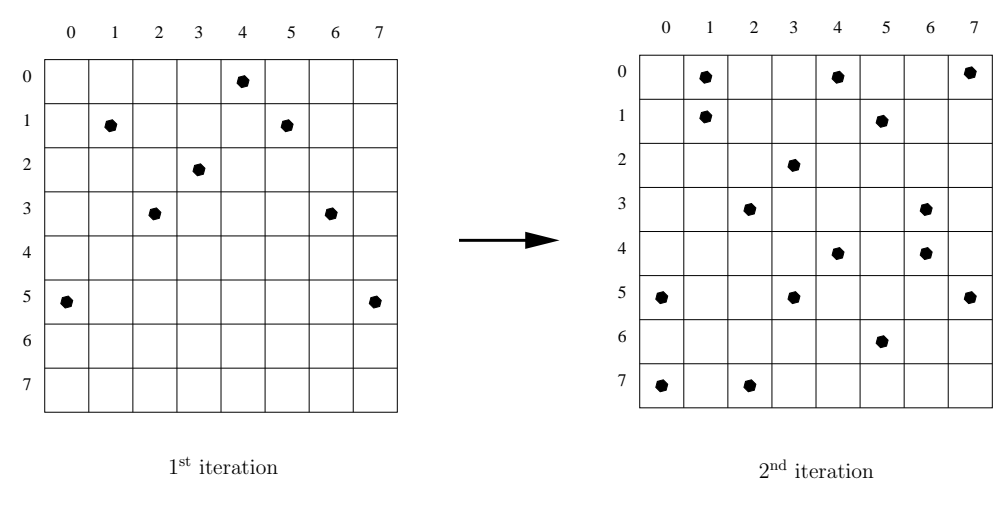
Subcarrier-oriented mode - (a) Remove subcarrier j^* from the set $\tilde{\mathcal{M}}$: $\tilde{\mathcal{M}} \leftarrow \tilde{\mathcal{M}} - \{j^*\}$; (b) Remove user k' from the set $\tilde{\mathcal{K}}$: $\tilde{\mathcal{K}} \leftarrow \tilde{\mathcal{K}} - \{k'\}$, if it has been assigned the required number of subcarriers.

User-oriented mode - (a) Remove subcarrier j' from the set $\tilde{\mathcal{M}}$: $\tilde{\mathcal{M}} \leftarrow \tilde{\mathcal{M}} - \{j'\}$; (b) Remove user k^* from the set $\tilde{\mathcal{K}}$: $\tilde{\mathcal{K}} \leftarrow \tilde{\mathcal{K}} - \{k^*\}$, if it has been assigned the required number of subcarriers.

Step 5 Repeat Steps 1 - 4 until $\tilde{\mathcal{M}} = \emptyset$.

3.6.2 Characteristics of Bidirectional Worst Subchannel Avoiding Subcarrier-Allocation Algorithm

In comparison with the other subcarrier-allocation algorithms, especially, the WSA algorithm, considered in Section 3.5.4, our proposed BWSA algorithm has the following advantages. First, in comparison with the WSA algorithm, the BWSA algorithm is capable of avoiding more worst subchannels that might be assigned to users. When operated under the WSA algorithm, for each of the subcarriers, the worst subchannel (user) can be avoided. By contrast, when the BWSA algorithm is employed, for each of the worst subchannels identified, both the worst and the second worst subchannels are avoided from the possible future assignments. Second, in the context of the WSA algorithm, the worst subchannels are identified at the start of the algorithm, which are then



Candidate subcarrier for allocation

Figure 3.4: **Stage I of BSS:** based on the example of Table 3.1, searching for the candidate subcarriers.

fixed during the process of subcarrier-allocation. By contrast, for the BWSA algorithm, the worst subchannel is dynamically identified during the subcarrier-allocation process, only those subchannels affecting future allocations are considered. Third, the BWSA algorithm can achieve a higher diversity gain than the other subcarrier-allocation algorithms. As shown in Section 3.5, in any of these other subcarrier-allocation algorithms, the subchannel for allocation is chosen from just one dimension. By contrast, in our BWSA algorithm, as shown in Section 3.6.1, it attempts to choose the best subchannel for allocation from two dimensions. Hence, it has a higher probability to obtain a better subchannel for allocation. Additionally, we should note that the complexity of the BWSA algorithm is only slightly higher than that of the WSA algorithm, as will be shown in Section 3.8.

3.7 Best Subchannel Seeking (BSS) Subcarrier-Allocation Algorithm

In this section, we propose a so-called best subchannel seeking (BSS) subcarrier-allocation scheme, which aims to find a sub-optimum solution for maximizing the achievable SNR in (3.12). Specifically, the BSS algorithm is designed for solving the optimization problem described in (3.14), which maximizes the channel qualities of all the data streams of all the users. In this section, the principle of the BSS algorithm is first introduced and, then, its characteristics are discussed.

3.7.1 Principles of Best Subchannel Seeking Subcarrier-Allocation Algorithm

Let us first illustrate the principles of the BSS algorithm with the aid of the example with the channel qualities shown in Table 3.1. During the first stage of the algorithm, the candidate subcarriers are identified iteratively as shown in Figure 3.4.

The BSS algorithm tries to find the sub-optimum subcarrier-allocation solutions for maximizing the achievable SNR that is close to the optimum. It is designed for solving the optimization problem described in (3.14), which aims to maximize the subchannel qualities of all data streams of all users. The BSS algorithm consists of two stages: Stage I for searching candidate subcarriers, and Stage II for allocating users the candidate subcarriers.

Let us first illustrate the principles of the BSS algorithm using the example with the subchannel qualities shown in Table 3.1. During Stage I of the algorithm, the candidate subcarriers are identified iteratively as shown in Figure 3.4. For each of the subcarriers, the user with the best subchannel quality is identified, and the subcarrier is taken as the candidate subcarrier of this user. According to Table 3.1, we can show that, after the first iteration, the sets of candidate subcarriers for the eight users are shown in Figure 3.4, which are $\tilde{\mathcal{F}}_0=\{4\},\,\tilde{\mathcal{F}}_1=\{1,5\},\,\tilde{\mathcal{F}}_2=\{3\},$ $\tilde{\mathcal{F}}_3=\{2,6\},\, \tilde{\mathcal{F}}_4=\varnothing,\, \tilde{\mathcal{F}}_5=\{0,7\},\, \tilde{\mathcal{F}}_6=\varnothing,\, \tilde{\mathcal{F}}_7=\varnothing.$ Consequently, for users 1, 3, 5, each one has two candidate subcarriers, while users 4, 6 and 7 do not have any candidate subcarriers at all. In this case, the BSS algorithm continues to the second iteration to search for more candidate subcarriers. During the second iteration, for each subcarrier, the user having the best subchannel quality but not a candidate yet is selected. Therefore, the candidate user selected has the second best subchannel quality on the considered subcarrier. Consequently, after the second iteration, the candidate subcarrier sets of the eight users are updated to $\tilde{\mathcal{F}}_0 = \{1,4,7\}, \, \tilde{\mathcal{F}}_1 = \{1,5\}, \, \tilde{\mathcal{F}}_2 = \{3\},$ $\tilde{\mathcal{F}}_3=\{2,6\},\, \tilde{\mathcal{F}}_4=\{4,6\},\, \tilde{\mathcal{F}}_5=\{0,3,7\},\, \tilde{\mathcal{F}}_6=\{5\},\, \tilde{\mathcal{F}}_7=\{0,2\},\, \text{as shown in Figure 3.4.}$ Furthermore, we can see that the number of candidate subcarriers for each of the users is at least the number of subcarriers required by the user. Hence, the BSS algorithm may stop the search process and forward to Stage II to try to allocate the candidate subcarriers.

In the general cases when every user has multiple data streams to transmit and, hence, requires multiple subcarriers, the operations of Stage I of the BSS algorithm can be stated as follows.

Algorithm 3. (Stage I of BSS: Candidate Subcarrier Search)

Initialization: Set $\tilde{\mathcal{F}}_k = \emptyset$, $\forall k \in \mathcal{K}$; $\tilde{\mathcal{K}}_i = \mathcal{K}$, $\forall j \in \mathcal{M}$.

Search:

- **Step 1** For all subcarriers $(\forall j \in \mathcal{M})$, the user with the best subchannel quality is identified, which is expressed as $k_i^* = \arg\max_{k \in \tilde{\mathcal{K}}_i} \{A_{k,j}\}$.
- **Step 2** Subcarrier j is taken as a candidate subcarrier of user k_j^* , yielding $\tilde{\mathcal{F}}_{k_i^*} \leftarrow \tilde{\mathcal{F}}_{k_i^*} \cup \{j\}$.
- **Step 3** Remove user k_j^* from the set $\tilde{\mathcal{K}}_j$: $\tilde{\mathcal{K}}_j \leftarrow \tilde{\mathcal{K}}_j \{k_i^*\}$.
- **Step 4** The above search process is repeated until the *Condition*: $|\tilde{\mathcal{F}}_k| \ge q_k, \forall k \in \mathcal{K}$ (the number of candidate subcarriers for each of the users is at least the number of subcarriers required by the user) is met.

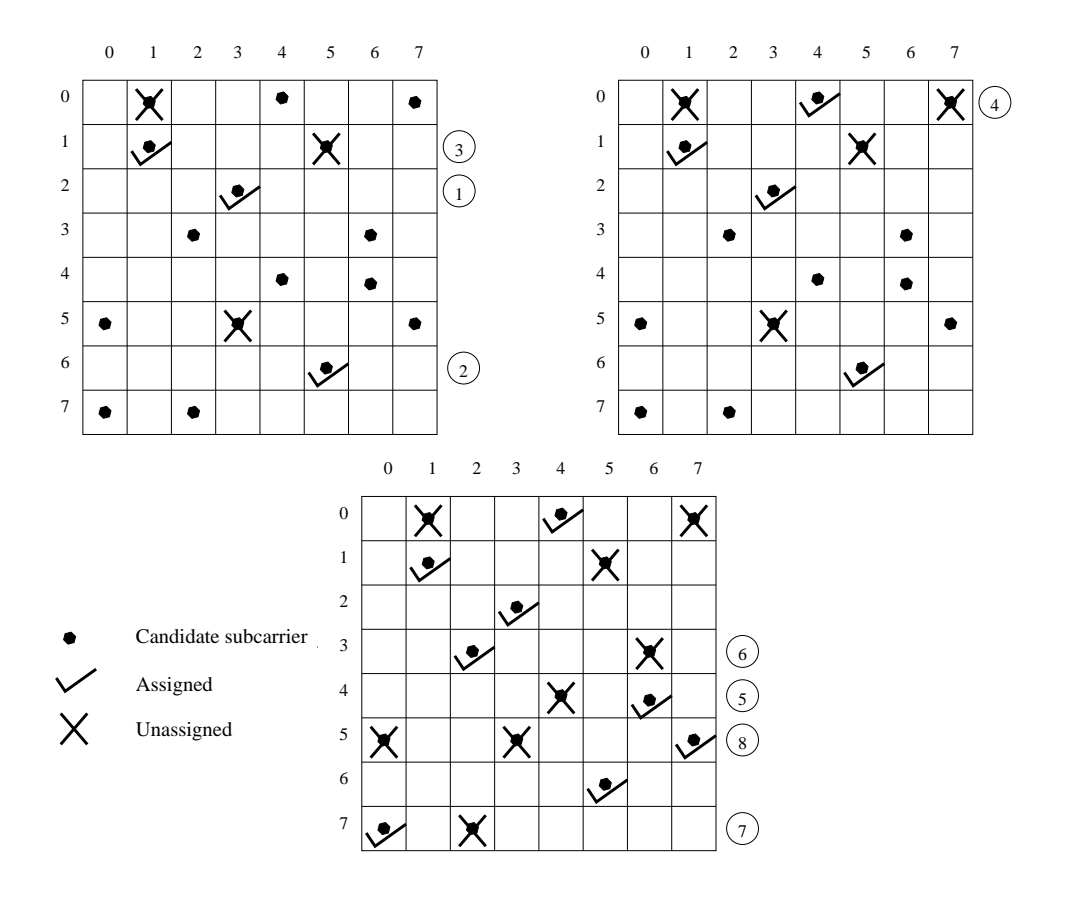


Figure 3.5: **Stage II of BSS:** based on the candidate subcarriers obtained from Stage I of the BSS, allocating the subcarriers to the users.

Step 5 The BSS algorithm forwards to Stage II.

The operations during Stage II of the BSS algorithm can be explained with the aid of the example shown in Figure 3.5. During this stage, one subcarrier is allocated at a time. Therefore, the subcarrier-allocation process requires eight allocation iterations to assign the eight subcarriers. At each iteration, the BSS algorithm allocates a subcarrier to the user having the least number of candidate subcarriers. For the considered example, first, both users 2 and 6 have the least number of candidate subcarriers of one. However, in order to avoid allocating users the worst subchannels, the BSS algorithm first allocates user 2 subcarrier 3, as the candidate subcarrier of user 2 is worse than that of user 6. Consequently, we have $\mathcal{F}_2 = \{3\}$. Since a subcarrier can only be assigned once, subcarrier 3 is then removed from the candidate subcarrier set of user 5, yielding $\tilde{\mathcal{F}}_5 = \{0,7\}$. In a similar way, as demonstrated by the top-left plot of Figure 3.5, user 6 is allocated subcarrier 5 during the second iteration, followed by allocating user 1 subcarrier 1 during the third iteration. After the above three iterations, the rest users 0, 3, 4, 5 and 7 all have two candidate subcarriers. Again, in order to avoid assigning the worst subchannels to users, the BSS algorithm first allocates a subcarrier to the user having the worst candidate subchannel among these users. As seen in Table 3.1, among these five users, user 0 has the worst candidate subchannel with the subchannel quality $A_{0,7} = 4.24$. Therefore, during the fourth iteration, user 0 is assigned the best subcarrier

4 in its candidate subcarrier set, as shown in the top-right plot of Figure 3.5. Similarly, the other subcarriers are allocated to the rest users during the following four iterations, as illustrated in the bottom plot of Figure 3.5. Finally, the allocation results are $\mathcal{F}_0 = \{4\}$, $\mathcal{F}_1 = \{1\}$, $\mathcal{F}_2 = \{3\}$, $\mathcal{F}_3 = \{2\}$, $\mathcal{F}_4 = \{6\}$, $\mathcal{F}_5 = \{7\}$, $\mathcal{F}_6 = \{5\}$ and $\mathcal{F}_7 = \{0\}$. The corresponding subchannel qualities of the allocated subcarriers are $\{5.27, 14.92, 6.58, 5.97, 5.17, 5.15, 8.15, 5.49\}$. From this set, we can see that the worst subchannel quality of the allocated subcarriers is 5.15, which is much larger than that obtained by the subcarrier-allocation algorithms discussed in Section 3.5. Furthermore, when the channel-inverse power-allocation is employed and assuming P = 1, the obtained SNR is $\gamma_c = 0.78$, which is also significantly higher than that attained by the other algorithms considered in Section 3.5.

Note that, if Stage II is unable to be fulfilled, as there are not enough candidate subcarriers, the BSS algorithm returns to Stage I to add more candidates. The above process repeats until all users are allocated their required number of subcarriers.

In summary, for the general cases when each user requires multiple data streams, the operations during Stage II of the BSS algorithm can be stated as follows.

Algorithm 4. (Stage II of BSS: Subcarrier – Allocation)

Initialization: Set
$$\hat{\mathcal{K}} = \mathcal{K}$$
; $\mathcal{K}' = \emptyset$; $\mathcal{F}_k = \emptyset$, $\hat{\mathcal{Q}}_k = \mathcal{Q}_k$, $\forall k \in \mathcal{K}$.

Allocation:

- **Step 1** Identify the users having the least number of candidate subcarriers, yielding a set expressed as $\mathcal{K}' = \arg\min_{k \in \hat{\mathcal{K}}} \{ |\tilde{\mathcal{F}}_k| \}$.
- **Step 2** In \mathcal{K}' , find the user having the worst candidate subcarrier, which is expressed as $k^* = \arg\min_{k \in \mathcal{K}', j \in \tilde{\mathcal{F}}_k} \{A_{k,j}\}.$
- **Step 3** Allocate user k^* the best subcarrier chosen from its candidate subcarrier set, i.e., $\mathcal{F}_{k^*} = \mathcal{F}_{k^*} \cup \{j^*\}$, where $j^* = \arg\max_{j \in \tilde{\mathcal{F}}_{k^*}} \{A_{k^*,j}\}$.
- **Step 4** Remove subcarrier j^* from the candidate subcarrier sets of all the users, which is expressed as $\forall k \in \hat{\mathcal{K}}, \tilde{\mathcal{F}}_k \leftarrow \tilde{\mathcal{F}}_k \{j^*\}, \text{ if } j^* \in \tilde{\mathcal{F}}_k.$
- **Step 5** Remove user k^* from the set $\hat{\mathcal{K}}$, if $|\mathcal{F}_{k^*}| = q_{k^*}$, i.e., $\hat{\mathcal{K}} \leftarrow \hat{\mathcal{K}} \{k^*\}$.
- **Step 6** Repeat the above 5 steps until the allocation process fulfills, or the allocation process is unable to carry on before completion. In the later case, the BSS algorithm returns to the search process of Stage I to add more candidate subcarriers.

3.7.2 Characteristics of Best Subcarrier Seeking Subcarrier-Allocation Algorithm

In comparison with the four low-complexity subcarrier-allocation algorithms considered in Section 3.5, the proposed BSS algorithm employs the following characteristics. First, it is in general

Table 3.2: Average number of iterations, S, for search of candidate subcarriers and the average number of allocation-search iterations, S', for completion of subcarrier-allocation. The values are expressed as (S, S').

L_p	Q K	1	2	4	8	
	4	3.14, 1.002	2.84, 1.04	2.43, 1.16	3.05, 1.77	
	8	5.51, 1.006	4.11, 1.12	3.41, 1.94	5.19, 2.97	
M/4	16	7.87, 1.03	5.65, 1.35	6.27, 2.54	9.79, 4.87	
	32	9.37, 1.09	7.51, 1.92	9.52, 4.24	13.75, 6.54	
	64	12.69, 1.12	9.23, 1.98	12.96, 5.12	18.22, 7.53	
	4	2.7, 1.01	2.41, 1.08	2.27, 1.34	3.08, 1.96	
	8	3.87, 1.06	3.38, 1.41	4.04, 2.47	5.69, 3.63	
<i>M</i> /2	16	5.13, 1.17	4.34, 1.76	6.65, 2.84	10.1, 5.24	
	32	6.4, 1.31	6.16, 2.36	10.64, 5.15	15.35, 7.76	
	64	7.64, 1.42	7.16, 2.55	13.79, 6.01	20.14, 9.02	

capable of achieving higher SNR than the three subcarrier-allocation algorithms. As shown in Section 3.5, with the greedy algorithm, the users allocated subcarriers later may have to accept very poor subchannels. The WSA algorithm can avoid allocating the worst subchannels, but it does not care whether the allocated subchannels belong to the best ones. By contrast, the proposed BSS algorithm aims to allocate users the best possible subchannels, motivating to maximize the attainable SNR and, hence, the reliability. Second, owing to the maximization of SNR, the BSS algorithm does not make a trade-off between reliability and throughput, as shown by the results in Section 3.10. Third, the BSS algorithm is highly efficient for the large OFDMA systems that use a big number of subcarriers to support many users. However, it might not be very efficient for the small OFDMA systems with a small number of subcarriers for supporting a low number of users, as explained in detail associated with Figure 3.13 in Section 3.10.

Fourth, the number of iterations required by the BSS algorithm for searching candidate subcarriers and for allocating subcarriers is usually much smaller than the number of subcarriers. As an example, Table 3.2 shows the average number of iterations S required for searching candidate subcarriers, and the average number of iterations S', where one iteration includes a searching process and an allocation process, required for finally completing subcarrier allocation. For this table, we assume a frequency-selective Rayleigh fading channel with L_p number of time-domain resolvable paths, and the same noise variance for all subcarriers of all users. The total number of subcarriers is M = KQ, where Q is the number of subcarriers per user. In the table, each of the results was obtained by the average of 10^5 realizations. From Table 3.2, we can find that, in relatively large OFDMA systems, the average number of iterations S is much smaller than the number of subcar-

riers. When M is small but there are relatively more users sharing the subcarriers, allocation can typically be completed in 1-2 iterations of S'. When the system is large, the number of iterations S' is still very small, in comparison with the number of subcarriers M.

Finally, we should note that, subcarrier-allocation can be understood in theory as a type of selection diversity. The performance of an algorithm depends on the portion of subchannels selected from the total KM subchannels. The BSS algorithm motivates to choose the set of subcarriers having the best subchannel qualities of the KM subchannels. Hence, it employs the capability to achieve the highest possible diversity gain, especially, when it is operated in a large OFDMA or other large multicarrier systems.

3.8 Complexity Analysis of Subcarrier-Allocation Algorithms

In this section, we analyze the complexity of the BWSA and BSS algorithms, and compare them with the other sub-optimum algorithms considered in this chapter. Specifically, we only consider the complexity of the subcarrier-allocation algorithms, as the same power-allocation scheme can be used for all the algorithms considered. Furthermore, the complexity is counted as the number of comparisons carried out. Specifically, in our analysis, we assume that an OFDMA system has M = KQ number of subcarriers and that each of the K users is allocated Q number of subcarriers.

Let us first consider the complexity of the greedy algorithm. We note first that the number of comparisons required to find the maximum of U real numbers is (U-1) [192]. It can be shown that the complexity of the greedy algorithm has an upper-bound, which happens when each of the first (M-K) subcarriers searches for the best subchannel quality among the K available users. Hence, in the greedy algorithm, during the first (M-K) allocation iterations, (M-K)(K-1) number of comparisons are required. During the last K allocation iterations, $\sum_{i=1}^{K-1} (K-i) = K(K-1)/2$ number of comparisons are required. Therefore, in total, the greedy algorithm requires at most (M-K)(K-1)-K(K-1)/2 number of comparisons, which can be expressed as

$$C^{(\text{greedy})} \le (M - K)(K - 1) - \frac{K(K - 1)}{2}$$
 (3.23)

yielding a complexity of $\mathcal{O}(MK)$, as M > K.

As the analysis in Section 3.5.3 shows, the maximal greedy algorithm executes α ($\alpha \geq M$) times of the greedy algorithm. Therefore, it has the complexity of $\mathcal{O}(\alpha MK)$.

The WSA algorithm needs to find both the maximum and the minimum of the K subchannel qualities for each of the M subcarriers, which requires 2M(K-1) number of comparisons. Moreover, the M minimum subchannel qualities are sorted from the best to the worst, which costs $2M \ln M$ number of comparisons. Therefore, the total number of comparisons for the WSA algorithm can be expressed as

$$C^{(WSA)} = 2M(K-1) + 2M\ln M$$
 (3.24)

which gives the complexity of $\mathcal{O}(MK)$.

We should note that the number of comparisons required by the BWSA algorithm is a variable, which depends on the specific subchannel quality matrix being processed. However, the BWSA algorithm requires the maximum number of comparisons, when the subchannel quality matrix results in that each user is assigned (Q-1) subcarriers after (M-K) iterations. In this case, to identify the worst subchannel qualities, we need M(K-1) comparisons during these (M-K) iterations, and (K-1)(K-2)/2 comparisons during the last K iterations. Moreover, at each iteration, the BWSA algorithm first searches for the worst subchannel quality among the left subchannels, which requires at most M(M-1)/2 comparisons. Once the worst subchannel quality is identified, the allocation processes requires (M-K)(K-1)+K(K-1) comparisons. Hence, in general, the total number of comparisons required by the BWSA algorithm satisfies

$$C^{(BWSA)} < (K-1)(2M + \frac{K-2}{2}) + \frac{1}{2}M(M-1)$$
(3.25)

which makes the complexity of the BWSA algorithm $\mathcal{O}(M^2)$.

As shown in Section 3.7, the BSS algorithm consists of two stages. At Stage I, the best candidate users are selected for each of the subcarriers. Although several iterations might be run between search and allocation, it can be shown that identifying the best candidates in different iterations can be achieved by one ordering process, which, for each of the subcarriers, orders the users from the best to the worst. According to [192], sorting K real numbers using the quick-sort algorithm requires $2K \ln K$ comparisons. Hence, the total number of comparisons required for searching candidates is $2MK \ln K$.

During Stage II, the BSS algorithm allocates the candidate subcarriers to users. Assume that an allocation can be fulfilled, the number of comparisons required can be analyzed as follows. The BSS algorithm first needs to identify the users having the least number of candidate subcarriers, which requires at most (M-K)(K-1)+K(K-1)/2 comparisons. Occasionally, it needs to find the specific user by comparing the minimum subchannel qualities when more than one user happens to have the same least number of candidate subcarriers. This process requires less than M(Q-1) comparisons. Then, the best candidate subcarrier is assigned to the identified user. In most cases, the best candidate is chosen from at most Q number of options, giving that this process requires about M(Q-1) comparisons.

Finally, when considering both the two stages, as well as the iterations between candidate subcarrier searching and subcarrier-allocation, the total number of comparisons required by the BSS algorithm satisfies

$$C^{(BSS)} < 2MK \ln K + \bar{S}'(M-K)(K-1) + \frac{\bar{S}'K(K-1)}{2} + 2\bar{S}'M(Q-1)$$
 (3.26)

where \bar{S}' denotes the average number of iterations between candidate subcarrier searching and subcarrier-allocation that the BSS algorithm actually uses. Note that, \bar{S}' is not necessary the same

Algorithm	Complexity
Direct Search	$\mathcal{O}(M!)$
Hungarian [185]	$\mathcal{O}(M^3)$
Greedy [80]	$\mathcal{O}(M^2)$
Maximal Greedy [86]	$\mathcal{O}(\alpha M^2)$
WUF Greedy [85]	$\mathcal{O}(M^2)$
WSA [83]	$\mathcal{O}(KM)$
BWSA	$\mathcal{O}(M^2)$
BSS	$\mathcal{O}(\min\{KM\ln K, \bar{S}'KM\})$

Table 3.3: The complexity of different subcarrier-allocation algorithms

value as S', for example, as shown in Table 3.2. In fact, with the information shown in Table 3.2, Stage II of the BSS algorithm may not be activated until the number of iterations is closing the value of S'. As an example, when K=32 and Q=8, we can see in Table 3.2 that S'=7.76. In this case, the BSS algorithm can keep its Stage II inactive during the first six iteration, and only starts activating it afterwards. Consequently, we have in average $\bar{S}'=1.76$ instead of S'=7.76 and, hence, the complexity of the BSS algorithm can be reduced. From (3.26), we can know that the BSS algorithm has a complexity of $\mathcal{O}(\min\{MK \ln K, \bar{S}'MK\})$.

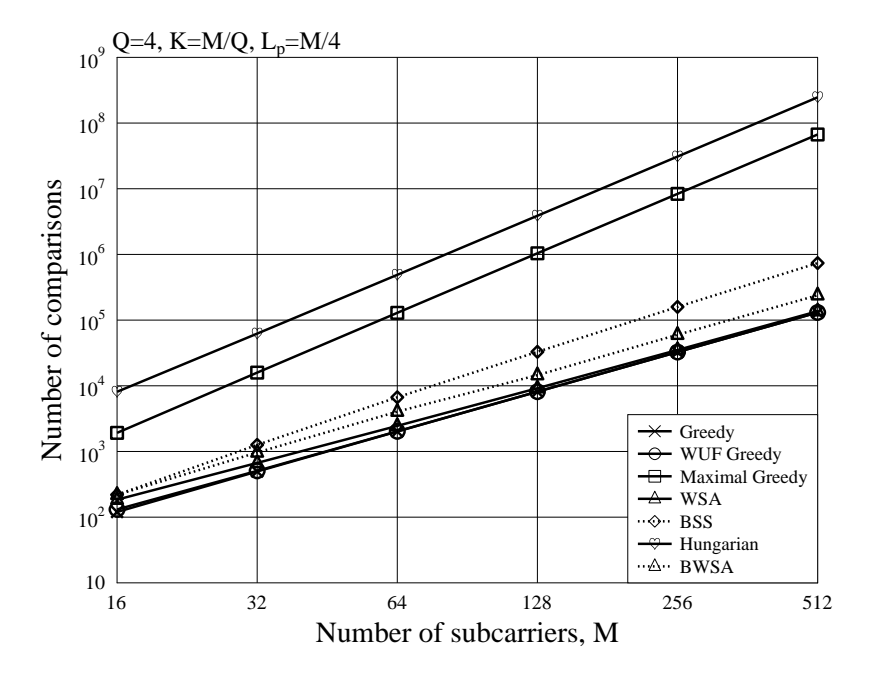


Figure 3.6: Comparisons of the number of comparisons required by the various subcarrierallocation algorithms for Q=4, when communicating over the frequency-selective Rayleigh fading channels with $L_p=M/4$ time-domain resolvable paths.

The complexity of the proposed BWSA and BSS algorithms and that of some other subcarrierallocation algorithms considered are summarized in Table 3.3. It can be observed that the greedy algorithm has the lowest complexity, while the direct exhaustive search algorithm demands the highest complexity. The Hungarian method [83, 86, 191], which is optimum as the direct search algorithm, has the complexity $\mathcal{O}(M^3)$. The proposed BWSA algorithm has the same complexity as the Greedy algorithm, and its complexity is lower than that of the proposed BSS algorithm. While, the complexity of the BSS algorithm relies on \bar{S}' of the average number of iterations between candidate subcarrier searching and subcarrier-allocation, which we can usually choose to be in the range 1-3, as shown by the analysis below (3.26).

In Figure 3.6, we compare the number of comparisons required by the various algorithms, when the system experiences frequency-selective fading, and each user is assigned Q=4 subcarriers. Furthermore, for the BSS algorithm, we used $\bar{S}'=3$, while for the maximal greedy algorithm, we used $\alpha=M$. Explicitly, both the proposed BWSA and the BSS algorithms require much lower comparisons than the maximal greedy algorithm and the Hungarian algorithm. However, the two algorithms proposed require more comparisons than the greedy, WUF greedy or the WSA algorithm. Due to its iterative characteristic, the BSS algorithm needs more comparisons than the BWSA algorithm.

3.9 Upper- and Lower-Bound Bit Error Rate of Subcarrier-Allocation Algorithms

Due to the non-linear operations used by the various subcarrier-allocation algorithms, it is usually very difficult to derive the closed-form expressions for the BER of the considered subcarrier-allocation algorithms. Instead, in this section, we analyze the upper- and lower-bound BER for all possible subcarrier-allocation algorithms operated in downlink OFDMA systems, by considering two specific subcarrier-allocation schemes: (a) fixed allocation, (b) *unfair* greedy algorithm. Note that, when the unfair greedy algorithm is employed, a subcarrier is always allocated to the user with the best subchannel quality, regardless of how many subcarriers it has. Explicitly, the fixed allocation provides the BER upper-bound, while the unfair greedy algorithm yields the BER lower-bound of all possible fair or unfair subcarrier-allocation schemes. In this section, the BER upper- and lower-bound are analyzed by assuming square quadrature amplitude modulation (QAM) baseband modulation. Let us first consider the BER upper-bound.

3.9.1 Upper-bound Bit Error Rate of Subcarrier-Allocation Algorithms

In the context of the fixed subcarrier-allocation algorithm, each subcarrier is always assigned to a same user regardless of its subchannel quality, when fairness is assumed. Therefore, the fixed subcarrier-allocation gives the upper-bound of error rate of the subcarrier-allocation algorithms.

When fixed subcarrier-allocation is assumed, the average BER of OFDMA systems can be

written as

$$P_e = \frac{1}{M} \sum_{k \in \mathcal{K}} \sum_{q \in \mathcal{Q}_k} P_e^{(k,q)} = P_e^{(k,q)}$$
 (3.27)

where $k \in \mathcal{K}$, $q \in \mathcal{Q}_k$, $P_e^{(k,q)} = E[P_e^{(k,q)}(\gamma_{k,q})]$ denotes the average BER of data stream q of user k, here $E[\cdot]$ denotes the expectation operation, while $P_e^{(k,q)}(\gamma_{k,q})$ is the error probability conditioned on a given SNR $\gamma_{k,q}$. Specifically, when R-ary QAM (R-QAM) baseband modulation is employed, the average BER of OFDMA systems with fixed subcarrier-allocation can be expressed as [193–195]

$$P_{e} = \frac{2}{\sqrt{R} \log_{2} \sqrt{R}} \sum_{n=1}^{\log_{2} \sqrt{R}} \sum_{i=0}^{1 - 2^{-n} \sqrt{R} - 1} (-1)^{\lfloor \frac{2^{n-1}i}{\sqrt{M}} \rfloor} \left(2^{k-1} - \lfloor \frac{2^{n-1}i}{\sqrt{R}} + \frac{1}{2} \rfloor \right) P_{e,i}$$
(3.28)

in associated with

$$P_{e,i} = E\left[Q\left((2i+1)\sqrt{\frac{2\gamma_c}{R-1}}\right)\right] \tag{3.29}$$

where $\lfloor \cdot \rfloor$ denotes the floored integer. In (3.29), the Q-function is defined as $Q(x) = \frac{1}{\sqrt{2\pi}} \int_x^\infty e^{-t^2/2} dt$. Furthermore, γ_c is the SNR per symbol.

As shown in Section 3.4.1, when the channel-inverse power-allocation algorithm is applied, all sub-streams of all users have the same SNR, which is given by (3.12) and is rewritten as

$$\gamma_c = \frac{P}{N_0} \left(\sum_{k \in \mathcal{K}} \sum_{q \in \mathcal{Q}_k} \frac{1}{|h_{k,q}|^2} \right)^{-1} = \frac{P}{N_0} \left(\frac{1}{|h_{\Sigma}|^2} \right)^{-1}$$
(3.30)

Therefore, when substituting (3.30) into (3.29), it can be shown that

$$P_{e,i} = \int_0^\infty Q\left(\frac{\zeta}{\sqrt{x}}\right) f_{1/|h_{\Sigma}|^2}(x) dx$$

$$= \frac{1}{2} - \frac{\zeta}{\sqrt{8\pi}} \int_0^\infty x^{-3/2} \exp\left(-\frac{\zeta^2}{2x}\right) F_{1/|h_{\Sigma}|^2}(x) dx$$
(3.31)

where by definition

$$\zeta = (2i+1)\sqrt{\frac{2P}{(R-1)N_0}}. (3.32)$$

In (3.31), $f_{1/|h_{\Sigma}|^2}(x)$ is the PDF of $1/|h_{\Sigma}|^2$ and $F_{1/|h_{\Sigma}|^2}(x)$ represents the corresponding cumulative distribution function (CDF) of $1/|h_{\Sigma}|^2$. With the aid of the results in [196], we can express (3.31) as

$$P_{e,i} = \frac{1}{2} - \frac{1}{\pi} \int_0^\infty \frac{\Re(M_{1/|h_{\Sigma}|^2}(j\alpha))}{\alpha} \exp(-\zeta\sqrt{\alpha}) \sin(\zeta\sqrt{\alpha}) d\alpha$$

$$= \frac{1}{2} - \frac{4}{\pi} \int_{-1}^1 \frac{\Re(M_{1/|h_{\Sigma}|^2}(j(\frac{1+u}{1-u})^2))}{1-u^2} \exp(-\zeta\frac{1+u}{1-u}) \sin(\zeta\frac{1+u}{1-u}) du \qquad (3.33)$$

where $\Re(z)$ is the real part of z, and $M_{1/|h_{\Sigma}|^2}(w)$ is the moment generation function (MGF) of $1/|h_{\Sigma}|^2$.

From (3.30), we have $1/|h_{\Sigma}|^2 = \sum_{k \in \mathcal{K}} \sum_{q \in \mathcal{Q}_k} \frac{1}{|h_{k,q}|^2}$. When communicating over Rayleigh or Nakagami-m fading channels, the square of channel gain $|h_{k,q}|^2$, $(\forall k \in \mathcal{K}, \forall q \in \mathcal{Q}_k)$, obeys the Gamma distribution with the PDF given by $f_{|h_{k,q}|^2}(x; m_{k,q}, \Omega_{k,q})$ [180], where the parameters $m_{k,q}$ and $\Omega_{k,q}$ determine the fading severity and power. Then, according to [37, 196], we can express the MGF of $1/|h_{\Sigma}|^2$ as

$$M_{1/|h_{\Sigma}|^{2}}(w) = \prod_{k \in \mathcal{K}} \prod_{q \in \mathcal{Q}_{k}} \frac{2}{\Gamma(m_{k,q})} \left(\frac{-w}{\Omega_{k,q}}\right)^{2} K_{m_{k,q}} \left(2\sqrt{\frac{-w}{\Omega_{k,q}}}\right)$$
(3.34)

where the modified Bessel function $K_m(z)$ is defined in [197].

Finally, by substituting (3.33) and (3.34) into (3.28), we can obtain the average BER of the downlink OFDMA systems employing the fixed subcarrier-allocation and channel-inverse power-allocation algorithms.

3.9.2 Lower-bound Bit Error Rate of Subcarrier-Allocation Algorithms

One lower-bound BER for OFDMA systems employing subcarrier-allocation can be obtained, when considering the unfair greedy subcarrier-allocation algorithm. In this case, each of the subcarriers is allocated without concerning about fairness to the user with the best subchannel quality. Therefore, for each subcarrier, selection diversity with the order equaling to the number of users can be attained. Consequently, when the channel-inverse power-allocation is employed, all subcarriers attain the same SNR, which is expressed as

$$\gamma_c = \frac{P}{N_0} \left(\sum_{j \in \mathcal{M}} \frac{1}{|h_j|_{\text{max}}^2} \right)^{-1} = \frac{P}{N_0} |h_{\Sigma}'|^2$$
 (3.35)

where $|h_j|_{\text{max}}^2$ is the best squared channel gain of subcarrier j. Assume i.i.d fading for the K users of the jth subcarrier, the CDF of $|h_j|_{\text{max}}^2$ can be derived as

$$F_{|h_j|_{\max}^2}(x) = \Pr\left\{\max_{k \in \mathcal{K}} \{Y_k\} < x\right\}$$

$$= \prod_{k=1}^K \Pr\{Y_k < y\}$$

$$= \prod_{k=1}^K F_{|h_{j,k}|^2}(y)$$
(3.36)

where $F_{|h_{j,k}|^2}(y)$ is the CDF of $|h_{j,k}|^2$. Correspondingly, the PDF can be found as $f_{|h_j|_{\max}^2}(x)=\frac{dF_{|h_j|_{\max}^2}(x)}{dx}$. However, at this stage, it is extremely difficult to derive the closed-form MGF, CDF or PDF of $|h_{\Sigma}'|^2$ seen in (3.35). In order to circumvent this problem, we introduce the **Gamma-Approximation** (Gamma-Ap) to approximate $|h_{\Sigma}'|^2$ in (3.35) as a Gamma distributed random variable with the PDF expressed as $f_{|h_{\Sigma}'|^2}(x;m',\Omega')$, where $\Omega'=E[|h_{\Sigma}'|^2]$ and $m'=(\Omega')^2/E[(|h_{\Sigma}'|^2-1)^2]$

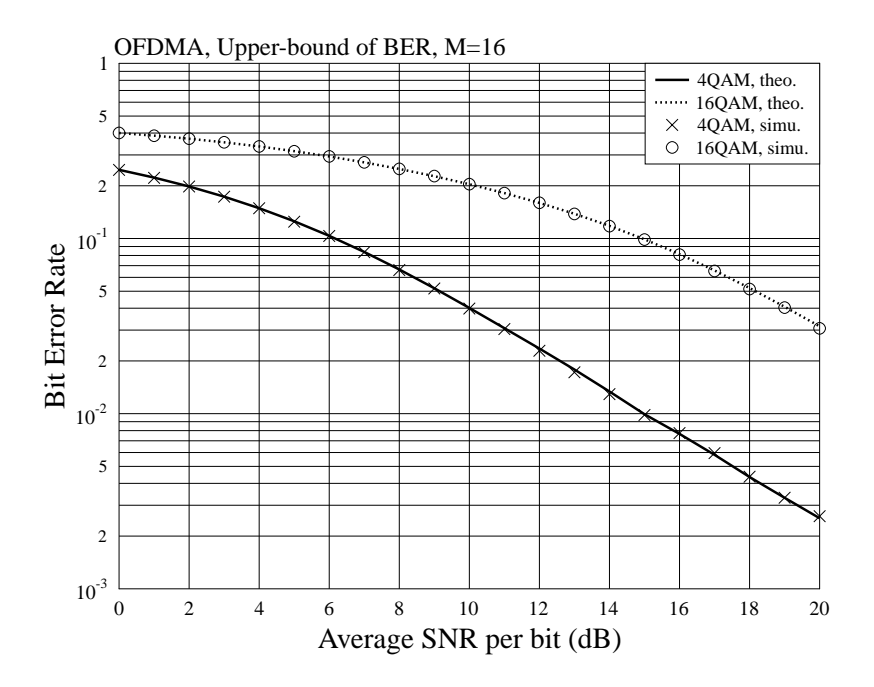


Figure 3.7: The BER upper-bound of subcarrier-allocation in the downlink OFDMA systems, where independent Rayleigh fading are assumed for all subcarriers of all users, and the 4QAM and 16QAM modulations are employed.

 $\Omega')^2$], which can be readily found by simulations based on about 10^4 realizations, as shown in [198].

With the aid of the Gamma-AP, it can be shown that, when the *R*-QAM baseband modulation is employed, the average lower-bound BER of OFDMA systems employing subcarrier-allocation can also be expressed as (3.28) and (3.29). Furthermore, (3.29) can be derived as [1,180]

$$P_{e,i}(m,\gamma_t) = \int_0^\infty Q\left((2i+1)\sqrt{\frac{2P}{(R-1)N_0}}x\right) f_{|h'_{\Sigma}|^2}(x;m',\Omega') dx$$

$$= \sqrt{\frac{\gamma_t}{\gamma_t + m'}} \frac{(1+\gamma_t/m')^{-m'}\Gamma(m'+1/2)}{2\sqrt{\pi}\Gamma(m'+1)} \times {}_2F_1\left(1,m'+1/2;m'+1;\frac{m'}{m'+\gamma_t}\right)$$
(3.37)

where $\gamma_t = P(2i+1)^2 \Omega' / [N_0(R-1)]$. In (3.37), ${}_2F_1(a,b;c;z)$ is the hypergeometric function that is defined as [181, 182].

In order to show the accuracy of the analytical results and the approximation, in Figures 3.7 and 3.8, we depict the BER of the OFDMA systems using the fixed subcarrier-allocation and the unfair greedy algorithm assisted subcarrier-allocation, where the theoretical and simulation results are compared. Explicity, in both figures, the BER results evaluated from the formulas perfectly match with that obtained from simulations. The accuracy of the Gamma-AP has also been illustrated in [198].

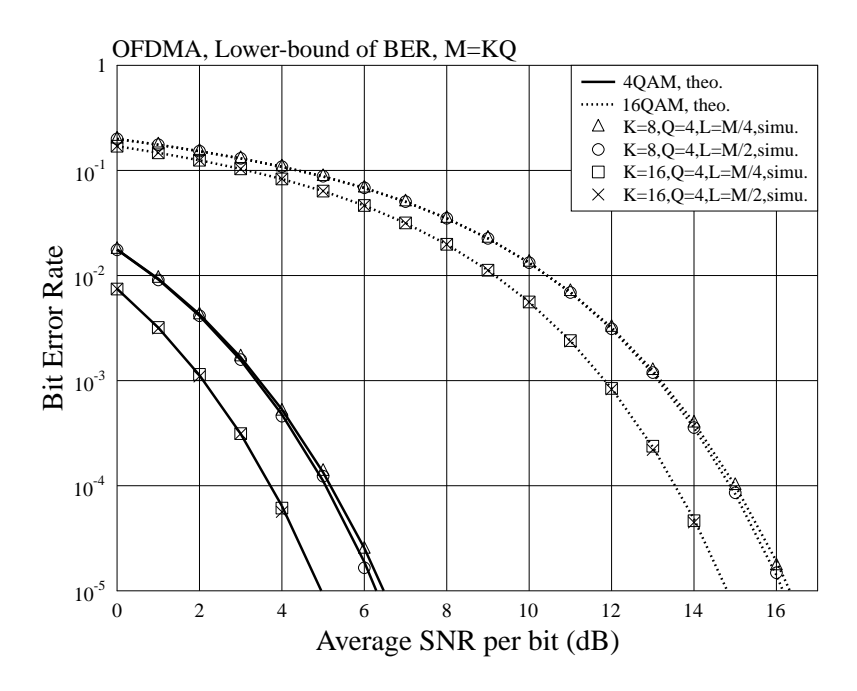


Figure 3.8: The BER lower-bound of subcarrier-allocation in the downlink OFDMA systems, where the 4QAM and 16QAM modulations are employed, when communicating over frequency-selective Rayleigh fading with L_p time-domain resolvable paths.

3.10 Performance Results

we demonstrate the achievable BER performance and spectrum-efficiency of the proposed BWSA and the BSS algorithms, and compare them with that of some other existing algorithms, when assuming either the channel-inverse or water-filling power-allocation algorithms. Specifically for BER performance, we assume that the OFDMA systems employ the quadrature phase-shift keying (QPSK) baseband modulation. For both the BER performance and spectrum-efficiency, we assume that the total transmission power per OFDM symbol is P = M = KQ, the downlink channels experience frequency-selective Rayleigh fading with L_p number of time-domain resolvable paths, and that, for the maximal greedy algorithm, a searching space containing $\alpha = M$ randomly-specified user orders is used. Note that, the spectrum-efficiency to be demonstrated in this section is evaluated by the formula

$$C = \frac{1}{M} \sum_{k=1}^{K} \sum_{j^* \in \mathcal{F}_k} \log_2 (1 + \gamma_{k,j^*})$$
 (3.38)

where γ_{k,j^*} represents the SNR of the j^* th subcarrier assigned to user k.

3.10.1 BER Performance

Figure 3.9 compares the BER performance of the BWSA, BSS and some other subcarrier-allocation algorithms from references. As marked in the figure, we assumed an OFDMA system having M =

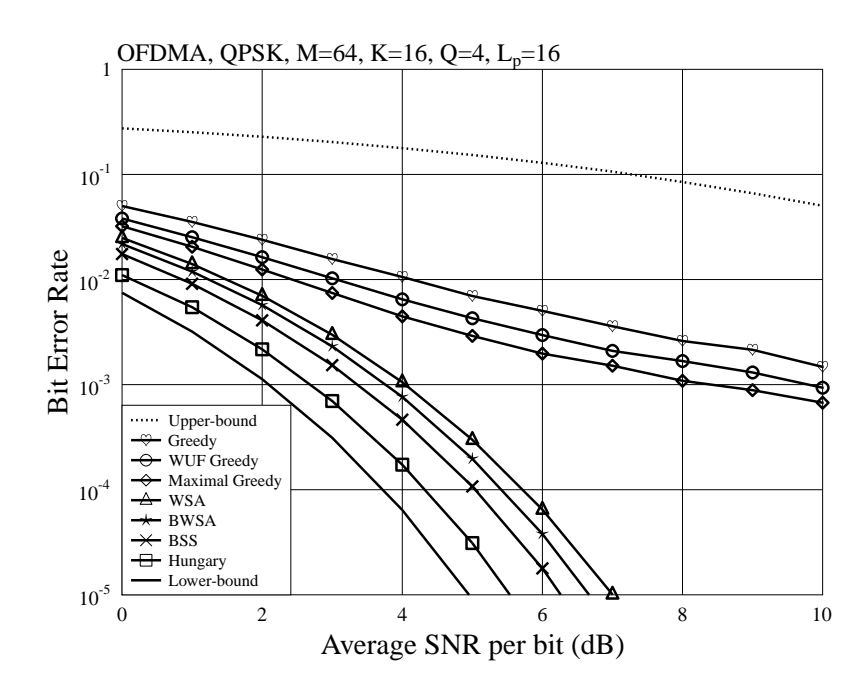


Figure 3.9: BER of downlink OFDMA systems employing various subcarrier-allocation algorithms and using M=64 subcarriers to support K=16 users, when communicating over frequency-selective Rayleigh fading with $L_p=16$ time-domain resolvable paths.

64 subcarriers to support K = 16 users. Clearly, we see that the BER curves of all the considered subcarrier-allocation schemes fall between the upper-bound BER of the fixed subcarrier-allocation and the lower-bound BER of the unfair greedy algorithm, which were derived in Section 3.9. All the dynamic subcarrier-allocation algorithms significantly outperform the fixed subcarrier-allocation corresponding to the upper bound. From Figure 3.9 we observe that the proposed BWSA and BSS algorithms achieve better BER performance than the other sub-optimum algorithms considered, but there is a small gap from the performance of the optimum Hungary algorithm. Both of them significantly outperform the greedy, WUF greedy and the maximal greedy algorithms. The BSS algorithm achieves a better BER performance than the BWSA algorithm, at the cost of higher complexity. In comparison with the WSA algorithm, the BWSA and the BSS algorithms have the gains of about 0.2 dB and 0.5 dB, respectively, at the BER of 10^{-5} .

In Figure 3.10, we consider to assign M=128 subcarriers to K=32 users, when communicating over the frequency-selective Rayleigh fading channels with $L_p=32$ time-domain resolvable paths. In addition to the observations in Figure 3.9, we can see that all the allocation algorithms now perform better than what they did in Figure 3.9. This is because assigning a larger number of subcarriers to more users results in a higher gain for any of the dynamic subcarrier-allocation schemes considered. Additionally, when comparing Figure 3.9 with Figure 3.10, we can see that the BER performance of both the BWSA and BSS algorithms becomes closer to that of the Hungarian algorithm, when M is increased from M=64 to M=128.

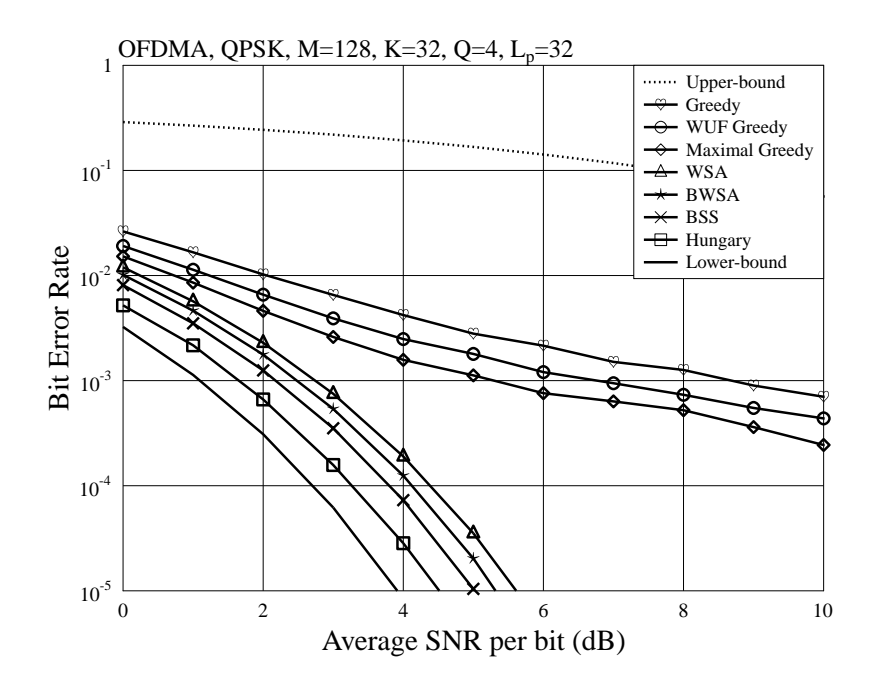


Figure 3.10: BER of downlink OFDMA systems employing various subcarrier-allocation algorithms and using M=128 subcarriers to support K=32 users, when communicating over frequency-selective Rayleigh fading with $L_p=32$ time-domain resolvable paths.

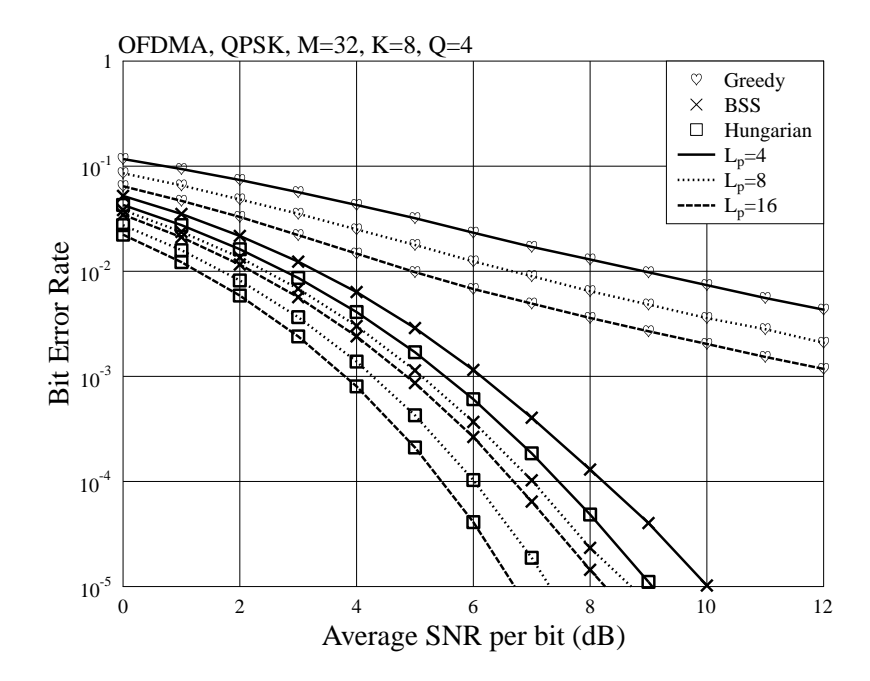


Figure 3.11: BER of the downlink OFDMA system employing various of subcarrier-allocation algorithms, experiencing frequency-selective Rayleigh fading, when K=8 users and M=32 subcarriers are considered.

In Figure 3.11, we compare of the BSS algorithm with the Hungarian algorithm when communicating over the frequency-selective fading channels with different numbers of multipaths. The

results clearly show performance improvement for all the three algorithms considered, as L_p increases. As shown in the figure, for the BSS and Hungarian algorithms, the slope slightly increases, as the value of L_p increases, which implies that the diversity gain slightly increases. However, for the greedy algorithm, the three BER curves are nearly in parallel, implying that there is no diversity gain, as L_p increases. Additionally, it can be noted that the error performance of the BSS algorithm gets closer to that of the Hungarian algorithm, as L_p increases.

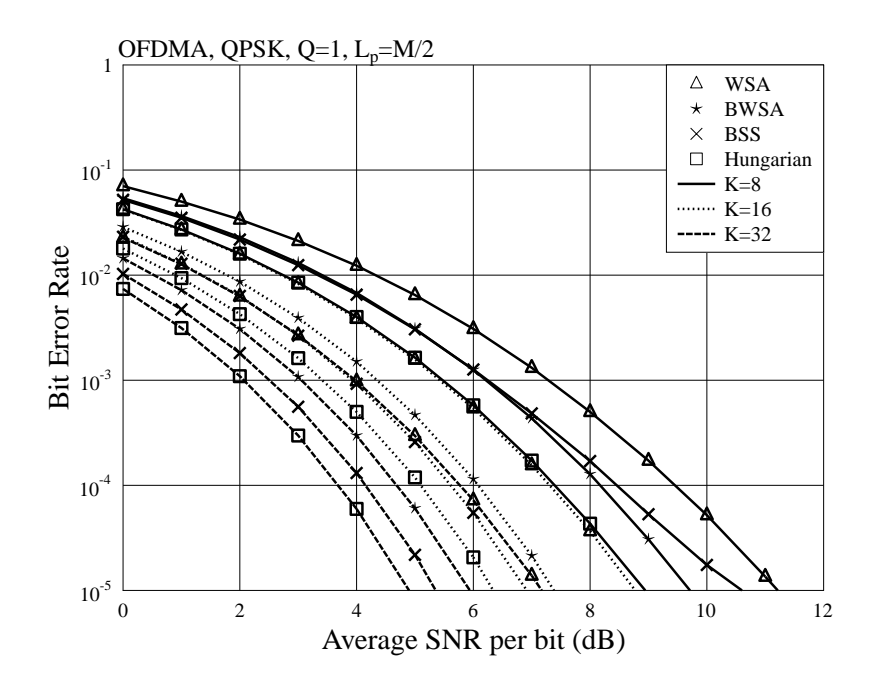


Figure 3.12: BER performance comparison of downlink OFDMA systems employing various subcarrier-allocation algorithms and using M subcarriers to support K=M users, when communicating over frequency-selective Rayleigh fading channels having $L_p=M/2$ time-domain resolvable paths.

Figure 3.12 compares the BER performance of the two proposed subcarrier-allocation algorithms, WSA and the Hungarian algorithms, when assuming that each user is assigned one subcarrier, i.e., when M=K, with respect to different number of subcarriers. As the results of Figure 3.12 show, for all the four algorithms considered, the BER performance improves, as the number of subcarriers/users involved increases, owing to the increased multiuser diversity gain. Both the BWSA and the BSS algorithms outperform the WSA algorithm, which becomes more declared, as the number of subcarriers/users increases. The BER performance achieved by the BSS algorithm becomes closer to that of the Hungarian algorithm, as the number of subcarriers/users becomes larger. This is because the probability of the BSS algorithm obtaining poor candidate subcarriers becomes smaller, when the number of subcarriers increases. When M=K=8, we observe that the BWSA algorithm outperforms the BSS algorithm when the average SNR is higher than 6 dB. However, when M=K=16 or 32, the BSS algorithm always achieves better BER performance than the BWSA algorithm. Furthermore, the performance gain of the BSS algorithm

Scrs Users	0	1	2	3
0	2.37	2.83	1.35	0.97
1	1.01	0.91	4.85	2.96
2	0.12	0.45	1.16	0.34
3	1.47	2.30	1.49	0.06

Table 3.4: An example for Channel Qualities of M = 4 Subcarriers of K = 4 Users.

over the BWSA algorithm is enhanced when M=K becomes larger. The above observations may imply that the BSS algorithm is near optimum, if it is operated in the large systems using many subcarriers to support many users, which are generally the cases in long-term evolution (LTE) and long-term evolution advanced (LTE-A) systems.

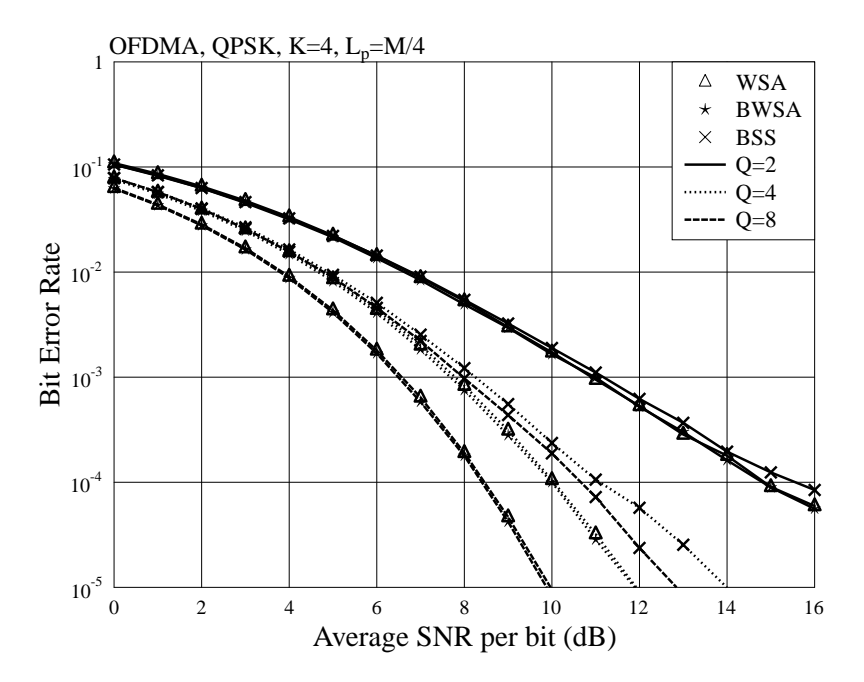


Figure 3.13: BER comparison of the BSS, BWSA and WSA algorithms for downlink OFDMA system supporting K=4 users and, experiencing frequency-selective Rayleigh fading with $L_p=M/4$ time-domain resolvable paths.

While the BSS algorithm is highly efficient, when it is operated in large OFDMA systems, it may not be as efficient as the WSA algorithm, when they are operated in small-sized OFDMA systems supporting a small number of users. Figure 3.13 addresses this issue, where the BSS and WSA algorithms are compared in the context of an OFDMA system supporting K=4 users. Explicitly, in this case, the BSS algorithm is always outperformed by the WSA algorithm. Therefore, the efficiency of the BSS algorithm is dependent on the number of users involved. It may become inefficient for operation in OFDMA systems supporting a small number of users. By contrast, the

proposed BWSA algorithm always outperforms the WSA algorithm, regardless of the size of the OFDMA systems considered, as shown in Figure 3.13. This is because the BWSA algorithm is an improved algorithm of the WSA algorithm, and it is capable of making use of more diversity than the WSA algorithm. However, we note that, when the system is small, as shown in Figure 3.13, the performance improvement of the BWSA algorithm over the WSA algorithm is small.

Let us explain the above observation using an example with the parameters M=4, K=4 and $q_k=1, \forall k\in\mathcal{K}$. The subchannel quality matrix for the four subcarriers of the four users are detailed in Table 3.4. According to Section 3.5.4, it can be shown that the allocation results obtained by the WSA algorithm are $\mathcal{F}_0=\{0\}$, $\mathcal{F}_1=\{3\}$, $\mathcal{F}_2=\{2\}$, $\mathcal{F}_3=\{1\}$. Correspondingly, the SNR attained is $\gamma_c=0.49$, when assuming the total transmission power of P=1. By contrast, when the BSS algorithm is applied, three iterations are required by the first stage to find the candidate subcarrier sets for the four users, which are $\tilde{\mathcal{F}}_0=\{0,1,2,3\}$, $\tilde{\mathcal{F}}_1=\{0,1,2,3\}$, $\tilde{\mathcal{F}}_2=\{3\}$ and $\tilde{\mathcal{F}}_3=\{0,1,2\}$. Then, according to Section 3.7.1, after the subcarrier-allocation, we obtain $\mathcal{F}_0=\{0\}$, $\mathcal{F}_1=\{2\}$, $\mathcal{F}_2=\{3\}$ and $\mathcal{F}_3=\{1\}$. From the allocation results, we can see that there are the third best, which are in fact the second worst, subcarriers allocated to users, giving the worst subchannel quality $A_{2,3}=0.34$ and the achieved SNR $\gamma_c=0.26$. This SNR is smaller than $\gamma_c=0.49$ obtained by the WSA algorithm.

3.10.2 Spectrum-Efficiency Performance

In this section, we investigate the spectrum-efficiency of the systems employing various subcarrierand power-allocation algorithms. The considered spectrum-efficiency in this section refers to the average throughput of the downlink OFDMA systems. For the sake of comparison, we consider both the channel-inverse and the water-filling assisted power-allocation schemes. Furthermore, for all the simulations in this section, we assume that the downlink transmissions experience frequencyselective Rayleigh fading with $L_p = M/4$ time-domain resolvable paths.

Above we have shown that the BWSA and BSS algorithms are capable of achieving the error performance that is close to the optimum Hungarian algorithm among the sub-optimum subcarrier-allocation algorithms considered, especially, when large OFDMA systems are considered. In Figure 3.14, we show that the BER performance of the BWSA and BSS algorithms are achieved without making a trade-off with the spectrum-efficiency, which determines the practically attainable throughput, of the OFDMA system. As seen in Figure 3.14, the BSS algorithm achieves the highest spectrum-efficiency among the considered sub-optimum subcarrier-allocation algorithms, which is also the one closest to the optimum Hungarian algorithm. The spectrum-efficiency attained by the BWSA algorithm is close to that of the BSS algorithm, and is higher than that of the other sub-optimum algorithms.

Furthermore, the probability density functions (PDFs) shown in Figure 3.15 explain that the BWSA and BSS algorithms also result in better fairness of data rates for the invoked users than

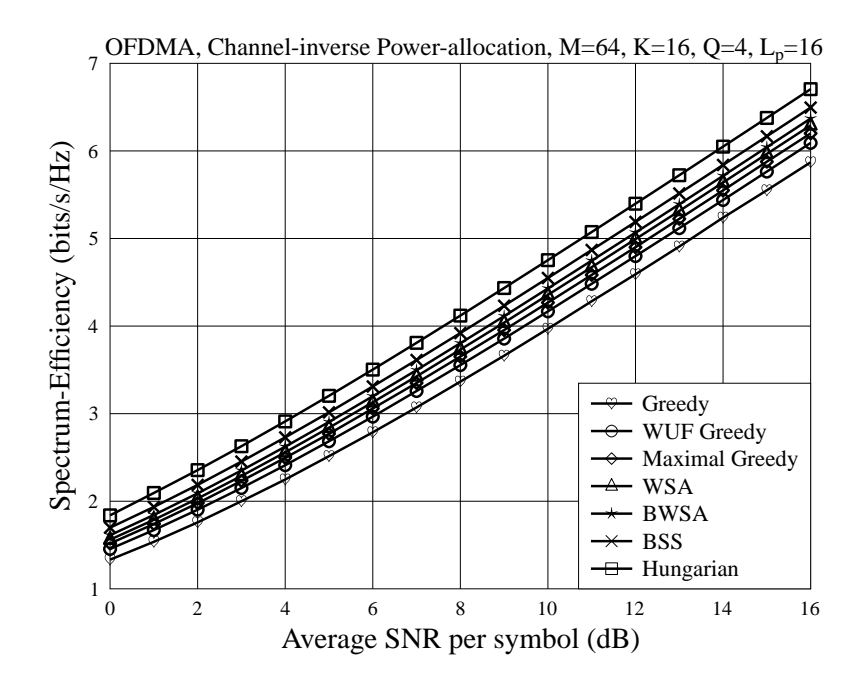


Figure 3.14: Spectrum-efficiency of downlink OFDMA systems employing the channel-inverse power-allocation algorithm and various subcarrier-allocation algorithms as well as using M=64 subcarriers to support K=16 users, when communicating over frequency-selective Rayleigh fading with $L_p=16$ time-domain resolvable paths.

the the Greedy and WSA algorithms considered. As shown in the figure, the obtained spectrum-efficiency by the Greedy algorithm distributes over a big range, meaning that there are often some users obtaining high throughput, while some others obtaining very low throughput. The BWSA algorithm is capable of improving the WSA algorithm by avoiding more worst subchannels than the WSA algorithm. Certainly, it achieves a higher minimum spectrum-efficiency and also better fairness. By contrast, the BSS algorithm cannot only provide users the highest possible throughput, but also protect their throughput to be stable and fair. These are reflected by the BSS's distributions, which have relatively high average spectrum-efficiency and relatively high peak values, in comparison to the other two schemes, as seen in Figure 3.15.

Finally, in Figure 3.16, we show the spectrum-efficiency of the OFDMA systems employing various subcarrier-allocation algorithms, when employing the water-filling power-allocation algorithm. Although in this case all the algorithms achieve a similar spectrum-efficiency, we can see that the proposed two algorithms are still slightly better than the other sub-optimum algorithms. The reason behind the above observations is that the water-filling algorithm maximizes the spectrum-efficiency of a system by allocating more power to the better subchannels. As a result, the system's spectrum-efficiency is dominated by the good subchannels, making the spectrum-efficiency of different subcarrier-allocation schemes similar. However, as the greedy algorithm as well as its some extensions may allocate users poor subchannels, the water-filling algorithm may make the fairness of these algorithms worse in terms of the data rate attained per user. By contrast, when the BWSA

3.11. Conclusions 105

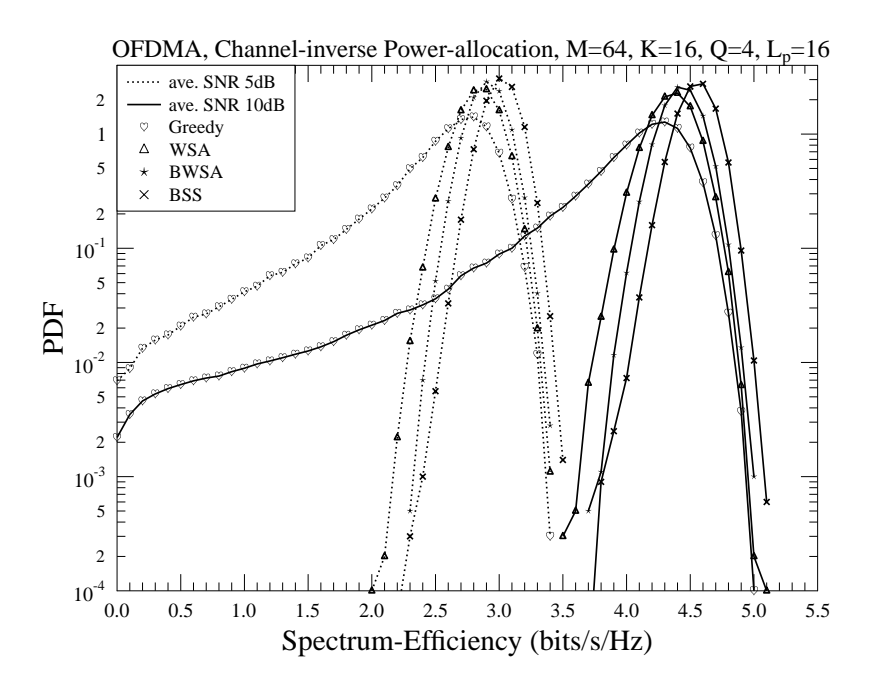


Figure 3.15: PDF of Spectrum-efficiency of downlink OFDMA systems employing the channel-inverse power-allocation algorithm and various subcarrier-allocation algorithms as well as using M=64 subcarriers to support K=16 users, when communicating over frequency-selective Rayleigh fading with $L_p=16$ time-domain resolvable paths.

or BSS algorithm is employed, users are rarely assigned with poor subchannels. Consequently, even when the water-filling power-allocation is used, relatively fair data rates across the users can be guaranteed.

3.11 Conclusions

Motivating to avoid assigning as many users as possible the worst subchannels, or to assign users the best possible subchannels, in this chapter, we have designed two low-complexity subcarrier-allocation algorithms for downlink OFDMA systems, namely, the BWSA and BSS algorithms. The BWSA algorithm represents a two-dimensional extension of the existing one-dimensional WSA algorithm. It outperforms the WSA algorithm, while the WSA algorithm outperforms many other existing sub-optimum subcarrier-allocation algorithms, such as, the greedy algorithm, as shown in [83]. In contrast to the BWSA algorithm considering the subcarrier-allocation starting from the worst subchannels, the BSS algorithm starts its operations from the best subchannels. Specifically, the BSS algorithm is operated in two stages: 1) a search stage to find the best possible candidate subchannels, and 2) an allocation stage to assign users the subchannels chosen from the candidate subchannels. Our studies illustrate that the search stage can usually be completed within a relatively small number of iterations, especially, when large OFDMA systems supporting a big number of users are considered. This property guarantees the BSS to have low complexity. When operated

3.11. Conclusions 106

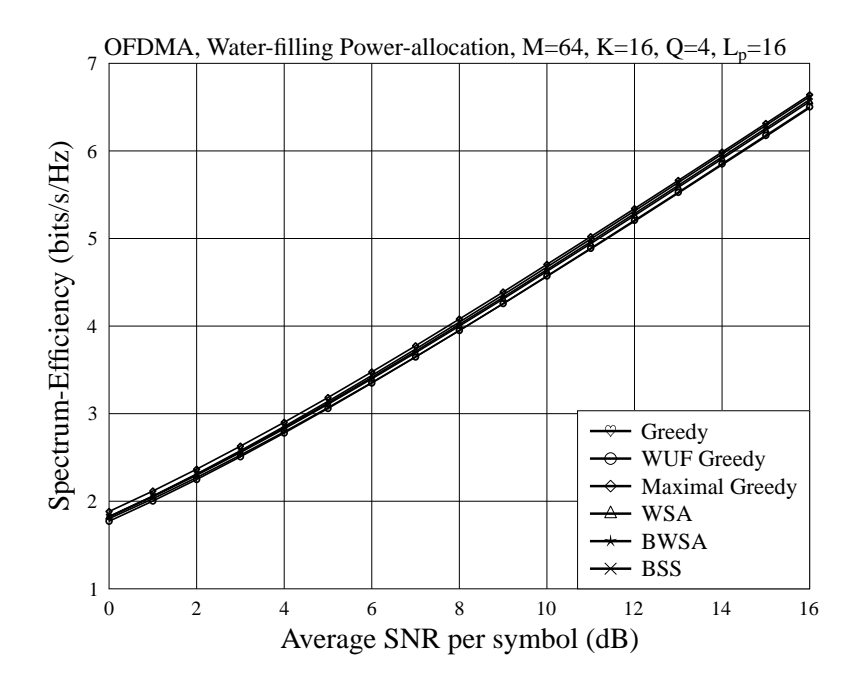
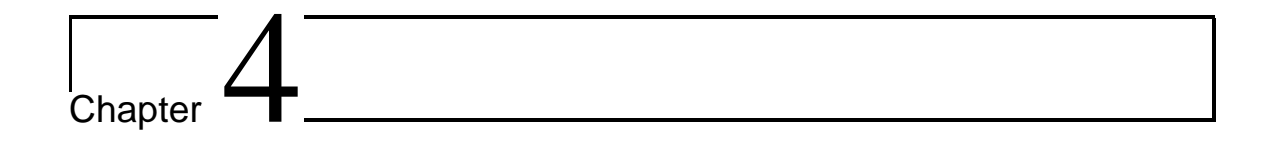


Figure 3.16: Spectrum-efficiency of downlink OFDMA systems employing the water-filling power-allocation algorithm and various subcarrier-allocation algorithms as well as using M=64 subcarriers to support K=16 users, when communicating over frequency-selective Rayleigh fading with $L_p=16$ time-domain resolvable paths.

in relatively large OFDMA systems, such as $K \ge 8$, the proposed BSS algorithm outperforms the other sub-optimum subcarrier-allocation algorithms considered in this chapter, as well as the BWSA algorithm. As the communication channel becomes more frequency-selective, the BSS algorithm's performance becomes close to that of the optimum Hungarian algorithm. The BSS algorithm's performance is dependent on the number of users K involved. As the number of users involved increases, the achievable BER and spectrum-efficiency performance move closer to that achieved by the Hungarian algorithm. However, the BSS algorithm may be outperformed by the BWSA or WSA algorithm, when the OFDMA systems are very small, such as, of using M=4 subcarriers to support K=4 users. By contrast, the BWSA algorithm is efficient, regardless of the size of the OFDMA systems. Certainly, in practice, the OFDMA systems are usually large. For example, the LTE/LTE-A OFDMA systems typically employ 64 - 2048 subcarriers. Additionally, our proposed BWSA and BSS algorithms are capable of providing users fairer data rates than the other sub-optimum algorithms, in addition to the relatively higher throughput.



Resource Allocation in Single-cell Downlink MC DS-CDMA Systems

4.1 Introduction

In Chapter 3, we have proposed two novel subcarrier-allocation algorithms for the downlink OFDMA systems. In this chapter, we consider the resource allocation for the more generalized multicarrier DS-CDMA systems, where each subcarrier transmits DS spreading signals.

In wireless communications, multicarrier signalling have attracted wide attention as one of the promising candidates for high speed broadband wireless communications. In multicarrier systems, multicarrier modulation/demodulation can be implemented with the aid of low-complexity fast Fourier transform (FFT) techniques. When appropriately configured, some multicarrier schemes, such as OFDMA and orthogonal multicarrier DS-CDMA, employ the capability to suppress intersymbol interference (ISI) [1,61]. Furthermore, the multicarrier DS-CDMA (MC DS-CDMA), in which each subcarrier uses direct-sequence (DS) spreading, employs a high number of degrees-of-freedom for high-flexibility design and reconfiguration [61].

It is now well-known that exploiting the time-varying characteristics of wireless channels is capable of significantly enhancing the quality-of-service (QoS) of wireless communication systems. Specifically, with the aid of dynamic subcarrier-allocation to users, promising energy- and spectrum-efficiency can be attained by making use of the embedded multiuser diversity [77]. Owing to its above-mentioned metrics, subcarrier-allocation in broadband multicarrier systems, such as in LTE/LTE-A OFDMA, now becomes highly important. In literature, such as in [77, 78, 80, 82–86], various subcarrier-allocation algorithms have been proposed and studied for downlink OFDMA systems and other multicarrier systems. Specifically, the (unfair) greedy algorithm has been investigated in [78] without considering the fairness, which aims at maximizing the total sum rate of downlinks. By contrast, in [80, 82], the (fair) greedy algorithm has been studied, when fairness

4.1. Introduction 108

is taken into account, making each user select the best subcarrier(s) from the available subcarriers. However, in terms of reliability, the users allocated the subcarriers at the late stages of the fair greedy algorithm often have poor performance. In order to circumvent the shortcomings of the fair greedy algorithm, in [83], a worst subcarrier avoiding (WSA) algorithm has been proposed for subcarrier-allocation in the downlink OFDMA and frequency division multiple access (FDMA) systems. The studies in [83] demonstrate that the WSA algorithm can effectively avoid assigning users the subchannels of the poorest qualities, and can hence attain higher reliability than the fair greedy algorithm. In subcarrier-allocation, the Hungarian algorithm [185] is recognized the optimum algorithm in the sense of maximum reliability, which has been investigated, for example, in [83, 86]. However, the Hungarian algorithm is of high complexity for implementation in the OFDMA systems with a high number of subcarriers supporting a high number of users.

In LTE/LTE-A downlink OFDMA systems, the number of subcarriers is usually very high, which is up to 2048, and the number of users supported may also be very high. These characteristics generate some problems, such as, the PAPR problem, and may prevent schedulers from employing the optimum or even some promising sub-optimum subcarrier-allocation schemes, due to their complexity constraint. As the complexity of the optimum or sub-optimum subcarrier-allocation algorithms is mainly dependent on the number of subcarriers, reducing the number of subcarriers may effectively decrease the operation complexity of these algorithms. It is well-known that, owing to the employment of DS spreading, the MC DS-CDMA can use a significantly lower number of subcarriers than the multicarrier schemes, such as the OFDMA, which do not employ DS spreading. For example, Figure 1.7 shows the transmitter schematic of a MC DS-CDMA system, where each data stream is DS spread before assigning a subcarrier. Furthermore, MC DS-CDMA employs the flexibility to configure its number of subcarriers according to the frequency-selectivity of wireless channels, so that each subcarrier experiences independent fading. In this case, the number of subcarriers of MC DS-CDMA will be at the order of the number of time domain resolvable paths of wireless channels and, hence, will usually be low [1]. Therefore, in MC DS-CDMA, the relatively high-complexity optimum or near-optimum subcarrier-allocation algorithms may be employed in order to achieve the best possible performance.

A range of researches [97–100, 105, 107, 125] have been dedicated to the field of resource allocation in the MC-CDMA and MC DS-CDMA systems. The allocations of transmission rate, subcarrier and power have been considered in MC-CDMA system in [97] for minimizing the total transmission power when given certain bit error rate (BER) requirements. The authors of [99, 100] have compared the capacity performance of the MIMO-OFDMA and MIMO-MC-CDMA systems, when adaptive power allocation is employed. In [125], adaptive allocations of subchannel, power and alphabet size have been addressed in a distributed MC DS-CDMA system, in order to minimize the transmit power under the constraint of packet rate.

Against this background, in this chapter we study the subcarrier-allocation issue in MC DS-CDMA systems. Specifically, some representative algorithms including the greedy and greedy-

4.2. System Model 109

class algorithms, WSA algorithm, etc., are introduced to and studied associated with the MC DS-CDMA systems. In this chapter, we propose a range of subcarrier-allocation algorithms with the aid of channel-inverse power-allocation scheme, aiming at maximizing the reliability of the downlink MC DS-CDMA system. The proposed algorithms includes the parallel Hungarian algorithm, worst case avoiding (WCA) and the worst case first (WCF) algorithms. Furthermore, we propose a so-called iterative worst excluding (IWE) algorithm, which allows the proposed subcarrier-allocation algorithms to achieve even better performance. In this chapter, the BER performance of the MC DS-CDMA systems employing various subcarrier-allocation algorithms is investigated, when assuming that subcarrier channels experience independent fading. Our simulation results reveal that the proposed algorithms may significantly outperform the existing sub-optimum algorithms. Furthermore, the IWE algorithm is effective for further improving the BER performance of some subcarrier-allocation algorithms.

Note that, the BWSA and BSS algorithms studied in Chapter 3 can also be straightforwardly extended to the MC DS-CDMA systems considered in this chapter. However, in this chapter, we focus on the other novel subcarrier-allocation algorithms.

The rest of this chapter is organized as follows. Section 4.2 gives the system model and makes the main assumptions. Section 4.3 briefly reviews three existing subcarrier-allocation algorithms for acting as benchmarks and Section 4.4 introduces the proposed algorithms. Section 4.5 presents a novel scheme which facilitates various subcarrier-allocation algorithms. Section 4.6 analyzes and compares the complexity of the considered subcarrier-allocation algorithms. Section 4.7 investigates and evaluates the error rate and the spectrum-efficiency performance of the downlink MC DS-CDMA systems employing various power- and subcarrier-allocation algorithms. At last, conclusions are summarized in Section 4.8.

4.2 System Model

We consider a single-cell downlink MC DS-CDMA system, which consists of one base station (BS) communicating with *K* mobile users. We assume that each of the communicating terminals, including BS and *K* mobile users, employs one antenna for signal receiving and transmission. Signals transmitted from BS to mobile users are MC DS-CDMA signals using time (T)-domain DS spreading [1] and the spreading factor is expressed as *N*. For clarity, the variables and notations used in this chapter are summarized as follows:

K Number of mobile users;

 \mathcal{K} Set of user indexes, defined as $\mathcal{K} = \{0, 1, \dots, K-1\}$;

N Spreading factor of DS spreading;

M Number of subcarriers of MC DS-CDMA systems;

4.2. System Model 110

 \mathcal{M} Set of subcarrier indexes, defined as $\mathcal{M} = \{0, 1, \dots, M-1\}$;

 $h_{k,j}$ Channel gain of subcarrier j of user k;

C $(N \times K)$ -dimensional spreading matrix with columns consisting of the spreading sequences taken from a $(N \times N)$ orthogonal matrix. Note that, some columns of C may be the same in the case of K > N. In this case, the corresponding users are operated on different subcarriers;

 \mathcal{F}_i Set of indexes for up to N users assigned to subcarrier j;

 $|\mathcal{F}|$ Cardinality of the set \mathcal{F} , representing the number of elements in set \mathcal{F} ;

 P_k Transmission power for user k;

P Total transmission power of BS, $P = \sum_{k \in \mathcal{K}} P_k$;

 $A_{k,j}$ Channel quality of subcarrier (subchannel) j of user k, $A_{k,j} = |h_{k,j}|^2/(2\sigma^2)$, where $\sigma^2 =$ $1/(2\bar{\gamma}_s)$ denotes the single-dimensional noise power at a mobile user and $\bar{\gamma}_s$ denotes the average signal-to-noise ratio (SNR) per symbol.

In this chapter, we assume that each user is allocated one spreading code of one subcarrier. Consequently, we have

$$\bigcup_{m \in \mathcal{M}} \mathcal{F}_m = \mathcal{K},\tag{4.1}$$

$$|\mathcal{F}_m| = N, \quad \forall m \in \mathcal{M}$$
 (4.2)

$$|\mathcal{F}_m| = N, \quad \forall m \in \mathcal{M}$$
 (4.2)
 $\mathcal{F}_m \cap \mathcal{F}_j = \emptyset, \quad \text{if } m \neq j, \ \forall m, j \in \mathcal{M}$

where \emptyset means an empty set. Constraint (4.1) implies that all subcarriers must be allocated to users, (4.2) means that there are N users sharing one subcarrier, and, moreover, (4.3) indicates that each user has only one data stream supported by a DS code on one subcarrier.

Let us assume that the data symbols to be transmitted by the BS to the K mobile users are expressed as $\mathbf{x} = [x_0, x_1, \dots, x_{K-1}]^T$, where x_k is the data symbol to user k, which is assumed to satisfy $E[x_k] = 0$ and $E[|x_k|^2] = 1$. Furthermore, let us assume that the j'th subcarrier is assigned to user k. Then, considering that the M subcarriers are orthogonal, the signal received by user k from the j'th subcarrier can be written as

$$\mathbf{y}_k = h_{k,j'} \mathbf{C}_k \mathbf{PWx} + \mathbf{n}_k \tag{4.4}$$

where, in addition to the notations mentioned previously, y_k is a length-N observation vector, $\mathbf{n}_k = [n_{k,0}, \dots, n_{k,N-1}]^T$ is a length-N noise vector at user k, while \mathbf{C}_k is a $(N \times K)$ matrix formed from C by setting those columns corresponding to the subcarriers different from the kth user's subcarrier to zero vectors, as the result of using orthogonal subcarriers. In this chapter, we assume that uplinks and downlinks are operated in the TDD mode. Hence, an uplink channel and

4.2. System Model

its corresponding downlink channel can be assumed to be reciprocal. In this way, the BS is capable of obtaining the knowledge of all the KM downlink subchannels and, hence, it can preprocess the signals to be transmitted by setting $\mathbf{W} = \text{diag}\{w_0, w_1, \dots, w_{K-1}\}$, where $w_k = h_{k,j'}^* / \sqrt{|h_{k,j'}|^2}$ and $(\cdot)^*$ denotes the conjugate operation.

In this chapter, we assume that the BS employs one of the two power-allocation schemes, namely the channel-inverse and the water-filling assisted power-allocation schemes, which have been detailed in Sections 3.4.1 and 3.4.2. In (4.4), the power assigned to each user can be expressed in matrix form as $\mathbf{P} = \text{diag}\{P_0, P_1, \dots, P_{K-1}\}$. Consequently, after the despreading for user k using its spreading code \mathbf{c}_k , the kth column of \mathbf{C} , it can be shown that the decision variable generated by user k is

$$z_k = P_k \sqrt{|h_{k,j'}|^2} x_k + n_k \tag{4.5}$$

which yields the SNR

$$\gamma_k = P_k |h_{k,j'}|^2 \bar{\gamma}_s = P_k A_{k,j'}. \tag{4.6}$$

Explicitly, when allocating user k a subcarrier with higher subchannel quality $A_{k,j'}$, it attains a higher SNR, hence, yielding a higher spectrum-efficiency and a lower error rate for a given modulation scheme.

Note that the above considered MC DS-CDMA scheme can be straightforwardly extended to the scenarios where each of the users demands multiple data streams depending on the data rate required by the user. In this case, let q_k represent the number of data streams of user k ($k \in \mathcal{K}$). Then, we have the constraint of $\sum_{k \in \mathcal{K}} q_k \leq MN$ on the resource allocation, meaning that the total number of data streams does not exceed MN in order to avoid interference. In this extended MC DS-CDMA system, if $q_k \leq N$, user k can be assigned one subcarrier and its q_k data streams can be supported by assigning the user q_k different spreading codes. By contrast, if $q_k > N$, then, user k may be assigned multiple spreading codes and multiple subcarriers, in order to support the q_k data streams.

Note furthermore that our MC DS-CDMA scheme represents a generalized multicarrier scheme for studying resource allocation. First, when N=1, i.e., when there is no DS spreading, the MC DS-CDMA scheme is reduced to the conventional OFDMA. Correspondingly, we only require subcarrier-allocation, but no code-allocation, as that studied in Chapter 3. Second, when given the total bandwidth of a MC DS-CDMA system, there exists a trade-off between the number of subcarriers M and the spreading factor N, which determines the bandwidth of the subchannels. Hence, in a MC DS-CDMA system, the number of subcarriers can be reconfigured according to the communication environments, so that each of the subchannels experiences flat fading, while different subchannels experience relatively independent fading. Specifically, when operated in an environment where fading is highly frequency-selective, the system may be configured with a relatively high number of subcarriers but a relatively low spreading factor, in order to guarantee that

all subcarriers experience flat fading. By contrast, when the communication environment becomes less frequency-selective, the system may be reconfigured to use a smaller number of subcarriers but a bigger spreading factor. Owing to the reduced number of subcarriers and the increased bandwidth per subchannel, different subchannels will experience less correlated fading, the complexity of subcarrier-allocation can be reduced and, furthermore, the PAPR problem can be mitigated.

The objective of our subcarrier-allocation in this chapter is the same as that in Chapter 3, as shown in Section 3.3. We motivate to assign the *K* users the best set of subcarriers, i.e., the best *K* subchannels chosen from the *KM* possible subchannels. By allocating subcarriers in such a way, as shown in Chapter 3, there is no trade-off between reliability and spectrum-efficiency. Let us first consider the application of some existing subcarrier-allocation algorithms for the MC DS-CDMA systems.

4.3 Existing Subcarrier-Allocation Algorithms

In this section, we briefly introduce how some existing representative subcarrier-allocation algorithms can be extended for application in the single-cell downlink MC DS-CDMA systems. Three algorithms, including the greedy algorithm, the WSA algorithm, and the optimum Hungarian algorithm, are considered. We have detailed the greedy and WSA algorithms in Section 3.5. Therefore, we only highlight their advantages and drawbacks in this section, against which a range of subcarrier-allocation algorithms are proposed and investigated in the following sections. Furthermore, we also describe the optimum Hungarian algorithm, which is the subcarrier-allocation algorithm minimizing the error rate of a considered system.

Along with our analysis, an example is introduced, which employs M=4 subcarriers to support K=8 mobile users. Therefore, each subcarrier can be assigned to two users, which are distinguished by their DS spreading codes of length N=2. In this example, the subchannel qualities corresponding to the four subcarriers of the eight users are illustrated in Table 4.1, where the first row and first column denote the user and subcarrier indices, respectively. Furthermore, in our discussion, we assume that the channel-inverse assisted power-allocation algorithm is employed, and the total transmission power is P=1. From the above discussion and Chapter 3, we can realize that the main difference between the subcarrier-allocation in OFDMA systems and that in MC DS-CDMA systems is that one subcarrier is only assigned to one user in the OFDMA systems, while one subcarrier may be assigned to multiple users in the MC DS-CDMA systems. Let us first discuss the greedy algorithm.

In the context of the greedy algorithm [80], a subcarrier is always allocated to the two users (in contrast to one in OFDMA) having the best subchannel qualities among the users still requiring subcarriers. For the example considered, the subcarrier-allocation is carried out one by one from the first subcarrier to the last. Specifically, subcarrier 0 is allocated to users 2 and 5, as they correspond

	U0	U1	U2	U3	U4	U5	U6	U7
S0	3.73	4.95	5.06	0.34	2.37	5.04	1.59	3.42
S1	1.39	2.01	0.52	4.71	5.02	8.32	10.60	2.12
S2	0.41	1.63	4.52	0.87	0.91	3.50	2.49	0.65
S3	2.13	5.07	4.57	2.55	3.22	0.49	1.20	0.02

Table 4.1: Subchannel Quality Matrix for K = 8 Users of M = 4 Subcarriers.

to the two highest subchannel qualities on subcarrier 0 among the eight users. Hence, the allocation set for subcarrier 0 is updated to $\mathcal{F}_0 = \{2,5\}$. Similarly, subcarrier 1 is allocated to users 4 and 6, as they have the best subchannel qualities among the remaining users for this subcarrier, yielding $\mathcal{F}_1 = \{4,6\}$. Similarly, we can obtain $\mathcal{F}_2 = \{1,3\}$ and $\mathcal{F}_3 = \{0,7\}$. According to the allocation results, when the channel-inverse power-allocation is employed, it can be shown that the attainable SNR is given by $\gamma_c = \left(\sum_{k \in \mathcal{F}_j} A_k^{-1}\right)^{-1} = 0.019$, while the worst (minimum) subchannel quality of the allocated subcarriers is $\min_{k \in \{\mathcal{F}_j\}} \{A_{k,j}\} = 0.02$, which dominates the attainable SNR and hence the achievable error performance.

Explicitly, the greedy algorithm has the advantage of low-complexity. However, at the later stages of allocation, the algorithm may have to assign users the subcarriers with very poor subchannel qualities, as there are no other options. As the above example shows, at the last stage, subcarrier 3 has to be allocated to user 7, which results in the poorest subchannel quality of $A_{7,3} = 0.02$.

The WSA algorithm is designed to avoid assigning users the subcarriers having the worst subchannel qualities [83]. With the aid of the example of Table 4.1, for each of the subcarriers, the worst subchannel quality is identified, denoted by bold value in (4.7). It can be readily known that the worst subchannel qualities corresponding to the four subcarriers are $A_0^{(\min)} = 0.34$ for subcarrier 0, $A_1^{(\min)} = 0.52$ for subcarrier 1, $A_2^{(\min)} = 0.41$ for subcarrier 2 and $A_3^{(\min)} = 0.02$ for subcarrier 3. Secondly, the subcarriers are arranged in the ascending order as $\{3,0,2,1\}$ according to their worst subchannel qualities, forming a matrix shown as

$$\begin{bmatrix} & U_0 & U_1 & U_2 & U_3 & U_4 & U_5 & U_6 & U_7 \\ S_3 & 2.13 & \underline{5.07} & \underline{4.57} & 2.55 & 3.22 & 0.49 & 1.20 & \textbf{0.02} \\ S_0 & \underline{3.73} & 4.95 & 5.06 & \textbf{0.34} & 2.37 & \underline{5.04} & 1.59 & 3.42 \\ S_2 & \textbf{0.41} & 1.63 & 4.52 & 0.87 & \underline{0.91} & 3.50 & \underline{2.49} & 0.65 \\ S_1 & 1.39 & 2.01 & \textbf{0.52} & \underline{4.71} & 5.02 & 8.32 & 10.60 & \underline{2.12} \end{bmatrix}$$
 (4.7)

where, the worst subchannel qualities are represented by boldface values. Finally, based on the above-derived matrix, the subcarriers are allocated to the eight users in the principles of the greedy algorithm, from the first row to the last row, yielding the allocation results $\mathcal{F}_0 = \{0,5\}$, $\mathcal{F}_1 = \{3,7\}$, $\mathcal{F}_2 = \{4,6\}$, and $\mathcal{F}_3 = \{1,2\}$, corresponding to the underlined numbers in (4.7). With the aid of (3.12), the attainable SNR is evaluated to be $\gamma_c = \left(\sum_{k \in \mathcal{F}_j} A_k\right)^{-1} = 0.29$, when assuming that the total transmission power is P = 1. Furthermore, from (4.7) we can know that the worst

subchannel quality of the allocated subcarriers is $\min_{k \in \{\mathcal{F}_i\}} \{A_{k,j}\} = 0.91$.

Explicitly, the WSA algorithm significantly improves both the worst subchannel quality and the attainable SNR per subcarrier, after the power-allocation, in comparison with that obtained by the greedy algorithm. Owing to the above, the WSA algorithm is expected to achieve better error performance than the greedy algorithm [83].

The Hungarian algorithm has originally been proposed to solve the assignment problem in graph theory [185, 191], and been designed to find the minimum cost for a complete one-to-one matching, when given a square cost matrix. The Hungarian algorithm has also been introduced to deal with the subcarrier-allocation problem in multicarrier communication systems, such as, OFDMA [83, 86], which provides the optimum solutions in the sense of maximizing the reliability, such as, SNR, etc. The detailed operations for the Hungarian algorithm can be found in many references, such as in [185], here we briefly summarize its operation as follows.

Algorithm 5. (Hungarian Algorithm)

- **Step 1** Subtract the minimum cost of each row from each row in the cost matrix, until all rows and columns of the cost matrix appear zeros.
- **Step 2** Draw the minimum number of lines to cover the zeros in the reduced cost matrix. The final assignment is obtained when the number of lines equals N_{cost} , where N_{cost} is the size of the cost matrix. Otherwise, update the cost matrix, go to step 3.
- **Step 3** Identify the minimum cost of the uncovered part of the cost matrix, and then add the minimum cost to the covered columns as well as subtract it from the uncovered rows. Repeat steps 2 and 3 until the assignment is derived.

As the Hungarian algorithm has to be operated based on a square cost matrix, for our example of Table 4.1, we first need to modify it to a (8×8) square matrix, and change $\{A_{k,m}\}$ in Table 4.1 to $\{1/A_{k,j}\}$, as the Hungarian algorithm aims to find out the minimum sum of costs. The modified subchannel quality matrix can be expressed as

$$\begin{bmatrix} & U_0 & U_1 & U_2 & U_3 & U_4 & U_5 & U_6 & U_7 \\ S_0 & \underline{0.27} & 0.20 & 0.197 & 2.94 & 0.42 & 0.198 & 0.63 & 0.29 \\ S_1 & 0.72 & 0.50 & 1.92 & \underline{0.21} & 0.199 & 0.12 & 0.09 & 0.47 \\ S_2 & 2.44 & 0.61 & \underline{0.221} & 1.15 & 1.09 & 0.29 & 0.40 & 1.54 \\ S_3 & 0.47 & \underline{0.197} & 0.219 & 0.39 & 0.31 & 2.04 & 0.83 & 50 \\ S_0 & 0.27 & 0.20 & 0.197 & 2.94 & 0.42 & 0.198 & 0.63 & \underline{0.29} \\ S_1 & 0.72 & 0.50 & 1.92 & 0.21 & 0.199 & 0.12 & \underline{0.09} & 0.47 \\ S_2 & 2.44 & 0.61 & 0.221 & 1.15 & 1.09 & \underline{0.29} & 0.40 & 1.54 \\ S_3 & 0.47 & 0.197 & 0.219 & 0.39 & \underline{0.31} & 2.04 & 0.83 & 50 \end{bmatrix}$$

Then, the Hungarian algorithm as above-stated is executed on (4.8), which yields the allocation results $\mathcal{F}_0 = \{0,7\}$, $\mathcal{F}_1 = \{3,6\}$, $\mathcal{F}_2 = \{2,5\}$, $\mathcal{F}_3 = \{1,4\}$. It can be shown that the obtained SNR is $\gamma_c = 0.53$, when the channel-inverse assisted power-allocation is employed, while the worst subchannel quality of the allocated subcarriers is $\min_{j \in \mathcal{M}, k \in \mathcal{F}_i} \{A_{k,j}\} = 3.42$.

The Hungarian algorithm is the optimum algorithm, which gives the best subcarrier-allocation in terms of minimization of the error rate. However, the Hungarian algorithm demands a high complexity of $\mathcal{O}(K^3)$, which becomes a bottleneck for the practical implementation, when the number of users involved is high.

4.4 Proposed Subcarrier-Allocation Algorithms

In this section, we propose a range of subcarrier-allocation algorithms, for operation in the MC DS-CDMA systems. These algorithms aim to minimize the average BER of the system, but without making a trade-off with the throughput. First, we propose a so-called parallel Hungarian algorithm, in order to mitigate the high complexity issue suffered by the Hungarian algorithm. Then, we propose two low-complexity algorithms, namely the WCA and the WCF algorithms. These two algorithms are designed to improve the allocation results obtained by the WSA algorithm. For the sake of showing the principle, we describe the proposed algorithms in this section with the aid of the example of Table 4.1. Let's first discuss the parallel Hungarian algorithm.

4.4.1 Parallel Hungarian Subcarrier-Allocation Algorithm

In order to reduce the computational complexity, in this section, we propose a so-called parallel Hungarian algorithm for subcarrier-allocation schemes in the downlink MC DS-CDMA systems. As the name suggests, the proposed algorithm is based on the Hungarian algorithm [185], while is operated in parallel form.

From Section 4.3 and [185], we can know that the complexity of the Hungarian algorithm highly depends on the size of the cost matrix and is $\mathcal{O}(K^3)$ for the subcarrier-allocation in the considered MC DS-CDMA system. Hence, reducing the size of the cost matrix can significantly reduce the number of operations required, and hence the operational complexity. In our MC DS-CDMA systems, the number of subcarriers is M and the number of users supported is up to K = MN. As each of the subcarriers supports N users, we may divide the subcarrier-allocation process into N parallel sub-processes, each sub-process deals with M users and allocates one user to each of the M subcarriers with the aid of the Hungarian algorithm. In this case, the overall complexity of subcarrier allocation becomes $\mathcal{O}(NM^3)$, instead of $\mathcal{O}(N^3M^3)$ of the Hungarian algorithm operated on the original $(K \times K)$ cost matrix, where K = MN.

For the considered example of Table 4.1, the parallel Hungarian algorithm is operated based

on two (4×4) cost matrices, which may be obtained by randomly grouping the 8 users into two groups. For example, we may let users 0, 3, 4 and 6 be group 1, and users 1, 2, 5 and 7 be group 2. Correspondingly, the two (4×4) subchannel quality matrices are given by

$$\begin{bmatrix} & U_0 & U_3 & U_4 & U_6 \\ S_0 & \underline{0.27} & 2.94 & 0.42 & 0.63 \\ S_1 & 0.72 & \underline{0.21} & 0.199 & 0.09 \\ S_2 & 2.44 & 1.15 & 1.09 & \underline{0.40} \\ S_3 & 0.47 & 0.39 & \underline{0.31} & 0.83 \end{bmatrix} \begin{bmatrix} & U_1 & U_2 & U_5 & U_7 \\ S_0 & 0.20 & 0.197 & 0.198 & \underline{0.29} \\ S_1 & 0.50 & 1.92 & \underline{0.12} & 0.47 \\ S_2 & 0.61 & \underline{0.221} & 0.29 & 1.54 \\ S_3 & \underline{0.197} & 0.219 & 2.04 & 50 \end{bmatrix}. \tag{4.9}$$

Then, the Hungarian algorithm can be operated respectively based on the cost matrices derived from the above subchannel quality matrices, yielding the allocation results $\mathcal{F}_0 = \{0,7\}$, $\mathcal{F}_1 = \{3,5\}$, $\mathcal{F}_2 = \{2,6\}$, $\mathcal{F}_3 = \{1,4\}$, as the underlined subchannel qualities in (4.9) indicate. When the channel-inverse assisted power-allocation is used, it can be shown that the obtained SNR is $\gamma_c = 0.49$, while the worst subchannel quality of the allocated subcarriers is $\min_{j \in \mathcal{M}, k \in \mathcal{F}_j} \{A_{k,j}\} = 2.49$, which is worse than that obtained by the Hungarian algorithm in Section 4.3. However, for this specific example considered, the SNR obtained by the proposed parallel Hungarian algorithm is higher than that obtained by the other sub-optimum algorithms, such as, the greedy and the WSA algorithms discussed in Section 4.3.

In summary, the parallel Hungarian algorithm can be summarized as follows.

Algorithm 6. (Parallel Hungarian Algorithm)

- **Step 1** User grouping: Randomly divide the K users into N groups, each group has M users.
- **Step 2** Cost matrix forming: Corresponding to the N user groups, N number of $(M \times M)$ cost matrices are formed from the original $(M \times K)$ subchannel quality matrix.
- **Step 3** Subcarrier Allocation: The Hungarian algorithm is executed in the context of the N cost matrices to derive the subcarrier-allocation results.

From the example and the algorithm, explicitly, the proposed parallel Hungarian algorithm is a modified version of the Hungarian algorithm. The complexity depends on the size of the sub-cost matrices. There is a trade-off between the performance of the parallel Hungarian and the size of the sub-cost matrices, or the number of sub-cost matrices. When fewer sub-cost matrices are used, making the size of the sub-cost matrices larger, the achieved performance will be closer to that of the optimum Hungarian algorithm. However, the complexity also becomes higher.

4.4.2 Worst Case Avoiding Subcarrier-Allocation Algorithm

From the analysis in Section 4.4, we may classify the WSA algorithm as a subcarrier-oriented WSA algorithm, which is capable of avoiding assigning the (M-1) worst subchannels when

there are in total *M* subcarriers [83]. Specifically, for the considered example, the WSA algorithm can guarantee not to assign the three worst subchannels and, in most cases, four worsts can be avoided. In the MC DS-CDMA systems where the number of users is more than the number of subcarriers, in order to achieve better error performance, the subcarrier-allocation may be operated in the user-oriented mode, which may avoid assigning more of the worst subchannels. Inspired by the observation, in this section, we generalize the WSA algorithm to a so-called worst case avoiding (WCA) algorithm, the principles of which is first illustrated below.

When the WCA algorithm is employed, it always tries to avoid as many as possible the worst subchannels. The WCA algorithm is operated either in the subcarrier-oriented mode, i.e., WSA, or in the user-oriented mode. Specifically, for the example considered, as the number of users is higher than the number of subcarriers, the user-oriented mode will avoid a higher number of worst subchannels than the subcarrier-oriented WSA algorithm. In this case, the WCA algorithm first arranges the users in an ascending order of $\{7, 3, 0, 5, 2, 4, 6, 1\}$ according to their worst subchannel qualities of four subcarriers, yielding

$$\begin{bmatrix} & U_7 & U_3 & U_0 & U_5 & U_2 & U_4 & U_6 & U_1 \\ S_0 & \underline{3.42} & \textbf{0.34} & \underline{3.73} & 5.04 & 5.06 & 2.37 & 1.59 & 4.95 \\ S_1 & 2.12 & \underline{4.71} & 1.39 & \underline{8.32} & \textbf{0.52} & 5.02 & 10.60 & 2.01 \\ S_2 & 0.65 & 0.87 & \textbf{0.41} & 3.50 & 4.52 & \textbf{0.91} & \underline{2.49} & \underline{\textbf{1.63}} \\ S_3 & \textbf{0.02} & 2.55 & 2.13 & \textbf{0.49} & \underline{4.57} & \underline{3.22} & \textbf{1.20} & 5.07 \end{bmatrix}. \tag{4.10}$$

In (4.10) the subchannel qualities in boldface are the worst subchannel qualities of the users. Then, based on the ordered matrix (4.10), the subcarrier-allocation is carried out based on the greedy algorithm, one user at a stage, from the first to the last column. Consequently, the allocation results are $\mathcal{F}_0 = \{0,7\}$, $\mathcal{F}_1 = \{3,5\}$, $\mathcal{F}_2 = \{1,6\}$, and $\mathcal{F}_3 = \{2,4\}$. It can be shown that the SNR achieved by the WCA algorithm is $\gamma_c = 0.41$, and the worst subchannel quality of the allocated subcarriers is $\min_{k \in \{\mathcal{F}_i\}} \{A_{k,j}\} = 1.63$.

Straightforwardly, the proposed WCA algorithm is capable of achieving better allocation results than the WSA algorithm, as the WSA is a special case of the WCA. For the considered example, both the worst subchannel quality and the achievable SNR are improved in comparison with that obtained by the WSA algorithm. Furthermore, it can be shown that the WCA algorithm is capable of preventing allocating at least $\max\{K-N, M-1\}$ worst subchannels, instead of at least (M-1) of the WSA algorithm.

In summary, the WCA algorithm can be stated as follows.

Algorithm 7. (Worst Case Avoiding Algorithm)

Initialization: Subcarrier-oriented mode is chosen when $M \geq K$, otherwise, user-oriented mode is selected when M < K. Set $\tilde{\mathcal{M}} = \mathcal{M}$, $\tilde{\mathcal{K}} = \mathcal{K}$.

Step 1 Worst subchannel quality identification:

User-oriented mode - Find each user's worst subchannel quality: $A_k^{(\min)} = \min_{j \in \mathcal{M}} \{A_{k,j}\}.$

Subcarrier-oriented mode - Find each subcarrier's worst subchannel quality:

$$A_j^{(\min)} = \min_{k \in \mathcal{K}} \{A_{k,j}\}.$$

Step 2 User (or Subcarrier) ordering:

User-oriented mode - Arrange users in ascending order according to the worst subchannel qualities as $\{i_0, i_1, \dots, i_{K-1}\}$, if $A_{i_0}^{(\min)} \leq A_{i_1}^{(\min)} \leq \dots \leq A_{i_{K-1}}^{(\min)}$.

Subcarrier-oriented mode - Arrange subcarriers in ascending order according to the worst subchannel qualities as $\{q_0,q_1,\ldots,q_{M-1}\}$, if $A_{q_0}^{(\min)} \leq A_{q_1}^{(\min)} \leq \ldots \leq A_{q_{M-1}}^{(\min)}$.

Step 3 Allocation:

Based on the above-derived order, subcarrier-allocation is carried out one-by-one:

User-oriented mode - First, at the i_k th stage, subcarrier j^* is allocated to user i_k : $j^* = \arg\max_{j \in \tilde{\mathcal{M}}} \{A_{i_k,j}\}, i_k \in \mathcal{K}$. Then, if subcarrier j^* has been assigned to N = K/M users, it is removed from $\tilde{\mathcal{M}}$: $\tilde{\mathcal{M}} \leftarrow \tilde{\mathcal{M}} - \{j^*\}$.

Subcarrier-oriented mode - First, at the q_m th stage, user k^* is allocated to subcarrier q_m : $k^* = \arg\max_{k \in \tilde{\mathcal{K}}} \{A_{k,q_m}\}, q_m \in \mathcal{M}$. Then, if user k^* has been assigned the required number of subcarriers, it is deleted from $\tilde{\mathcal{K}}$: $\tilde{\mathcal{K}} \leftarrow \tilde{\mathcal{K}} - \{k^*\}$.

4.4.3 Worst Case First Subcarrier-Allocation Algorithm

According to the WCA algorithm described in Section 4.4.2, as the example shows, user 2 is allocated the subcarrier at the fifth stage, as its worst subchannel quality is $A_{2,1}=0.52$, which is the fifth worst of the users. However, from (4.10) we observe that subcarriers 0 and 1 cannot be the options for user 2, as each of these two subcarriers has been assigned to two users. In this case, the worst subchannel quality of user 2's available subcarriers becomes $A_{2,2}=4.52$, which is much larger than that of users 4, 6, and 1's available subcarriers (which are 0.91, 1.2 and 1.63, respectively). Therefore, in order to maximize the system's reliability, it would be beneficial to allocate the subcarriers to users 4, 6 and 1 before assigning the subcarrier to user 2.

Based on the above observation, we propose the WCF algorithm, which re-order the users (or subcarriers) according to the worst subchannel qualities of the available subcarriers (users). Specifically, for the MC DS-CDMA with K > M, during each stage, the algorithm first finds the worst subchannel quality of the unassigned users among only the subcarriers available for allocation, rather than finding the worst subchannel quality of the unsigned users among all the subcarriers, as done by the WCA algorithm. In detail, for the example considered, the WCF algorithm completes

the allocation user by user in 8 stages, which can be demonstrated as

$$\begin{bmatrix} & U_7 & U_3 & U_0 & U_5 & U_4 & U_6 & U_1 & U_2 \\ S_0 & \underline{3.42} & \textbf{0.34} & \underline{3.73} & 5.04 & 2.37 & 1.59 & 4.95 & 5.06 \\ S_1 & 2.12 & \underline{4.71} & 1.39 & \underline{8.32} & 5.02 & 10.60 & 2.01 & 0.52 \\ S_2 & 0.65 & 0.87 & \textbf{0.41} & 3.50 & \textbf{0.91} & \underline{2.49} & \textbf{1.63} & \underline{\textbf{4.52}} \\ S_3 & \textbf{0.02} & 2.55 & 2.13 & \textbf{0.49} & \underline{3.22} & \textbf{1.20} & \underline{5.07} & 4.57 \end{bmatrix}$$

where the eight columns stand for the eight stages of allocation, the subchannel qualities in boldface are the minimum of the users' subchannel qualities of the available subcarriers at the eight stages.

As shown in (4.11), at the first stage, the eight users' worst subchannel qualities of the subcarriers are the same as those in boldface in (4.11). In this case, user 7 ($A_{7,3} = 0.02$) is the worst and it is first assigned subcarrier 0 with the best subchannel quality of 3.42 among the four subcarriers. Similarly, as seen in (4.11), users 3, 0 and 5 are assigned subcarriers 1, 0 and 1, respectively, during the second, third and fourth stages. At this moment, we can see from (4.11) that the worst subchannel qualities of the available subcarriers for the four remaining users are $A_{1,2} = 1.63$ for user 1, $A_{2,2} = 4.52$ for user 2, $A_{4,2} = 0.91$ for user 4 and $A_{6,3} = 1.20$ for user 6, respectively. As we can see, the worst subchannel quality of the subcarriers available to user 2 becomes $A_{2,2} = 4.52$ instead of $A_{2,1} = 0.52$, as subcarrier 1 (also subcarrier 0) has already been assigned to two users in the previous four stages and cannot be assigned to other users. Therefore, at the fifth stage, a subcarrier is assigned to user 4, which is subcarrier 3. Similarly, subcarriers can be assigned to users 6, 1 and 2. From (4.11) we can know that the final allocation results are $\mathcal{F}_0 = \{0,7\}$, $\mathcal{F}_1 = \{3,5\}$, $\mathcal{F}_2 = \{2,6\}$ and $\mathcal{F}_3 = \{1,4\}$. The achievable SNR of the system is $\gamma_c = 0.49$ and the worst subchannel quality of the assigned subcarriers is $\min_{k \in \{\mathcal{F}_i\}} \{A_{k,j}\} = 2.49$.

In comparison with the WCA algorithm, as shown in Section 4.4.2, user 1 is forced to select subcarrier 2 at the last stage, which results in the poorest subchannel quality of $A_{1,2} = 1.63$. By contrast, under the WCF algorithm, user 1 has two options to choose either subcarrier 2 or subcarrier 3 at the seventh stage, and is then assigned the better subcarrier 3, which results in a subchannel quality of $A_{1,3} = 5.07$, which is significantly higher than $A_{1,2} = 1.63$ obtained by the WCA algorithm.

When comparing the WCF with the WCA, it is not hard to know that the WCF algorithm is capable of yielding the highest achievable SNR as well as the highest worst subchannel quality, as demonstrated by the above example. As the above example shows, the WCF algorithm successfully avoids assigning the worst subchannel quality by preventing the unreasonable allocation for user 2 at the fifth stage by the WCA algorithm. Therefore, the proposed WCF algorithm provides a more reliable and efficient way of subcarrier-allocation, while simultaneously captures all the advantages of the WCA algorithm. In summary, the WCF algorithm is stated as follows.

Algorithm 8. (Worst Case First Algorithm)

Initialization: User-oriented mode is chosen when M < K, subcarrier-oriented mode is used when $M \ge K$. Set $\tilde{\mathcal{K}} = \mathcal{K}$, $\tilde{\mathcal{M}} = \mathcal{M}$. Set $\mathcal{F}_j = \emptyset$ for all $j \in \mathcal{M}$.

Repeat:

Step 1 *User-oriented mode* - Identify the worst subchannel quality of each user:

$$A_k^{(min)} = \min_{j \in \tilde{\mathcal{M}}} \{A_{k,j}\}, \text{ for all } k \in \tilde{\mathcal{K}}.$$

Subcarrier-oriented mode - Identify the worst subchannel quality of each subcarrier:

$$A_i^{(min)} = \min_{k \in \tilde{\mathcal{K}}} \{A_{k,j}\}, \text{ for all } j \in \tilde{\mathcal{M}}.$$

Step 2 User-oriented mode - Find the user with the minimum of the worst subchannel qualities:

$$k^* = \arg \min_{k \in \tilde{\mathcal{K}}} \{A_k^{(\min)}\}.$$

 $\label{eq:subcarrier-oriented mode - Find the subcarrier with the minimum of the worst subchannel qualities: $j^* = \arg\min_{j \in \tilde{\mathcal{M}}} \{A_j^{(\min)}\}.$$

Step 3 User-oriented mode - Assign user k^* the subcarrier with the best subchannel quality: $q' = \arg\max_{a \in \tilde{\mathcal{M}}} \{A_{k^*,q}\}$, then $\mathcal{F}_{q'} \leftarrow \mathcal{F}_{q'} \cup \{k^*\}$.

Subcarrier-oriented mode - Allocate subcarrier j^* to the user with the best subchannel quality: $i' = \arg\max_{i \in \tilde{\mathcal{K}}} \{A_{i,j^*}\}$, then $\mathcal{F}_{j^*} \leftarrow \mathcal{F}_{j^*} \bigcup \{i'\}$.

Step 4 User-oriented mode - Remove user k^* from $\tilde{\mathcal{K}}$: $\tilde{\mathcal{K}} \leftarrow \tilde{\mathcal{K}} - \{k^*\}$. Remove subcarrier q' from $\tilde{\mathcal{M}}$ if $|\mathcal{F}_{q'}| = N$: $\tilde{\mathcal{M}} \leftarrow \tilde{\mathcal{M}} - \{q'\}$.

Subcarrier-oriented mode - Remove subcarrier j^* from $\tilde{\mathcal{M}}$: $\tilde{\mathcal{M}} \leftarrow \tilde{\mathcal{M}} - \{j^*\}$. Remove user i' from $\tilde{\mathcal{K}}$ if it has been assigned the required number of subcarriers: $\tilde{\mathcal{K}} \leftarrow \tilde{\mathcal{K}} - \{i'\}$.

Stop if
$$\tilde{\mathcal{K}} = \emptyset$$
, or $\tilde{\mathcal{M}} = \emptyset$.

Note again that the BWSA and BSS algorithms proposed in Chapter 3 can also be applied straightforwardly for subcarrier-allocation in the MC DS-CDMA systems. Since the principles and performance have been detailed in Chapter 3, they are not repeated in this chapter.

4.5 Iterative Worst Excluded (IWE) Algorithms

In this section, we propose a general algorithm called as the iterative worst excluding (IWE), which can be employed in associated with various of subcarrier-allocation algorithms, including the WSA, WCA and the WCF. With the aid of the IWE algorithm, the error rate performance of subcarrier-allocation algorithms may achieve further improvement. Let us first illustrate the principles of the IWE algorithm.

4.5.1 Principles of Iterative Worst Excluding Algorithms

As the name suggests, the proposed IWE algorithm aims to achieve an improved BER performance by iteratively updating the associated subchannel quality matrix. During each iteration, the IWE algorithm removes the worst subchannel qualities of the candidate subcarriers or the candidate users, before carrying out the subcarrier-allocation. After the subcarrier-allocation at an iteration, the allocation results obtained are compared with those obtained from the last iteration, in order to observe whether any performance improvement is gained. If there is performance gain, the algorithm continues to the next iteration. Finally, the algorithm stops, when there is no further performance improvement or when the maximum number of iterations is reached. In the following, we demonstrate the principles of the IWE algorithm in conjunction with the WCF subcarrier-allocation algorithm, which can be referred to as the IWE assisted WCF (IWE-WCF) algorithm. Furthermore, we compare the IWE-WCF algorithm with the other algorithms proposed in Section 4.4.

In the context of the IWE-WCF algorithm, the WCF algorithm is first carried out based on the subchannel quality matrix given in Table 4.1 during the first (initial) iteration. Correspondingly, the allocation results are given in Section 4.4.3 and the attainable SNR is $\gamma_c^{(1)} = 0.49$, where the superscript of (1) indicates the first iteration. At the second iteration, the worst subchannel qualities of the eight users are eliminated before operating again the WCF algorithm, in order to avoid assigning them to users. More specifically, the process of the second iteration can be shown with the aid of (4.12)

$$\begin{bmatrix} U_7 & U_3 & U_0 & U_6 & U_4 & U_5 & U_2 & U_1 \\ S_0 & 3.42 & \times & 3.73 & \textbf{1.59} & 2.37 & 5.04 & 5.06 & 4.95 \\ S_1 & 2.12 & \underline{4.71} & \textbf{1.39} & \underline{10.60} & 5.02 & 8.32 & \times & 2.01 \\ S_2 & \textbf{0.65} & \textbf{0.87} & \times & 2.49 & \times & \underline{\textbf{3.50}} & \underline{\textbf{4.52}} & \times \\ S_3 & \times & 2.55 & 2.13 & \times & \underline{\textbf{3.22}} & \times & 4.57 & \underline{\textbf{5.07}} \end{bmatrix}$$

$$(4.12)$$

where 'x' stands for the worst subchannel quality of an user which is removed before the subcarrier allocation, referred to as worst excluding (WE). After the WE, we can see in (4.12) that subcarrier 0 can be allocated to any of the remaining 7 users. We define these 7 users as the candidate users of subcarrier 0, expressed as $\tilde{\mathcal{F}}_0 = \{0, 1, 2, 4, 5, 6, 7\}$. Simultaneously, we can see that subcarrier 1 also has 7 candidate users. However, both subcarrier 2 and 3 have only five candidate users.

Following the WE process, the algorithm carries out the condition checking, in order to know whether the subcarrier-allocation can be completed based on the updated subchannel quality matrix. In order to fulfill the allocation, two conditions have to be met. Otherwise, the following subcarrier-allocation will not be carried out and the algorithm stops. In detail, the two conditions are as follows.

Condition (a): The number of candidate users of each subcarrier exceeds, K/M, of the number of

users to be assigned to one subcarrier. This condition can be expressed as

$$|\tilde{\mathcal{F}}_j| \ge K/M, \quad \forall j \in \mathcal{M}.$$
 (4.13)

Condition (b): Each subcarrier can only be assigned to K/M different users and each user is only assigned one subcarrier, which can be expressed as

$$|\tilde{\mathcal{F}}_j \cup \tilde{\mathcal{F}}_q| \ge 2K/M, \qquad j \ne q, \forall j, q \in \mathcal{M}.$$
 (4.14)

Specifically, for the example considered, we can observe from the updated matrix in (4.12) that the above two conditions can be met. Thus, it guarantees that each subcarrier can be allocated to two different users and each user attains one subcarrier. Therefore, we can proceed the WCF algorithm based on the updated matrix of (4.12). This process can also be shown with the aid of (4.12), where the boldface value under each user is the worst subchannel quality among the remaining users. Upon following the principles of the WCF algorithm, the new allocation results can be obtained, which are shown by the underlined values in (4.12). The results are $\mathcal{F}_0^{(2)} = \{0,7\}$, $\mathcal{F}_1^{(2)} = \{3,6\}$, $\mathcal{F}_2^{(2)} = \{2,5\}$ and $\mathcal{F}_3^{(2)} = \{1,4\}$. It can be shown that the achievable SNR of the system is $\gamma_c^{(2)} = 0.53$, while the worst subchannel quality of the allocated subcarriers is $\min_{k \in \{\mathcal{F}_i^{(2)}\}} \{A_{k,j}\} = 3.42$.

From the results of the second iteration, we can see that both the SNR and the worst subchannel quality are improved in comparison with those obtained from the first iteration. Therefore, the IWE-WCF algorithm continues to the third iteration, and the WE process is again first carried out, yielding

$$\begin{bmatrix} U_0 & U_1 & U_2 & U_3 & U_4 & U_5 & U_6 & U_7 \\ S_0 & 3.73 & 4.95 & 5.06 & \times & \times & 5.04 & \times & 3.42 \\ S_1 & \times & \times & \times & 4.71 & 5.02 & 8.32 & 10.60 & 2.12 \\ S_2 & \times & \times & \times & \times & \times & \times & 2.49 & \times \\ S_3 & 2.13 & 5.07 & 4.57 & 2.55 & 3.22 & \times & \times & \times \end{bmatrix}. \tag{4.15}$$

Then, the two required conditions are checked. Explicitly, the candidate user set of subcarrier 2 contains only one user and becomes $\tilde{\mathcal{F}}_2 = \{6\}$. However, for the example considered, each subcarrier is required to be allocated to N=2 users. Hence, condition (a) described in (4.13) is not satisfied, and the algorithm hence stops. Consequently, the results obtained from the second iteration are taken as the final allocation results.

For convenience, the main steps of the IWE assisted subcarrier-allocation algorithms can be described by the flow chart in Figure 4.1. In detail, during the initialization of the IWE algorithm, with the specific subcarrier-allocation algorithm is chosen, and the initial (first) iteration of subcarrier-allocation is carried out. After the initialization, the IWE scheme proceeds to the second iteration,

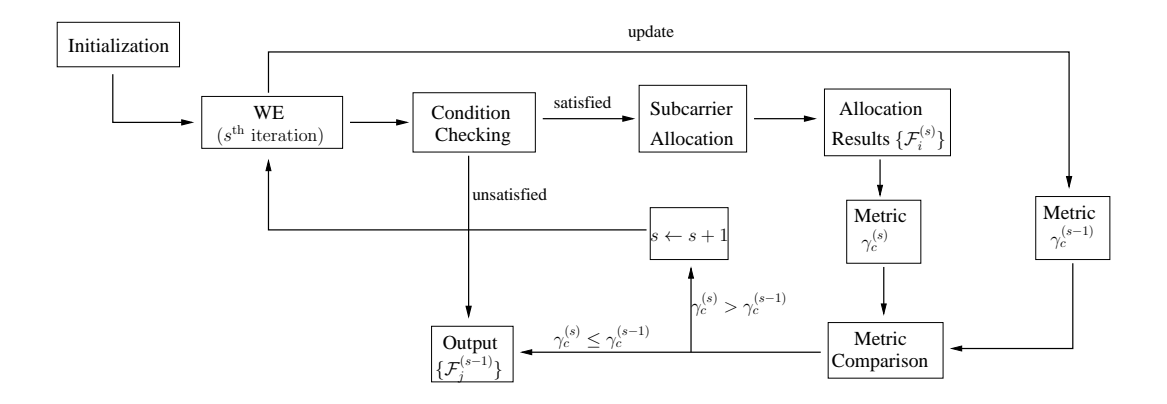


Figure 4.1: Flow chart showing the steps of the IWE algorithm.

and sets s=2. During each iteration with $s\geq 2$, the WE process is first carried out, as shown in the figure. Note that, the WE can be operated either in user direction or in subcarrier direction, which is dependent on the subcarrier-allocation algorithm employed, the number of subcarriers as well as the number of users involved. For example, when the IWE-WCF algorithm is employed, the WE is carried out in user direction. By contrast, when the IWE-WSA algorithm is used, the WE process is operated in subcarrier direction, i.e., the worst subchannel quality of each of the subcarriers is removed. As shown in Figure 4.1, following the WE block, the algorithm checks the conditions for assignment. When the two conditions as mentioned in this section are satisfied, it proceeds to the subcarrier-allocation. Otherwise, the IWE algorithm stops and takes the results obtained in the (s-1)th (previous) iteration as the final subcarrier-allocation. If the sth iteration of subcarrier-allocation is carried out, the allocation results of the sth (current) iteration are compared with those of the previous iteration against the performance metric. If performance is improved, the algorithm continues to the next iteration. Otherwise, the IWE algorithm stops and the allocation results from the previous iteration are taken as the final allocation results.

4.5.2 Characteristics of Iterative Worst Excluding Algorithms

The IWE algorithm employs a range of advantages in the sense of improving the error performance in comparison with the various subcarrier-allocation algorithms found in references. First, the IWE algorithm can be easily implemented in conjunction with an existing subcarrier-allocation algorithm, in order to enhance its performance, as discussed in Section 4.5.1. The core of the IWE algorithm is the WE process, which meliorates the subchannel quality matrix prior to operating subcarrier-allocation. Based on the improved subchannel quality matrix, the subcarrier-allocation followed can hence improve the error performance. Second, the subcarrier-allocation algorithm assisted by the IWE algorithm can always guarantee error performance improvement in comparison with that without using the IWE. In Section 4.5.1, we only described the operation procedure of the IWE-WCF algorithm. Similarly, we can also form the IWE aided WSA (IWE-WSA) algorithm,

Algorithm	IWE-WCF				IWE-WCA				IWE-WSA			
M N	4	8	16	32	4	8	16	32	4	8	16	32
1	1.76	2.14	2.44	2.58	2.20	2.75	2.74	2.73	2.20	2.75	2.74	2.73
2	1.70	2.12	2.40	2.55	1.96	2.45	2.65	2.72	2.42	2.64	2.67	2.71
4	1.60	2.03	2.34	2.52	1.78	2.30	2.61	2.71	2.43	2.55	2.65	2.70
8	1.49	1.89	2.25	2.46	1.63	2.18	2.56	2.70	2.42	2.51	2.64	2.69

Table 4.2: Average number of iterations for the IWE aided subcarrier-allocation algorithms.

the IWE aided WCA (IWE-WCA) algorithm, etc., the performance of which will be evaluated in Section 4.7. It should be noted that, the greedy algorithm was designed not to maximize the minimum of subchannel qualities. Hence, the IWE algorithm may not assist the greedy algorithm and its extensions in improving the error performance. Finally, from our studies, we find that the IWE algorithm converges fast and is usually operated with a low number of iterations, which guarantees the IWE aided algorithms low complexity.

As the number of iterations required by the IWE algorithm is an important factor, which affects the performance and complexity of the associated subcarrier-allocation algorithms, in Table 4.2, we summarize the average number of iterations required by the various IWE aided subcarrierallocation algorithms for some cases. For this table, we assumed for the considered downlink MC DS-CDMA system that all subcarriers of all users experience independent Rayleigh fading and the Gaussian noise of the same variance. Furthermore, we assumed that the number of users supported by the system is K = MN. Each of the results in the table was obtained by averaging over the outcomes of 10⁵ simulations. From the results, we can observe that the three IWE aided subcarrierallocation algorithms always require a low average number of iterations, which is $\bar{S} < 3$ for all the considered cases. Moreover, from the table, a few other observations can be identified. First, given a constant N value, it can be shown that the average number of iterations normalized by the number of subcarriers M, i.e., \bar{S}/M , decreases explicitly as M increases, even though, for most cases, the average number of iterations \bar{S} slightly increases as M becomes larger. Second, for most cases, \bar{S} in general becomes smaller as the spreading factor increases for a constant M. Furthermore, the IWE-WSA algorithm requires in average a slightly bigger number of iterations than the other two algorithms considered. This is mainly because the IWE-WSA algorithm carries out the WE operations in subcarrier direction, while the other two algorithms run the WE operations in user direction.

Furthermore, in Figure 4.2, we illustrate the probability mass function (PMF) of the number of iterations required by the three IWE aided subcarrier-allocation algorithms, where the results are obtained from 10^5 realizations. Associated with the studies, we assumed M = 16, K = 64

and N=4. It can be observed that the number of iterations is a variable and, for most cases, the allocation requires 2 iterations. However, the allocation process sometimes requires up to 6 iterations. Furthermore, the probability of requiring 8 iterations is nearly zero, which is still much smaller than the number of users K=64. From Table 4.2 and Figure 4.2, we therefore can conclude that the IWE aided algorithms usually demand a low number of iterations, which ensures a low complexity for implementation. Note that, in practice, we may set the maximum number of iterations to three or four, which guarantees the most of the available gain, while limits the complexity.

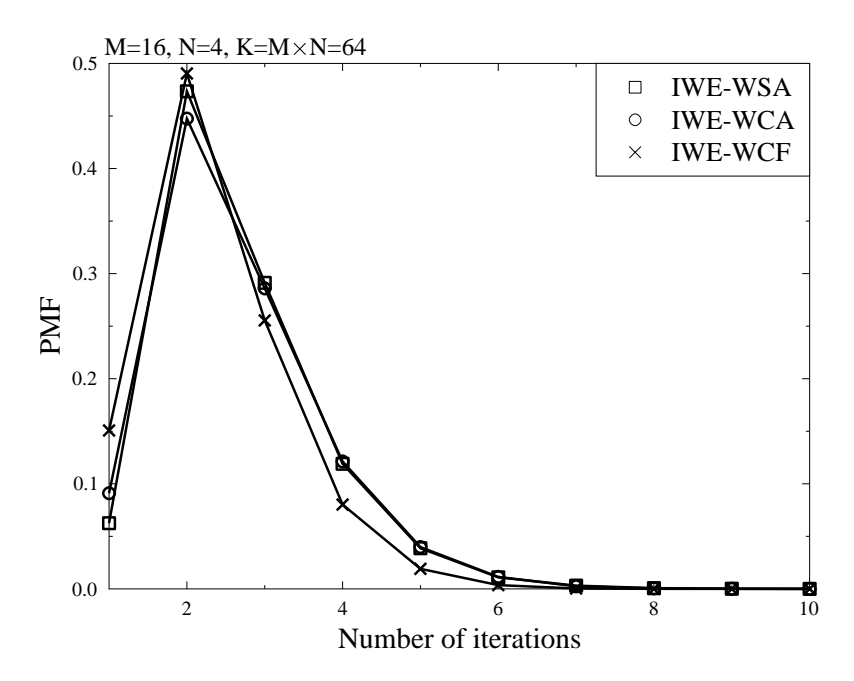


Figure 4.2: Distribution of the number of iterations required by the IWE aided subcarrierallocation algorithms.

4.6 Complexity Analysis of Subcarrier-allocation Algorithms

In this section, we analyze the complexity of the proposed subcarrier-allocation algorithms and that of the other considered existing algorithms. In our analysis, we assume that the same power-allocation scheme is used for all the subcarrier-allocation algorithms. Furthermore, the complexity reflects the number of comparisons required by the subcarrier-allocation algorithms.

First, the complexity of the greedy algorithm and that of the WSA algorithm can be found, for example, in [83], which are both $\mathcal{O}(K^2)$ for the MC DS-CDMA systems with $K \geq M$. Specifically, the number of comparisons required by the WSA algorithm can be expressed as

$$C^{(\text{WSA})} = M(K-1) + 2M \ln M + \frac{1}{2}K(K-1). \tag{4.16}$$

The complexity of the WCA algorithm depends on the specific operations. First, the K users are ordered from the worst to the best according to their worst subchannel qualities. This process requires $K(M-1)+2K\ln K$ comparisons. Then, for the subcarrier-allocation, the upper-bound happens when each subcarrier is assigned to (N-1) users during the first (K-M) stages. In this case, (K-M)(M-1)+M(M-1)/2 comparisons are required. When considering the above analysis, the number of comparisons required by the WCA algorithm satisfies

$$C^{(WCA)} \le K(M-1) + 2K \ln K + (K-M)(M-1) + \frac{1}{2}M(M-1)$$

$$\le (2K - \frac{M}{2})(M-1) + 2K \ln K.$$
(4.17)

From (4.17), we can be implied that the WCA algorithm has a complexity of $\mathcal{O}(KM)$.

Similarly, the complexity of the WCF algorithm has an upper-bound, which happens when each of the M subcarriers is assigned to (N-1) users during the first (K-M) allocation stages. In this case, K(M-1) comparisons are needed for the K users to find their worst subchannel qualities during the first (K-M+1) stages. Then, $\sum_{m=2}^{M-1} (M-m) = (M-1)(M-2)/2$ comparisons are required for re-identifying the worst subchannel quality during the last (M-1) stages. Moreover, during each stage, the WCF algorithm finds the minimum of the subchannel qualities of the k ($k = K, K-1, \ldots, 1$) available users, which requires K(K-1)/2 comparisons. Except user ordering, the allocation process of the WCF algorithm is the same as that of the WCA algorithm, which requires (K-M)(M-1) + M(M-1)/2 comparisons. Consequently, the upper-bound for the number of comparisons required by the WCF algorithm can be expressed as

$$C^{(WCF)} \le K(M-1) + \frac{1}{2}(M-1)(M-2) + \frac{1}{2}K(K-1) + (K-M)(M-1) + \frac{1}{2}M(M-1)$$

$$\le (2K-1)(M-1) + \frac{1}{2}K(K-1). \tag{4.18}$$

According to (4.18), we can readily know that the WCF algorithm has a complexity of $\mathcal{O}(K^2)$, when K > M is assumed.

From Section 4.4.1, we know that our proposed parallel Hungarian algorithm has a lower complexity than the original Hungarian algorithm. The parallel Hungarian algorithm carries out the allocation based on N separate cost matrices with the size of $(M \times M)$, each of which is operated with the Hungarian algorithm. With the aid of [185], where the complexity of the Hungarian algorithm has been analyzed, we readily know that the number of comparisons required by the parallel Hungarian algorithm is

$$C^{(Par. Hungarian)} = N \times \frac{11M^3 + 12M^2 + 31M}{6}$$
 (4.19)

giving a complexity of $\mathcal{O}(NM^3)$.

Let us now consider the complexity of the IWE-WSA algorithm. First, during the sth iteration, the WE process searches for the worst subchannel qualities of the M subcarriers, which has already been identified by the WSA operations during the (s-1)th iteration. Therefore, there is no complexity contribution by the WE process during the sth iteration. Second, we can easily find that the condition checking requires $\mathcal{C}^{(\mathrm{checking})} = M + M(M-1)/2$ operations during the sth $(s \geq 2)$ iteration. Note that, at the sth iteration, the number of comparisons required by the WSA-assisted subcarrier-allocation is $\mathcal{C}^{(\mathrm{allocation})}(s) = \mathcal{C}^{(\mathrm{WSA})} - \mathcal{C}^{(\mathrm{reduce})}(s)$, where $\mathcal{C}^{(\mathrm{reduce})}(s) = 2M(s-1)$ denotes the number of comparisons reduced as a result that some of the worst subchannels are removed by the WE process. When considering all the above, the number of comparisons required by the IWE-WSA algorithm can be expressed as

$$\mathcal{C}^{(\text{IWE-WSA})} = (S-1)\mathcal{C}^{(\text{checking})} + \sum_{s=1}^{S} \mathcal{C}^{(\text{allocation})}(s)$$

$$= \left(\frac{1}{2}SK + SM\right)(K-1) + \left(\frac{1}{2}M^2 + \frac{1}{2}M - SM\right)(S-1) + 2SM\ln M \quad (4.20)$$

when assuming that S iterations are used. (4.20) shows a complexity of $\mathcal{O}(SK^2)$ for the IWE-WSA algorithm.

In the context of the IWE-WCA and IWE-WCF algorithms, their complexity can be analyzed in the similar way as that for the IWE-WSA algorithm, in conjunction with WCA and WCF algorithms, respectively. It can be shown that the number of comparisons required by these two algorithms can be expressed as

$$C^{\text{(IWE-WCA)}} \le \left(2SK - \frac{1}{2}SM\right)(M - 1) + \left(\frac{1}{2}M^2 + \frac{1}{2}M - SK\right)(S - 1) + 2SK\ln K, \quad (4.21)$$

$$C^{\text{(IWE-WCF)}} \le \frac{1}{2}SK(K-1) + (2SK-S)(M-1) + \left(\frac{1}{2}M^2 + \frac{1}{2}M - SK\right)(S-1), \quad (4.22)$$

respectively. Therefore, the complexity of both the IWE-WCA and the IWE-WCF algorithms are $\mathcal{O}(SK^2)$.

In Table 4.3, we summarize the complexity of the various subcarrier-allocation algorithms. Note that, the maximal greedy algorithm [86] requires a complexity of $\mathcal{O}(\alpha K^2)$, where $\alpha (\geq M)$ is the size of the search space. In Section 4.7, we assume that the maximal greedy algorithm uses a random search space having the size $\alpha = M$. Furthermore, in Figures 4.3 and 4.4, we compare the number of operations required by the various subcarrier-allocation algorithms with respect to the number of subcarriers employed by the MC DS-CDMA systems.

Note that, in both figures, the number of operations are either the exact values or the upperbound of the algorithms considered. The number of comparisons of the IWE algorithms were obtained from (4.20) - (4.22). From both figures, we can see that the greedy and WCA algorithms always require the least number of comparisons, while the Hungarian algorithm [185, 191] needs the highest number of comparisons. When N=4 in Figure 4.3, the greedy algorithm demands

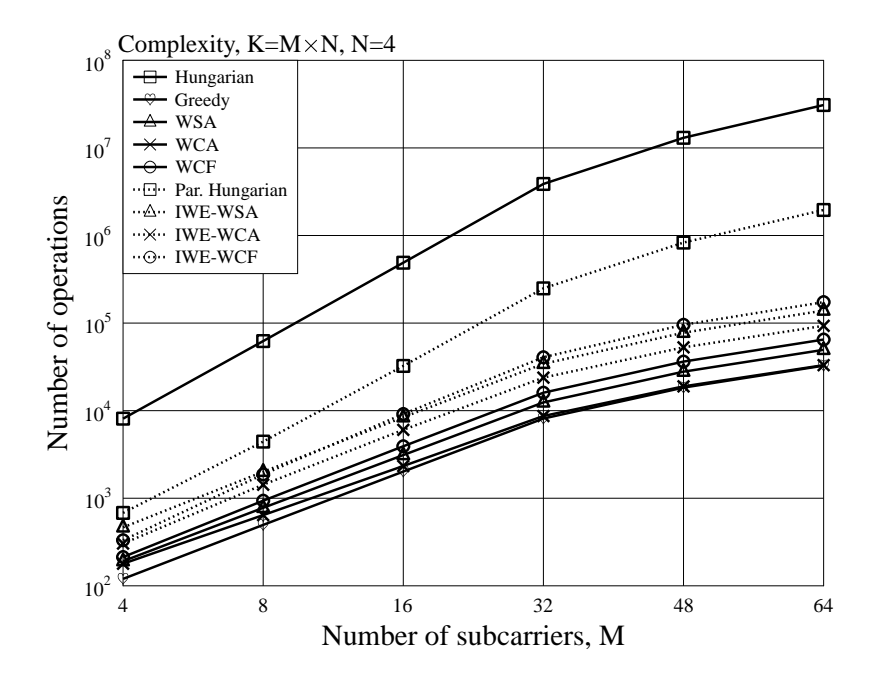


Figure 4.3: Number of comparisons required by various subcarrier-allocation algorithms when N=4.

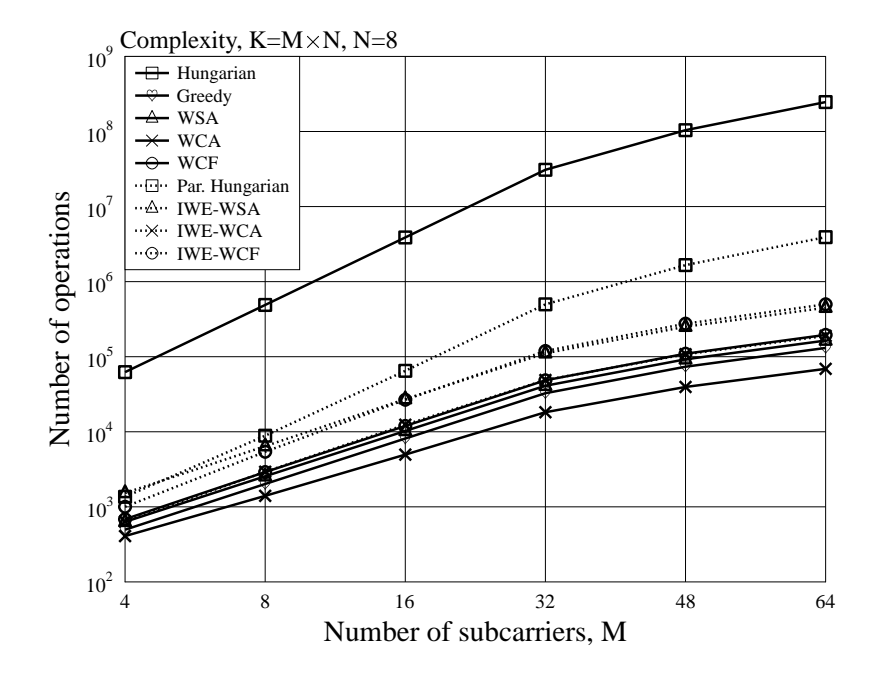


Figure 4.4: Number of comparisons required by various subcarrier-allocation algorithms when N=8.

the lowest number of comparisons when $M \leq 32$. However, when N = 8 in Figure 4.4, the WCA algorithm always has the lowest operations. Observing from the two figures, we can know that the complexity of the proposed WCA and WCF algorithms are at the same level as that of the WSA and greedy algorithm. Moreover, for the considered examples, we find that the number of

4.7. Performance Results 129

Table 4.3: Complexity of various subcarrier-allocation algorithms in single-cell downlink MC DS-CDMA systems.

Algorithm	Complexity
Hungarian	$O(K^3)$ [185]
Greedy	$\mathcal{O}(K^2)$
WUF Greedy	$\mathcal{O}(K^2)$
Maximal Greedy	$\mathcal{O}(\alpha K^2)$
WSA	$\mathcal{O}(K^2)$
Par. Hungarian	$\mathcal{O}(NM^3)$
WCA	$\mathcal{O}(KM)$
WCF	$\mathcal{O}(K^2)$
IWE-WSA	$\mathcal{O}(SK^2)$
IWE-WCA	$\mathcal{O}(SK^2)$
IWE-WCF	$\mathcal{O}(SK^2)$

comparison required by the IWE-aided subcarrier-allocation algorithms is slightly less than twice of the number of comparisons required by the original corresponding algorithms without invoking the IWE algorithm. Furthermore, from the two figures, we observe that the proposed parallel Hungarian algorithm has a significant lower complexity than the Hungarian algorithm, when various number of subcarriers and users are considered. Their complexity gap becomes larger as the length of the spreading code increases.

4.7 Performance Results

In this section, we provide a range of simulation results, in order to demonstrate and compare the achievable error rate and spectrum-efficiency performance of the downlink MC DS-CDMA systems employing various resource allocation schemes, which include two power-allocation algorithms and different subcarrier-allocation algorithms considered. For the error rate, we assume the quadrature phase-shift keying (QPSK) baseband modulation and that all the subcarriers experience independent flat Rayleigh fading or frequency selective Rayleigh fading. The number of users supported by the MC DS-CDMA is K = MN, with M being the number of subcarriers and N the length of the orthogonal DS spreading codes. In this chapter, both the channel-inverse and water-filling assisted power-allocation algorithms are considered, under the constraint that the total transmission power is P = K.

4.7.1 Bit Error Rate Performance

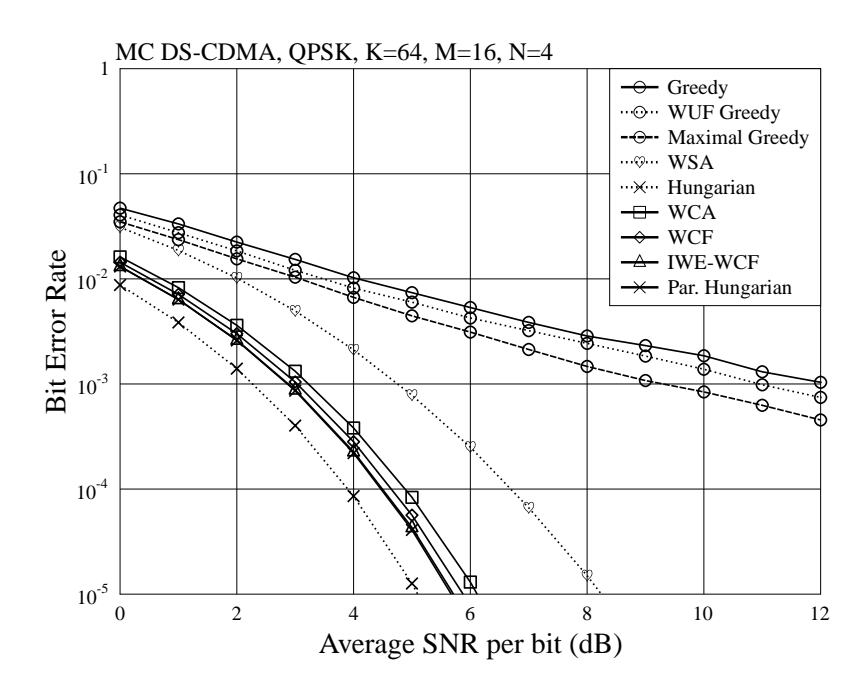


Figure 4.5: BER comparison of the single-cell downlink MC DS-CDMA systems employing the channel-inverse power-allocation and various subcarrier-allocation algorithms, when subcarriers experience independent Rayleigh fading.

Figure 4.5 demonstrates the BER performance of the MC DS-CDMA system employing various of subcarrier-allocation algorithms, when K = 64 users are supported by M = 16 subcarriers. Hence, each subcarrier supports 4 users. From the figure, we can obtain the following observations. First, the Hungarian algorithm gives the best BER performance, while the greedy algorithm yields the worst BER performance. Both the WUF greedy algorithm [85] and the maximal greedy algorithm [86], which assumes a random search space of size $\alpha = M$, slightly outperform the greedy algorithm. As the greedy-class algorithms aim to maximize the sum of the subchannel qualities, rather than maximizing the reliability, the greedy-class algorithms in general achieve poorer BER performance than the other reliability motivated algorithm. Second, from Figure 4.5, we observe that the proposed parallel Hungarian algorithm achieves the second best BER performance among the algorithms considered. Note that, the parallel Hungarian algorithm slightly outperforms the IWE-WCF algorithm under the considered scenarios. However it requires higher complexity than the IWE-WCF algorithm. Third, as seen in Figure 4.5, the proposed WCA, WCF, especially the IWE-WCF algorithms are capable of significantly outperforming the greedy-class algorithms as well as the WSA algorithm. Fourth, for the specific system parameters considered, the WCF algorithm has better BER performance than the WCA algorithm. This is because the WCF algorithm can avoid assignment of more number of worst subchannels than the WCA algorithm. Finally, by invoking the IWE scheme, further error performance improvement can be attained with a penalty of double complexity. The achievable BER of the IWE-WCF algorithm is close to that achieved by

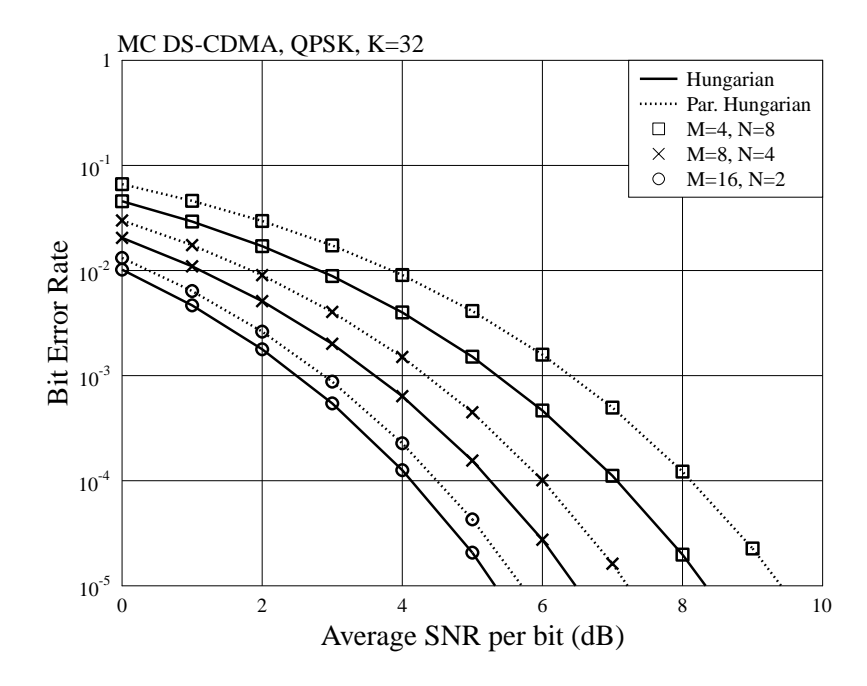


Figure 4.6: BER comparison of the single-cell downlink MC DS-CDMA systems employing the channel-inverse power-allocation and the Hungarian, the parallel Hungarian subcarrier-allocation algorithms, when subcarriers experience independent Rayleigh fading.

the Hungarian algorithm, with the difference of about 0.7 dB.

In Figure 4.6, we compares the BER performance of the proposed parallel Hungarian algorithm with that of the Hungarian algorithm, when considering K=32 users in the downlink MC DS-CDMA system. From this figure, we observe that the BER performance becomes better as the number of subcarriers M increases, which results in a higher diversity for subcarrier-allocation. As shown in Figure 4.6, when given K=MN a constant, the error performance of the parallel Hungarian algorithm is closer to that of the Hungarian algorithm, as the number of subcarriers increases. Specifically, there is about 0.5 dB performance gap between these two algorithms, when M=16. This observation implies that BER performance of the parallel Hungarian algorithm converges to the BER performance of the Hungarian algorithm, as the ratio of M/N becomes bigger. Nevertheless, as shown in Section 4.6, the parallel Hungarian algorithm requires a higher complexity, when the ratio of M/N becomes bigger.

Figure 4.7 compares the BER performance of the MC DS-CDMA systems employing the WSA, WCA and the WCF algorithms for K=32 users. In general, the proposed WCA and WCF algorithms always yield better BER performance than the WSA algorithm. As discussed in Section 4.3, the WSA algorithm implements the assignment by avoiding the worst subchannel qualities in a subcarrier-oriented mode. Hence, its performance depends on the frequency-selective diversity relating to the number of subcarriers. By contrast, for the MC DS-CDMA systems employing

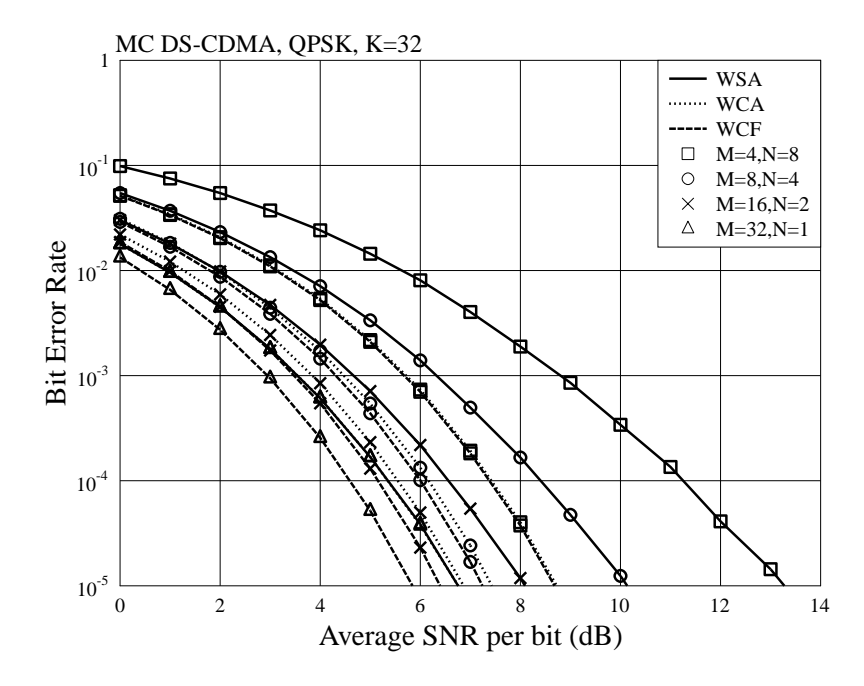


Figure 4.7: BER comparison of the single-cell downlink MC DS-CDMA systems employing the channel-inverse power-allocation as well as the WSA, WCA and the WCF subcarrier-allocation algorithms, when subcarriers experience independent Rayleigh fading.

DS spreading, the number of users supported is usually higher than the number of subcarriers, as considered in Figure 4.7. In this case, the WCA and WCF algorithms avoid the worst subchannel qualities in a user-oriented mode and achieve much higher diversity than the WSA scheme. Furthermore, from Figure 4.7 we observe that, when given K = MN a constant, the BER performance of the three algorithms improves as M becomes larger. The reason behind the observation is that we assumed that all subcarriers experience independent fading regardless of the number of subcarriers. This assumption implies that more subcarriers results in higher diversity. In this case, the advantage of the WCA algorithm over the WSA algorithm becomes smaller as the ratio of K/M becomes bigger. Furthermore, when M = K = 32 and N = 1, both the WCA and WSA achieve the same BER, as, in this case, the MC DS-CDMA is reduced to an OFDMA system without T-domain spreading. Consequently, the user-oriented diversity is the same as the subcarrier-oriented diversity. By contrast, as shown in Figure 4.7, the advantage of the WCF algorithm over the WCA algorithm is enhanced as M increases, when given K = MN a constant. Specifically, when M = 32 and N=1, the WCF algorithm has 0.6 dB SNR gain over the WCA algorithm at the BER of 10^{-5} . From the above, we can know that, when all subcarriers experience independent fading, the number of subcarriers has a significant impact on the performance of the considered subcarrier-allocation algorithms.

Figures 4.8, 4.9 and 4.10 show the BER gain of employing the IWE algorithm for the WCF, WCA and WSA algorithms, respectively. Under the various cases, the BER improvement can be

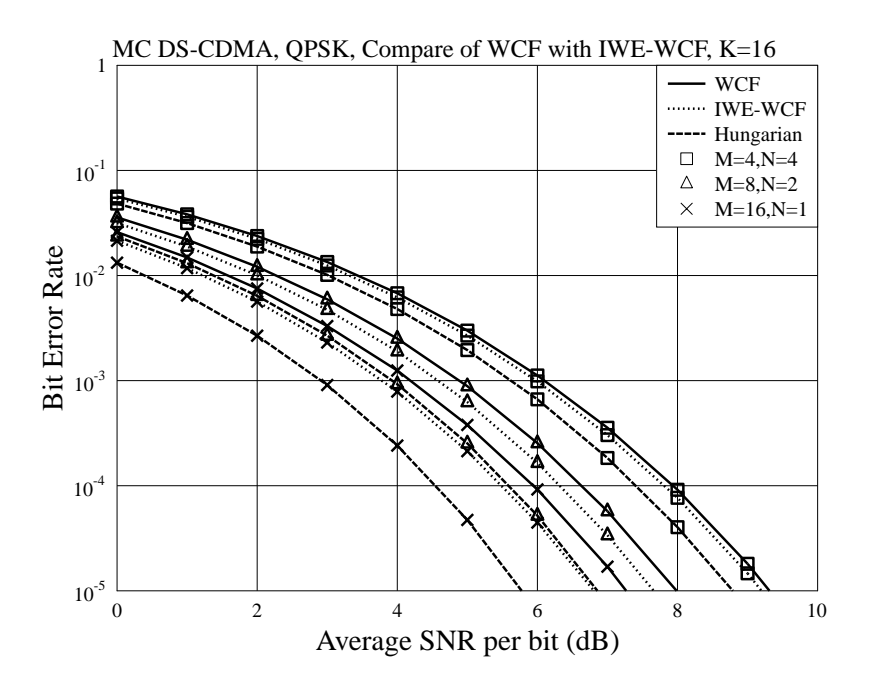


Figure 4.8: BER comparison of the single-cell downlink MC DS-CDMA systems employing the channel-inverse power-allocation and the WCF, the IWE-WCF subcarrier-allocation algorithms, when subcarriers experience independent Rayleigh fading.

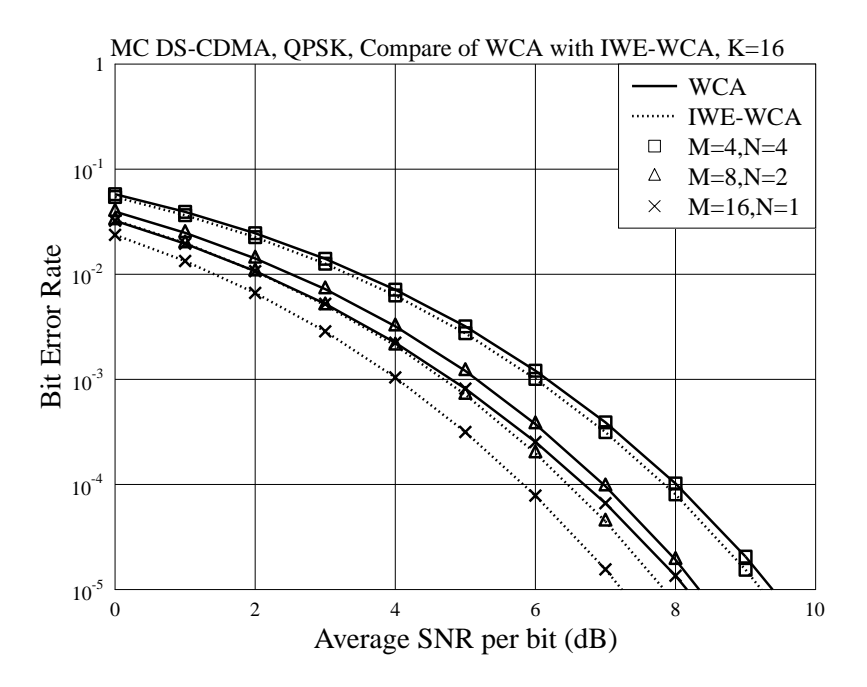


Figure 4.9: BER comparison of the single-cell downlink MC DS-CDMA systems employing the channel-inverse power-allocation and the WCA, the IWE-WCA subcarrier-allocation algorithms, when subcarriers experience independent Rayleigh fading.

obtained by introducing the IWE algorithm. Thus, this observation confirms the benefit of using the IWE algorithm in association with subcarrier-allocation algorithms. By comparing the three

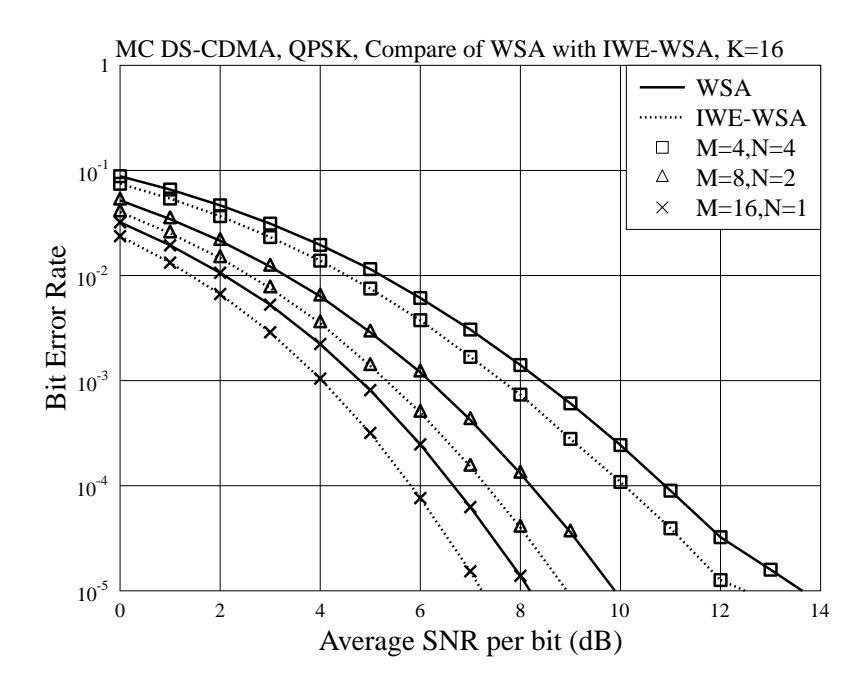


Figure 4.10: BER comparison of the single-cell downlink MC DS-CDMA systems employing the channel-inverse power-allocation and the WSA, the IWE-WSA subcarrier-allocation algorithms, when subcarriers experience independent Rayleigh fading.

figures, we observe that the IWE-WCF algorithm always has the best BER performance, while the IWE-WSA has the worst performance among the three IWE aided algorithms. This observation maintains the same for the three algorithms without using the IWE algorithm in Figure 4.7. From Figures 4.8 and 4.9, we observe that the improvement of using the IWE scheme for the WCF and the WCA algorithms gets larger as the number of subcarriers M becomes bigger. By contrast, in Figure 4.10, the BER advantage of using the IWE remains the same, which is about 1 dB, as the number of subcarriers M becomes bigger. As discussed in Section 4.5, the WE process of the IWE-WCA and IWE-WCF algorithms excludes the worst subcarrier for each user during an iteration, but the worst user of each subcarrier is eliminated during every iteration for the IWE-WSA algorithm. Therefore, the BER performance of the IWE-WCF and IWE-WCA algorithms is highly affected by the subcarrier diversity, whereas that of the IWE-WSA algorithm is dominated by the user diversity. In Figure 4.10, the number of users is K=16 for all cases, thus they obtain a similar BER gain when employing the IWE algorithm.

So far, we have assumed that all subcarriers of a MC DS-CDMA system experience independent fading, regardless of the number of subcarriers. When given the frequency selectivity of a wireless channel, this assumption may not be true. In this case, the fading experienced by different subcarriers in fact becomes more correlated, as the number of subcarriers increases. Therefore, in Figure 4.11, we study the BER performance of the MC DS-CDMA employing the WCF algorithm, when the number of time-domain resolvable paths is fixed to $L_p=2$ or 4, i.e., when given the frequency selectivity of wireless channels. In general, the BER performance of the downlink MC

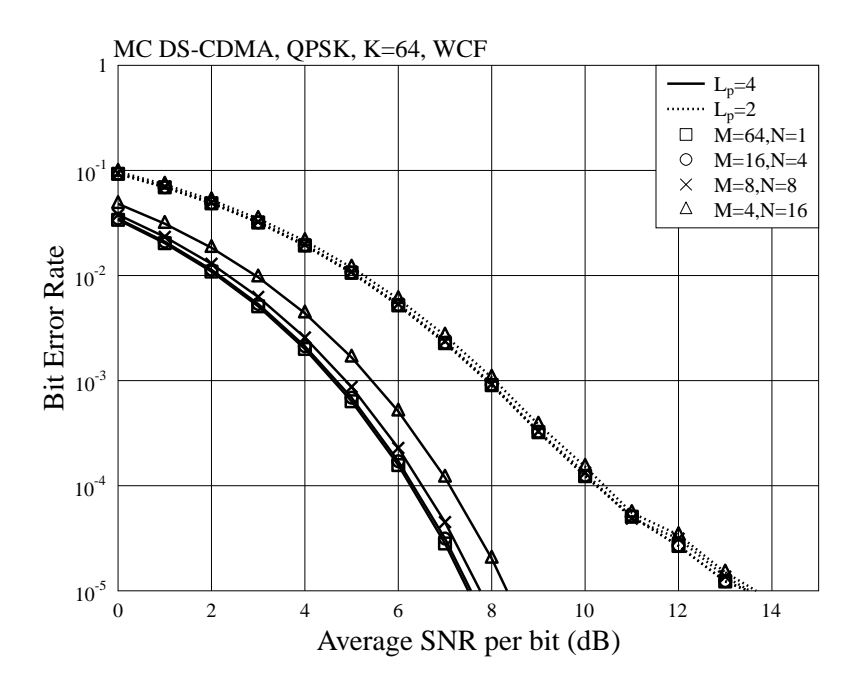


Figure 4.11: BER of the single-cell downlink MC DS-CDMA systems employing the channel-inverse power-allocation and the WCF subcarrier-allocation algorithm, when subcarriers experience frequency selective Rayleigh fading with L_p number of time domain resolvable paths.

DS-CDMA system becomes better when there are more number of time domain resolvable paths L_p , i.e., when the subcarriers experience the less correlated Rayleigh fading. Furthermore, when $L_p = 2$, we find that using M = 4 subcarriers is sufficient for attaining all the frequency diversity. By contrast, when $L_p = 4$, M = 16 subcarriers are required to achieve all the frequency diversity.

Figure 4.12 compares the various subcarrier-allocation algorithms employed by the single-cell downlink MC DS-CDMA systems, when considering the special case of N=1. In this case, the MC DS-CDMA system is reduced to the OFDMA system. As we discussed in Section 4.4.2, the proposed WCA algorithm is the same as the WSA algorithm when there is no time domain spreading, i.e., when N=1. Therefore we obtain the same performance result for the WCA and WSA algorithms in the figure. Further that, it can be known that the proposed parallel Hungarian algorithm becomes the Hungarian algorithm, when N=1. From Figure 4.12, we can observe that the BER performance of the systems employing any of the subcarrier-allocation algorithms becomes better, as the number of users increases. Additionally, the proposed WCF and IWE-WCF algorithms have significant BER performance gain over the WSA algorithm, when frequency selective Rayleigh fading channel is assumed.

By comparing Figure 4.12 with Figures 4.8 and 4.10, we can explicitly see the BER performance improvement, when the MC DS-CDMA systems experience independent Rayleigh fading, which once again prove that higher frequency diversity results in a better BER performance of the

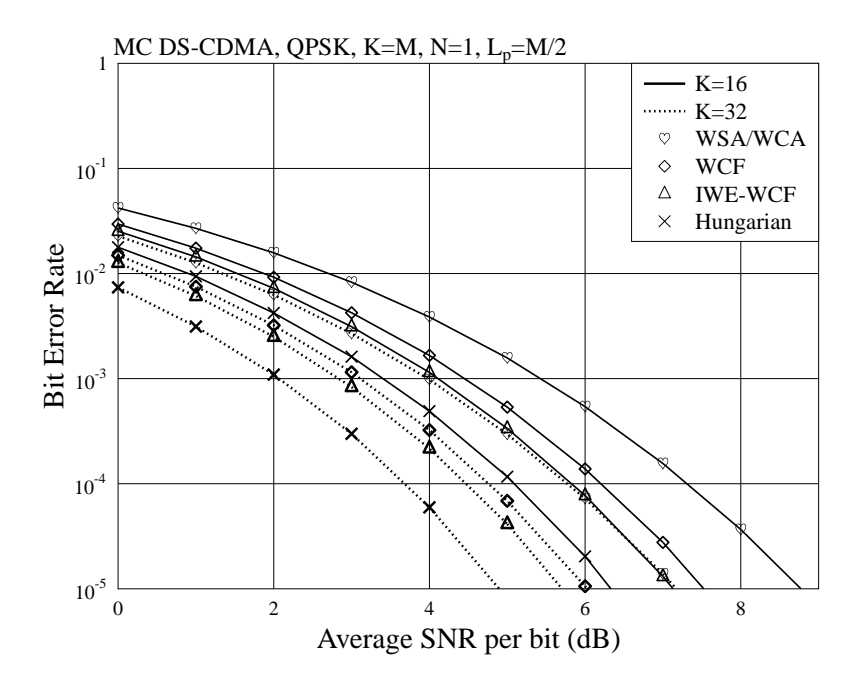


Figure 4.12: BER of the single-cell downlink MC DS-CDMA systems employing the channel-inverse power-allocation and various subcarrier-allocation algorithms, when subcarriers experience frequency selective Rayleigh fading with $L_p = M/2$ number of time domain resolvable paths.

subcarrier-allocation algorithms. Additionally, when we compare the algorithms proposed in this chapter with the BSS algorithm proposed in Chapter 3, as shown in Figure 4.12 and Figure 3.12. we can observe that, under the single-cell downlink OFDMA systems, the BSS algorithm outperforms the WCF algorithm, and also slightly outperforms the IWE-WCF algorithm with about 0.1 dB performance gain. However, as the complexity analysis in Sections 4.6 and 3.8 shows, the BSS algorithm has a higher complexity than the IWE-WCF algorithm.

4.7.2 Spectrum-Efficiency Performance

In this section, we investigate the spectrum-efficiency of the single-cell downlink MC DS-CDMA systems employing the various subcarrier- and power-allocation algorithms. As we mentioned in Chapter 3, the spectrum-efficiency considered here is the average throughput expressed in terms of bits per second per Hertz of the downlink MC DS-CDMA systems. In this section, the spectrum-efficiency of using both the channel-inverse and water-filling assisted power-allocation schemes are considered, to show that our proposed subcarrier-allocation schemes do not make a trade-off between throughput and reliability. Note that, for all the simulations in this section, we assume that the downlink MC DS-CDMA experiences independent Rayleigh fading.

Figure 4.13 shows the spectrum-efficiency of the downlink MC DS-CDMA systems employing various subcarrier-allocation algorithms. From the figure and referring to the results shown in

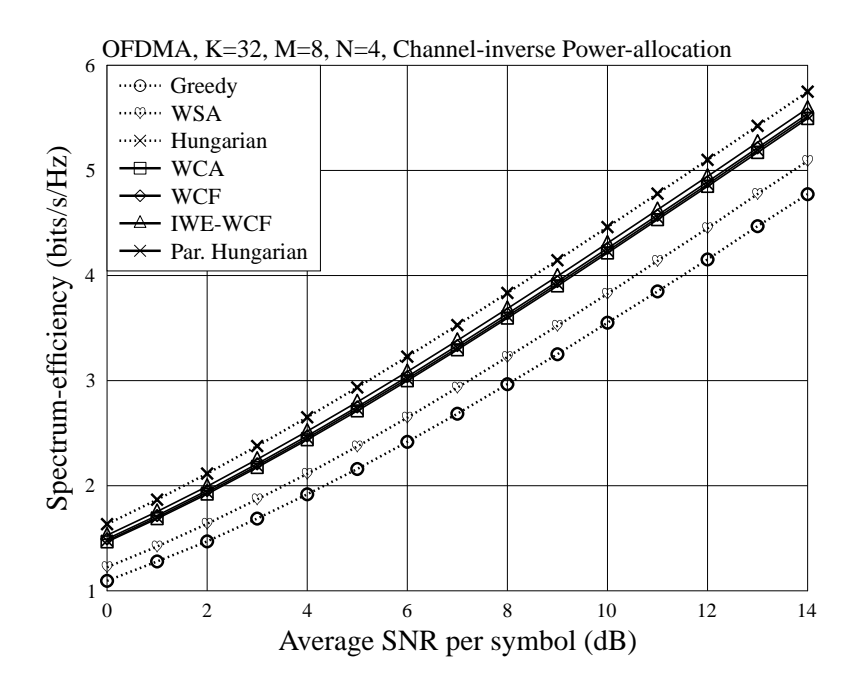


Figure 4.13: Spectrum-efficiency of single-cell downlink MC DS-CDMA systems employing the channel-inverse power-allocation and various subcarrier-allocation algorithms, when subcarriers experience independent Rayleigh fading.

Section 4.7.1, we can know that our proposed subcarrier-allocation algorithms motivating to maximize BER performance do not make a trade-off with the spectrum-efficiency, which determines the practically attainable throughput of the downlink MC DS-CDMA systems. As shown in Figure 4.13, the Hungarian algorithm achieves the highest spectrum-efficiency, followed by those of the proposed subcarrier-allocation algorithms, in the decreasing order the IWE-WCF, WCF, parallel Hungarian and the WCA algorithms. Explicitly, the spectrum-efficiency of the the proposed algorithms is higher than that of the greedy and that of the WSA algorithms. As shown in the figure, there is about 2 dB performance gain of the WCA algorithm over the greedy algorithm.

Figure 4.14 evaluates the spectrum-efficiency of the MC DS-CDMA systems employing various subcarrier-allocation algorithms, when assuming K=64 users supported by the MC DS-CDMA systems having M=16 subcarriers. By comparing Figure 4.14 with Figure 4.13, which have the parameters of K=32 and M=8, we can see that the relative relationship among the subcarrier-allocation algorithms is the same in both figures. Moreover, as the number of users or subcarriers for Figure 4.14 is more than that for Figure 4.13, we observe that, at a given SNR, the spectrum-efficiency in Figure 4.14 is slightly higher than the corresponding one shown in Figure 4.13.

In literature, water-filling power-allocation is used, when the optimization objective is to maximize the spectrum-efficiency. Therefore, in Figure 4.15, the spectrum-efficiency performance of the downlink MC DS-CDMA system employing the water-filling power-allocation is demonstrated,

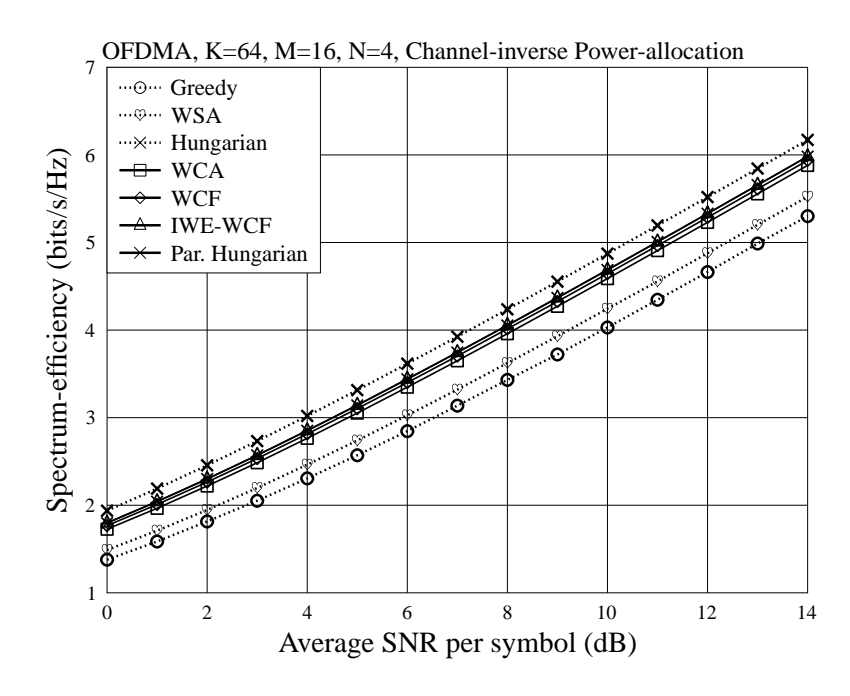


Figure 4.14: Spectrum-efficiency of single-cell downlink MC DS-CDMA systems employing the channel-inverse power-allocation and various subcarrier-allocation algorithms, when subcarriers experience independent Rayleigh fading.

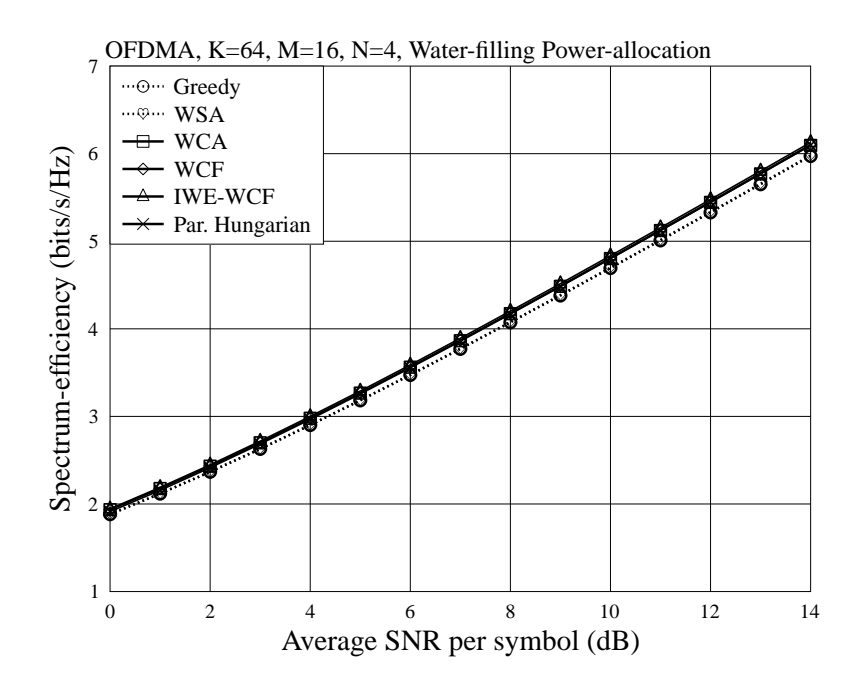


Figure 4.15: Spectrum-efficiency of single-cell downlink MC DS-CDMA systems employing the water-filling power-allocation and various subcarrier-allocation algorithms, when subcarriers experience independent Rayleigh fading.

when various subcarrier-allocation algorithms are considered. As shown in Figure 4.15, all the algorithms achieve nearly the same spectrum-efficiency, implying that all these subcarrier-allocation

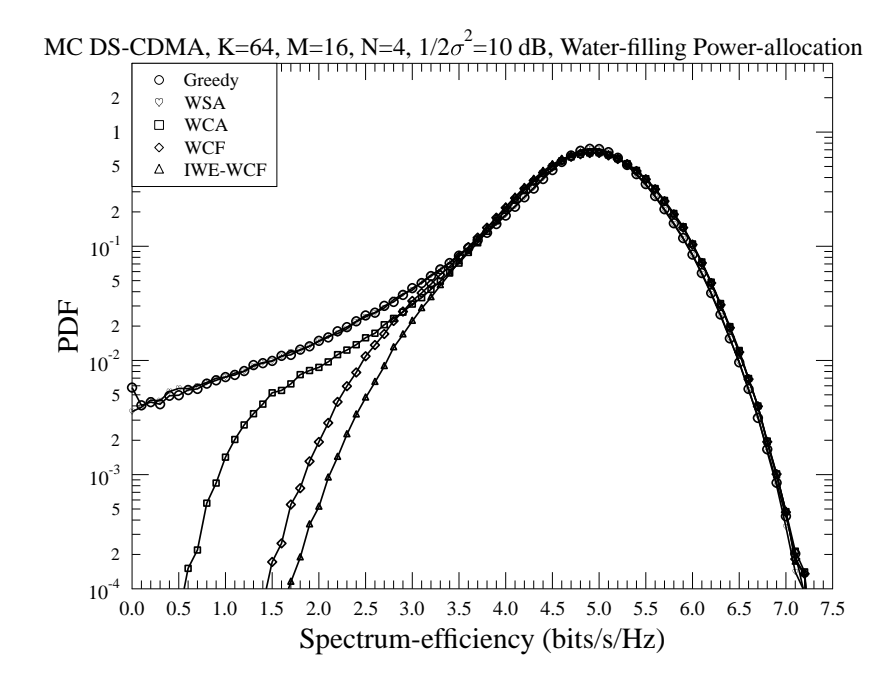


Figure 4.16: PDF of spectrum-efficiency of single-cell downlink MC DS-CDMA systems employing the water-filling power-allocation and various subcarrier-allocation algorithms, when subcarriers experience independent Rayleigh fading.

algorithms are near optimum from the point of view of spectrum-efficiency maximization. The reason behind the observation is that employing the water-filling power-allocation minimizes the difference of the spectrum-efficiency of different subcarrier-allocation algorithms. As discussed in Section 3.4.2, the water-filling scheme aims to maximize the system throughput by allocating more power to the subcarriers with better subchannel qualities. Therefore, when the water-filling algorithm is employed, the subcarriers allocated with the best subchannel qualities dominate the spectrum-efficiency performance of the MC DS-CDMA systems. However, the BER performance of these algorithms has big difference, as shown in Section 4.7.1, and our proposed subcarrier-allocation algorithms in general outperform the other sub-optimum subcarrier-allocation algorithms. Therefore, although our algorithms are motivated to maximize the reliability, they do not impose any trade-off on the spectrum-efficiency, and, in fact, achieve slightly higher spectrum-efficiency than the existing sub-optimum algorithms. When comparing Figure 4.15 with Figure 4.14, we can see that the water-filling algorithm achieves a slightly higher spectrum-efficiency than the channel-inverse algorithm.

In addition to the higher spectrum-efficiency, our proposed algorithms are also capable of providing higher fairness data rates. These can be reflected by the PDFs of spectrum-efficiency shown in Figure 4.16. As shown in the figure, the spectrum-efficiency obtained by the Greedy and WSA algorithms distributes over a relatively large range, meaning that there are some users often obtaining very high throughput, while some other users have obtaining very low throughput, and, therefore, relatively poor fairness. By contrast, for the proposed algorithms, from the WCA, to

4.8. Conclusions 140

the WCF and to the IWE-WCF algorithm, the distribution range becomes smaller and smaller, and the distribution range of all the three algorithms are narrower than that of the Greedy and WSA algorithms. Therefore, we are implied that the proposed three algorithms result in better fairness than the greedy and WSA algorithms. Furthermore, according to Figure 4.16, we can know that the fairness of the IWE-WCF algorithm is better than that of the WCF algorithm, and both of them can provide higher fairness services than the WCA algorithm.

4.8 Conclusions

In this chapter, we have investigated the resource allocation in the single-cell downlink MC DS-CDMA systems. Various subcarrier- and power-allocation algorithms have been considered. Our resource allocation in downlink MC DS-CDMA system motivates to maximize the systems' reliability, by maximizing the SNR of the systems. According to the references, subcarrier- and power-allocation can be carried out separately without losing much performance. Therefore, in our MC DS-CDMA systems, subcarriers are first allocated and, then, power-allocation is implemented. In this chapter, we have reviewed three existing subcarrier-allocation algorithms, including the greedy, WSA and the Hungarian algorithms, and illustrated how to apply them to the downlink MC DS-CDMA systems. Furthermore, we have analyzed the drawbacks of the above-mentioned algorithms. Specifically, although it is low-complexity, the greedy algorithm has a shortcoming of assigning poor subcarriers to the users obtaining subcarrier later. The WSA algorithm can significantly improve the error performance of the greedy algorithm, but it does not exploit the maximum possible diversity provided by the systems. Although the Hungarian algorithm is able to achieve the optimum error rate performance, it requires extremely high complexity, especially, when the number of users is high, which limits its practical application.

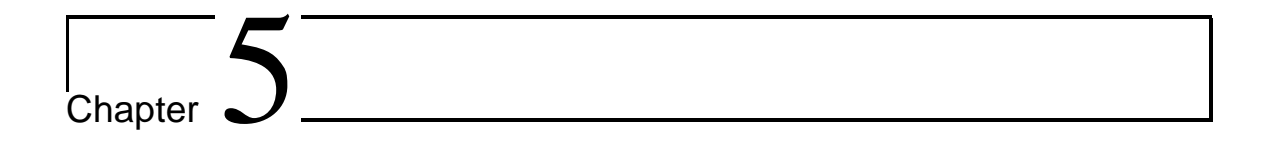
Against the existing subcarrier-allocation algorithms, in this chapter, we have proposed a range of fair subcarrier-allocation algorithms and investigated their performance in the context of the MC DS-CDMA systems, where the number of users supported is assumed to be higher than the number of subcarriers. Specifically, in order to mitigate the high complexity of the conventional Hungarian algorithm, we have proposed the parallel Hungarian algorithm, which, instead of operating on a $(MN \times MN)$ matrix, but processes N number of $(M \times M)$ cost matrices. By doing this, the complexity can be reduced from $\mathcal{O}(M^3N^3)$ of the Hungarian algorithm to $\mathcal{O}(NM^3)$ of the parallel Hungarian algorithm. By analyzing the characteristics of the WSA algorithm, we find that it is mainly beneficial to the multicarrier systems with subcarriers more than users. Therefore, we have generalized the WSA algorithm to the WCA algorithm, which is suitable for operation in any multicarrier systems. Our studies show that the proposed WCA algorithm is capable of achieving better BER and spectrum-efficiency performance than the WSA algorithm. Then, we have proposed the WCF algorithm, which is capable of further improving the BER and spectrum-efficiency performance of the MC DS-CDMA systems. Our studies show that the WCF algorithm can be

4.8. Conclusions 141

operated in a more efficient and reliable way, while maintains all the advantages of the WCA algorithm. Furthermore, in this chapter, an IWE algorithm has been proposed for further improving the performance of the WSA, WCA and the WCF algorithms, resulting in the so-called IWE-WSA, IWE-WCA and the IWE-WCF algorithms, respectively. The IWE assisted algorithms are the iterative algorithms, which can usually be accomplished within a very low number of iterations, as our studies show. Additionally, the complexity of the proposed subcarrier-allocation algorithms has been analyzed and compared with that of the low-complexity greedy algorithm. We can argue that all our proposed subcarrier-allocation algorithms have the merit of low-complexity.

We have demonstrated the BER and spectrum-efficiency performance of our proposed algorithms, and compared them with a range of existing subcarrier-allocation algorithms. Our studies show that the proposed subcarrier-allocation algorithms are capable of attaining better BER performance than the greedy-class algorithms and the WSA algorithm. When considering the MC DS-CDMA systems with a high ratio of M/N, the proposed parallel Hungarian algorithm can achieve better BER performance than the other proposed algorithms, and its BER performance is close to that of the optimum Hungarian algorithm. The WCF algorithm outperforms the proposed WCA algorithm for all the cases considered. Furthermore, an IWE-assisted algorithm always improves the reliability of the original subcarrier-allocation algorithm. The IWE-WCA algorithm outperforms the IWE-WSA algorithm, both of which are outperformed by the IWE-WCF algorithm. Additionally, our results demonstrate that the reliability attained by the IWE-WCF algorithm is close to that achieved by the high-complexity optimum Hungarian algorithm. Besides the error performance, we have investigated the spectrum-efficiency of the MC DS-CDMA systems employing various subcarrier-allocation algorithms. We have considered both the channel-inverse power-allocation, which is beneficial to maximization of reliability, and the water-filling power-allocation algorithm, which achieves maximum sum rate. Our studies show that our proposed subcarrier-allocation algorithms motivating to maximize reliability do not make a trade-off with the attainable spectrumefficiency of the downlink MC DS-CDMA systems. Instead, our proposed subcarrier-allocation algorithms are capable of achieving higher (or slightly higher) spectrum-efficiency than the existing sub-optimum subcarrier-allocation algorithms considered in this chapter. Owing to its motivation of maximizing spectrum-efficiency, the water-filling algorithm can attain higher spectrum-efficiency than the channel-inverse algorithm. Furthermore, according to the PDFs of spectrum-efficiency, we have shown that the proposed subcarrier-allocation algorithms can provide better fairness data rates to users than the other existing sub-optimum algorithms.

Note that, the observations derived from our studies in this chapter are in general suitable for the MC DS-CDMA systems, where different users may be allocated with different numbers of subcarriers or/and spreading codes. This is because the relative advantages and disadvantages of the different subcarrier-allocation algorithms are mainly determined by the diversity gain available to the systems, i.e., by the values of *K* and *M*, but not by the numbers of data streams of the users.



Resource Allocation in Multicell Downlink OFDMA Systems

5.1 Introduction

Orthogonal frequency division multiple access (OFDMA) has emerged as one of the key techniques for high-speed broadband wireless communication systems. OFDMA employs a range of advantages, including the facility for high achievable data rate, the capability of efficiently combating inter-symbol interference, low-complexity FFT based modulation/demodulation implementation, etc. However, in multicell OFDMA systems, the scarce spectrums (or frequencies) are inevitable reused, and, furthermore, it is expected to be fully reused in the fourth generation (4G) wireless systems and beyond. Hence, in multicell OFDMA systems, users experience the intercell interference (InterCI), which may significantly reduce the system performance, if it is not cleverly managed. To mitigate the strong InterCI problem, one of the approaches is to exploit dynamic resource allocation, which efficiently allocates subcarrier, power and other resources available according to the communication environment, so as to minimize the InterCI and to maximize the energy-efficiency and spectrum-efficiency of the multicell systems [199]. However, in multicell OFDMA systems, the resource allocation faces a lot of challenges, including the possible of huge signalling overhead, limited backhaul resources, high-complexity from optimization problem itself and backhaul operations, the issues caused by the expansive servicing area, diverse services, large number of users, etc.

In literature, resource allocation approaches in multicell systems can be categorized into two classes, the centralized and distributed resource allocation, based on where the resource allocation algorithms are carried out. Specifically, in the centralized resource allocation, a central control unit is used to collect all the information required, including, such as, the CSI of the wireless channels of all users in all cells, the information about the radio resources, etc. The central unit is also

5.1. Introduction 143

responsible for managing and allocating the resources jointly to all the users in all cells. Apparently, such a centralized resource allocation scheme can exploit an enormous number of degrees of freedom, which are provided by the number of cells, the number of users, the number of subcarriers, the number of scheduling slots, the number of codes, the power levels, etc., that can be exploited to optimize the network performance [116]. In literature, there are a range of researches, including [118–121, 123], having proposed and studied the centralized resource allocation in multicell OFDMA systems. Specifically, in [121], the authors have proposed a concept called load matrix, based on which the InterCI and intracell interference (IntraCI) experienced by users are jointly managed in wireless cellular networks. Considering a two-cell OFDMA system, the authors of [119, 120] have investigated the centralized resource allocation, where the resources include power and subcarriers. Furthermore, in [120], the NP-hard joint resource allocation problem has been approximated by a novel weighted sum throughput maximization (WSTM) problem, which is solved by using a centralized convex power-allocation algorithm and a non-convex subcarrierallocation algorithm. A two-stage resource allocation scheme has been proposed in [118], in which joint subcarrier-allocation and scheduling is carried out in the first stage, followed by the interference-aware power-allocation in the second stage.

Centralized resource allocation may demand a huge amount of feedback for the channel information, which requires possibly huge signalling overhead and energy. For this sake, distributed resource allocation has attracted intensive attention in recent years. In distributed resource allocation, every BS independently allocates its resources, usually based only on the intracell channel information and the interference measured locally. In comparison with the centralized approaches, distributed resource allocation has the main advantages of fast response to dynamic resource environments and fast time-varying fading channels, as well as low complexity for implementation, which make them highly attractive in practice. Distributed resource allocation in multicell OFDMA systems has been widely studied, e.g., in [135-140]. The distributed resource allocation scheme proposed in [135] has involved jointly subcarrier, bit and power-allocation for multicell OFDMA systems, which has linear complexity via the operations in a round-robin manner. In [136], the authors have studied the distributed subcarrier- and power-allocation for the multicell OFDMA networks with cognitive radio functionality. By contrast, in [137], a distributed power-allocation scheme has been proposed for the multicell multiple input single output (MISO) based OFDMA networks, where the CSI of all users is shared among the BSs. The resource allocation in DF relayassisted multicell OFDMA systems has been considered in [138], where a semi-distributed iterative allocation algorithm is operated under the interference temperature constraints. More recently, interference aware resource allocation has drawn more and more research attentions, as shown, e.g., in [139, 140].

It can be understood that, in order to combat the InterCI in multicell OFDMA systems, one can employ a sophisticated InterCI mitigation technique at the receiver side, by using, such as, maximum likelihood (ML) detection, successive interference cancellation (SIC), multiple-antenna

5.1. Introduction 144

based interference nulling, etc. On the other hand, BS cooperation can be another high-efficiency InterCI mitigation approach, which shifts the processing overhead to the BSs, rather than causing too much computational complexity at mobile terminals. For example, X.D. Wang et al. [200, 201] have studied the scheduling and power-allocation in the multicell downlink OFDMA systems and other networks, which treat the InterCI problem via BS coordination. However, in [138, 200, 201], the BS cooperation cannot fully exploit the potential of cooperation, since in these schemes only CSI is shared but there is no data exchange among the BSs. By contrast, the researches in [123,202– 204] have devoted to the resource allocation in multicell OFDMA systems with full BS cooperation by assuming that both CSI and data are shared among the BSs. In this case, certainly, there is a high demand on the backhual system. Under certain constraints of backhaul capacity, a novel heuristic BS assignment algorithm has been proposed in [203] and a user scheduling algorithm has been developed in [204], respectively. Furthermore, the trade-off among energy-efficiency, backhaul capacity, and network capacity has been addressed in [123], and based on finding a good trade-off, an efficient iterative resource allocation algorithm has been proposed by allowing the BSs to jointly carry out the zero-forcing beam-forming assisted transmission. Furthermore, in [132, 205], the authors have addressed the energy-efficiency issue of the BS cooperation based resource allocation in multicell OFDMA systems.

Against the background, in this chapter, we design and compare two novel InterCI mitigation algorithms for the multicell downlink OFDMA systems on the basis of the subcarrier-allocation algorithms proposed in the previous chapters. Specifically, we first extend the on-off power (OOP) InterCI mitigation algorithm [116] to our multicell downlink OFDMA systems, which mitigates the InterCI by turning off the subchannels suffering from strong InterCI. Inspired by the OOP algorithm, our first proposed InterCI mitigation algorithm is the distributed decision making assisted cooperation (DDMC) algorithm, which is designed for maximizing the pay-off of cooperation while simultaneously minimizing the cost caused. In our DDMC algorithm, all the BSs first independently allocate subcarriers to their users and, then, each of the BSs independently makes its InterCI mitigation decisions, which are exchanged among the BSs to set up cooperation. In this chapter, we assume that, if there is a cooperation available, the DDMC algorithm sets up a space time block coding (STBC) aided cooperative transmission to a user with poor signal-to-interference ratio (SIR). Hence, if there is a cooperation for a user, the cooperating BSs are assumed to share the data of the user. However, if the cooperation for a user with poor SIR cannot be established, the transmission to the user is switched off. The second InterCI mitigation algorithm proposed is namely the centralized decision making assisted cooperation (CDMC) algorithm, which motivates to make the best InterCI mitigation decisions, based on limited InterCI information shared among the BSs, in order to maximize the sum rate of the users sharing a subcarrier, and to maximize the frequency reuse factor of the subcarriers. In the context of the CDMC algorithm, decisions are efficiently made by the BSs for the users sharing a subcarrier according to the three cases identified based on the InterCI matrix formed. Our studies and performance results in this chapter show that 5.2. System Model

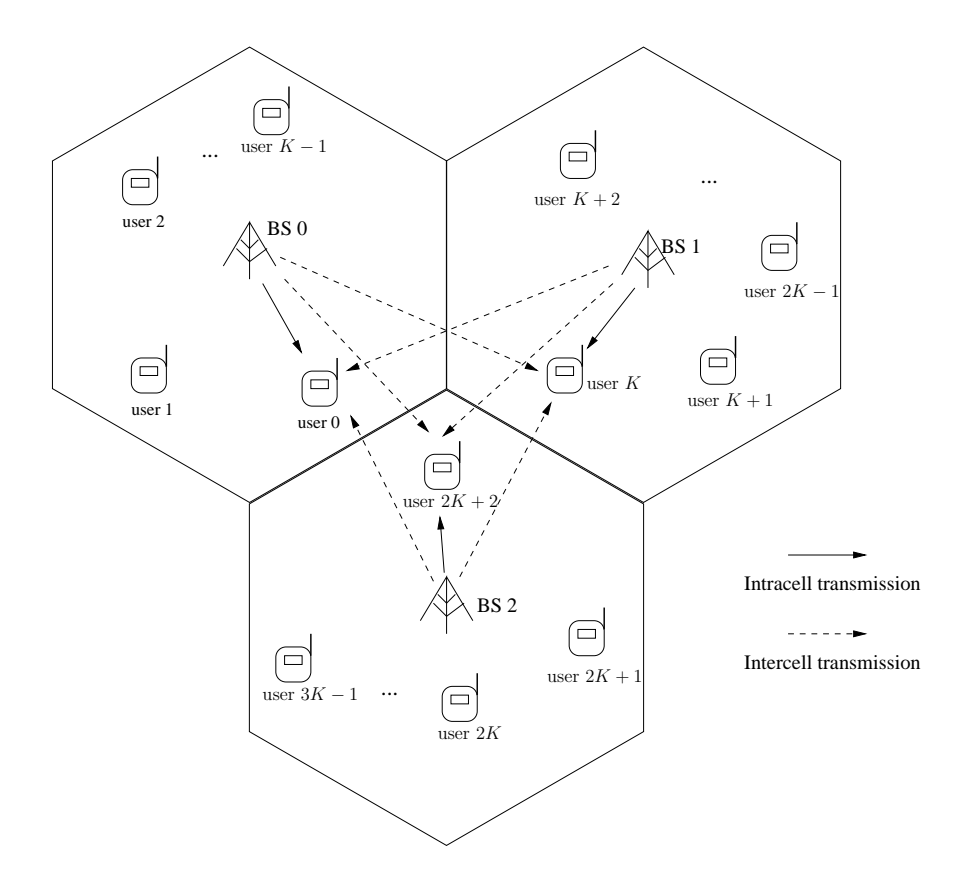


Figure 5.1: Conceptual structure of the multicell downlink OFDMA systems.

both the proposed DDMC and CDMC algorithms can outperform the OOP algorithm in terms of the achievable spectrum-efficiency. The CDMC algorithm provides the highest frequency reuse factor. Furthermore, in this chapter, we also analyze the overhead required by the various InterCI mitigation algorithms proposed and considered.

The rest of this chapter is organized as follows. Section 5.2 introduces the system model and makes the main assumptions. Section 5.3 analyses the general principles of the distributed subcarrier-allocation in the multicell downlink OFDMA systems. Section 5.4 extends the famous InterCI mitigation algorithm of OOP to our multicell downlink OFDMA systems. Sections 5.5 and 5.6 introduce the proposed DDMC and CDMC algorithms, respectively, and analyze their characteristics. Section 5.7 demonstrates and discusses the simulation results concerning the spectrum-efficiency, frequency reuse factor and the overhead. At last, conclusions are made in Section 5.8.

5.2 System Model

We consider the resource allocation in a multicell downlink OFDMA system, as depicted in Figure 5.1. In order to describe the main features of multicell systems but for the sake of simplicity, we assume that the system consists of three cells, each of which has one base station (BS) supporting *K* mobile users. We assume that each of the communication terminals, including both BSs and

5.2. System Model 146

mobile users, employs one antenna for signal receiving and transmission. Furthermore, we assume that the OFDMA signalling is used for the downlink transmissions from BSs to mobile users [1]. In total, there are M number of subcarriers in the downlink of the considered three-cell OFDMA system. In order to make our description clear, we first define the following sets:

 $\mathcal{K}^{(u)}$ Set of user indexes in cell u, defined as $\mathcal{K}^{(u)} = \{uK + 0, uK + 1, \dots, uK + K - 1\}, u = 0,1,2;$

 \mathcal{K} Set of user indexes in all cells, defined as $\mathcal{K} = \bigcup_{u \in \{0,1,2\}} \mathcal{K}^{(u)} = \{0,1,\ldots,3K-1\};$

 $\hat{\mathcal{K}}^{(u)}$ Set of indexes of the users with SIR below the pre-defined SIR threshold in cell u;

 $\tilde{\mathcal{K}}^{(u)}$ Set of indexes of the cell-edge users in cell u, including the users in $\hat{\mathcal{K}}^{(u)}$, and the users in $\mathcal{K}^{(u)} - \hat{\mathcal{K}}^{(u)}$, which share the same subcarriers as the users in $\hat{\mathcal{K}}^{(u')}$ and $\hat{\mathcal{K}}^{(u'')}$ in cells u', u'' $(u \neq u' \neq u'')$;

 $\tilde{\mathcal{K}}$ Set of indexes of the cell-edge users in the system, i.e., $\tilde{\mathcal{K}}=\tilde{\mathcal{K}}^{(0)}\cup \tilde{\mathcal{K}}^{(1)}\cup \tilde{\mathcal{K}}^{(2)};$

 \mathcal{M} Set of subcarrier indexes, defined as $\mathcal{M} = \{0, 1, \dots, M-1\}$;

 $\mathcal{F}_m^{(u)}$ Set of indexes for the users assigned to subcarrier m in cell u.

In this chapter, for simplicity, we assume that each user in a cell is assigned a single subcarrier, i.e., K = M. Note that, the IntraCI to each user can be avoided by assigning different subcarriers to the users in a cell, but each user still suffers from the InterCI imposed by the other two users in the adjacent cells assigned the same subcarrier. Therefore, our subcarrier-allocation satisfies that

$$\bigcup_{m \in \mathcal{M}} \mathcal{F}_m^{(u)} = \mathcal{K}^{(u)}, \ \forall u \in \{0, 1, 2\},\tag{5.1}$$

$$\mathcal{F}_{m}^{(u)} \cap \mathcal{F}_{m'}^{(u)} = \emptyset, \ m \neq m', \ \forall m, m' \in \mathcal{M}, \ \forall u \in \{0, 1, 2\}, \tag{5.2}$$

$$|\mathcal{F}_{m}^{(u)}| = 1, \ \forall m \in \mathcal{M}, \ \forall u \in \{0, 1, 2\}.$$
 (5.3)

As shown in Figure 5.1, we assume that each BS locates at the center of a hexagonal cell, and K users uniformly distribute in the cell. We assume that, in each cell, ideal power control is applied to maintain the same received power by its K intracell users, which is normalized to one. We assume that each BS transmits signals only to its intracell users, and InterCI exists only between adjacent cells owing to the propagation pathloss. Let the InterCI be characterized by a factor α , which, when taking into account of the combined effects of propagation pathloss, shadowing and transmit power, can be expressed as [206]

$$\alpha = \sqrt{\left(\frac{d_0}{d_1}\right)^{\mu} 10^{\frac{\zeta_0 - \zeta_1}{10}}} \tag{5.4}$$

5.2. System Model

where d_0 and d_1 represent the distances from a BS to the considered intracell and intercell users, respectively. In (5.4), μ is the pathloss exponent, and ζ_0 , ζ_1 (in dB) are zero-mean Gaussian distributed random variables with standard deviation Y (in dB), which account for the shadowing effect. Owing to ζ_0 and ζ_1 having the correlation depending on the propagation attenuation from a BS to the two users, ($\zeta_0 - \zeta_1$) has been illustrated to obey the log-normal distribution with zero mean and standard deviation of Y (in dB) [206]. In addition to the propagation pathloss and shadowing effects, signals transmitted from BSs to users also experience the fast fading, which, is assumed to be the independent Rayleigh flat fading in terms of different users.

Let us assume that the data symbol to be transmitted by BS u to an intracell user k ($k \in \mathcal{K}^{(u)}$) is expressed as x_k , which is assumed to satisfy $E[x_k] = 0$ and $E[|x_k|^2] = 1$. Furthermore, let us assume that subcarrier m is assigned to user k. Then, considering that the M subcarriers are orthogonal, the signal received by user k of cell u can be written as

$$y_{k} = h_{k,m}^{(u)} w_{k}^{(u)} x_{k} + \sum_{\substack{u' \in \{0,1,2\}, u' \neq u \\ \text{InterCI}}} h_{k,m}^{(u')} \alpha_{k',k}^{(u')} w_{k'}^{(u')} x_{k'} + n_{k},$$

$$(5.5)$$

$$k \in \mathcal{K}^{(u)}, \ k' \in \mathcal{K}^{(u')}, \ u \in \{0,1,2\}$$

when users k and k' are all assigned subcarrier m, satisfying

$$\mathcal{F}_m^{(u)} = \{k\}, \ \mathcal{F}_m^{(u')} = \{k'\}, \ m \in \mathcal{M}.$$
 (5.6)

In (5.5), y_k is the received signal of user k, and n_k is the noise variable at user k. The noise variables of all users in the system are assumed to obey the complex Gaussian distribution with zero mean and a variance of $2\sigma^2$, where $2\sigma^2=1/\bar{\gamma}_s$ and $\bar{\gamma}_s$ denotes the average SNR per symbol. Note that, in (5.5), $h_{k,m}^{(u)}$ is the channel gain of fast fading from BS u to its intracell user k assigned with subcarrier m. Furthermore, in (5.5), $h_{k,m}^{(u')}\alpha_{k',k}^{(u')}$ is the channel gain of the InterCI of user k imposed by BS u'. While $h_{k,m}^{(u')}$ is the channel gain of fast fading from BS u' to user k on subcarrier m, and the factor $\alpha_{k',k}^{(u')}$ characterizes the slow fading from BS u' to user k, by assuming that user k' is assigned the same subcarrier as user k. The slow fading factor $\alpha_{k',k}^{(u')}$ is defined by (5.4), which incorporates the effects of pathloss, shadowing and transmit power. In this chapter, we assume that the uplinks and downlinks are operated in the TDD mode. In this way, each BS has the CSI of the fast fading channels of all subcarriers between the BS and all the k' intracell users, i.e., k' is a capable of preprocessing the signals to be transmitted to its intracell users by setting

$$w_k^{(u)} = \frac{(h_{k,m}^{(u)})^*}{\sqrt{|h_{k,m}^{(u)}|^2}}$$
 (5.7)

where $(\cdot)^*$ denotes the conjugate operation. However, we assume that a BS does not have the CSI of the InterCI channels (including both the fast and slow fading) between a BS and the 2K users in the other two cells. In this case, if a BS simply carries out the subcarrier-allocation for its K users

based only on the knowledge about its KM downlink intracell channels, the performance achieved might be very poor, due to the InterCI.

Assume that users in different cells generate interference independently. Then, from (5.5), the signal-to-interference-plus-noise ratio (SINR) for user k is

$$\gamma_{k} = \frac{|h_{k,m}^{(u)}|^{2}}{\sum_{u' \in \{0,1,2\}, u' \neq u} |h_{k,m}^{(u')} \alpha_{k',k}^{(u')} w_{k'}^{(u')}|^{2} + 2\sigma^{2}}
= \frac{|h_{k,m}^{(u)}|^{2}}{I_{k} + 2\sigma^{2}}, \quad k \in \mathcal{K}^{(u)}, k' \in \mathcal{K}^{(u')}, m \in \mathcal{M}$$
(5.8)

where $I_k = \sum_{u' \in \{0,1,2\}, u' \neq u} |h_{k,m}^{(u')} \alpha_{k',k}^{(u')} w_{k'}^{(u')}|^2$ is the power of InterCI on user k. From (5.8), explicitly, when user k is allocated a subcarrier with a higher channel quality of $|h_{k,m}^{(u)}|^2$, while its InterCI users are allocated the subcarriers generating a lower value of $|h_{k,m}^{(u')} \alpha_{k',k}^{(u')}|^2$, user k can obtain a relatively high SINR and, hence, a lower error rate, if a given baseband modulation scheme is considered, or a higher data rate, if variable rate transmission is possible.

5.3 General Theory

In this section, we discuss the general theory for design of the subcarrier-allocation algorithms for the multicell downlink OFDMA system, as discussed in Section 5.2. In cellular communication systems, reliability and spectrum-efficiency are the two most important metrics for performance measurement. As mentioned before, in our three-cell OFDMA system, we employ M subcarriers to support 3K users distributed in three cells. Hence, when the objective is to maximize the system's reliability, the subcarrier-allocation optimization problem can be described as

$$\bigcup \left\{ \mathcal{F}_{m}^{(u)} \middle| u \in \{0, 1, 2\} \right\}^{*} = \arg \min_{\bigcup \left\{ \mathcal{F}_{m}^{(u)} \middle| u \in \{0, 1, 2\} \right\}} \left\{ \frac{1}{3K} \sum_{k \in \mathcal{K}} \bar{P}_{e}^{(k)}(\gamma_{k}) \right\}, \tag{5.9}$$
s.t. (5.1), (5.2), (5.3)

where 's.t.' stands for 'subject to'. In (5.9), $\cup \left\{ \mathcal{F}_m^{(u)} | u \in \{0,1,2\} \right\}$ stands for testing all the possible allocations for all users, while $\cup \left\{ \mathcal{F}_m^{(u)} | u \in \{0,1,2\} \right\}^*$ contains the final allocation results for all the users. Note that, in this chapter, no power-allocation is considered owing to using power control. As mentioned in Chapter 3, it is often very hard to solve the optimization problem of (5.9), due to the nonlinear relationship between $\bar{P}_e^{(k)}(\gamma_k)$ and γ_k . However, the average BER \bar{P}_e is usually dominated by the user with the lowest SINR [84]. As done in [75,83,188], the subcarrier-allocation algorithm can be designed to maximize the minimum SINR of the users. Correspondingly, the optimization problem can be described as

$$\bigcup \left\{ \mathcal{F}_{m}^{(u)} \middle| u \in \{0, 1, 2\} \right\}^{*} = \arg \max_{\bigcup \left\{ \mathcal{F}_{m}^{(u)} \middle| u \in \{0, 1, 2\} \right\}} \left\{ \min_{u \in \{0, 1, 2\}, k \in \mathcal{K}^{(u)}} \left\{ \gamma_{k} \right\} \right\}, \qquad (5.10)$$
s.t. (5.1), (5.2), (5.3).

As in the previous chapters, in this chapter we motivate to design the subcarrier-allocation algorithms that do not make a trade-off between reliability and spectrum-efficiency of the system. Therefore, while guaranteeing that the minimum SINR of users (which is in fact equivalent to the minimum signal-to-interference ratio (SIR) of users, as shown later) is higher than a threshold, our objective of subcarrier-allocation is to maximize the spectrum-efficiency of users, with the optimization problem described as

$$\cup \left\{ \mathcal{F}_{m}^{(u)} | u \in \{0, 1, 2\} \right\}^{*} = \arg \max_{0 \in \mathcal{F}_{m}^{(u)} | u \in \{0, 1, 2\} } \left\{ \sum_{k \in \mathcal{K}} \log_{2}(1 + \gamma_{k}) \right\},$$
 (5.11)

$$\eta_k > \eta_t, \ \forall k \in \mathcal{K}$$
(5.12)

where γ_k is the SINR of user k, which is given by (5.8), and η_k , η_t are the SIR of user k and the SIR threshold. Alternatively, the SINR of (5.8) can be written as

$$\gamma_k = \frac{1}{\eta_k^{-1} + A_k^{-1}}, \ k \in \mathcal{K}^{(u)}$$
 (5.13)

where A_k is the signal to noise ratio (SNR) of user k, which are expressed as

$$\eta_k = \frac{|h_{k,m}^{(u)}|^2}{I_k}, \ A_k = \frac{|h_{k,m}^{(u)}|^2}{2\sigma^2}, \ k \in \mathcal{K}^{(u)}.$$
(5.14)

It can be shown that (5.10) and (5.11) are non-convex problems, which are extremely difficult to solve for the optimum solutions. In order to find the promising sub-optimum solutions simultaneously approximating (5.10) and (5.11), in this chapter, we propose two novel subcarrier-allocation algorithms, which first carry out subcarrier-allocation independently at each of the BSs. Then, minimum cooperation among the three BSs is operated, in order to mitigate the InterCI. The procedure is summarized in Figure 5.2, each BS first independently allocates the subcarriers to its K users. Then, InterCI is mitigated with the aid of some information exchange among the BSs, as will become explicit in our forthcoming discourses.

In this chapter, we assume that, for subcarrier-allocation, a BS only knows the CSI of its intracell channels, i.e., BS u ($u \in \{0,1,2\}$) carries out the subcarrier-allocation only based on the CSI of the KM intracell subchannels, which are $\{h_{k,m}^{(u)}|k\in\mathcal{K}^{(u)},m\in\mathcal{M}\}$. Furthermore, we assume that all the K users in the same cell suffer from the Gaussian noise signals with the same variance of $2\sigma^2$. In this case, BS u has the knowledge of the SNRs of its K users with respect to the M subcarriers, i.e., BS u knows $\{A_k|k\in\mathcal{K}^{(u)},\cup\{\mathcal{F}_m^{(u)}\}\}$, which are referred to as the subchannel qualities of the K users. Therefore, when BS u carries out the subcarrier-allocation motivating to maximize the subchannel qualities of all its K users, the optimization problem can be described as

$$\bigcup \{\mathcal{F}_{m}^{(u)}\}^{*} = \arg \max_{\bigcup \{\mathcal{F}_{m}^{(u)}\}} \left\{ A_{k}, \ k \in \mathcal{K}^{(u)} \right\}, \ \forall u \in \{0, 1, 2\},
\text{s.t. (5.1), (5.2), (5.3).}$$

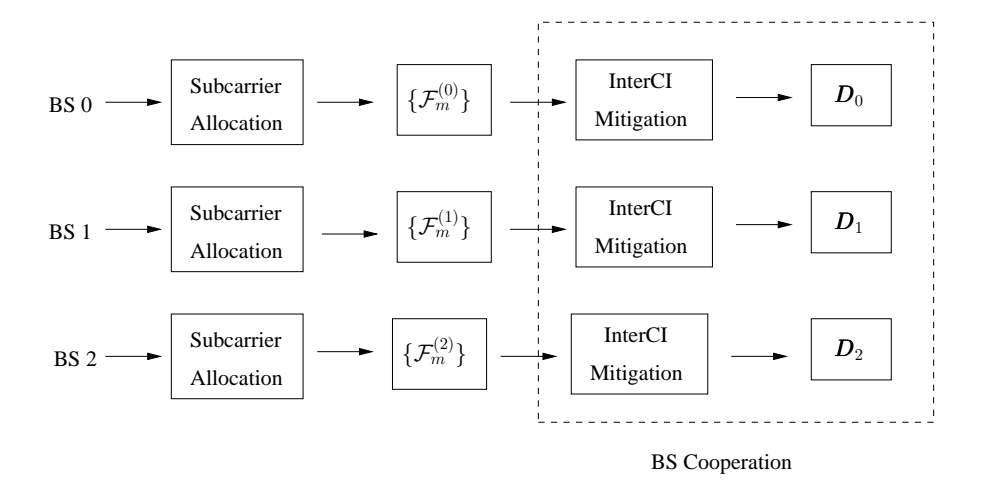


Figure 5.2: Flow chart illustrating the proposed distributed subcarrier-allocation and InterCI mitigation in the multicell downlink OFDMA systems.

Based on the knowledge of the intracell subchannel qualities, the subcarrier-allocation may achieve the best performance when without InterCI. However, according to (5.8) and (5.13), the SINR of a user may be very low, if it suffers from strong InterCI, even though the SNR of the user is high. For this sake, after the subcarrier-allocation, an InterCI mitigation algorithm is operated, trying to solve the optimization problem

$$\mathbf{D}^* = \arg\max_{\{\mathbf{D}\}} \left\{ \sum_{k \in \mathcal{K}_m} \log_2(1 + \gamma_k), \ \forall m \in \mathcal{M} \mid \bigcup \{\mathcal{F}_m^{(u)}\}^* \right\}, \tag{5.16}$$

$$\gamma_k = 0$$
, if $\eta_k < \eta_t$, $\forall k \in \mathcal{K}$ (5.17)

where K_m contains the indexes of the users in the three cells sharing subcarrier m. η_t is the SIR threshold required for all users to achieve certain quality of service (QoS), which can be set a value according to given communication scenarios. As described in (5.17), the SIR of a user activated is higher than the SIR threshold η_t . In (5.16), D is a length-3M vector, which is referred to as the InterCI mitigation decision (IMD) vector. The IMD vector is in the form of

$$\mathbf{D} = \left[\mathbf{D}_0^T \ \mathbf{D}_1^T \ \mathbf{D}_2^T \right]^T \tag{5.18}$$

where $\mathbf{D}_u = [D_{u,0}, D_{u,1}, \dots, D_{u,M-1}]^T$ is the IMD vector of BS u ($u \in \{0,1,2\}$), which provides the transmission states on M subcarriers by BS u. Specifically, the mth element of \mathbf{D}_u , i.e., $D_{u,m}$, has three states defined as

$$D_{u,m} = \begin{cases} k & \text{if BS } u \text{ transmits } x_k \text{ of its intracell user } k \text{ on subcarrier } m, \\ -1 & \text{if BS } u \text{ turns off transmission on subcarrier } m, \\ k' & \text{if BS } u \text{ helps to transmit } x_{k'} \text{ of user } k' \text{ in cell } u' \neq u \text{ on subcarrier } m. \end{cases}$$
 (5.19)

5.3. General Theory 151

Note that, when $D_{u,m} = -1$, BS u switches off the transmission on subcarrier m. In this case, when assuming that subcarrier m is allocated to user k' in cell u', and to user k'' in cell u'', then, the SINRs of these two users become

$$\gamma_{k'} = \frac{|h_{k',m}^{(u')}|^2}{|h_{k',m}^{(u'')}\alpha_{k'',k'}^{(u'')}|^2 + 2\sigma^2}, \qquad \gamma_{k''} = \frac{|h_{k'',m}^{(u'')}|^2}{|h_{k'',m}^{(u')}\alpha_{k',k''}^{(u')}|^2 + 2\sigma^2}$$
(5.20)

which show that both users k' and k'' experience only one InterCI. Furthermore, it can be easily understood that the SINRs of users k' and k'' can be significantly improved, if user k imposes strong InterCIs on them. Hence, in multicell communications, it is sometimes very efficient for a BS to turn off some transmissions on some subcarriers, as shown in [116].

By contrast, when $D_{u,m} = k'$ in (5.19), BS u chooses to cooperate with BS u', and helps it to transmit $x_{k'}$ to user k' in cell u'. Note that, in order to achieve the cooperative transmission, in this chapter, we assume that symbol $x_{k'}$ is known to BS u, which requires a small amount of overhead. However, for those non-cooperative subcarriers, there is no sharing of data. Since we assume that there is no CSI exchange among the BSs, the optimum cooperation scheme for the two BSs is the classic space time block coding (STBC) [207], which achieves transmit diversity. Specifically, when BS u cooperates with BS u' to transmit $x_{k'}(t)$ and $x_{k'}(t+T)$ to user k' at time t and t+T (t is the symbol duration), respectively, while experiencing interference from BS t', the observations received by user t' in two consecutive time slots can be expressed as

$$y_{k'}(t) = h_{k',m}^{(u')} x_{k'}(t) + h_{k',m}^{(u)} \alpha_{k,k'}^{(u)} x_{k'}(t+T) + h_{k',m}^{(u'')} \alpha_{k'',k'}^{(u'')} x_{k''}(t) + n_{k'}(t),$$
(5.21)

$$y_{k'}(t+T) = -h_{k',m}^{(u')} x_{k'}^*(t+T) + h_{k',m}^{(u)} \alpha_{k,k'}^{(u)} x_{k'}^*(t) + h_{k',m}^{(u'')} \alpha_{k'',k'}^{(u'')} x_{k''}(t+T) + n_{k'}(t+T)$$
 (5.22)

when assuming that the related channels stay the same during two symbol durations (or two transmission time slots when transmission of packets is considered). Assume that user k' is capable of estimating the channels from both BS u and BS u'. Then, user k' can form the decision variables as

$$r_{k'}(t) = (h_{k',m}^{(u')})^* y_{k'}(t) + h_{k',m}^{(u)} \alpha_{k,k'}^{(u)} (y_{k'}(t+T))^*,$$
(5.23)

$$r_{k'}(t+T) = (h_{k',m}^{(u)}\alpha_{k,k'}^{(u)})^* y_{k'}(t) - h_{k',m}^{(u')}(y_{k'}(t+T))^*.$$
(5.24)

Based on (5.23) and (5.24), it can be shown that the SINR of user k' at both time t and t + T is

$$\gamma_{k'} = \frac{|h_{k',m}^{(u')}|^2 + |h_{k',m}^{(u)}\alpha_{k,k'}^{(u)}|^2}{|h_{k',m}^{(u'')}\alpha_{k'',k'}^{(u'')}|^2 + 2\sigma^2}.$$
(5.25)

Since BS u helps BS u' to send information to user k', only when it generates strong InterCI on user k', the SINR of (5.25) may be significantly enhanced, in comparison with (5.8) of the case without BS cooperation.

As shown in (5.16), our objective of InterCI mitigation is to maximize the sum rate of the users sharing the same subcarrier in the system. This can be achieved by properly design of the

IMD vector. In this chapter, we will consider three approaches, including two proposed distributed InterCI mitigation algorithms. In a little more detail, we first consider a benchmark InterCI mitigation algorithm, namely the on-off power (OOP) algorithm [116, 143, 144], which is a distributed algorithm without any BS cooperation. Then, we propose a so-called distributed decision making assisted cooperation (DDMC) algorithm, and the centralized decision making assisted cooperation (CDMC) algorithm. We will see that both of the proposed algorithms require only little BS cooperation, although the CDMC algorithms demands a little more information exchange among the BSs than the DDMC algorithm.

5.4 On-Off Power InterCI Mitigation

The OOP algorithm is an efficient method to combat InterCI, and it has been widely studied and used in multicell communication systems, such as, in [116, 143, 144]. The OOP algorithm has mainly been considered for power-allocation in literature, e.g., in [116]. In this section, we extend the OOP algorithm to our multicell OFDMA system for the purpose of InterCI mitigation, which hence results in performance improvement. The basic principle of the OOP algorithm is that a BS turns off the transmission on the subchannels that are suffering from strong InterCI. By doing this, there are two-fold of benefits. First, transmission on the subchannels with poor quality can be avoided, which can save power for future transmission, when the subchannels have good quality. Second, the InterCI imposed by these subchannels can also be removed. In our downlink OFDMA system, we assume that a BS does not know the InterCI on its *K* users. However, each mobile user is capable of estimating the signal strength from its own BS as well as the InterCI from other BSs. Hence, the user knows the received SIR. Consequently, mobile users may inform their BSs to turn off the transmission or not, based on the measured SIR values.

Let us assume that subcarrier m is allocated to users k, k', k'' in cells u, u' and u'', respectively. Then, we can express the subchannel qualities (some of them in fact generate InterCI) on subcarrier m in a matrix form as

$$\mathbf{A}_{m} = \begin{bmatrix} A_{k,m}^{(u)} & A_{k',m}^{(u)} & A_{k'',m}^{(u)} \\ A_{k,m}^{(u')} & A_{k',m}^{(u')} & A_{k'',m}^{(u')} \\ A_{k,m}^{(u'')} & A_{k',m}^{(u'')} & A_{k'',m}^{(u'')} \end{bmatrix}$$

$$= \begin{bmatrix} \frac{|h_{k,m}^{(u)}|^{2}}{2\sigma^{2}} & \frac{|h_{k',m}^{(u)}\alpha_{k,k'}^{(u)}|^{2}}{2\sigma^{2}} & \frac{|h_{k'',m}^{(u)}\alpha_{k,k''}^{(u)}|^{2}}{2\sigma^{2}} \\ \frac{|h_{k,m}^{(u')}\alpha_{k',k}^{(u')}|^{2}}{2\sigma^{2}} & \frac{|h_{k',m}^{(u')}\alpha_{k',k'}^{(u')}|^{2}}{2\sigma^{2}} & \frac{|h_{k'',m}^{(u')}\alpha_{k',k''}^{(u')}|^{2}}{2\sigma^{2}} \\ \frac{|h_{k,m}^{(u'')}\alpha_{k'',k}^{(u'')}|^{2}}{2\sigma^{2}} & \frac{|h_{k',m}^{(u'')}\alpha_{k',k'}^{(u'')}|^{2}}{2\sigma^{2}} & \frac{|h_{k'',m}^{(u'')}\alpha_{k',k''}^{(u'')}|^{2}}{2\sigma^{2}} \end{bmatrix}$$

$$(5.26)$$

where $A_{j,m}^{(i)}$ represents the subchannel quality of the transmission from BS i to user j on subcarrier m. Based on a column of A_m , a user can estimate its SIR, and when the OOP algorithm is employed, the user can inform its BS to turn off the transmission on subcarrier m, if the SIR is lower than the

SIR threshold. For example, user *k* can inform its BS to take the actions:

Power off, if
$$\eta_k < \eta_t$$
, (5.27)

Power on, if
$$\eta_k \ge \eta_t$$
 (5.28)

where η_k is the derived SIR of user k, and η_t is the SIR threshold.

Note that, the OOP algorithm is carried out by a BS at a time, in order to avoid that two or three cells simultaneously turn off the transmission on the same subcarrier. Therefore, when three cells are considered, three stages are required to complete one cycle of the OOP algorithm. Note furthermore that, when there are more cells, similar 'on-off' strategies can be designed. However, in cellular communications, as one mobile user can only be close to at most three cells. Three stages are usually enough for complete the OOP algorithm.

Let us below illustrate the OOP algorithm with the aid of an example. Suppose that, in a three-cell OFDMA system, there are M=8 subcarriers supporting 3K=24 users with each cell supporting K=8 users. Furthermore, let us assume that subcarrier 0 is allocated to users 4, 10, 19, which can be written as $\mathcal{F}_0^{(0)}=\{4\}$, $\mathcal{F}_0^{(1)}=\{10\}$ and $\mathcal{F}_0^{(2)}=\{19\}$, in cells 0, 1 and 2. Then, the subchannel quality matrix for subcarrier 0 is given by

$$\mathbf{A}_{0} = \begin{bmatrix} A_{4,0}^{(0)} & A_{10,0}^{(0)} & A_{19,0}^{(0)} \\ A_{4,0}^{(1)} & A_{10,0}^{(1)} & A_{19,0}^{(1)} \\ A_{4,0}^{(2)} & A_{10,0}^{(2)} & A_{19,0}^{(2)} \end{bmatrix} = \begin{bmatrix} 2.1909 & 0.0018 & 0.5078 \\ 1.4294 & 1.8621 & 0.1583 \\ 0.1168 & 3.3187 & 1.6459 \end{bmatrix}.$$
 (5.29)

When the OOP algorithm is employed, by setting different SIR thresholds we may obtain different ON-OFF results, such as, the IMD variables, $\{D_{u,m}\}$, and the corresponding sum rate $C_{\Sigma} = \sum_{k \in \{4,10,19\}} \log_2(1+\gamma_k)$. For the example of (5.29), the OOP algorithm gives the InterCI mitigation decisions as

$$\begin{cases}
(a): D_{0,0} = 4, D_{1,0} = 10, D_{2,0} = 19 & \text{if } \eta_t = -5 \text{ dB,} \\
(b): D_{0,0} = 4, D_{1,0} = -1, D_{2,0} = 19 & \text{if } \eta_t = 0 \text{ dB,} \\
(c): D_{0,0} = -1, D_{1,0} = -1, D_{2,0} = 19 & \text{if } \eta_t = 5 \text{ dB.}
\end{cases}$$
(5.30)

Specifically, if we let $\eta_t = -5$ dB= 0.316, there will be no user with power off, since the SIRs of the three users are all higher than the SIR threshold. In this case, the IMD variables are given by (5.30)(a) and the sum rate achievable by subcarrier 0 is $C_{\Sigma} = 2.4039$. Correspondingly, no InterCI mitigation actions are taken.

By contrast, when the SIR threshold is 0 dB, i.e., $\eta_t = 0$ dB= 1.0, the OOP algorithm will be executed as follows. During the first stage, user 4 estimates its SIR, giving $\eta_4 = \frac{A_{4,0}^{(0)}}{A_{4,0}^{(1)} + A_{4,0}^{(2)}} = 1.4171$, which is higher than the threshold. Therefore, user 4 stays on and BS 0 transmits signal to it on subcarrier 0. During the second stage, user 10 estimates its SIR, obtaining $\eta_{10} = 0.5608$, which is lower than the required threshold. Hence, user 10 changes to the off state and informs BS 1 to stop transmitting signal to it. During the third stage, user 19 finds that its SIR is higher than the

threshold and, certainly, it stays on. Consequently, when $\eta_t = 0$ dB, we have the IMD variables of (5.30)(b), and the sum rate of $C_{\Sigma} = 2.6311$, which is higher than $C_{\Sigma} = 2.4039$ of the case without using the InterCI mitigation.

Furthermore, when $\eta_t = 5 \, \mathrm{dB} = 3.1623$, then, the OOP algorithm has the following operations. During the first stage, user 4 informs BS 0 to turn off the transmission to it, since $\eta_4 \leq \eta_t$. During the second stage, user 10 estimates its SIR, giving $\eta_{10} = A_{10,0}^{(1)}/A_{10,0}^{(2)} = 0.5611$, which is still lower than the threshold. Hence, it informs BS 2 to stop transmitting it information. As user 4 in cell 0 and user 10 in cell 1 have been turned off, there are no InterCIs on user 19 in cell 2. Hence, during the third stage, user 19 will stay on, as its SIR becomes infinite. As a result, when $\eta_t = -5 \, \mathrm{dB}$, we have the IMD variables of (5.30)(c), and, correspondingly, the sum rate of subcarrier 0 is $C_{\Sigma} = 1.4038$, which is lower than that obtained by setting $\eta_t = 0 \, \mathrm{dB}$.

From the above example, we are implied that the performance of the system employing the OOP algorithm is highly dependent on the SIR threshold. If an improper SIR threshold is set, it may cause to turn off some very good subchannels or to keep the transmissions on some very poor subchannels, both of which may lead to decrease of throughput performance. Therefore, it is very important to set up a proper SIR threshold for the OOP algorithm, in order to efficiently mitigate the InterCI and achieve the highest possible sum rate.

In general, the OOP algorithm can be described as follows.

Algorithm 9. (On - Off Power Algorithm)

Initialization: Set $D_{u,m} = k$ if $F_m^{(u)} = \{k\}, \forall u \in \{0,1,2\}$ and $\forall m \in \mathcal{M}$.

For Stage u = 0, 1, 2:

Step 1 All users in cell
$$u$$
 estimate their SIRs, using the formula $\eta_k = \frac{|h_{k,m}^{(u)}|^2}{\sum_{u' \in \{0,1,2\}, u' \neq u} I_{u',k}}$ where $I_{u',k} = 0$ if $D_{u',m} = -1$ and $F_m^{(u')} = \{k'\}$, otherwise $I_{u',k} = |h_{k,m}^{(u')} \alpha_{k',k}^{(u')}|^2$.

Step 2 Let the set of users whose SIRs are lower than the threshold be expressed as $\hat{\mathcal{K}}^{(u)}$, i.e., $\hat{\mathcal{K}}^{(u)} = \{\hat{k}|\eta_{\hat{k}} < \eta_t, \hat{k} \in \mathcal{K}^{(u)}\}$. Then, the users in $\hat{\mathcal{K}}^{(u)}$ inform BS u to stop their transmissions.

Step 3 BS u updates the corresponding IMD variables as $D_{u,\hat{m}} = -1$, if $F_{\hat{m}}^{(u)} = \{\hat{k}\}, \forall \hat{k} \in \hat{\mathcal{K}}^{(u)}$.

5.5 Distributed Decision Making Assisted Cooperation InterCI Mitigation

In this section, we propose a novel InterCI mitigation scheme, which is called as the distributed decision making assisted cooperation (DDMC) algorithm. As its name suggests, the DDMC algorithm introduces cooperation among BSs to enhance the performance.

In Section 5.3, we have shown how a user can benefit from the cooperative transmission. Specifically, as shown in (5.25), when the STBC is employed for two BSs to transmit to one user, the SINR of a user can be significantly improved, if the cooperative BS imposes large InterCI on the user. The cost for the above-mentioned cooperation is the increased complexity for information exchange between BSs and that some BSs have to stop transmitting information to some of their own users. Therefore, our DDMC algorithm is designed for maximizing the pay-off from the cooperation, while simultaneously minimizing the cost caused.

In our DDMC algorithm, the following assumptions are introduced. First, we assume that a BS is capable of sharing the data of its users with another BS, whenever necessary. Specifically, if two BSs decide to cooperate to send information to one user, the BS holding the data of the user will forward them to the cooperative BS. Second, we assume that the BSs do not share their CSI of their users. Hence, we assume that two BSs transmit to a user by employing the STBC scheme [207]. In this case, we assume that every user is able to estimate the required CSI and can carry out coherent detection or STBC decoding. Note that, our proposed DDMC algorithm is a distributed decision-making algorithm, which is independently operated at the individual BSs.

In the DDMC algorithm, we also introduce a SIR threshold. When the SIR measured by a user is lower than the threshold, it informs its BS to take one of the actions: 1) Setting up a cooperative transmission for the user, and 2) switching off the transmission to the user. Let us below explain the principles. Let us assume that user k in cell u suffers the InterCI from both BSs u' and u'' (where $u \neq u' \neq u''$), and the InterCI power is $I_{u',k}$ and $I_{u'',k}$. Then, the rules for user k to make the decision are as follows:

Ask for cooperation from BS
$$u'$$
, if $\eta_k < \eta_t$, and $I_{u',k} > I_c$, $I_{u'',k} \le I_c$, (5.31)

Ask for cooperation from BS
$$u''$$
, if $\eta_k < \eta_t$, and $I_{u',k} \le I_c$, $I_{u'',k} > I_c$, (5.32)

Power off, if
$$\eta_k < \eta_t$$
, and either $I_{u',k} > I_c$, $I_{u'',k} > I_c$, or $I_{u',k} \le I_c$, $I_{u'',k} \le I_c$. (5.33)

In the above rules, I_c is the InterCI threshold for cooperation, which can be set according to the various communication objectives, such as, maximization of sum rate. As shown in (5.31) and (5.32), in our DDMC scheme, user k can only ask for cooperation, when only one BS imposes high InterCI on it, while the InterCI from the other BS is below the threshold I_c . However, if user k suffers strong InterCI from two BSs, as described in (5.33), user k simply inform its BS to stop transmitting it information. The reason for us to use this strategy will become clear during our forthcoming discussion. Additionally, when the InterCI from both interfering BSs is low, but the SIR is still lower than the threshold η_t , the BS also switches off the transmission to the user. This scenario is mainly that the channel from the BS to its user is very poor.

Let us now explain in detail why the rules in (5.31)-(5.33) are introduced. Suppose subcarrier m is allocated to user k in cell u, user k' in cell u' and user k'' in cell u''. Assume that only user k has a SIR being lower than the threshold η_t due to the high InterCI from BS u'. Then, when user k

obtains the cooperation from BS u', the SINRs of users k, k' and k'' become

$$\gamma_k = \frac{|h_{k,m}^{(u)}|^2 + I_{u',k}}{I_{u'',k} + 2\sigma^2}, \qquad \gamma_{k'} = 0, \qquad \gamma_{k''} = \frac{|h_{k'',m}^{(u'')}|^2}{I_{u,k''} + I_{u',k''} + 2\sigma^2}.$$
 (5.34)

From (5.34), we can see that the SINR of user k may be significantly improved, as (5.31) is met. In this case, the sum rate of the three users is most probably increased, owing to making use of the strong interference of $I_{u',k}$. However, if the case of (5.33) is met, the SINR of user k may not be improved too much, when both $I_{u',k}$ and $I_{u'',k}$ are very weak. When both $I_{u',k}$ and $I_{u'',k}$ are very strong, the cooperation of BS u' (or u''), or both of them with BS u is beneficial to user k. However, the cost is too much, as BS u' and u'' have to turn off their transmissions to users k', k''. Consequently, the sum rate of the three users may decrease, in comparison with the case without cooperation. Therefore, in the case of (5.33), it might be more beneficial to improve the sum rate of the users by simply turning off the transmission from BS u to user k.

As an example, when the DDMC algorithm is applied to a three-cell system with the subchannel quality matrix of subcarrier 0 is given by (5.29), the operations can be described as follows. First from (5.29) we can find that the SIRs of the three uses are $\eta_4 = 1.417$, $\eta_{10} = 0.5608$ and $\eta_{19} = 2.471$, respectively. By setting the various SIR thresholds and InterCI thresholds for cooperation, the IMD variables obtained by the DDCM algorithm are

$$\begin{cases}
(a): D_{0,0} = 4, D_{1,0} = 10, D_{2,0} = 10 & \text{if } \eta_t = 0 \text{ dB, } I_c = 1, \\
(b): D_{0,0} = 4, D_{1,0} = 4, D_{2,0} = -1 & \text{if } \eta_t = 5 \text{ dB, } I_c = 1.
\end{cases}$$
(5.35)

Then, let us first consider the scenario that $\eta_t=0$ dB=1.0 and $I_c=1$. In this case, during the first stage, user 4 finds that its SIR is higher than the SIR threshold η_t , it hence stays on. During the second stage, user 10 in cell 1 knows that its SIR is lower than the SIR threshold η_t . Then, it checks whether it can ask a BS for cooperation, by checking the InterCI from BSs 0 and 2. It can be shown that $I_{0,10} < I_c$ and $I_{2,10} > I_c$. Hence, according to the rules given in (5.31)-(5.33), user 10 informs BS 1 to request the cooperation from BS 2, and, as a result, BS 1 obtains the cooperation from BS 2 to send information to user 10. During the third stage, BS 2 informs user 19 the switch-off of transmission, as it is unable to transmit information to user 19. Assume that BSs 1 and 2 transmit information to user 19 using the STBC. Then, we can find that the sum rate of subcarrier 0 is $C_{\Sigma}=3.5213$, which is higher than that achieved by the OOP algorithm.

By contrast, when the SIR threshold becomes $\eta_t = 5$ dB=3.1623, and $I_c = 1$ during the first stage, user 4 finds that its SIR is $\eta_4 = 1.417 < \eta_t$, and $I_{1,4} = 1.4294 > I_c$, $I_{2,4} = 0.1168 < I_c$. Hence, user 4 informs BS 0 to request the cooperation from BS 1. After BS 1 accepts the cooperation request from BS 0, it stops the transmission to user 10. During the second stage, user 10 finds that its SIR is $\eta_4 = 0.5608 < \eta_t$, and $I_{0,10} = 0.0018 < I_c$, $I_{2,10} = 3.3187 > I_c$. Hence, it informs BS 1 to request the cooperation from BS 2. However, BS 1 has to refuse the request, as it has accepted the cooperation request from BS 0. Hence, BS 1 informs user 10 the turning off

of the transmission. During the third stage, user 19 informs BS 2 to turn off its transmission, as its SIR is lower than the threshold η_t and $I_{0,19} < I_c$, $I_{1,19} < I_c$, which satisfy the conditions in (5.33). Consequently, with BS 0 and BS 1 jointly transmitting to user 4 and BS 2 turning off the transmission to user 19, the sum rate achieved on subcarrier 0 is $C_{\Sigma} = 2.2080$. Clearly, the sum rate is higher than 1.4038 obtained by the OOP algorithm for the corresponding case.

Based on the above analysis and the examples, we can now summarize the DDMC algorithm as follows.

Algorithm 10. (Distributed Decision Making Assisted Cooperation Algorithm)

Initialization:

- (1) Set $D_{u,m} = k$ if $F_m^{(u)} = \{k\}, \forall u \in \{0,1,2\}$ and $\forall m \in \mathcal{M}$.
- (2) All users in the three cells estimate their SIRs, which can be expressed as $\eta_k = \frac{|h_{u,k,m}|^2}{\sum_{u' \in \{0,1,2\}, u' \neq u} I_{u',k}}$, when assuming that $F_m^{(u)} = \{k\}$, $F_m^{(u')} = \{k'\}$ and $F_m^{(u'')} = \{k''\}$, $\forall k \in \mathcal{K}^{(u)}$ and $\forall u \in \{0,1,2\}$. Let $\hat{\mathcal{K}}^{(u)} = \{\hat{k} | \eta_{\hat{k}} < \eta_t, \hat{k} \in \mathcal{K}^{(u)}\}$, $\forall u \in \{0,1,2\}$.

For Stage u = 0, 1, 2:

- **Step 1** In cell u, any of the users in $\hat{\mathcal{K}}^{(u)}$ informs BS u either to request for the cooperation from an identified BS, or to turn off its transmission, according to the rules defined in (5.31)-(5.33). The algorithm proceeds to Step 2, if BS u receives a request of turning off from user \hat{k} , while it proceeds to Step 3, if BS u receives a request from user \hat{k} , say, for cooperation from BS u'.
- **Step 2** BS u turns off the transmission to user \hat{k} , and updates the corresponding IMD variable to $D_{u,\hat{m}} = -1$.
- **Step 3** BS u requests BS u' for the cooperation to transmit information to user \hat{k} , and
 - (1) BS u' accepts the request if it has not cooperated with another BS, and updates the corresponding IMD variable to $D_{u',\hat{m}} = \hat{k}$, when assuming $F_{\hat{m}}^{(u)} = \{\hat{k}\}$. Then, it proceeds to Step 4.
 - (2) Otherwise, BS u' refuses the request of BS u, and proceeds to Step 2.
- **Step 4** BS u sends the data of user \hat{k} to BS u', and they transmit the data to user \hat{k} based on a STBC.

5.6 Centralized Decision Making Assisted Cooperation InterCI Mitigation

In this section, we propose and analyze another InterCI mitigation scheme, which carries out centralized decision making assisted cooperation (CDMC) with limited InterCI information sharing among the BSs. Similar to the DDMC, the CDMC algorithm considers turning off transmission to some users on some subcarriers, and cooperation between two BSs for transmission to a user on a

subcarrier. Our CDMC algorithm motivates to make the best InterCI mitigation decisions, based on limited InterCI information, in order to maximize the sum rate of users on a subcarrier, but also to improve the frequency reuse factor of the subcarriers.

As done in the DDMC algorithm, in the CDMC algorithm, we assume that the cooperative BSs share the data of the users that they jointly send information to. However, CSI is not shared between BSs. Hence, we assume that, once two BSs cooperate to send information to one user, the STBC transmission scheme is employed. Furthermore, we assume that each mobile user is capable of acquiring the required CSI to carry out coherent detection. In addition to the above assumptions similar to those used in the DDMC algorithm, the BSs operated under the CDMC are also assumed to share the "three-valued InterCI information" of users. As the name indicates, the three-valued InterCI information is characterized by one of three possible integer values, namely -1, 0, 1, which is determined by the power of the corresponding InterCI. Let us first use the example (5.29) to briefly explain the disadvantage of the DDMC algorithm considered in Section 5.5.

As the example discussed in Section 5.5 shows, when the SIR threshold is $\eta_t = 5$ dB, the DDMC algorithm finally gives the decision that BS 1 cooperating with BS 0 transmit to user 4, while BS 2 turns off its transmission to user 19. However, this is explicitly not the best InterCI mitigation strategy, and there are better solutions. For example, we may let BS 2 cooperate with BS 1 to transmit information to user 10, while BS 0 keeps transmitting to its own user 4. In this case, we can find that the sum rate on subcarrier 0 is $C_{\Sigma} = 3.5213$, which is higher than that $C_{\Sigma} = 2.208$ obtained by the DDMC algorithm. In order to make the above better decisions, BSs require the information about the InterCIs of users 4, 10 and 19, which yields a little bit higher complexity than the DDMC algorithm.

Inspired by the above example, in the CDMC algorithm, the BSs make the decisions based on the three-valued InterCI information shared among the BSs. Specifically, the three values for the InterCI suffered by a user are determined as

$$v_{u',k} = \begin{cases} -1 & \text{if } I_{u',k} < I_o, \\ 0 & \text{if } I_o \le I_{u',k} < I_c, \\ 1 & \text{if } I_{u',k} \ge I_c \end{cases}$$
 (5.36)

where $v_{u',k}$ denotes the digitized InterCI from BS u' to user k in cell u. In (5.36), $I_{u',k}$ is the InterCI on user k from user u', while I_o and I_c are two thresholds introduced. Furthermore, we refer to I_o as the "off-power threshold", and to I_c as the "cooperation threshold" which was used in (5.31)-(5.33). As shown in (5.36), the InterCI on user k is divided into three regions by the two thresholds. For convenience, we refer to these three regions as 1) ignorable InterCI, when $v_{u',k} = -1$, 2) moderate InterCI, if $v_{u',k} = 0$, and 3) strong InterCI, when $v_{u',k} = 1$. Suppose that subcarrier m is allocated to users k, k' and k'' in cells u, u' and u''. Let the corresponding digitized InterCI is expressed in

matrix form as

$$\mathbf{V}_{m} = \begin{bmatrix} v_{k} & v_{u,k'} & v_{u,k''} \\ v_{u',k} & v_{k'} & v_{u',k''} \\ v_{u'',k} & v_{u'',k''} & v_{k''} \end{bmatrix} = \begin{bmatrix} \mathbf{v}_{k,m} & \mathbf{v}_{k',m} & \mathbf{v}_{k'',m} \end{bmatrix}.$$
 (5.37)

Here, V_m is referred to as the digitized InterCI matrix, or simply the InterCI matrix, of subcarrier m, and $v_{k,m} = [v_k \ v_{u',k} \ v_{u'',k}]^T$ is the digitized InterCI vector of user j on subcarrier m. In (5.37), a non-diagonal element explains the strength of the InterCI between a BS and a user, which is derived from (5.36). By contrast, a diagonal element indicates whether the corresponding user has its SIR below or above the SIR threshold η_t , defined as

$$\nu_i = \begin{cases} 1 & \text{if } \eta_i < \eta_t, \\ 0 & \text{if } \eta_i \ge \eta_t \end{cases}$$
 (5.38)

for i = k, k' and k''.

In the context of the CDMC algorithm, the decisions made by the BSs for a user are according to the four cases determined by the digitized InterCI matrix V_m given by (5.37).

- Case 0 (No Actions): When $\nu_0 = \nu_1 = \nu_2 = 0$. All BSs transmit to their users on the allocated subcarriers.
- Case 1 (**Cooperation**): At least one of the three users on a subcarrier satisfies the conditions in (5.39).

$$\nu_k = 1 \& v_{u'k} = 1 \& v_{u''k} \neq 1 \tag{5.39}$$

where $k \in \mathcal{K}^{(u)}$, $u \neq u' \neq u''$, $\forall u \in \{0, 1, 2\}$.

• Case 2 (**Possible Cooperation**): Any of the three users on a subcarrier does not satisfy the conditions in (5.39), but at least one of the users satisfies the conditions of (5.40).

$$v_k = 1 \& v_{u',k} = 1 \& v_{u'',k} = 1$$
 (5.40)

where $k \in \mathcal{K}^{(u)}$, $u \neq u' \neq u''$, $\forall u \in \{0, 1, 2\}$.

• Case 3 (**No Cooperation**): Any of the three users on a subcarrier does not satisfy the conditions of (5.39) and (5.40), but at least one of the users satisfies the conditions of (5.41).

$$v_k = 1 \& v_{u',k} \neq 1 \& v_{u'',k} \neq 1 \tag{5.41}$$

where $k \in \mathcal{K}^{(u)}$, $u \neq u' \neq u''$, $\forall u \in \{0, 1, 2\}$.

Let us below discuss the operations under Cases 1-3 in more detail.

When the InterCI matrix V_m belongs to Case 1, the CDMC algorithm will be operated as the flow chart shown in Figure 5.3. Note that, in Case 1, we can always set up a cooperative transmission for a user whose SIR is below the SIR threshold η_t . However, there are sometimes more than one cooperation options possible. In this case, the CDMC algorithm aims to find the best one, in order to maximize the sum rate of the considered subcarrier. As shown in Figure 5.3, specifically, the decisions are made within three iterations, where s denotes the iteration index. Furthermore, in order to evaluate the decision made in an iteration, we introduce a metric, denoted as, $\varepsilon_m^{(s)}$, for the sth iteration in terms of subcarrier s. It can be shown that, in Case 1, there are three possible strategies for InterCI mitigation.

- **Strategy 1**: Two BSs cooperate for a user and the other BS stops transmission on a subcarrier. In this case, we have $\varepsilon_m^{(s)} = 1$, and the IMD variables are in the form of $D_{u,m} = k$, $D_{u',m} = k$, $D_{u'',m} = -1$.
- **Strategy 2**: Two BSs cooperate for a user and the other BS transmits to its own user with the SIR lower than the SIR threshold η_t . In this case, we have $\varepsilon_m^{(s)} = 2$ associated with the IMD variables given by $D_{u,m} = k$, $D_{u',m} = k$, $D_{u'',m} = k''$.
- **Strategy 3**: Two BSs cooperate for a user and the other BS transmits to its own user with the SIR higher than the SIR threshold η_t . In this case, we have $\varepsilon_m^{(s)} = 3$ and $D_{u,m} = k$, $D_{u'',m} = k''$.

Note that, in the above strategies, we assumed that $u \neq u' \neq u''$, and $u, u', u'' \in \{0, 1, 2\}$.

As mentioned previously, our CDMC algoirthm motivates to maximize the sum rate as well as the frequency reuse factor of the system. Clearly, in Case 1, Strategy 1 generates smaller sum rate (or metric) than Strategies 2 and 3, since in Strategy 1 there is only one information transmission flow on a considered subcarrier. By contrast, in strategies 2 and 3, the algorithm allows two information transmission flows, including the one generated by Strategy 1. Moreover, we can know that Strategy 3 is the most desirable one, since it allows a cooperation between two BSs and a transmission from a BS to its user having a high SIR. By contrast, in Strategy 2, in addition to the two cooperative BSs, the link from the other BS to its user is weak. It hence generates lower sum rate than Strategy 3. As Figure 5.3 shows, our CDMC algorithm in Case 1 always makes the final decision that results in the highest metric value among the available decisions.

Let us now return to the example of (5.29), when the CDMC algorithm associated with Case 1 is applied. This case corresponds to setting the SIR threshold $\eta_t = 5$ dB. Furthermore, we assume that $I_c = 1$, $I_o = 0.1$. Under these assumptions, we can readily know that the SIRs of the three users on subcarrier 0 are all below the threshold η_t . Let us assume that BS 0 makes the InterCI mitigation decisions for the three users. Hence, both BS 1 and BS 2 send the digitized InterCIs to BS 0, after they receive from their users. Consequently, based on the InterCI values in (5.29), the

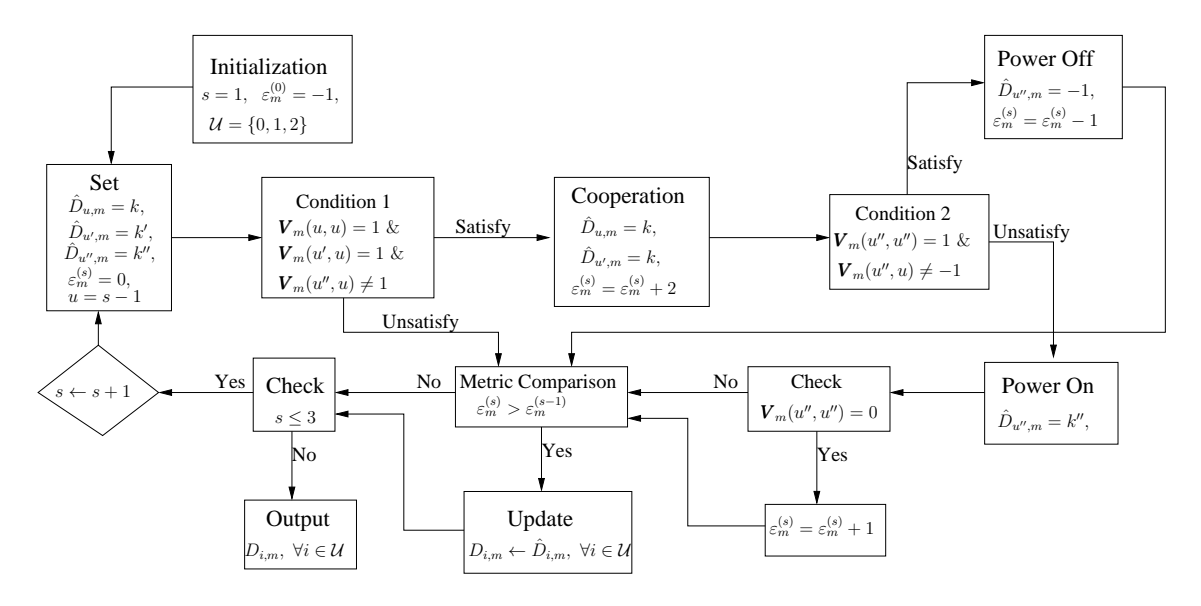


Figure 5.3: Flow chart showing the operations of the CDMC algorithm in Case 1, when assuming $u \neq u' \neq u''$, and users k, k', k'' are in cells u, u' and u'', respectively.

InterCI received by BS 0 can be expressed in matrix form as

$$\mathbf{V}_{0} = \begin{bmatrix} v_{4} & v_{0,10} & v_{0,19} \\ v_{1,4} & v_{10} & v_{1,19} \\ v_{2,4} & v_{2,10} & v_{19} \end{bmatrix} = \begin{bmatrix} 1 & -1 & 0 \\ 1 & 1 & 0 \\ 0 & 1 & 1 \end{bmatrix}$$
 (5.42)

Explicitly, the operational situation is in Case 1, as the conditions of (5.39) are met for both users 4 and 10. Then, following Figure 5.3, we have the decisions of the IMD variables as

$$D_{0.0} = 4$$
, $D_{1.0} = 10$, $D_{2.0} = 10$ if $\eta_t = 5$ dB, $I_c = 1$, $I_0 = 0.1$. (5.43)

According to the operations in Figure 5.3, during the first (s = 1) iteration, BS 0 checks if a cooperation can be set up for user 4 in cell 0. Since Condition 1 in the figure is met, a cooperation between BS 0 and BS 1 can be set up for user 4. However, BS 2 has to turn off the transmission to user 19, as Condition 2 in Figure 5.3 is satisfied, $V_0(2,0) = 0$. As a result, at the end of the first iteration, the decisions derived are $\hat{D}_{0,0}=4$, $\hat{D}_{1,0}=4$ and $\hat{D}_{2,0}=-1$, which belongs to Strategy 1 and has a metric of $\varepsilon_0^{(1)} = 1$. During the second iteration, BS 0 tries to build a cooperation for user 10 between BS 1 and BS 2, since it satisfies Condition 1. Furthermore, as shown in (5.42), $V_0(0,1) = -1$, meaning that user 10 suffers ignorable InterCI from BS 0. Hence, BS 0 can keep transmission to user 4. Consequently, the second iteration yields the decisions of $\hat{D}_{0,0}=4$, $\hat{D}_{1,0}=10$ and $\hat{D}_{2,0}=10$, and a metric of $\varepsilon_0^{(1)}=2$, which is better than that obtained during the first iteration. During the third iteration, BS 0 finds that a cooperation for user 19 cannot be set up, as Condition 1 in Figure 5.3 is not satisfied. Therefore, the final InterCI mitigation decisions are given by the second iteration, which are $D_{0,0} = 4$, $D_{1,0} = 10$ and $D_{2,0} = 10$, and sent by BS 0 to BS 1 and BS 2. It can be shown that the sum rate achieved is $C_{\Sigma}=3.5213$. In comparison with $C_{\Sigma} = 2.208$ achieved by the DDMC algorithm, better InterCI mitigation decisions have been made by the CDMC algorithm for the example considered.

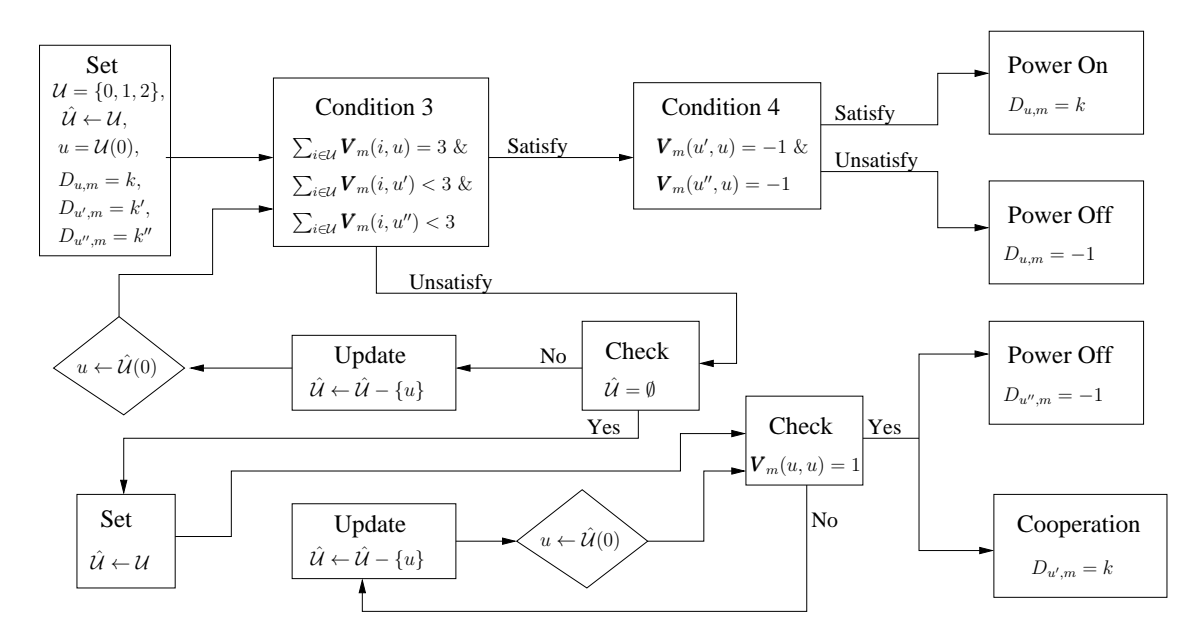


Figure 5.4: Flow chart showing the operations of the CDMC algorithm in Case 2, when assuming that $u \neq u' \neq u''$, u' < u'', and users k, k', k'' are in cells u, u' and u'', respectively.

In order to further explain the operations of the CDMC algorithm under Case 1, let us consider another example, in which subcarrier m is allocated to users i, j, q in cells 0, 1 and 2, respectively. In this case, the digitized InterCI matrix of subcarrier m is given by

$$\mathbf{V}_{m} = \begin{bmatrix} v_{i} & v_{0,j} & v_{0,q} \\ v_{1,i} & v_{j} & v_{1,q} \\ v_{2,i} & v_{2,j} & v_{q} \end{bmatrix} = \begin{bmatrix} 0 & 1 & -1 \\ -1 & 1 & 1 \\ 0 & -1 & 1 \end{bmatrix}$$
(5.44)

which is known to BS 0, when we assume that BS 0 makes the decisions. First, there is no cooperation set up during the first iteration, as $v_i = 0$, resulting in that Condition 1 in Figure 5.3 is not satisfied. As for user j, Condition 1 is satisfied. Hence, during the second iteration, BS 0 tries to set up a cooperation between BS 0 and BS 1. Meanwhile, BS 2 is allowed to transmit to its user q with SIR lower than the threshold. This belongs to Strategy 2, and gives a metric of $\varepsilon_m^{(2)} = 2$. During the third iteration, a cooperation is assumed for user q between BS 1 and BS 2. Furthermore, BS 0 can keep transmitting to user i, whose SIR is higher than the threshold. This decision belongs to Strategy 3, and results in a metric of $\varepsilon_m^{(3)} = 3$. Consequently, the decisions made in the third iteration are taken as the final decisions, which are $D_{0,m} = i$, $D_{1,m} = q$ and $D_{2,m} = q$. From both of the examples of (5.42) and (5.44), we can know that, under Case 1, the CDMC algorithm can always make the best decisions in terms of InterCI mitigation and maximization of system's frequency reuse factor. Let us now describe the operation of the CDMC algorithm operated under Case 2.

Figure 5.4 describes the flow chart of the operations of the CDMC algorithm under Case 2. In the context of Case 2, the conditions defined in (5.39) are not met, while the conditions in (5.40)

are satisfied for at least one of the three users sharing a subcarrier in cells 0, 1 and 2. Under Case 2, as shown in Figure 5.4, the CDMC algorithm will not establish a cooperation for a user with the SIR below η_t , when Condition 3 is satisfied, i.e., when only one of the users suffers from two strong InterCI signals. In this case, the transmission to the user experiencing two strong InterCI signals will be kept on or turned off, depending on whether Condition 4 in Figure 5.4 is satisfied or not. If Condition 4 is satisfied, which means that both the other two users have the required channel qualities for communication, this strong interfered user will be kept on. Otherwise, when Condition 4 is not satisfied, this user will be switched off. However, a cooperation can be set up for a user with poor SIR, in the circumstance that this user and at least another user both suffer from the strong InterCI from two BSs. Therefore, as shown in Figure 5.4, when the CDMC algorithm is operated under Case 2, there are three possible InterCI mitigation strategies, which can be described as

Strategy 4: One user turns off while the other two BSs transmit respectively to their users, having the IMD variables as $D_{u,m} = -1$, $D_{u',m} = k'$, $D_{u'',m} = k''$.

Strategy 5: All users stay on, corresponding to the values for the IMD variables: $D_{u,m} = k$, $D_{u',m} = k'$, $D_{u'',m} = k''$.

Strategy 6: Two BSs cooperate while the other one switches off its transmission to its user. Correspondingly, the values for the IMD variables are $D_{u,m} = k$, $D_{u',m} = k$, $D_{u'',m} = -1$.

Note that, in the above strategies, we assumed that $u \neq u' \neq u''$, and $u, u', u'' \in \{0, 1, 2\}$.

Let us below consider two examples to show the operations under Case 2. In these examples, we assume that subcarrier m is allocated to users i, j, q in cells 0, 1 and 2. In the first example, the InterCI matrix V_m of subcarrier m is given by

$$\mathbf{V}_{m} = \begin{bmatrix} v_{i} & v_{0,j} & v_{0,q} \\ v_{1,i} & v_{j} & v_{1,q} \\ v_{2,i} & v_{2,j} & v_{q} \end{bmatrix} = \begin{bmatrix} 0 & -1 & 1 \\ -1 & 0 & 1 \\ -1 & 0 & 1 \end{bmatrix}$$
(5.45)

From (5.45), we can see that the conditions in (5.39) are not satisfied, but those in (5.40) are satisfied, as we have $V_m(2,2) = 1$, $V_m(0,2) = 1$ and $V_m(1,2) = 1$. Hence, the CDMC algorithm operates in Case 2. Therefore, as shown in Figure 5.4, the CDMC algorithm first checks whether Condition 3 is satisfied for the users in cells u = 0, 1, 2. Here, we find that Condition 3 is only satisfied with u = 2, which means that only user q in cell 2 suffers strong InterCI from two BSs, i.e., from BSs 0 and 1. Then, the algorithm goes further to decide whether the transmission to user q should be switched off or not, by checking Condition 4. It can be seen that Condition 4 is unsatisfied, as $V_m(2,1) = 0$, meaning that BS 2 does not impose small InterCI on user j. Hence, the transmission from BS 2 to user q is terminated. As the results, the algorithm gives the decisions of $D_{0,m} = i$, $D_{1,m} = j$ and $D_{2,m} = -1$.

Let us consider another example, there are two users of both suffering strong InterCI from two

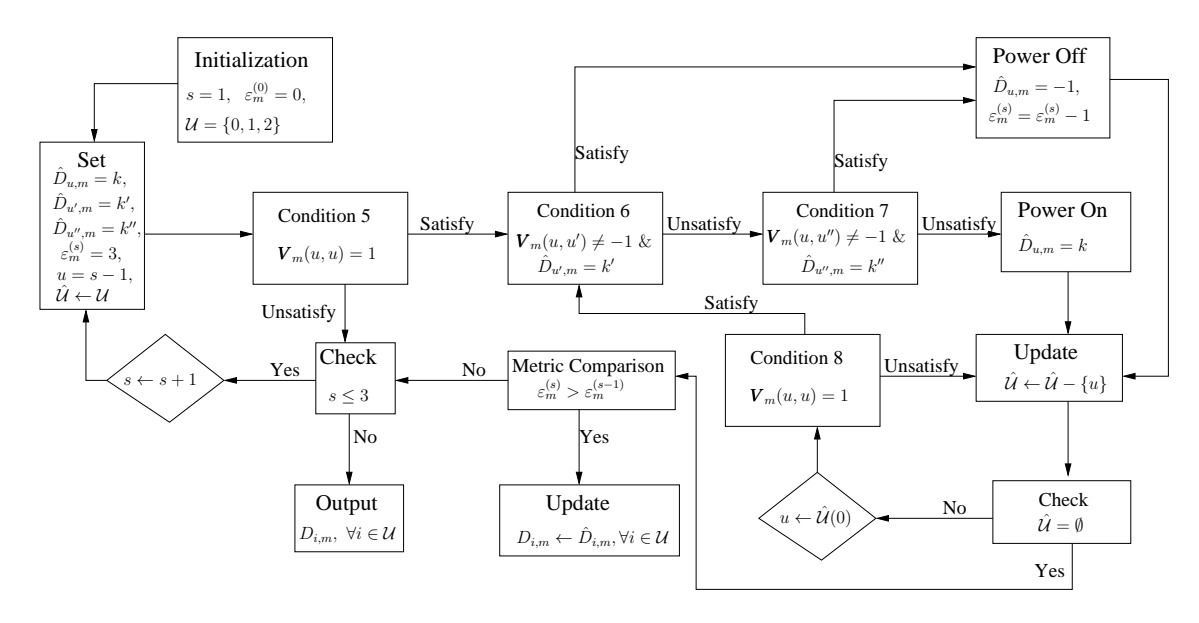


Figure 5.5: Flow chart of Case 3 showing the operations of the CDMC algorithm, when assuming that $u \neq u' \neq u''$, u' < u'', and users k, k', k'' are in cells u, u' and u'', respectively.

BSs. The InterCI matrix V_m of subcarrier m is given by

$$\mathbf{V}_{m} = \begin{bmatrix} v_{i} & v_{0,j} & v_{0,q} \\ v_{1,i} & v_{j} & v_{1,q} \\ v_{2,i} & v_{2,j} & v_{q} \end{bmatrix} = \begin{bmatrix} 1 & 0 & 1 \\ 1 & 0 & 1 \\ 1 & -1 & 1 \end{bmatrix}.$$
 (5.46)

In this case, Condition 3 is not satisfied, as both user i in cell 0 and user q in cell 2 experience strong InterCI from two BSs. Therefore, it is beneficial to first switch off the transmission to a user with its SIR lower than η_t , and, then to set up a cooperation for the other user with its SIR lower than η_t . Specifically, according to our previous analysis, it can be shown that the CDMC algorithm will derive the decisions that BS 1 cooperating with BS 0 transmits to user i, while BS 2 stops transmission to user q. Consequently, the values for the IMD variables are $D_{0,m} = i$, $D_{1,m} = i$, $D_{2,m} = -1$. Note that, for the example of (5.46), our CDMC may give the decisions that a cooperation for user q is set up while the transmission to user i is switched off, which do not make a big difference with the above derived decisions.

Finally, when the CDMC algorithm is carried out under Case 3, the operations can be described by the flow chart in Figure 5.5. It can be shown that, in Case 3, no cooperation for users with SIRs below the threshold η_t can be established. The algorithm can only turn off some users to mitigate the InterCI on a users with poor SIR. As discussed before, the transmission to a user is turned off, only when its transmission imposes strong InterCI on the other active users. Hence, under Case 3, the CDMC algorithm motivates to make the best InterCI mitigation decisions, when there are more than one user having their SIRs below the threshold η_t . As shown in Figure 5.5, the final InterCI mitigation decisions can be made after three iterations for evaluating all the possible options. Similar to the operations of Case 1, here a metric $\varepsilon_m^{(s)}$ is introduced for evaluating the

quality of the decisions made during an iteration. Furthermore, from Figure 5.5, we can know that there are three possible InterCI mitigation strategies, which are described as follows.

- **Strategy 7**: All transmissions to users are on. In this case, we have $\varepsilon_m^{(s)} = 3$, and the IMD variables are $D_{u,m} = k$, $D_{u',m} = k'$, $D_{u'',m} = k''$.
- **Strategy 8**: One user switches off, while the other two are on. In this case, we have $\varepsilon_m^{(s)} = 2$, and the IMD variables are $D_{u,m} = -1$, $D_{u',m} = k'$, $D_{u'',m} = k''$.
- **Strategy 9**: Two users are off, while the other user is on. In this case, we have $\varepsilon_m^{(s)} = 1$, and the IMD variables are $D_{u,m} = -1$, $D_{u',m} = -1$, $D_{u'',m} = k''$.

Note that, in the above description for strategies, we assume that $u \neq u' \neq u''$, and $u, u', u'' \in \{0, 1, 2\}$.

Let us now show the principles of the CDMC algorithm under Case 3 with the aid of an example, where two users have their SIR below the threshold η_t . Assume that subcarrier m is allocated to users i, j, q in cells 0, 1 and 2, and the InterCI matrix V_m of subcarrier m is given by

$$\mathbf{V}_{m} = \begin{bmatrix} v_{i} & v_{0,j} & v_{0,q} \\ v_{1,i} & v_{j} & v_{1,q} \\ v_{2,i} & v_{2,j} & v_{q} \end{bmatrix} = \begin{bmatrix} 0 & 0 & 0 \\ -1 & 1 & 0 \\ 0 & -1 & 1 \end{bmatrix}.$$
 (5.47)

Explicitly, the CDMC algorithm operates in the principles of Case 3, as the conditions in (5.41) are met for both users j and q, while the conditions in (5.39) and in (5.40) are not satisfied for all the three users. Hence, as shown in Figure 5.5, during the first iteration, the algorithm checks if Condition 5 is satisfied, which tries to find the operational option for user i. Since user i has a SIR higher than η_t , it does not need an InterCI mitigation action. Therefore, during the second iteration, the algorithm checks for user j. It finds that the transmission to user j needs to be turned off, as Condition 5 ($V_m(1,1)=1$) is met and Condition 6 ($V_m(1,0)=-1$) is not met, as well as Condition 7 ($V_m(1,2)=0$) is met. Meanwhile, the transmission to user q is also turned off, since Conditions 5 and 6 in Figure 5.5 are met. Hence, the decisions given by the algorithm are $\hat{D}_{0,m}=i$, $\hat{D}_{1,m}=-1$ and $\hat{D}_{2,m}=-1$, which belongs to Strategy 9 and has a decision metric of $\varepsilon_m^{(2)}=1$. During the third iteration, the CDMC algorithm first deals with user q in cell 2. Similar to the procedure in the second iteration, it results in the decisions of $\hat{D}_{0,m}=i$, $\hat{D}_{1,m}=j$ and $\hat{D}_{2,m}=-1$, which has a decision metric of $\varepsilon_m^{(3)}=2$. Therefore, after three iterations, the final decisions made are given by that obtained during the third iteration.

In summary of the operations of the CDMC algorithm under Cases 1, 2 and 3, the algorithm can now be described as follows. In our description, we assume that there is a head BS, which is responsible for the decision making for a subcarrier.

5.7. Performance Results 166

Algorithm 11. (Centralized Decision Making Assisted Cooperation Algorithm)

Initialization: For all subcarriers $m \in \mathcal{M}$:

- (1) All users estimate their SIRs, which can be expressed as $\eta_k = \frac{|h_{u,k,m}|^2}{\sum_{u' \in \{0,1,2\}, u' \neq u} I_{u',k}}$, where $F_m^{(u)} = \frac{|h_{u,k,m}|^2}{\sum_{u' \in \{0,1,2\}, u' \neq u} I_{u',k}}$
- $\{k\}, F_m^{(u')} = \{k'\} \text{ and } F_m^{(u'')} = \{k''\}, \forall k \in \mathcal{K}^{(u)}, \forall u \in \{0, 1, 2\}.$
- (2) Set $\mathcal{K}_m = \{k | \mathcal{F}_m^{(u)} = \{k\}\}$, where $k \in \mathcal{K}^{(u)}$, $u \in \{0, 1, 2\}$.
- (3) Set $\hat{\mathcal{K}}_m = \left\{ \hat{k} | \eta_{\hat{k}} < \eta_t, \ \hat{k} \in \mathcal{K}_m \right\}$.

For subcarrier m, the algorithm takes no actions, if $\hat{\mathcal{K}}_m = \emptyset$; Otherwise, it executes the following operations:

- **Step 1** The digitized InterCI $v_{u',\hat{k}}$, $v_{u'',\hat{k}}$ derived from (5.36) for all the users in $\hat{\mathcal{K}}_m$ are sent to the head BS.
- **Step 2** The head BS asks for the digitized InterCI of all the users in $\hat{\mathcal{K}}'_m = \mathcal{K}_m \hat{\mathcal{K}}_m$. (Note that, after Steps 1 and 2, the head BS has the knowledge of V_m , which is enough for it to make the InterCI mitigation decisions.)
- **Step 3** Based on V_m , the head BS makes the InterCI mitigation decisions based on the rules under the three cases described in Figures 5.3-5.5, respectively.
- **Step 4** The head BS informs the other two BSs the InterCI decisions by sending them the corresponding values of the IMD variables $D_{u,m}$, $\forall u \in \{0,1,2\}$.

As described above, under our current CDMC algorithm, the InterCI mitigation decisions are made by the head BS, which holds all the InterCI information. Alternatively, we may let all the BSs know all the InterCI information about the three users sharing a subcarrier. In this case, based on the InterCI information, each BS can make the decisions, which should be the same for all the three users. Hence, there is no need for a BS to inform the other two BSs the decisions. Specifically, in this approach, when a BS knows that one of its users has the SIR lower than the threshold η_t , it then broadcasts the digitized InterCI vector of the user, such as the vector $\boldsymbol{v}_{k,m}$ in (5.37), to the other two BSs. Once receiving the InterCI vector, the other two BSs also broadcast the InterCI information of their users sharing the same subcarrier, regardless of the SIR values of their users. In this way, all the three BSs have the full knowledge of the digitized InterCI matrix of a subcarrier. Consequently, they can make the decisions in the same principles of the CDMC under cases 1, 2 or 3.

5.7 Performance Results

In this section, we provide a range of simulation results, in order to demonstrate and compare the achievable spectrum-efficiency performance of the multicell downlink OFDMA systems employing various subcarrier-allocation algorithms and InterCI mitigation algorithms. We assume that all subcarriers experience independent flat Rayleigh fading. We assume that, in each of the three cells,

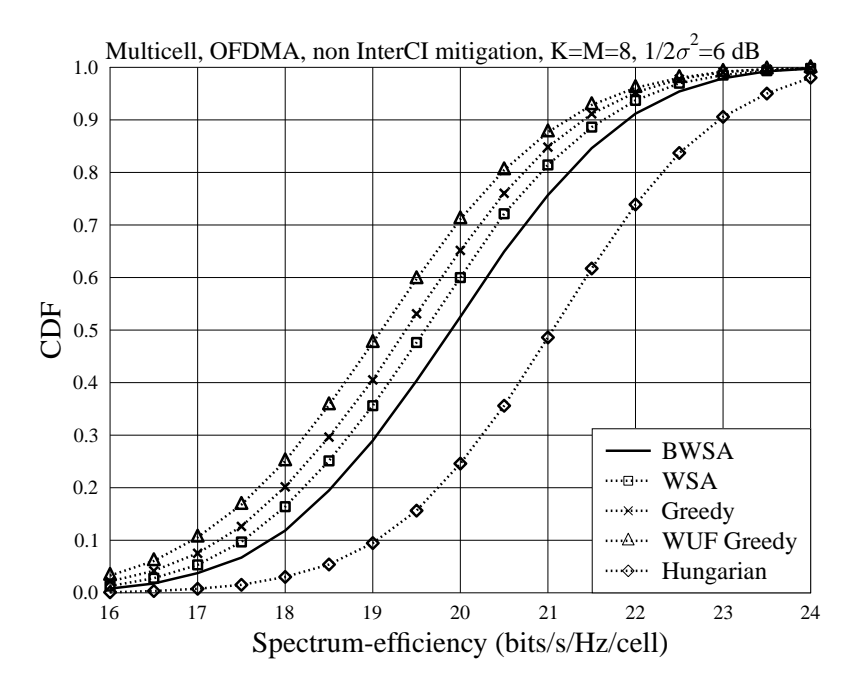


Figure 5.6: CDF of spectrum-efficiency of the multicell downlink OFDMA systems employing various subcarrier-allocation algorithms, when assuming M=8 subcarriers and average SNR per symbol of $\bar{\gamma}_s=1/2\sigma^2=6$ dB.

the number of users supported by the OFDMA is K=M, where M is the number of subcarriers. In each cell, we assume K users are uniformly distributed. All users in the system are assumed to experience the AWGN with the same noise variance. The effect of the pathloss exponent in (5.4) is assumed to be $\mu=4.0$, and the standard deviation of the shadowing effect is Y=8 dB. Note that, in this section, as power control is employed in each cell, there is no power-allocation.

Figure 5.6 shows the CDF of the spectrum-efficiency of the multicell downlink OFDMA systems, when using various subcarrier-allocation algorithms are distributively operated in three cells. In Figure 5.6, we assume that the system does not attempt any InterCI mitigation. Since the Hungarian algorithm [83,86] is the optimum subcarrier-allocation algorithm of providing the optimum solutions in the sense of maximizing the SNR of all users. As shown in Figure 5.6, it achieves the best spectrum-efficiency performance. From Figure 5.6, we observe that the greedy algorithms, including the greedy and WUF greedy algorithms, have the worst spectrum-efficiency performance among these considered algorithms. Our proposed BWSA algorithm in Chapter 3 is only outperformed by the Hungarian algorithm, but it achieves better spectrum-efficiency performance than any of the other subcarrier-allocation algorithms considered. The parameters for Figure 5.7 are the same as those in Figure 5.6, except that, in Figure 5.7, the noise variance is smaller, with the average SNR per symbol being $\bar{\gamma}_s = 12$ dB. By comparing Figure 5.7 with Figure 5.6, we observe that the spectrum-efficiency attained by all the subcarrier-allocation algorithms increases, when the noise variance becomes smaller. Again, in Figure 5.7, we can see that our BWSA algorithm proposed in Chapter 3 can outperform any of the other algorithms, except the Hungarian algorithm.

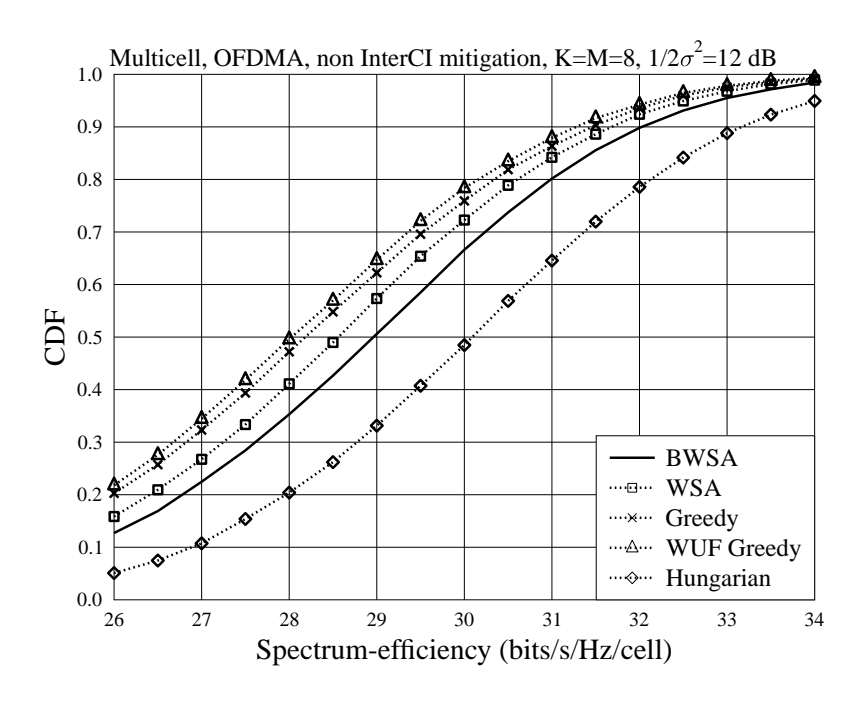


Figure 5.7: CDF of spectrum-efficiency of the multicell downlink OFDMA systems employing various of subcarrier-allocation algorithms, when assuming M=8 subcarriers and average SNR per symbol of $\bar{\gamma}_s=1/2\sigma^2=12$ dB.

Below we start considering the performance of the multicell downlink OFDMA systems, when the InterCI mitigation algorithms are applied. For the sake of explicit comparison, we address the performance by focusing on the cell-edge users in the system. Let us define $\hat{\mathcal{K}}^{(u)} = \{k | \eta_k < \eta_t, k \in \mathcal{K}^{(u)}\}$ as the set of indexes of the users with SIR below the SIR threshold in cell u ($u \in \{0,1,2\}$). Here, the cell-edge users in cell u include the users in $\hat{\mathcal{K}}^{(u)}$, and the users in $\mathcal{K}^{(u)} - \hat{\mathcal{K}}^{(u)}$, which share the same subcarriers as the users in $\hat{\mathcal{K}}^{(u')}$ and $\hat{\mathcal{K}}^{(u'')}$ in cells u', u'' ($u \neq u' \neq u''$). Let us now denote $\tilde{\mathcal{K}}^{(u)}$ as the set of the cell-edge users in cell u. In this case, an InterCI mitigation algorithm may be applied to combat or make use of the InterCI. In the figure, the average spectrum-efficiency of cell-edge users per cell is given by

$$C = \frac{1}{3} \sum_{u \in \{0,1,2\}} \sum_{k \in \tilde{K}^{(u)}} \log_2(1 + \gamma_k), \text{ (bits/s/Hz/cell)}.$$
 (5.48)

Correspondingly, the average spectrum-efficiency per cell-edge user is

$$C = \frac{1}{|\tilde{\mathcal{K}}|} \sum_{u \in \{0,1,2\}} \sum_{k \in \tilde{\mathcal{K}}^{(u)}} \log_2(1+\gamma_k), \text{ (bits/s/Hz/user)}$$

$$(5.49)$$

where $\tilde{\mathcal{K}}$ contains the indexes of the cell-edge users in the system, i.e., $\tilde{\mathcal{K}} = \tilde{\mathcal{K}}^{(0)} \cup \tilde{\mathcal{K}}^{(1)} \cup \tilde{\mathcal{K}}^{(2)}$. In (5.48) and (5.49), γ_k is the SINR of user k, which is given by (5.8) or (5.13).

Figure 5.8 compares the spectrum-efficiency performance of the different InterCI mitigation algorithms employed by the three-cell downlink OFDMA systems, where the average spectrum-efficiency for cell-edge users is depicted, when we assume that the SIR threshold η_t is -4 dB, 0 dB

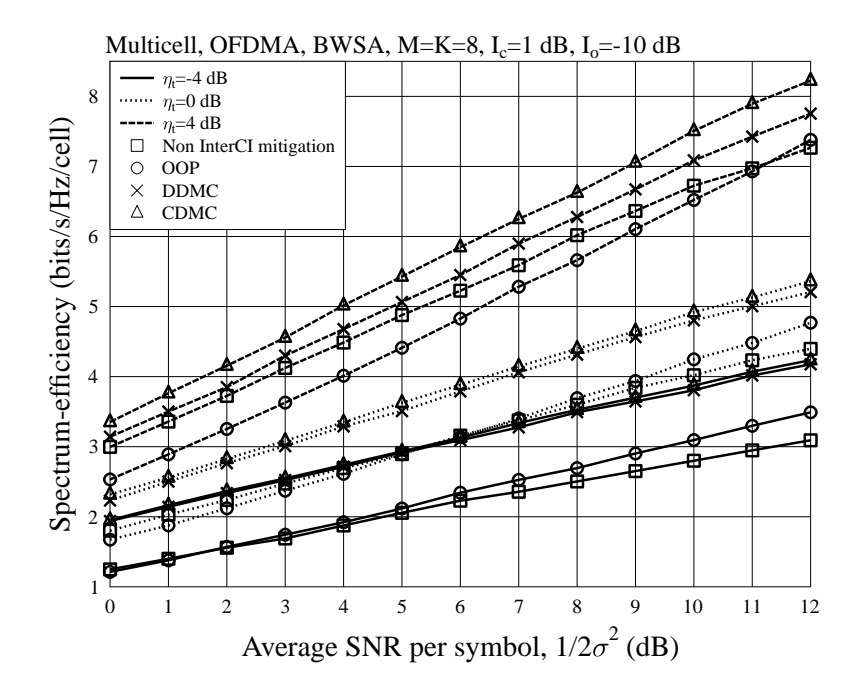


Figure 5.8: Spectrum-efficiency of cell-edge users in the multicell downlink OFDMA systems employing the BWSA subcarrier-allocation algorithm and various InterCI mitigation algorithms.

or 4 dB. The other parameters used in the investigation can be found on the top the figure. From the figure, we can obtain the following observations. First, for all the considered SIR thresholds, both the proposed DDMC and CDMC algorithms achieve a higher spectrum-efficiency than the OOP algorithm, and than the case without employing any InterCI mitigation, which is labelled as "non InterCI mitigation" in the figure. As shown in the figure, the DDMC and CDMC algorithms become more advantageous over the OOP algorithm as the threshold η_t reduces. This is because, as described in Sections 5.5 and 5.6, the DDMC and CDMC algorithms are motivated to establish cooperative transmissions for the cell-edge users, instead of turning off their transmissions. We can know that the number of users needing cooperation or turned off becomes less, as η_t reduces. In other words, those "edge-users" move further to the cell edge. Therefore, setting up cooperation for the cell-edge users will be more beneficial than simply turning off them. Second, we can observe that the CDMC algorithm always outperforms the DDMC algorithm, and the gain becomes bigger, as the SIR threshold η_t increases. This is because, the CDMC algorithm finds a joint InterCI mitigation strategy for the three users assigned the same subcarrier, based on the knowledge about the InterCI of the three users. By contrast, under the DDMC algorithm, each BS makes distributed InterCI mitigation decisions for its own users. Therefore, the CDMC algorithm is capable of achieving a higher spectrum-efficiency than the DDMC algorithm. Furthermore, the CDMC algorithm attains more SNR gain than the DDMC algorithm, when the number of cell-edge users increases, resulted from the increase of the SIR threshold η_t . Third, Figure 5.8 shows that the spectrum-efficiency achieved by the OOP algorithm is dependent on the SIR threshold. The

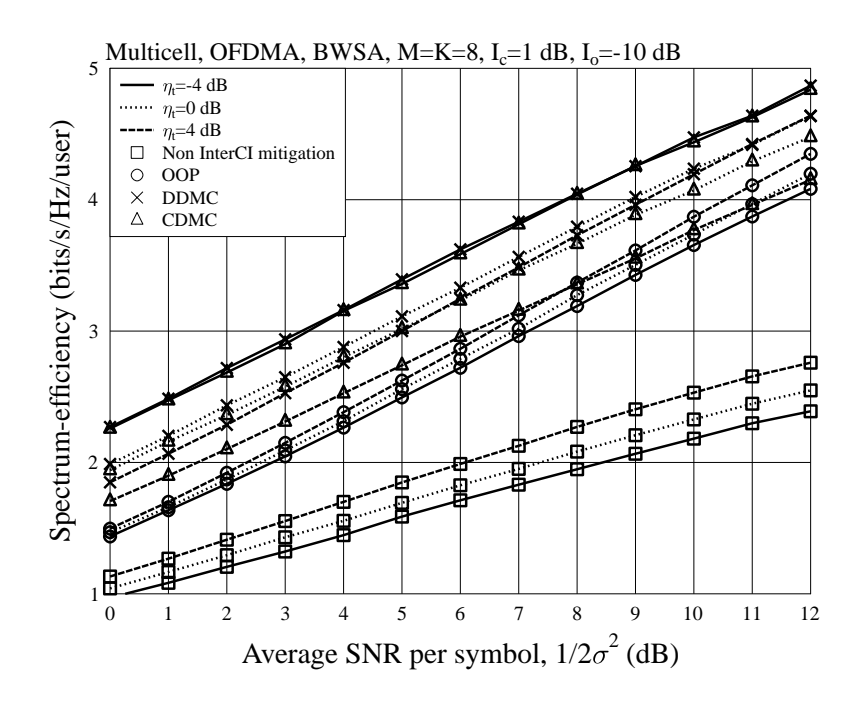


Figure 5.9: Spectrum-efficiency per active cell-edge user in the multicell downlink OFDMA systems employing the BWSA subcarrier-allocation algorithm and various InterCI mitigation algorithms.

OOP algorithm is capable of achieving a spectrum-efficiency gain over the "non InterCI mitigation" case, when a small SIR threshold $\eta_t = -4$ dB is applied. However, the OOP algorithm may become useless in terms of InterCI mitigation, when the SIR threshold is high, such as $\eta_t = 4$ dB. In this case, there may be too many users turned off. Fourth, as shown in Figure 5.8, the OOP algorithm becomes more effective, when the average SNR becomes large. In comparison with the case without InterCI mitigation, the OOP algorithm can only achieve a spectrum-efficiency gain, when the average SNR is sufficiently high. Therefore, when the system is too noisy or when the turning off threshold is too high, too many users may be turned off, which is not beneficial to the OOP algorithm. Explicitly, our proposed DDMC and CDMC algorithms are capable of avoiding these drawbacks of the OOP algorithm, by seeking cooperation for cell-edge users, instead of simply turning off them.

In Figure 5.9, we investigate the average spectrum-efficiency per active cell-edge user in the systems employing various InterCI mitigation algorithms. First, we can observe that any of the three InterCI mitigation algorithms significantly outperforms the case of "non InterCI mitigation". Second, the CDMC algorithm achieves a lower spectrum-efficiency than the DDMC algorithm for all the SIR thresholds considered. This observation is surprise but we can explain it as follows. As discussed in Section 5.6, the CDMC algorithm aims to maximize the system's sum rate as well as maximizing the frequency reuse factor. By contrast, the DDMC algorithm is mainly throughput motivated. Specifically, when a cooperation cannot be set up for a user with SIR below the threshold, the DDMC algorithm simply turns off the transmission to the user. However, the CDMC

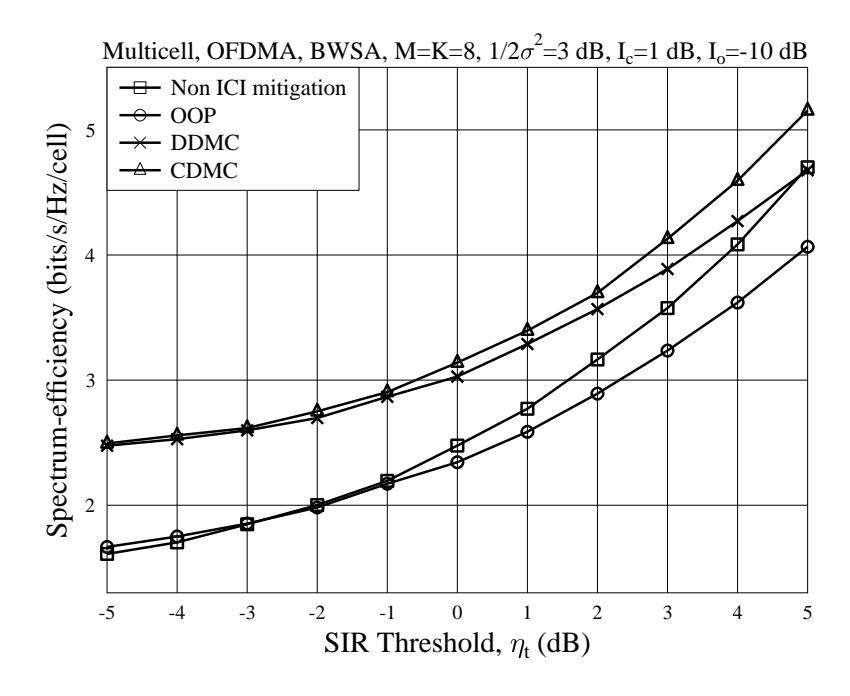


Figure 5.10: Comparison of spectrum-efficiency performance of cell-edge users in the multicell downlink OFDMA systems employing various InterCI mitigation algorithms, when different SIR thresholds are applied.

algorithm still allows the transmission to the user, provided that its transmission does not cause strong InterCI to the other users. Consequently, for the same SIR threshold, the number of active cell-edge users resultant from the CDMC algorithm is higher than that resultant from the DDMC algorithm. Among the active cell-edge users given by the CDMC algorithm, there are possibly many users having low rates, which makes the average spectrum-efficiency in terms of "bits/s/Hz/user" small. Note that, as shown in Figure 5.8, if the spectrum-efficiency of the total cell-edge users in a cell is considered, the CDMC algorithm always outperforms the DDMC algorithm. As shown in Figure 5.9, when $\eta_t = -4$ dB, the CDMC algorithm has a similar spectrum-efficiency per active cell-edge user as the DDMC algorithm. Third, when $\eta_t = 4$ dB, the CDMC algorithm attains a lower spectrum-efficiency per active cell-edge user than the OOP algorithm, when SNR per bit is higher than 8 dB. This is because, when the SIR threshold is higher, the CDMC algorithm allows more weak cell-edge users to transmit, which results in the decrease of the spectrum-efficiency per active cell-edge user. Finally, from the figure we can see that, when the system does not employ any InterCI mitigation algorithm, the spectrum-efficiency per active cell-edge user gets higher, as the SIR threshold becomes bigger. This is because, more users close to the BS will become the cell-edge users considered, as the SIR threshold becomes higher.

In Figures 5.10 and 5.11, we compare the spectrum-efficiency per cell performance of cell-edge users in the three-cell downlink OFDMA systems employing various InterCI mitigation algorithms, when the SIR threshold is in the range of -5 dB $\leq \eta_t \leq 5$ dB. In both figures, we can observe that the proposed DDMC and CDMC algorithms outperform the other two algorithms considered.

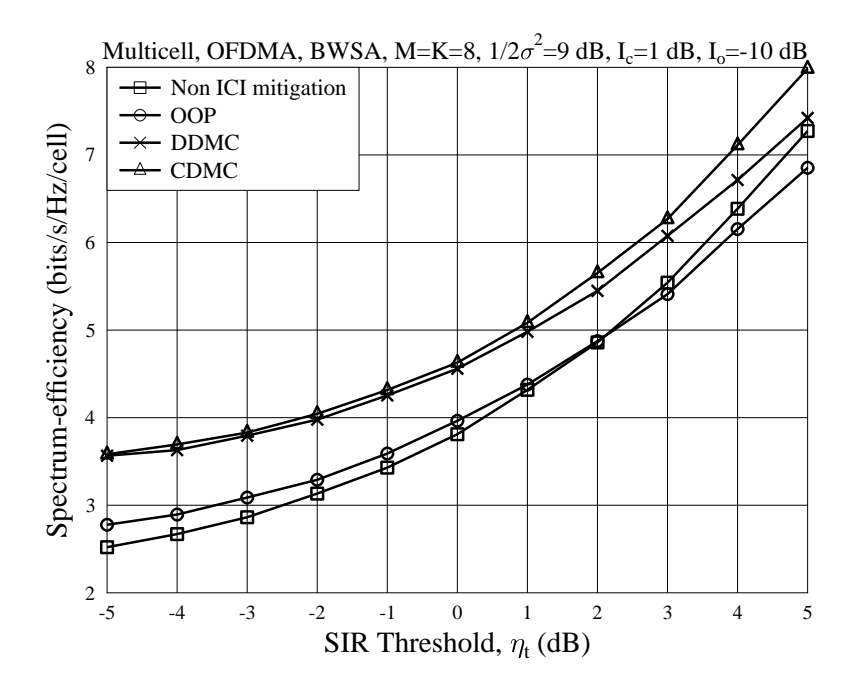


Figure 5.11: Comparison of spectrum-efficiency performance of cell-edge users in the multicell downlink OFDMA systems employing various InterCI mitigation algorithms, when different SIR thresholds are applied.

Since the spectrum-efficiency per cell is considered, the CDMC algorithm always gives the highest spectrum-efficiency among the four schemes. From Figures 5.10 and 5.11, we find that, when the SIR threshold becomes higher, the spectrum-efficiency per cell achieved by the non InterCI mitigation gets closer to that of the proposed DDMC algorithm, and it is higher than that achieved by the OOP algorithm. From the above observations, we can conclude that the spectrum-efficiency performance of our proposed DDMC and CDMC algorithms as well as the OOP algorithm are all dependent on the SIR threshold applied. By comparing Figure 5.10 with Figure 5.11, we can see that the intersection between the curves of the OOP algorithm and the non InterCI mitigation case shifts from $\eta_t = -2$ dB to $\eta_t = 2$ dB, when the average SNR per symbol is increased from $\bar{\gamma}_s = 3$ dB to $\bar{\gamma}_s = 9$ dB. Note that, at a given SNR, when η_t increases, more users will be included as the cell-edge users, among which more users could be turned off, when the OOP algorithm is applied. This makes the spectrum-efficiency per cell achieved by the OOP algorithm become lower than that obtained by doing nothing.

Figure 5.12 evaluates the spectrum-efficiency per cell performance of cell-edge users in the three-cell downlink OFDMA systems employing various InterCI mitigation algorithms. Again, we can observe that the proposed DDMC and CDMC algorithms outperform both the OOP algorithm and the case of "non InterCI mitigation". From Figure 5.12, we observe that the spectrum-efficiency per cell increases, as the number of users per cell increases and, as a result, the number of cell-edge users also increases. In Figure 5.12, we can see that the spectrum-efficiency difference between the DDMC and the CDMC algorithm stays similar, regardless of the number of users per cell.

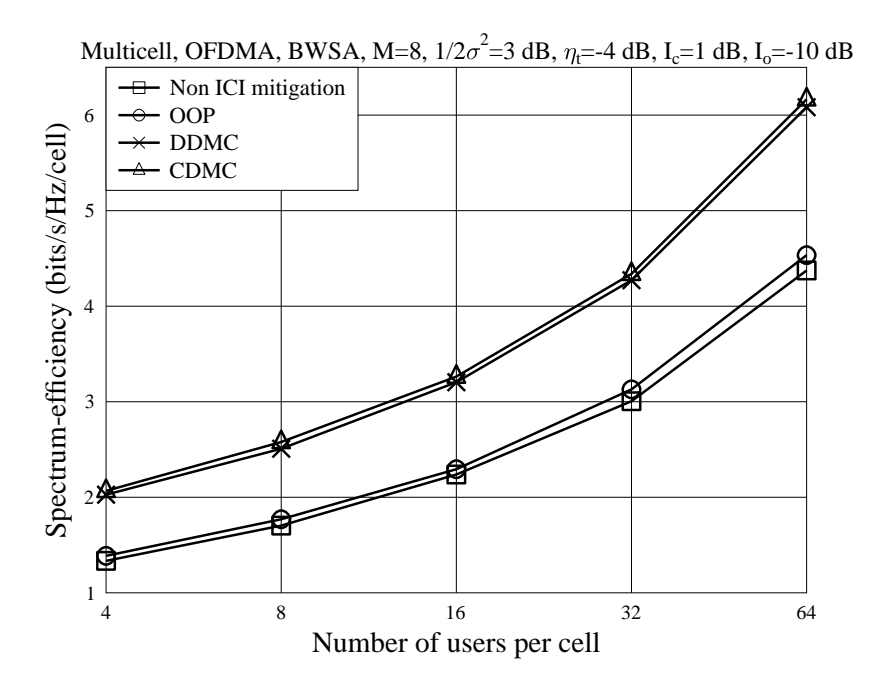


Figure 5.12: Comparison of spectrum-efficiency performance of cell-edge users in the multicell downlink OFDMA systems employing various InterCI mitigation algorithms with respect to different number of users per cell.

However, the spectrum-efficiency difference between the DDMC, the CDMC algorithms and the OOP algorithm becomes bigger, as the number of users increases. This is because the proposed DDMC and CDMC algorithms encourage more cooperative transmissions for cell-edge users, when the number of users increases, instead of turning off. Furthermore, we also see that the OOP algorithm has a larger spectrum-efficiency advantage over the non InterCI mitigation case, when the number of users per cell gets bigger, as the result that the OOP algorithm turns off those users experiencing strong InterCI.

As discussed in Sections 5.5 and 5.6, both the proposed DDMC and CDMC algorithms invoke a decision threshold I_c for finding the cell-edge users for possible cooperation. Given the other parameters, more users will be viewed as the users generating strong InterCI, when I_c decreases. In addition to evaluating the effect of the SIR threshold, in Figure 5.13, we investigate the spectrum-efficiency per cell performance of the multicell downlink OFDMA systems employing the DDMC and CDMC algorithms, when the InterCI cooperation threshold I_c is in the range of -15 dB $\leq I_c \leq$ 15 dB. As seen in Figure 5.13, we find that, for both the proposed algorithms, there are desirable I_c values, which result in the highest spectrum-efficiency. Generally, when the threshold I_c gets smaller, the proposed algorithms try to establish cooperation for more users. By contrast, when I_c becomes larger, they allow cooperation for fewer users. The above observation implies that, in a multicell OFDMA system, we only need to identify a 'good' fraction of users, which usually experience strong InterCI, in order to achieve the highest spectrum-efficiency. Note that, when $\eta_t = -4$ dB, Figure 5.13 show that the best spectrum-efficiency per cell performance achieved by

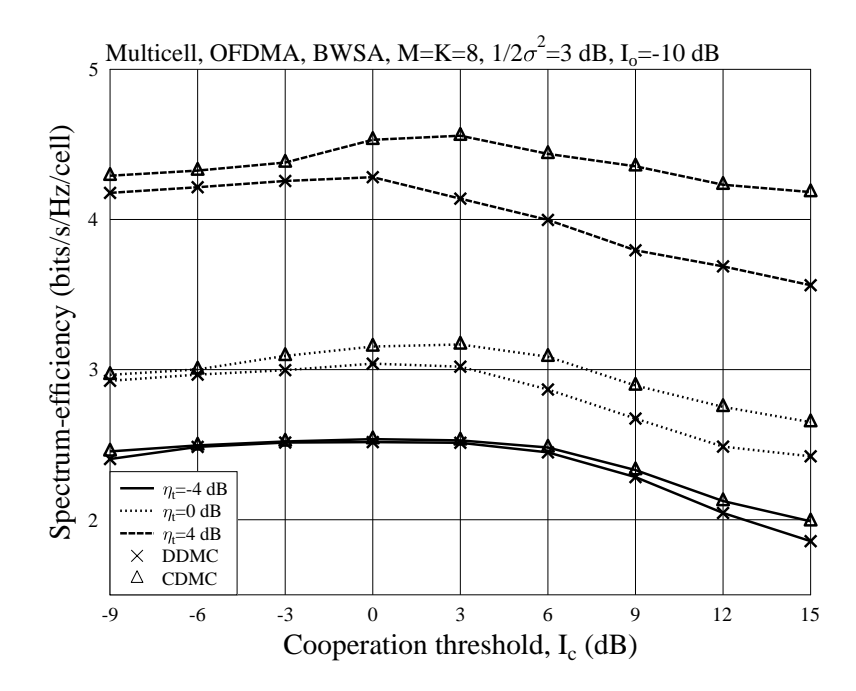


Figure 5.13: Comparison of spectrum-efficiency performance of cell-edge users in the multicell downlink OFDMA systems employing various InterCI mitigation algorithms with different InterCI cooperation thresholds I_c , when using M=K=8 subcarriers and the average SNR per symbol of $\bar{\gamma}_s=3$ dB.

the DDMC and CDMC algorithms is in the range of $-6 \text{ dB} \le I_c \le 6 \text{ dB}$. However, the best I_c range for the two algorithms is reduced to $-3 \text{ dB} \le I_c \le 3 \text{ dB}$, when $\eta_t = 0 \text{ dB}$, and to $-1 \text{ dB} \le I_c \le 1 \text{ dB}$, when $\eta_t = 4 \text{ dB}$. This observation implies that the spectrum-efficiency performance of the two proposed algorithms becomes more sensitive to the cooperation threshold I_c , as the SIR threshold increases. Moreover, Figure 5.13 once again confirms our previous conclusion that the CDMC algorithm yields a larger performance gain over the DDMC algorithm, as the SIR threshold η_t increases. In addition, this gain is enhanced, as the value of I_c increases.

Figure 5.14 investigates how the InterCI off-power threshold affects the spectrum-efficiency per cell performance of the CDMC algorithm. As shown in Section 5.6, the InterCI off-power threshold I_o cannot exceed the InterCI cooperation threshold I_c . Hence, in Figure 5.14, for different I_c values, we have different ranges for I_o . From the figure, we observe that, for a low SIR threshold, such as $\eta_t = -4$ dB, the spectrum-efficiency per cell performance of the CDMC algorithm slightly varies, when different values of I_o is employed. However, the CDMC algorithm yields a more explicit fluctuating spectrum-efficiency per cell with respect to I_o , as the SIR threshold η_t gets higher. However, in general, we can conclude that the spectrum-efficiency performance of the CDMC algorithm is not very sensitive to the InterCI off-power threshold I_o .

In Figures 5.15 and 5.16, we investigate the frequency reuse factor of the three-cell downlink OFDMA systems employing the InterCI mitigation algorithms. In Figures 5.15, the frequency

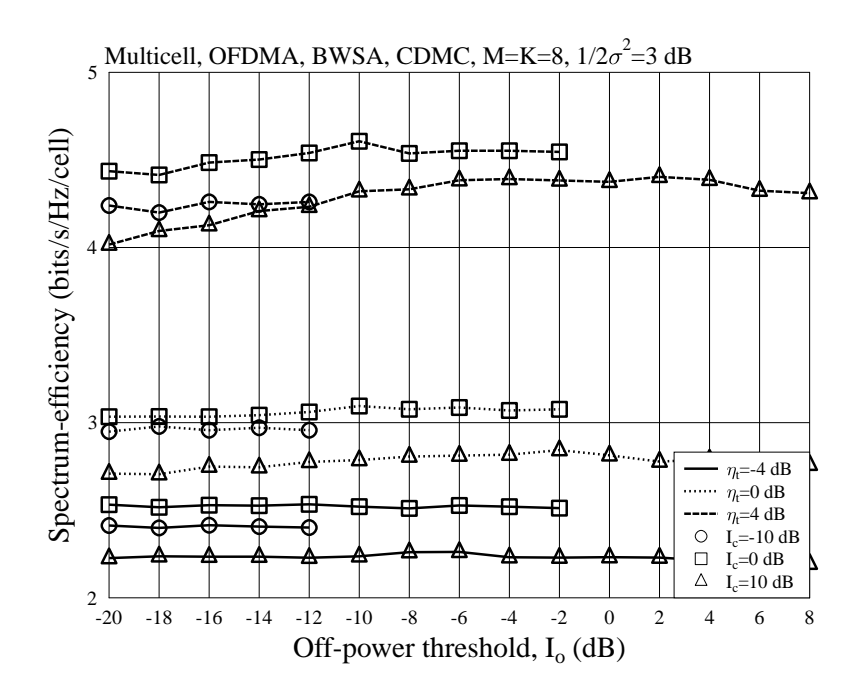


Figure 5.14: Spectrum-efficiency performance of cell-edge users in the multicell downlink OFDMA systems employing the CDMC algorithm with respect to different off-power thresholds I_0 .

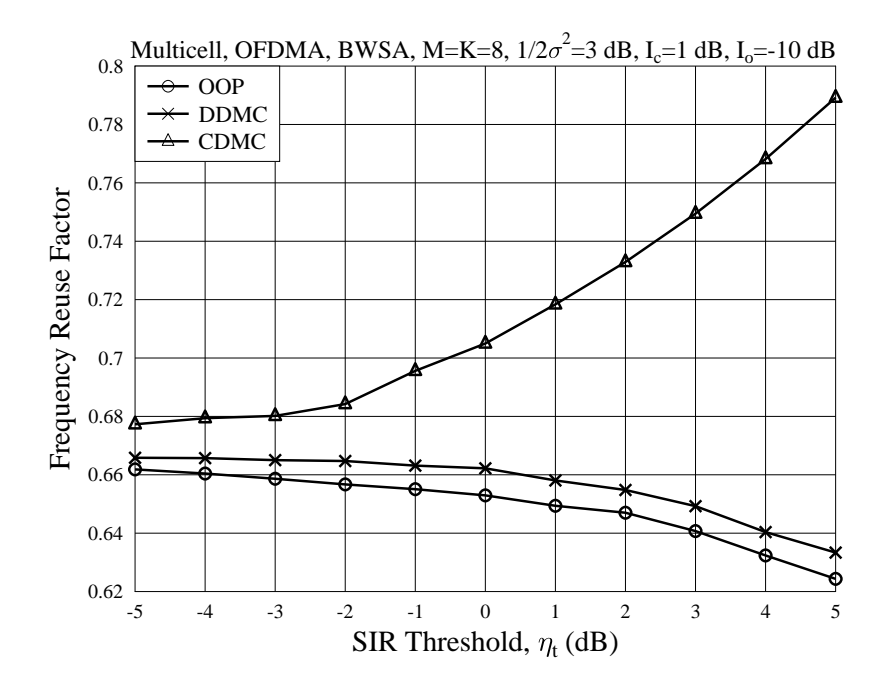


Figure 5.15: Frequency reuse factor of cell-edge users in the multicell downlink OFDMA systems employing various InterCI mitigation algorithms with respect to different SIR thresholds η_t .

reuse factor for the three algorithms is depicted against the SIR threshold η_t . From this figure, we clearly see that the frequency reuse factor obtained by the CDMC algorithm is significantly

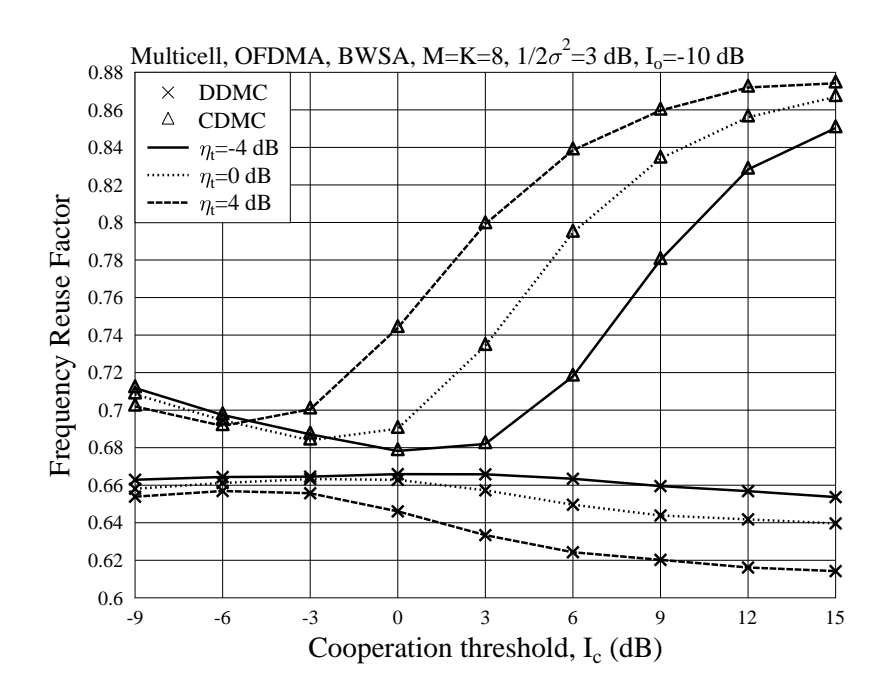


Figure 5.16: Frequency reuse factor of cell-edge users in the multicell downlink OFDMA systems employing various InterCI mitigation algorithms with respect to different InterCI cooperation thresholds I_c .

higher than those given by the DDMC and the OOP algorithms. We also observe that the frequency reuse factor obtained by the CDMC algorithm increases, as η_t increases. However, the frequency reuse factor achieved using the other two algorithms decreases, as the SIR threshold η_t increases. These observations imply that, with the CDMC algorithm, the multicell downlink OFDMA system is capable of providing services simultaneously for more users, even though some of them might have a relatively low rate. By contrast, when the DDMC algorithm is employed, the number of users turned off increases, as η_t increases, which results in the drop of the frequency reuse factor. Furthermore, regardless of the transmission quality of cell-edge users, the OOP algorithm directly stops the transmissions to them, which also results in the drop of the frequency reuse factor, as the SIR threshold η_t increases. Additionally, from Figures 5.15 we can also find that the frequency reuse factor achieved by our proposed DDMC algorithm is slightly higher than that obtained by the OOP algorithm, which is due to the cooperation introduced.

Figure 5.16 compare the frequency reuse factor of the multicell downlink OFDMA system employing the DDMC and CDMC algorithms with respect to the InterCI cooperation threshold I_c . From the figure, generally, we can observe that the frequency reuse factor obtained by the CDMC algorithm increases towards one, as the InterCI cooperation threshold I_c increases. This is because, when the cooperation threshold I_c gets higher, it is more difficult for the CDMC algorithm to establish the cooperation for cell-edge users, and it, therefore, continues transmitting to more cell-edge users, if the InterCI off-power threshold I_o is fixed. Furthermore, we can notice that, in the range of $I_c \leq 0$ dB, the frequency reuse factor achieved by the CDMC algorithm slightly decreases, as the

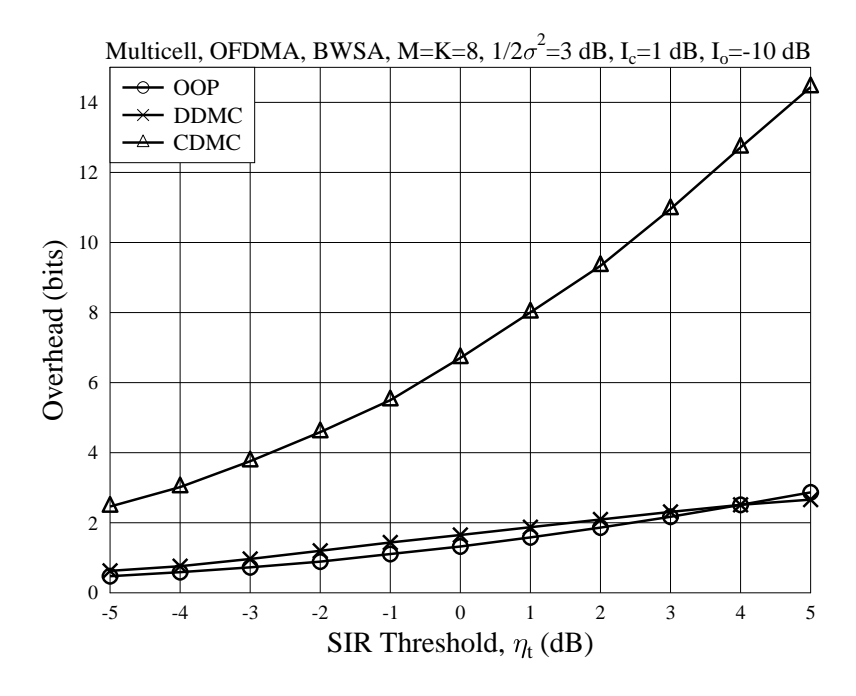


Figure 5.17: Overhead required by the various InterCI mitigation algorithms.

SIR threshold increases. For the DDMC algorithm, as shown in Figure 5.16, the frequency reuse factor slightly decreases, as the threshold I_c increases. This is because the DDMC algorithm turns off more users, when the threshold I_c becomes higher. From the previous results, we can conclude that the DDMC and CDMC algorithms are capable of achieving spectrum-efficiency per cell performance, as well as attaining higher frequency reuse factors than the OOP algorithm. Moreover, the CDMC algorithm does not make a trade-off between the spectrum-efficiency performance and the achievable frequency reuse factor of the system.

Explicitly, the operations of the OOP, DDMC and CDMC algorithms require different overhead. Hence, in Figure 5.17, we compare the overhead required by the various InterCI mitigation algorithms. In the figure, the overhead is measured by the number of bits per user, which is obtained from the total overhead (bits) per cell divided by the number of users in a cell. The overhead considered includes the control information transmitted between users and their BSs, and those among BSs, as well as the data symbols shared among the BSs for cooperation. For all the three InterCI mitigation algorithms, we assume that one bit overhead is required for transmitting a request of cooperation or off-power. Furthermore, in Figure 5.17, we assume that, under the CDMC algorithm, the decisions are made by the head BS, as described in Algorithm 11. The digitized InterCI vector of a subcarrier, such as $v_{k,m}$ in (5.37), has 18 different states. Hence, a BS needs 4 bits to convey the digitized InterCI vector of a subcarrier. Therefore, in total 8 bits of overhead are required for the two BSs to inform the head BS the InterCI information of a subcarrier. In addition, another 3 bits are required for the head BS to broadcast the InterCI mitigation decisions of a subcarrier to the other two BSs, since the decisions have 9 states in total.

5.8. Conclusions 178

Table 5.1: Requirements comparison of the various InterCI mitigation algorithms.

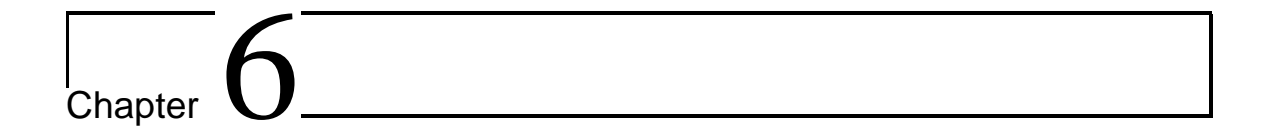
	OOP	DDMC	CDMC
Intracell CSI sharing	No	No	No
Intercell CSI sharing	No	No	Yes
Data exchange	No	Yes	Yes
BS cooperation	No	Yes	Yes
Overheads per subcarrier	2 bits	4 bits	11 bits

In Figure 5.17, we compare the overhead required by the various InterCI mitigation algorithms, when considering a range of values for the SIR threshold. From the figure, we first observe that the required overhead for all the three algorithms increases, as the SIR threshold gets higher. This is because that, when the SIR threshold gets higher, the number of cell-edge users increases. Hence, the InterCI mitigation algorithms are operated for more users, which certainly needs a higher amount of overhead. Therefore, we may conclude that the overhead required by the considered InterCI mitigation algorithms is mainly affected by the SIR threshold. Furthermore, our proposed CDMC algorithm requires higher overhead than the other two algorithms. By contrast, the proposed DDMC algorithm needs a very low overhead, which is similar to that of the OOP algorithm. In summary, the requirements for operations of the various InterCI mitigation algorithms are shown in Table 5.1.

5.8 Conclusions

In this chapter, we have proposed two efficient InterCI mitigation algorithms, namely, the DDMC and the CDMC algorithms, for operation in the multicell downlink OFDMA systems. Both the DDMC and the CDMC algorithms aim at maximizing the spectrum-efficiency of the users with their SIRs lower than the SIR threshold η_t . Owing to this, the spectrum-efficiency of the overall system can be maximized. Our DDMC algorithm is a distributed decision-making algorithm, in which each BS independently makes the InterCI mitigation decisions. Based on the decisions, then a STBC aided cooperative transmission to a user with poor SIR may be set up, or the transmission to a user with poor SIR may be turned off. By contrast, the CDMC InterCI mitigation algorithm makes the decisions in a centralized approach. It motivates to make the best InterCI mitigation decisions based on limited InterCI information shared by the BSs, in order to maximize the sum rate of the users sharing a subcarrier. The CDMC algorithm also attempts to improve the frequency reuse factor of the subcarriers. As our algorithm shows, the CDMC algorithm makes the decisions for the three users sharing a subcarrier according to one of the three cases determined by the InterCI matrix. The principles of the CDMC algorithm associated with the three cases are described in Figures 5.3-5.5. Specifically, in Case 1, the CDMC algorithm can set up a cooperation for a user with poor SIR. In Case 2, it may establish a cooperation for a user. However, under Case 5.8. Conclusions 179

3, the algorithm will switch off the transmission to one or more users with their SIR below the threshold η_t . In this chapter, in order to make the performance comparison more explicit, we have addressed the spectrum-efficiency performance in Section 5.7 by focusing on the cell-edge users in the system. Our studies and performance results also show that both the proposed DDMC and CDMC algorithms can achieve a higher spectrum-efficiency than the OOP algorithm, and also than the case without employing any InterCI mitigation. This is because that our DDMC and CDMC algorithms have been designed with the motivation to establish cooperative transmissions for the users with poor SIRs, instead of simply turning off their transmissions. In comparison with the DDMC algorithm, the CDMC algorithm is able to find a better InterCI mitigation strategy in a joint way, based on the more knowledge about the InterCI information that is shared among the three BSs. Therefore, the CDMC algorithm is capable of attaining a higher spectrum-efficiency (per cell) and a higher frequency reuse factor than the DDMC algorithm, while the frequency reuse factor resulted from these two algorithms is higher than that of the the OOP algorithm. In addition, we have analyzed and compared the overhead required by the various InterCI mitigation algorithms. The results show that our DDMC algorithm requires a similar amount of overhead as the OOP algorithm, while the CDMC algorithm demands much higher overhead than these two algorithms. Overall, our studies in this chapter demonstrate that using distributed resource allocation followed by some efficient InterCI mitigation schemes, such as, the DDMC and CDMC algorithms, may significantly improve the performance of the multicell downlink OFDMA systems. In the next chapter, we will consider the code-allocation in the multicell downlink MC DS-CDMA systems with limited information sharing among the BSs.



Resource Allocation in Multicell Downlink MC DS-CDMA Systems

6.1 Introduction

It is well-known that exploiting the time-varying characteristics of wireless channels is capable of significantly increasing the capacity and enhancing the quality-of-service (QoS) of wireless communication systems. As demonstrated in the previous chapters, with the aid of dynamic resource allocation to communication users, promising energy- and spectrum-efficiency can be attained by making use of the embedded multiuser diversity [77]. Owing to the above-mentioned merits, resource allocation in broadband multicarrier communication systems now becomes very important. However, in wireless communications, the fundamental challenge lies in how to make efficient use of the expensive spectrum resources available, and to deal with the issues caused by the expansion of service area, service types, high diversity and large number of users. As a result, wireless spectrums (or frequency bands) are inevitably reused geographically in multiple cells of the wireless communication networks, which leads to a main performance-limiting factor, namely, the intercell interference (InterCI).

As mentioned in Chapter 4, in the LTE/LTE-A downlink OFDMA systems, the number of subcarriers can be very high, which is up to 2048, and the number of communication users simultaneously supported may also be very high. These OFDMA systems may experience some problems, such as, the PAPR problem. Furthermore, in these systems, scheduling becomes highly challenging, making them hard to employ the optimum or even sub-optimum subcarrier-allocation schemes, due to their complexity constraint [1, 190]. The scheduling issue becomes even more concerned, when multicell cellular communication is considered, as there exists InterCI. As discussed in Chapter 4, owing to the employment of DS spreading, the MC DS-CDMA can employ a significantly lower number of subcarriers than the other multicarrier schemes, such as the OFDMA,

6.1. Introduction 181

which do not employ DS spreading [1]. Furthermore, the MC DS-CDMA employs the flexibility to configure its number of subcarriers according to the frequency-selectivity of wireless channels, so that each subcarrier experiences independent fading. In this case, the number of subcarriers of MC DS-CDMA is at the order of the number of T-domain resolvable paths of wireless channels and, hence, it is usually a small number.

A range of researches, such as [97-100, 105, 107, 125], have proposed some resource allocation algorithms in the singlecell MC-CDMA and MC DS-CDMA systems. In Chapter 4 and also in [208], we have studied the resource allocation issues in the single-cell downlink MC DS-CDMA systems. The resources considered include power, subcarrier and DS spreading codes. However, in the single-cell scenario, the DS spreading codes are assumed orthogonal. Hence, the code-allocation becomes very simple. In other words, in the single-cell downlink MC DS-CDMA systems, resource allocation only needs to consider the power- and subcarrier-allocation. By contrast, when the multicell downlink MC DS-CDMA systems are considered, resource allocation becomes much more challenging. Due to the existence of InterCI, efficient resource allocation may have to consider the code-allocation in addition to power- and subcarrier-allocation. Therefore, in this chapter, we motivate to investigate the resource allocation in the multicell downlink MC DS-CDMA systems, which, to the best of our knowledge, has not been addressed in the existing references. Specifically, in this chapter, we consider the resource allocation in the multicell downlink MC DS-CDMA systems, when assuming that all subcarriers can be used in all cells. We assume that power-control is employed in each individual cell, which is usually the case in practice. Hence, our resource allocation mainly includes the subcarrier- and code-allocation, which are designed to minimize the average error rate of the system, or maximize the spectrum-efficiency of the system. However, for the sake of simplicity and robust to implement, in this chapter, we propose a novel resource allocation scheme, which first carries out the subcarrier-allocation independently by each of the BSs, and, then, executes the code-allocation jointly by multiple BSs. To be more specific, our subcarrier-allocation algorithms proposed in [208] and Chapter 4, which include the worst case avoiding (WCA), the worst case first (WCF) and iterative worst excluding (IWE) algorithms, are extend to the multicell MC DS-CDMA systems. Through our investigation and performance comparison with some existing subcarrier-allocation algorithms, we again verify that our proposed subcarrier-allocation algorithms outperform the existing sub-optimum subcarrier-allocation algorithms, when they are operated in the multicell scenarios. After the subcarrier-allocation carried out independently by each of the BSs, then, the code-allocation is operated with the motivation to mitigate the InterCI.

In this chapter, for the sake of achieving low-complexity code-allocation, we assume that, the BSs only share the information about large-scale fading, which includes the propagation pathloss and shadowing effect. Based on the information shared among the BSs, two code-allocation schemes are proposed, namely, the simplified strong InterCI avoiding (SSIA) and the enhanced strong InterCI avoiding (ESIA) algorithms. Specifically, the SSIA algorithm operates the code-

6.2. System Model

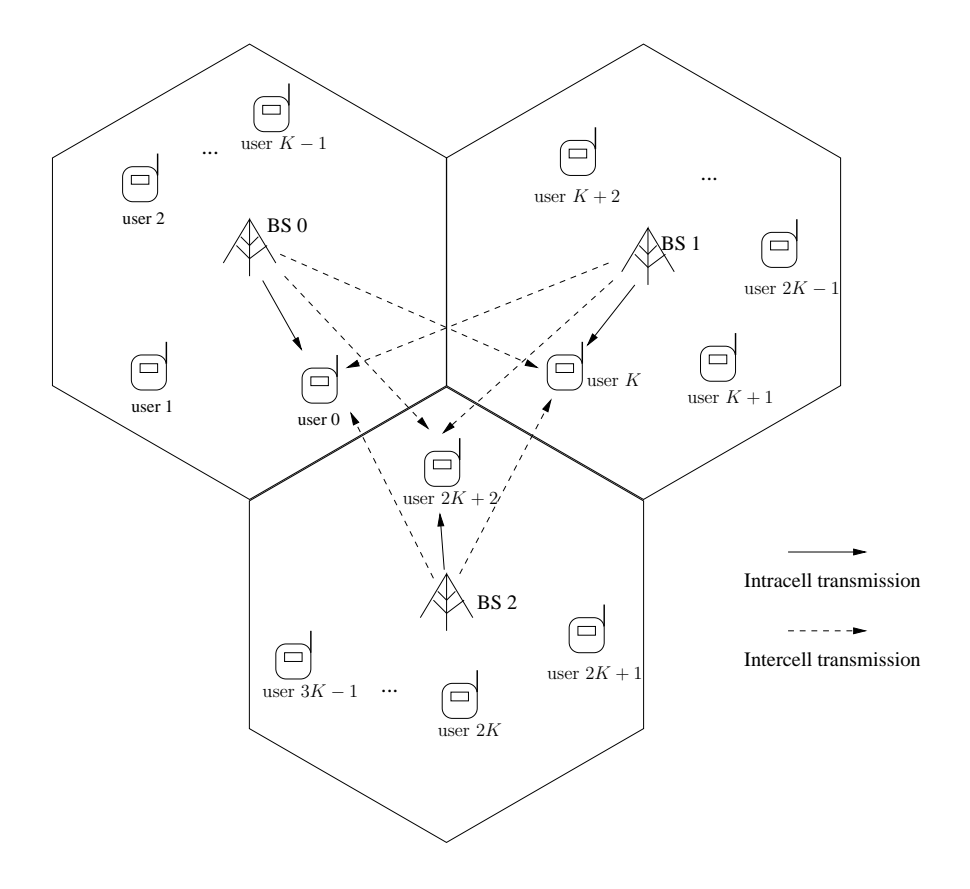


Figure 6.1: Conceptual structure of the multicell downlink MC DS-CDMA systems.

allocation by considering only one of the so-called InterCI factor matrices at a time. By contrast, in the ESIA algorithm, all the three InterCI factor matrices are simultaneously considered for code-allocation. In this chapter, the bit error rate (BER) and spectrum-efficiency performance of the multicell downlink MC DS-CDMA systems are investigated and compared, when various subcarrier- and code-allocation algorithms are employed, and when assuming that subcarrier channels experience independent fading. Our studies and performance results reveal that, the proposed code-allocation algorithms are highly efficient and significant performance gain can be attained, in comparison with the systems without code-allocation (or, in other words, random code-allocation).

6.2 System Model

We consider the resource allocation in a multicell downlink MC DS-CDMA system, as depicted in Figure 6.1. In order to catch the main features of multicell systems but for the sake of simplicity, we assume that the system consists of three cells, each of which has one base station (BS) supporting *K* mobile users. We assume that each of the communication terminals, including both BSs and mobile users, employs one antenna for signal receiving and transmission. Signals transmitted from BSs to mobile users are MC DS-CDMA signals employing time (T)-domain DS spreading [1]. For clarity, the variables and notations used in this chapter are summarized as follows:

6.2. System Model 183

K Number of mobile users in each cell;

 $\mathcal{K}^{(u)}$ Set of user indexes in cell u, defined as $\mathcal{K}^{(u)} = \{uK, uK+1, \dots, uK+K-1\}, u=0,1,2$;

N Spreading factor of DS spreading;

 \mathcal{N} Set of indexes of spreading codes, defined as $\mathcal{N} = \{0, 1, \dots, N-1\}$;

M Number of subcarriers of the MC DS-CDMA;

 \mathcal{M} Set of subcarrier indexes, defined as $\mathcal{M} = \{0, 1, \dots, M-1\}$;

 $h_{k,m}^{(u)}$ Channel gain of subcarrier m between BS u and user k in cell u;

C $(N \times K)$ -dimensional spreading matrix with columns consisting of the spreading codes taken from a $(N \times N)$ orthogonal matrix. Note that, some columns of C may be the same in the case of K > N. In this case, the corresponding users are allocated on different subcarriers;

 $\mathcal{F}_{m}^{(u)}$ Set of indexes for up to the N users assigned to subcarrier m in cell u;

 $\mathcal{V}_n^{(u)}$ Set of indexes for up to the M users assigned with spreading code n in cell u;

 $|\mathcal{F}|$ Cardinality of set \mathcal{F} , representing the number of elements in set \mathcal{F} .

In this chapter, we assume that each user in every cell is allocated one subcarrier and one spreading code (or, simply, code). In order to avoid intracell interference (IntraCI), users in the same cell are allocated either different subcarriers or different codes, or both are different. Expressed in mathematics, our allocations satisfy that

$$\bigcup_{m \in \mathcal{M}} \mathcal{F}_m^{(u)} = \mathcal{K}^{(u)}, \ \mathcal{F}_m^{(u)} \cap \mathcal{F}_{m'}^{(u)} = \emptyset, \qquad m' \neq m, \ \forall m', m \in \mathcal{M}, \ \forall u \in \{0, 1, 2\};$$
 (6.1)

$$\bigcup_{n\in\mathcal{N}}\mathcal{V}_n^{(u)}=\mathcal{K}^{(u)},\ \mathcal{V}_n^{(u)}\cap\mathcal{V}_{n'}^{(u)}=\emptyset,\qquad n'\neq n,\ \forall n',n\in\mathcal{N},\ \forall u\in\{0,1,2\}. \tag{6.2}$$

In our MC DS-CDMA system, in each cell, there are possibly N users sharing one subcarrier as well as M users sharing one code. From equations (6.1) and (6.2), we know that different users in a cell are guaranteed to have different subcarriers, if they possibly share the same code, as constrained by (6.1), or guaranteed to have different codes, if they share the same subcarrier, as explained in (6.2). Therefore, there is no IntraCI among users in a same cell. However, users in different cells may be allocated the same subcarrier and also the same code. In this case, there is intercell interference (InterCI).

As shown in Figure 6.1, we assume that each BS locates at the center of a hexagonal cell, and *K* users uniformly distribute in the cell. We assume that, in each cell, ideal power control is applied to maintain the same received power by its *K* intracell users, which is normalized to one. We assume that each BS transmits signals only to its intracell users, and InterCI exists only between adjacent

6.2. System Model 184

cells owing to the propagation pathloss. Let the InterCI be characterized by a factor α , which, when taking into account of the combined effects of propagation pathloss, shadowing and transmit power, can be expressed as [206]

$$\alpha = \sqrt{\left(\frac{d_0}{d_1}\right)^{\mu} 10^{\frac{\zeta_0 - \zeta_1}{10}}} \tag{6.3}$$

where d_0 and d_1 represent the distances from a BS to the considered intracell and intercell users, respectively. In (6.3), μ is the pathloss exponent, and ζ_0 , ζ_1 (in dB) are zero-mean Gaussian distributed random variables with standard deviation Y (in dB), which accounts for the shadowing effect. Owing to ζ_0 and ζ_1 having the correlation depending on the propagation attenuation from a BS to the two users, ($\zeta_0 - \zeta_1$) is illustrated to obey the log-normal distribution with zero mean and standard deviation of Y (in dB) [206]. In addition to the propagation pathloss and shadowing effects, signals transmitted from BSs to users also experience the fast fading, which, is assumed to be independent Rayleigh flat fading in terms of different users.

Let us assume that the data symbols to be transmitted by BS u to its K intracell users are expressed as $\mathbf{x}^{(u)} = [x_{uk}, x_{uK+1}, \dots, x_{uK+K-1}]^T$, where x_k is the data symbol to user k, which is assumed to satisfy $E[x_k] = 0$ and $E[|x_k|^2] = 1$. Furthermore, let us assume that subcarrier m is assigned to user k of cell u. Then, considering that the M subcarriers are orthogonal, the signal received by user k can be written as

$$\mathbf{y}_{k} = h_{k,m}^{(u)} \mathbf{C}_{m} \mathbf{W}^{(u)} \mathbf{x}^{(u)} + \sum_{u'=0, u' \neq u}^{2} h_{k,m}^{(u')} \alpha_{k',k}^{(u')} \mathbf{C}_{m} \mathbf{W}^{(u')} \mathbf{x}^{(u')} + \mathbf{n}_{k}$$
(6.4)

where, in addition to the notations mentioned previously, \mathbf{y}_k is a length-N observation vector. The vector $\mathbf{n}_k = [n_{k,1}, \dots, n_{k,N}]^T$ is a length-N noise vector at user k, and it is assumed to obey the complex Gaussian distribution with zero mean and a covariance matrix $2\sigma^2\mathbf{I}_N$, where $2\sigma^2 = 1/\bar{\gamma}_s$ is the noise variance and \mathbf{I}_N is a $(N \times N)$ identity matrix. In (6.4), $h_{k,m}^{(u)}$ is the fast fading channel gain from BS u to its intracell user k assigned with subcarrier m, while $\alpha_{k',k}^{(u')}$ characterizes the InterCI from BS u' to user k, by assuming that user k' is assigned with subcarrier m. Furthermore, \mathbf{C}_m is a $(N \times K)$ matrix formed from \mathbf{C} by setting those columns corresponding to the subcarriers other than m to zero vectors, as the result of using orthogonal subcarriers.

In this contribution, we assume that each BS employs the channel state information (CSI) of the KM intracell downlink channels. Hence, the BS is capable of preprocessing the signals to be transmitted by setting $\mathbf{W}^{(u)} = \operatorname{diag}\{w_{uK}^{(u)}, w_{uK+1}^{(u)}, \ldots, w_{uK+K-1}^{(u)}\}$ with $w_k^{(u)} = \left(h_{k,m}^{(u)}\right)^* / \sqrt{|h_{k,m}^{(u)}|^2}$, where $(\cdot)^*$ denotes the conjugate operation, and suppose that $k \in \mathcal{K}^{(u)}$, $k' \in \mathcal{K}^{(u')}$. However, we assume that the three BSs do not have the channel information $\left\{h_{k,m}^{(u')}|u,u'\in\{0,1,2\},u\neq u'\}\right\}$ of the intercell channels, in order to minimize the complexity of resource allocation. By contrast, since the pathloss and shadowing do not vary fast, we assume that the BSs are capable of sharing the information of the InterCI, i.e., $\left\{\alpha_{k',k}^{(u')}|u,u'\in\{0,1,2\},u\neq u'\}\right\}$. Consequently, after the despreading for user k using its spreading code \mathbf{c}_k , the kth column of \mathbf{C} , it can be shown that the

6.3. General Theory 185

decision variable generated by user k is

$$z_{k} = \sqrt{|h_{k,m}^{(u)}|^{2}} x_{k} + \underbrace{\sum_{u'=0, u' \neq u}^{2} h_{k,m}^{(u')} \alpha_{k',k}^{(u')} w_{k'}^{(u')} x_{k'}}_{\text{InterCI}} + n_{k}.$$

$$(6.5)$$

In (6.5), the first term is the desired signal for user k of cell u, and the second term is the InterCI from the other two cells. Furthermore, to obtain (6.5), we assumed that user k' of cell u' is assigned with the same subcarrier and also the same code as those assigned to user k.

From (6.5), we can know that the signal-to-interference-plus-noise ratio (SINR) for user k is

$$\gamma_k = \frac{|h_{k,m}^{(u)}|^2}{\sum_{u'=0, u' \neq u}^2 |h_{k,m}^{(u')} \alpha_{k',k}^{(u')} w_{k'}^{(u')}|^2 + 2\sigma^2}.$$
(6.6)

Explicitly, when allocating user k a subcarrier with higher channel quality $|h_{k,m}^{(u)}|^2$ while allocating its InterCI users have the subcarriers with lower values of $|h_{k,m}^{(u')}\alpha_{k',k}^{(u')}|^2$, we can obtain a relatively high SINR and, hence, a lower error rate, if a given baseband modulation scheme is considered.

6.3 General Theory

In the considered multicell MC DS-CDMA system, we employ M subcarriers and N spreading codes to support 3K users, which may be as high as 3MN, in three cells. Our resource allocation is aimed to maximize the system reliability, and the optimization problem can be described as

$$\bigcup \{\mathcal{F}_{m}^{(u)}, \mathcal{V}_{n}^{(u)}\}^{*} = \arg \min_{\bigcup \{\mathcal{F}_{m}^{(u)}, \mathcal{V}_{n}^{(u)}\}} \{\bar{P}_{e}\}
= \arg \min_{\bigcup \{\mathcal{F}_{m}^{(u)}, \mathcal{V}_{n}^{(u)}\}} \left\{ \frac{1}{3K} \sum_{k=0}^{3K-1} \bar{P}_{e}^{(k)}(\gamma_{k}) \right\},
\text{s.t. (6.1), (6.2)}$$
(6.7)

where 's.t.' stands for 'subject to', \bar{P}_e denotes the system's average BER and $\bar{P}_e^{(k)}$ denotes the average BER of user k. In (6.7), $\cup \{\mathcal{F}_k^{(u)}, \mathcal{V}_n^{(u)}\}$ stands for testing all the possible allocations for all the 3K users, while $\cup \{\mathcal{F}_k^{(u)}, \mathcal{V}_n^{(u)}\}^*$ contains the final allocation results for all the 3K users. Note that, in this chapter, no power-allocation is considered owing to using power control.

In practice, however, it is often very hard to solve the optimization problem of (6.7), due to the nonlinear relationship between $\bar{P}_e^{(k)}(\gamma_k)$ and γ_k . Since the average BER \bar{P}_e in various multicarrier communications systems is usually dominated by the subcarrier with the lowest SINR [84]. Consequently, our resource allocation algorithms are designed to maximize the minimum SINR of users, such as in [75, 83, 188]. Therefore, when we jointly consider the resource allocation including

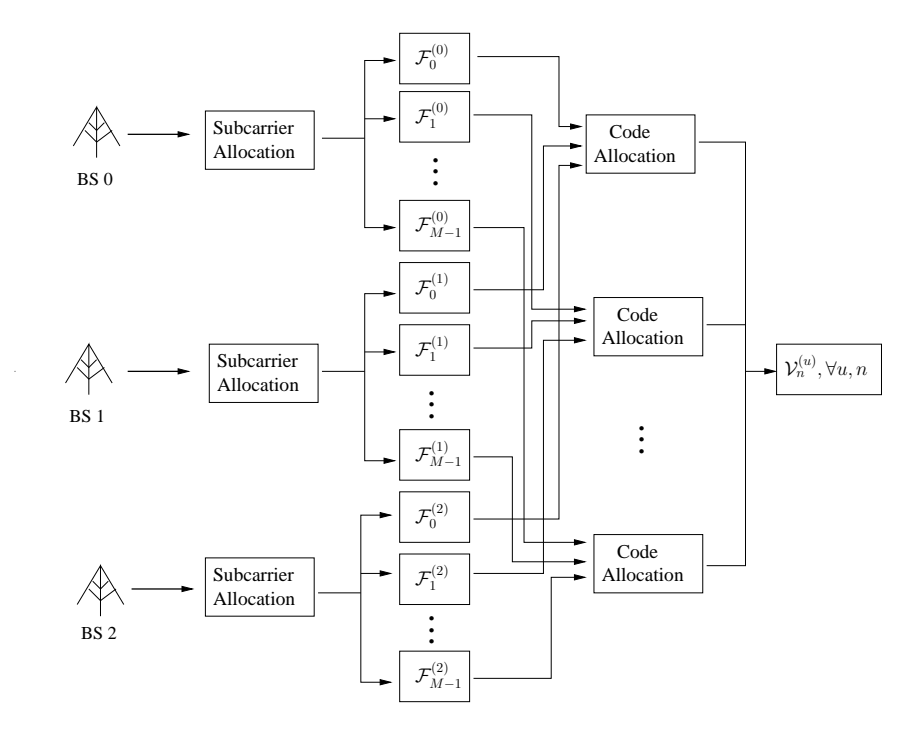


Figure 6.2: Flow chart illustrating the proposed resource allocation scheme for the multicell downlink MC DS-CDMA systems.

subcarrier- and code-allocation, the optimization problem can be expressed as

$$\bigcup \{\mathcal{F}_{m}^{(u)}, \mathcal{V}_{n}^{(u)}\}^{*} = \arg \max_{\bigcup \{\mathcal{F}_{m}^{(u)}, \mathcal{V}_{n}^{(u)}\}} \left\{ \min_{u \in \{0,1,2\}, k \in \mathcal{K}^{(u)}} \{\gamma_{k}\} \right\},$$
s.t. (6.1), (6.2) (6.8)

where γ_k is given by (6.6).

The optimization problem of (6.8) represents a non-convex problem, which is extremely difficult to solve. In order to simplify the resource allocation, in this chapter, we assume that subcarriers and codes are allocated separately. Specifically, the BSs first independently carry out the subcarrierallocation based only on the CSI of the *KM* intracell channels. Correspondingly, the optimization problem for subcarrier-allocation can be described as

$$\bigcup \{\mathcal{F}_{m}^{(u)}\}^{*} = \arg \max_{\bigcup \{\mathcal{F}_{m}^{(u)}\}} \left\{ \min_{k \in \mathcal{K}^{(u)}} \{A_{k}\} \right\}, \ \forall u,$$
s.t. (6.1)

where $A_k = \frac{|h_{k,m}^{(u)}|^2}{2\sigma^2}$. (6.9) aims to maximize the minimum subchannel quality of all the intracell users in the three cells, in contrast to [208], where subcarrier-allocation has been considered in single-cell MC DS-CDMA systems.

Overall, our resource allocation scheme may be viewed with the aid of the flow chart in Figure 6.2. After the three BSs independently allocate the subcarriers, they operate the code-allocation based on the results of the subcarrier-allocation. From (6.6), we can know that a user only experiences the InterCI from the two intercell users assigned the same subcarrier and code. Therefore, as shown in Figure 6.2, code-allocation are only need to be considered for the users in the three cells, which share the same subcarrier, with the objective of minimizing the InterCI of each user. As the BSs only share the InterCI factors of $\{\alpha_{k',k}^{(u')}|u'\in\{0,1,2\}\}$, the optimization problem of code-allocation can be described as

$$\bigcup \{\mathcal{V}_{n}^{(u)}\}^{*} = \arg \min_{\bigcup \{\mathcal{V}_{n}^{(u)}\}} \left\{ \max_{u \in \{0,1,2\}, k \in \mathcal{F}_{m}^{(u)}} \{E_{k}\} \right\}, \ \forall m \in \mathcal{M},$$
s.t. (6.2)

where
$$E_k = |\alpha_{k',k}^{(u')}|^2 + |\alpha_{k'',k}^{(u'')}|^2$$
 if $\mathcal{F}_m^{(u)} = \{k\}$, $\mathcal{F}_m^{(u')} = \{k'\}$, $\mathcal{F}_m^{(u'')} = \{k''\}$, $m \in \mathcal{M}$.

Although solving the optimization problems of (6.9) and (6.10) has much lower complexity, than solving (6.8), exhaustive search is still required, which however has extremely high complexity and prevents the algorithm from practical implementation, when the number of users in the system is relatively high. In order to further reduce the complexity, in this chapter, we focus on finding the sub-optimum solutions for the optimization problem of (6.10). Specifically, two algorithms are proposed for (6.10), which are the simplified strong InterCI avoiding (SSIA) and enhanced strong InterCI avoiding (ESIA) code-allocation algorithms.

In summary, our resource allocation consists of two stages, subcarrier- and code-allocation. First, each BS independently executes the subcarrier-allocation to obtain the allocation results $\{\mathcal{F}_m^{(u)}\}$. Then, code-allocation is carried out based on the subcarrier-allocation results, yielding the code-allocation results $\{\mathcal{V}_n^{(u)}\}$. In literature, such as in [77, 78, 80, 82–86], various subcarrier-allocation algorithms have been proposed and studied for downlink OFDMA systems and other multicarrier systems. In Chapter 4, we have proposed a range of subcarrier-allocation algorithms for single-cell downlink MC DS-CDMA systems, which include the worst case avoiding (WCA), worst case first (WCF) and the iterative worst excluding (IWE) algorithms. In the considered MC DS-CDMA systems, each BS may employ a subcarrier-allocation algorithm discussed in Chapter 4. In this chapter, we do not further discuss the subcarrier-allocation algorithms, but focus on the code-allocation in the multicell MC DS-CDMA systems. Furthermore, in Section 6.7, we compare the BER and spectrum-efficiency performance of the multicell MC DS-CDMA systems employing the various subcarrier-allocation algorithms proposed in Chapter 4.

6.4 Simplified Strong InterCI Avoiding Code-Allocation

In our multicell MC DS-CDMA systems, code-allocation is carried out after subcarrier-allocation. As discussed in Section 6.3, after the subcarrier-allocation, each user suffers the InterCI only from two users in the other two cells, which are allocated the same subcarrier and code as itself. As shown in (6.6), the SINR obtained by a user is dominated by the InterCI, when the power of back-

ground noise becomes small. Therefore, the objective of code-allocation should keep the InterCI as small as possible. In this chapter, for the sake of achieving low implementation complexity, we assume that the BSs only share the knowledge of the InterCI factors $\{\alpha_{k',k}^{(u')}\}$, which take into account of both propagation pathloss and shadowing effect. In this case, code-allocation may be optimized to minimize the average InterCI of the three users sharing the same subcarrier and the same code.

In this section and Section 6.5, we propose two code-allocation algorithms, which are the simplified strong InterCI avoiding (SSIA) and the enhanced strong InterCI avoiding (ESIA) code-allocation algorithms. In order to make our algorithms easy to follow, we introduce them with the aid of an example, which employs M=4 subcarriers and N=4 orthogonal spreading codes for supporting 16 users in each cell. Therefore, the frequency reuse factor is one. In this example, we assume that, after the subcarrier-allocation, we have obtained the allocation results for subcarrier 0, $\mathcal{F}_0^{(0)}=\{0,3,6,7\}$ in cell 0, $\mathcal{F}_0^{(1)}=\{18,21,22,26\}$ in cell 1 and $\mathcal{F}_0^{(2)}=\{32,33,36,41\}$ in cell 2. The InterCI factors between two of the users allocated subcarrier 0 are illustrated in Tables 6.1-6.3, where, in each of the tables, the first element is the InterCI factor imposed by a column user to the corresponding row user, while the second element is the InterCI factor from a row user to the corresponding column user. Let us first consider the SSIA code-allocation algorithm.

Table 6.1: An example showing the InterCI factors $\left(\alpha_{k',k}^{(u')},\alpha_{k,k'}^{(u)}\right)$ between any two users allocated with subcarrier 0 in cells 0 and 1.

users	18	21	22	26
0	0.018, 0.005	0.108, 0.003	0.117, 0.106	0.143, 0.006
3	0.067, 0.126	0.01, 0.131	0.026, 1.958	0.116, 1.199
6	0.038, 0.165	0.011, 0.137	0.194, 0.368	0.147, 0.205
7	0.065, 0.022	0.167, 0.083	0.019, 0.177	0.081, 0.571

The SSIA algorithm aims at minimizing the maximum InterCI factor between two of the users sharing the same subcarrier. Hence, it carries out code-allocation jointly with the users in adjacent cells based on the knowledge about the InterCI factors of users in different cells. However, in order to reduce the complexity for implementation, our SSIA algorithm first carries out the code-allocation for the users in any two neighbouring cells. Then, codes are assigned to the users in the other cell. Let us now illustrate the SSIA algorithm in association with the example shown in Tables 6.1-6.3.

In the considered example, let us first carry out the code-allocation for the eight users in cells 0 and 1 assigned with subcarrier 0. The allocation are based on three InterCI factor matrices $\Theta_0^{(0,1)}$, $\Theta_0^{(0,2)}$ and $\Theta_0^{(1,2)}$, 1 which are obtained by modifying the InterCI factor matrices shown in

¹InterCI factor matrix $\Theta_m^{(u,u')}$ can be also expressed as $\Theta_m^{(u',u)}$, $\forall m, u, u'$.

Table 6.2: An example showing the InterCI factors $\left(\alpha_{k',k}^{(u')},\alpha_{k,k'}^{(u)}\right)$ between any two users allocated with subcarrier 0 in cells 0 and 2.

users	32	33	36	41
0	0.136, 0.004	0.624, 0.002	0.049, 0.007	0.218, 0.008
3	0.054, 0.031	0.102, 0.101	0.012, 0.146	0.064, 0.201
6	0.167, 0.033	0.013, 0.14	0.228, 0.464	0.13, 0.019
7	2.243, 0.034	0.656, 0.127	0.089, 0.058	0.063, 0.139

Table 6.3: An example showing the InterCI factors $\left(\alpha_{k',k}^{(u')},\alpha_{k,k'}^{(u)}\right)$ between any two users allocated with subcarrier 0 in cells 1 and 2.

users	32	33	36	41
18	0.095, 0.052	0.057, 0.125	0.04, 0.23	0.098, 0.017
21	0.129, 0.229	0.215, 0.024	1.127, 0.166	0.144, 0.044
22	0.009, 0.045	0.096, 0.912	0.077, 0.47	0.011, 0.133
26	0.245, 0.014	0.729, 0.015	0.18, 0.623	0.041, 0.068

Tables 6.1-6.3. Specifically, $\Theta_0^{(0,1)}$ is given by

where U_i is for user i, the circled numbers denote the allocation iterations, and the element value is obtained as

$$\tilde{\alpha}_{k,k'} = \max\left\{\alpha_{k',k}^{(u')}, \alpha_{k,k'}^{(u)}\right\}, \ k \in \mathcal{F}_0^{(0)}, \ k' \in \mathcal{F}_0^{(1)}.$$
 (6.12)

Similar to (6.11), we can obtain the other two matrices $\Theta_0^{(0,2)}$ and $\Theta_0^{(1,2)}$. For example, we can express $\Theta_0^{(0,2)}$ as

$$\Theta_0^{(0,2)} = \begin{bmatrix}
 U_{32} & U_{33} & U_{36} & U_{41} \\
 U_0 & 0.136 & 0.624 & 0.049 & 0.218 \\
 U_3 & 0.054 & 0.102 & 0.146 & 0.201 \\
 U_6 & 0.167 & 0.14 & 0.464 & 0.13 \\
 U_7 & 2.243 & 0.656 & 0.089 & 0.139
\end{bmatrix}.$$
(6.13)

Since for the cases of the InterCI factor being greater than 1, such as $\alpha_{k',k}^{(u')} > 1.0$, the InterCI signal is amplified. As shown in (6.6), we define the users generating the elements $\{\tilde{\alpha}_{k,k'} > 1.0\}$

in the matrices of (6.11) and (6.13) as 'undesirable' users. Furthermore, once a user is allocated a code, this user is referred to as 'unavailable' user. In the SSIA algorithm, each allocation iteration first identifies the row user, which has the maximum number of the 'unavailable' plus 'undesirable' users. Specifically, for the example considered, as shown in (6.11), the circled numbers indicate the allocation iterations. During the first allocation iteration, among the four users of cell 0, user 3 has the maximum number of 'undesirable' users in cell 1, which are user 22 corresponding to $\tilde{\alpha}_{3,22}=1.958$, and user 26 corresponding to $\tilde{\alpha}_{3,26}=1.199$. By contrast, the minimum value on this row is 0.126, which corresponds to user 3 in cell 0 and user 18 in cell 1. Therefore, user 18 in cell 1 is identified as the 'co-code' user of user 3 in cell 0, as the underlined element indicates. Consequently, during the first iteration, we allocate users 3 and 18 code 0. During iteration 2, we can see that, in (6.11), each of the rest three users in cell 0 has one 'unavailable' user of U_{18} but no 'undesirable' users. In this case, we first allocate a code to the user having the the largest "maximum InterCI factor", which hence avoids the assignment of strong InterCI. As shown in (6.11), $\tilde{\alpha}_{7,26} = 0.571$ is the largest one, which corresponds to user 7 in cell 0 and user 26 in cell 1. Therefore, like the procedure in iteration 1, we make user 21 in cell 1 as the 'co-code' user of user 7 in cell 0, and allocate them code 1. Similarly, we can identify the other 'co-code' users and allocate them codes. In the end, as the underlined elements in (6.11) show, during iterations 3 and 4, we allocate code 2 to users 6 and 26, and code 3 to users 0 and 22. Hence, from allocation iterations 1-4 we derive the code-allocation results, which are expressed as $\mathcal{V}_0^{(0)}=\{3\},\,\mathcal{V}_0^{(1)}=\{18\},$ $\mathcal{V}_{1}^{(0)} = \{7\}, \, \mathcal{V}_{1}^{(1)} = \{21\}, \, \mathcal{V}_{2}^{(0)} = \{6\}, \, \mathcal{V}_{2}^{(1)} = \{26\}, \, \mathcal{V}_{3}^{(0)} = \{0\}, \, \mathcal{V}_{3}^{(1)} = \{22\}.$

After the code-allocation to the users in cells 0 and 1, we can now start allocating codes to the four users in cell 2. The allocation can be carried out based either on the matrix $\Theta_0^{(0,2)}$ or on the matrix $\Theta_0^{(1,2)}$, which results in the same performance. For example, let us use the InterCI factor matrix $\Theta_0^{(0,2)}$ to illustrate the allocation principle, which is expressed as (6.13). After considering the allocation results from iterations 1-4, we modify $\Theta_0^{(0,2)}$ to

the allocation results from iterations 1-4, we modify
$$\Theta_0^{(0,2)}$$
 to
$$\Theta_0^{(0,2)} = \begin{bmatrix} U_{32} & U_{33} & U_{36} & U_{41} \\ U_0 & \underline{0.136} & 0.624 \rightarrow \textbf{0.912} & 0.049 \rightarrow 0.47 & 0.218 \\ U_3 & 0.054 \rightarrow 0.095 & \underline{0.102 \rightarrow 0.125} & 0.146 \rightarrow 0.23 & 0.201 \\ U_6 & 0.167 \rightarrow 0.245 & 0.14 \rightarrow \textbf{0.729} & \underline{0.464 \rightarrow 0.623} & 0.13 \\ U_7 & 2.243 & 0.656 & 0.089 \rightarrow 1.127 & \underline{0.139 \rightarrow 0.144} \end{bmatrix}$$
 (5) where the element ' $a \rightarrow b$ ' means updating ' a ' in (6.13) to ' b '. For example, users 0 and 22

where the element ' $a \to b$ ' means updating 'a' in (6.13) to 'b'. For example, users 0 and 22 are a pair of 'co-code' users, then $\tilde{\alpha}_{0,33}$ in the above matrix is updated to 0.912, as 0.912 = $\max{\{\tilde{\alpha}_{0,33}, \tilde{\alpha}_{22,33}\}}$. Similarly, each element in the matrix $\Theta_0^{(0;2)}$ can be updated as

$$\tilde{\alpha}_{k,k''} = \max\left\{\tilde{\alpha}_{k,k''}, \tilde{\alpha}_{k',k''}\right\}, \ k \in \mathcal{V}_n^{(0)}, \ k' \in \mathcal{V}_n^{(1)}, \ k'' \in \mathcal{F}_0^{(2)}$$
(6.15)

where we assume that users k and k' are a pair of 'co-code' users sharing code n.

For the users in cell 2, the code-allocations are carried out based on the matrix of (6.14), where the InterCI factors have been updated. Similar to the allocations for the users in cells 0 and 1, we

can identify user 7 during iteration 5, which has the maximum number of 'unavailable' InterCI factor, as $\tilde{\alpha}_{7,32}=2.243$ and $\tilde{\alpha}_{7,36}=1.127$. Therefore, we could find its 'co-code' user in cell 2, which is user 41, since the underlined value of $\tilde{\alpha}_{7,41}=0.144$ is the minimum available InterCI factor for user 7. As user 7 has been allocated code 1 at iteration 2, user 41 is therefore allocated code 1. By a similar way, the code-allocations for the rest users in cell 2 can be done at iterations 6, 7 and 8. Finally, as indicated by the underlined elements in (6.14), we have the code-allocation results given by $\mathcal{V}_0^{(2)}=\{33\}$, $\mathcal{V}_1^{(2)}=\{41\}$, $\mathcal{V}_2^{(2)}=\{36\}$, $\mathcal{V}_3^{(2)}=\{32\}$.

For the example considered, the code-allocation results for the users sharing subcarrier 0 are: users 7, 21 and 41 sharing code 0, users 3, 18 and 33 sharing code 1, users 6, 26 and 36 sharing code 2, users 0, 22 and 32 sharing code 3. Furthermore, with the aid of Table 6.3, we can know that the maximum InterCI factor after the SSIA assisted code-allocation is $\alpha^{(max)} = \alpha^{(1)}_{26,36} = 0.623$, while the average shadowing effect is $\alpha^{(ave)} = 0.145$.

In summary, the SSIA assisted code-allocation algorithm can be stated as follows.

Algorithm 12. (Simplified Strong InterCI Avoiding Code – Allocation Algorithm)

Set
$$\mathcal{V}_n^{(u)} = \emptyset$$
, $\forall n \in \mathcal{N}$, $\forall u \in \{0, 1, 2\}$.

For subcarrier $m = 0, 1, \dots, M - 1$:

Initialization:

Form the InterCI factor matrices $\Theta_m^{(u,u')}$ according to (6.11), $\forall u, u'$; Set $\tilde{\mathcal{N}} = \mathcal{N}$, $\tilde{\mathcal{F}}_m^{(u)} = \mathcal{F}_m^{(u)}$, $\tilde{\mathcal{F}}_m^{(u')} = \mathcal{F}_m^{(u')}$, $\forall u, u'$; Set u = 0, u' = 1 and u'' = 2.

Code-allocation:

For allocation iterations s = 1, ..., 2N, carry out the operations:

Step 1 User identification:

- (a) Find the user/users $\tilde{\mathcal{K}}_s$ in cell u with the maximum number of the 'unavailable' plus 'undesirable' users in cell u'.
- (b) Find the user in $\tilde{\mathcal{K}}_s$, which has the largest InterCI factor: $\hat{k} = \arg\max_{k \in \tilde{\mathcal{K}}_s} \left\{ \tilde{\alpha}_k^{(\max)} \right\}$, where $\tilde{\alpha}_k^{(\max)} = \arg\max\left\{ \tilde{\alpha}_{k,k'}, \ k' \in \tilde{\mathcal{F}}_m^{(u')} \right\}$.

Step 2 Allocating the code:

Allocate users
$$\hat{k}$$
 and \hat{k}' code n : $\mathcal{V}_n^{(u)} = \{\hat{k}\}, \mathcal{V}_n^{(u')} = \{\hat{k}'\},$ where $\hat{k}' = \arg\min_{k' \in \tilde{\mathcal{F}}_m^{(u')}} \left\{\tilde{\alpha}_{\hat{k},k'}\right\}$. $n = j$ if $\hat{k} \in \mathcal{V}_j^{(u)}$ or $\hat{k}' \in \mathcal{V}_j^{(u')}$; otherwise $n = \tilde{N}(0)$.

Step 3 Update:

Update
$$\Theta_m^{(u,u'')}$$
 by (6.15), if $s \leq N$; Set $\tilde{\mathcal{F}}_m^{(u)} \leftarrow \tilde{\mathcal{F}}_m^{(u)} - \{\hat{k}\}, \tilde{\mathcal{F}}_m^{(u')} \leftarrow \tilde{\mathcal{F}}_m^{(u')} - \{\hat{k}'\}$; Set $\tilde{\mathcal{N}} \leftarrow \tilde{\mathcal{N}} - n$; Set $u' = 2$ if $s = N$.

Step 4 Repeat Steps 1-3 until $\tilde{\mathcal{N}}=\emptyset$.

6.5 Enhanced Strong InterCI Avoiding Code-Allocation

The SSIA algorithm has a main advantage of low-complexity, as it operates based on the $(N \times N)$ InterCI factor matrices. However, the SSIA also has one shortcoming. During each allocation iteration, the SSIA code-allocation algorithm only considers the InterCI between the users in the two neighboring cells of being considered, but ignores the InterCI from the users in the other cell not considered at moment. This may cause that the users allocated in later iterations obtain the codes with strong InterCI. In order to improve the SSIA algorithm, but not to increase too much complexity, in this section, we design a code-allocation algorithm called as the ESIA algorithm, which also aims at minimizing the maximum InterCI factor of the users in the downlink multicell MC DS-CDMA systems. Let us below illustrate the principles of the ESIA algorithm with the aid of the example shown in Tables 6.1-6.3.

For the considered example, our ESIA algorithm is operated by simultaneously considering the three InterCI factor matrices, $\Theta_0^{(0,1)}$, $\Theta_0^{(0,2)}$ and $\Theta_0^{(1,2)}$. The elements in the matrix $\Theta_0^{(1,2)}$ are obtained from (6.12). Based on the three matrices, the ESIA algorithm can be explained in detail as follows, in association with (6.16)-(6.18).

$$\Theta_0^{(0,1)} = \begin{bmatrix}
 U_{18} & U_{21} & U_{22} & U_{26} \\
 U_0 & 0.018 & 0.108 \to 0.229 & 0.117 & \underline{0.143 \to 0.245} \\
 U_3 & \underline{0.126} & 0.131 & 1.958 & 1.199 \\
 U_6 & 0.165 & \underline{0.137 \to 0.215} & 0.368 \to 0.912 & 0.205 \to 0.729 \\
 U_7 & 0.065 & 0.167 & \underline{0.177} & 0.571
\end{bmatrix}$$
(6.16)

$$\Theta_0^{(0,2)} = \begin{bmatrix}
 U_{32} & U_{33} & U_{36} & U_{41} \\
 U_0 & \underline{0.136} & 0.624 & 0.049 & 0.218 \\
 U_3 & 0.054 \to 0.095 & 0.102 \to 0.125 & \underline{0.146 \to 0.23} & 0.201 \\
 U_6 & 0.167 & \underline{0.14} & 0.464 & 0.13 \\
 U_7 & 2.243 & 0.656 & 0.089 & \underline{0.139}
\end{bmatrix} (6.17)$$

$$\Theta_0^{(1,2)} = \begin{bmatrix} U_{32} & U_{33} & U_{36} & U_{41} \\ U_{18} & 0.095 & 0.125 & \underline{0.23} & 0.098 \to 0.201 \\ U_{21} & 0.229 & \underline{0.215} & 1.127 & 0.144 \to 0.167 \\ U_{22} & 0.045 \to 0.117 & 0.912 & 0.47 & \underline{0.133 \to 0.177} \\ U_{26} & \underline{0.245} & 0.729 & 0.623 & 0.068 \to 0.571 \end{bmatrix}$$

$$\tag{6.18}$$

The difference between the SSIA and the ESIA algorithms is that the ESIA algorithm identifies the user having the maximum number of 'unavailable' plus 'undesirable' users simultaneously

from all the three InterCI factor matrices, in order to exploit higher diversity. By contrast, the SSIA algorithm finds the user having the maximum number of 'unavailable' plus 'undesirable' users in one InterCI factor matrix, as shown in Section 6.4. Furthermore, the ESIA algorithm searches for the user having the above characteristics from both the row and column directions.

As shown in (6.16), (6.17) and (6.18), the ESIA algorithm needs eight allocation iterations to implement the code-allocation for the twelve users in the three cells. During iteration 1, we can readily find that among all the 12 users, user 3 in $\Theta_0^{(0,1)}$ has the maximum number of 'unavailable' plus 'undesirable' users, as $\tilde{\alpha}_{3,22}=1.958$, $\tilde{\alpha}_{3,26}=1.199$. Therefore, user 18 in cell 2 is identified as the 'co-code' user of user 3 in cell 1, owing to $\tilde{\alpha}_{3,18}=0.126$ is the minimum available InterCI factor. As, at this allocation iteration, neither of the two users has been assigned a code yet, we can allocate an available code to both of them. Hence, we allocate code 0 to users 3 and 18. After the code-allocation for these two users, the algorithm updates the corresponding InterCI factors in the other two matrices, $\Theta_0^{(0,2)}$ and $\Theta_0^{(1,2)}$, based on the same principles of (6.15). After the updating, we can observe that $\tilde{\alpha}_{3,k''}=\tilde{\alpha}_{18,k''}, \forall k''\in\mathcal{F}_0^{(2)}$ in (6.17) and (6.18).

During the second allocation iteration of the ESIA algorithm, we identify the user with the maximum number of 'unavailable' plus 'undesirable' users. However, as known from (6.17) and (6.18), all the ten users without allocated codes have the same number of 'unavailable' plus 'undesirable' users, which is one. For this sake, we propose a method named as the InterCI Scoring (IS) to identify which one of the ten users is first allocated a code, in order to further minimize the maximum InterCI factor for the allocated users. In detail, the IS method can be described as follows.

InterCI Scoring (IS): The InterCI factor $\tilde{\alpha}_{k,k'}$ is mapped to a corresponding InterCI score $e_{k,k'}$ defined as

$$e_{k\,k'} = i$$
, if $\tilde{\alpha}_{k\,k'} \in \mathcal{B}_i$, $i = 0, 1, \dots, N_b + 1$ (6.19)

where \mathcal{B}_i denotes the *i*th InterCI factor bin and there are in total $(N_b + 2)$ number of InterCI factor bins. Here, \mathcal{B}_i can be defined as

$$\mathcal{B}_{i} = \begin{cases} [1, +\infty), & \text{if } i = 0, \\ (1 - 0.9i/N_{b}, 1 - 0.9(i - 1)/N_{b}], & \text{if } i = 1, \dots, N_{b}, \\ (0, 0.1), & \text{if } i = N_{b} + 1. \end{cases}$$

$$(6.20)$$

According to (6.19) and (6.20), with the IS method, the InterCI factors are mapped to the integer scores, higher InterCI factors are awarded lower scores. Roughly, the InterCI is classified into three types: a) ignorable InterCI, if $0 < \tilde{\alpha}_{k,k'} < 0.1$; b) moderate InterCI, if $0.1 \ge \tilde{\alpha}_{k,k'} < 1$; and c) strong InterCI, if $\tilde{\alpha}_{k,k'} \ge 1$. Their corresponding scores are $e_{k,k'} = N_b + 1$ for ignorable InterCI, $e_{k,k'} = 0$ for strong InterCI, while $e_{k,k'} = 1, \ldots, N_b$ for moderate InterCI. Therefore, when the IS of a user is relatively low, it means that it suffers from relatively strong InterCI.

With the aid of the IS method, during iteration 2 of the ESIA algorithm, we can identify the user from the ten options via finding the one having the minimum sum of the IS. For the example

considered, we assumed that the number of bins is $N_b+2=4$. In this case, we can identify user 36 in cell 2 for code-allocation, as the sum of its IS is $e_{18,36}+e_{21,36}+e_{22,36}+e_{26,36}=2+0+2+1=5$, which is the smallest IS among the ten users. From (6.18), we can find that user 18 in cell 1 is user 36's 'co-code' user, as, corresponding to user 36, $\tilde{\alpha}_{18,36}=0.23$ is the minimum available InterCI factor, as shown in $\Theta_0^{(1,2)}$. Consequently, users 3, 18 and 36 from the three cells form a group of 'co-code' users, which are allocated code 0. Note that, as shown in (6.17), the InterCI factor $\tilde{\alpha}_{3,36}$ has also been changed to an underlined element, due to the fact that user 36 in cell 3 becomes the 'co-code' user of user 3. In the following six iterations, code-allocation to the remaining users can be carried out in the same way as iterations 1 and 2 described above. Note furthermore that, during iteration 5, users 6 and 33 directly become a pair of 'co-code' users, as they are the only users having not been allocated a code in cell 0 and 2.

Finally, as the underlined elements in (6.16), (6.17) and (6.18) show, the code-allocation results are: users 3, 18 and 36 sharing code 0, users 7, 22 and 41 sharing code 1, users 0, 26 and 32 sharing code 2, users 6, 21 and 33 sharing code 3. In comparison with the SSIA algorithm, the maximum InterCI factor achieved by the ESIA is much smaller, which is $\alpha^{(max)} = \alpha_{32,26}^{(2)} = 0.245$. Furthermore, the average InterCI factor also becomes smaller, which is $\alpha^{(ave.)} = 0.093$. The above improvement is achieved because the ESIA algorithm is capable of exploiting a higher order of diversity during the code-allocation.

The ESIA code-allocation algorithm is summarized as follows.

Algorithm 13. (Enhanced Strong InterCI Avoiding Code – Allocation Algorithm)

Set
$$V_n^{(u)} = \emptyset$$
, $\forall n \in \mathcal{N}$, $\forall u \in \{0,1,2\}$.

For subcarrier m = 0, 1, ..., M - 1:

Initialization:

Form the InterCI factor matrices
$$\Theta_m^{(0,1)}$$
, $\Theta_m^{(0,2)}$, $\Theta_m^{(1,2)}$ according to (6.11); Set $\tilde{\mathcal{N}} = \mathcal{N}$, $\tilde{\mathcal{F}}_m^{(u)} = \mathcal{F}_m^{(u)}$, $\tilde{\mathcal{F}}_m^{(u')} = \mathcal{F}_m^{(u')}$, $\tilde{\mathcal{F}}_m^{(u'')} = \mathcal{F}_m^{(u'')}$. Set $u \neq u' \neq u''$ and $u, u', u'' \in \{0, 1, 2\}$;

Code-allocation:

For allocation iteration s = 1, ..., 2N, carry out the operations:

Step 1 User identification:

- (a) By searching from the three InterCI factor matrices, find the user/users of $\tilde{\mathcal{K}}_s$ related to the specified InterCI factor matrices, which has/have the maximum number of the 'unavailable' plus 'undesirable' users in a cell.
- (b) Find the user $\hat{k} \in \tilde{\mathcal{K}}_s \cap \mathcal{K}^{(u)}$, which has the minimum sum of InterCI score. $\hat{k} = \arg\max_{k \in \tilde{\mathcal{K}}_s} \{E_k\}$, where $E_k = \sum_{k' \in \tilde{\mathcal{F}}_m^{(u')}} e_{k,k'}$ if user k in $\tilde{\mathcal{K}}_s$ is related to $\Theta_m^{(u,u')}$, or $E_k = \sum_{k' \in \tilde{\mathcal{F}}_m^{(u')}} e_{k',k}$ if user k in $\tilde{\mathcal{K}}_s$ is related to $\Theta_m^{(u',u)}$.

Step 2 Allocating code:

Allocate users \hat{k} and \hat{k}' code n: $\mathcal{V}_n^{(u)} = \{\hat{k}\}, \, \mathcal{V}_n^{(u')} = \{\hat{k}'\}, \, \text{where } n = j \text{ if } \hat{k} \in \mathcal{V}_j^{(u)} \text{ or } i \in \mathcal{V}_j^{(u)}$

$$\begin{split} \hat{k}' &\in \mathcal{V}_j^{(u')}; \text{ otherwise } n = \tilde{N}(0). \\ \hat{k}' &= \text{arg } \min_{k' \in \tilde{\mathcal{F}}_m^{(u')}} \left\{ \tilde{\alpha}_{\hat{k},k'} \right\} \text{ if user } \hat{k} \text{ is related to } \Theta_m^{(u,u')}, \text{ or } \hat{k}' = \text{arg } \min_{k' \in \tilde{\mathcal{F}}_m^{(u')}} \left\{ \tilde{\alpha}_{k',\hat{k}} \right\} \\ \text{if user } \hat{k} \text{ is related to } \Theta_m^{(u',u)}. \end{split}$$

Step 3 Update:

Update
$$\Theta_m^{(0,1)}$$
 and/or $\Theta_m^{(0,2)}$ and/or $\Theta_m^{(1,2)}$ by (6.15); Set $\tilde{\mathcal{F}}_m^{(u)} \leftarrow \tilde{\mathcal{F}}_m^{(u)} - \{\hat{k}\}, \ \tilde{\mathcal{F}}_m^{(u')} \leftarrow \tilde{\mathcal{F}}_m^{(u')} - \{\hat{k}'\}; \text{Set } \tilde{\mathcal{N}} \leftarrow \tilde{\mathcal{N}} - n.$

Step 4 Repeat Steps 1-3 until $\tilde{\mathcal{N}}=\emptyset$.

6.6 Characteristics of Code-Allocation

When operated in the multicell downlink MC DS-CDMA systems, our code-allocation algorithms employ a range of characteristics and advantages.

First, both the SSIA and the ESIA code-allocation algorithms aim to minimize the maximum InterCI factor, i.e., $\min\left\{\max_{k\in\mathcal{K}^{(u)},k'\in\mathcal{K}^{(u')}}\tilde{\alpha}_{k,k'}\right\}$, in order to reduce the InterCI to the value as small as possible, so as to improve the SINR in (6.6) of the multicell MC DS-CDMA system. As shown in Section 6.3, our code-allocations are operated based on the results of subcarrier-allocation. For each of the subcarriers, both of the proposed code-allocation algorithms deal with 3N users, which may be significantly smaller than the total 3MN users, if the system employs a relatively big number of subcarriers. Hence, the SSIA and ESIA code-allocation algorithms are guaranteed to have a low complexity for implementation. From the above, we know that the complexity is mainly dependent on the length N of the DS spreading codes.

Second, the SSIA algorithm can be operated with a lower complexity than the ESIA algorithm. As shown in Section 6.4, when the SSIA algorithm is employed, code-allocation is carried out first for the users in two adjacent cells. Then, it allocates the codes to the users in the other cell. This design ensures that the SSIA algorithm can be easily extended to the multicell systems with more than three cells.

Third, during an allocation iteration, the SSIA algorithm selects the users for code-allocation based only on one of the three InterCI factor matrices. By contrast, during an iteration, the ESIA algorithm allocates the users a code by simultaneously considering all the three InterCI factor matrices. Therefore, the ESIA algorithm can exploit a higher diversity for code-allocation than the SSIA algorithm. Consequently, in comparison with the SSIA algorithm, the ESIA algorithm may achieve a higher SINR for the users, and, hence has better BER performance or higher spectrum-efficiency.

Furthermore, in the ESIA algorithm, the IS method is proposed to identify which users should be first allocated a code. From (6.19) and (6.20), we can know that the performance of the IS method is affected by the number of bins, i.e., $N_b + 2$. In Fig. 6.3, we show the impact of N_b on the BER performance of the multicell MC DS-CDMA systems employing the ESIA-assisted

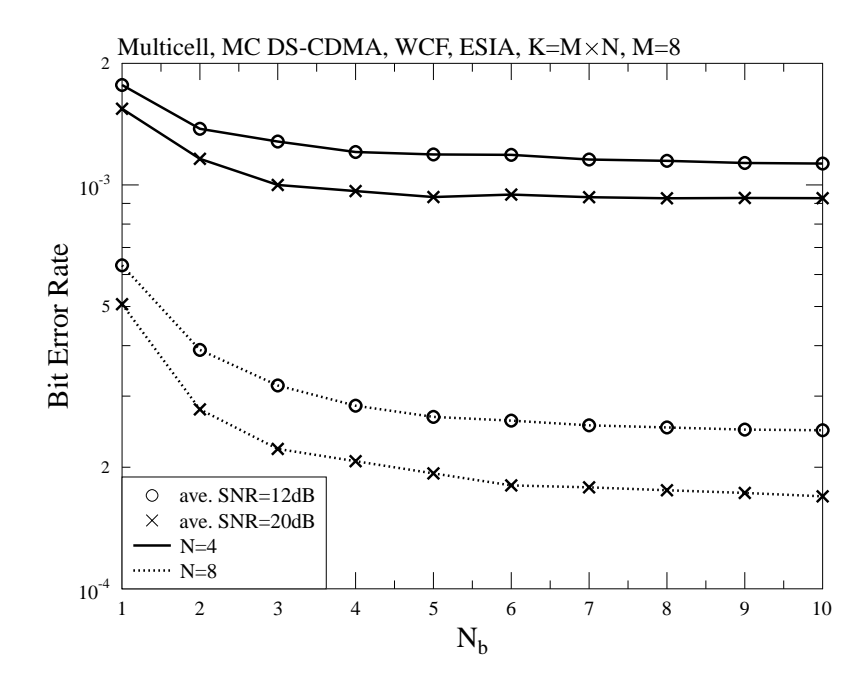


Figure 6.3: BER comparison, when the ESIA algorithm is applied with different number of bins, i.e., different values of N_b , for the IS method.

code-allocation. Note that, the number of bins for the IS is $N_b + 2$. From Fig. 6.3, we observe that, in general, the BER performance first improves and, then, converges to a constant value, as the number of bins used by the ESIA increases. When the number of DS spreading codes per subcarrier is increased from N = 4 to N = 8, more bins are required by the IS approach to achieve the minimum BER. However, in general and in practice when we consider the implementation complexity, we may choose $N_b + 2 = 5 - 6$ bins for the IS. Additionally, as seen in this figure and Fig. 6.3, the number of DS spreading codes per subcarrier has a big impact on the achievable BER performance of the multicell MC DS-CDMA system. Using more DS spreading codes per subcarrier yields better BER performance, as the result of higher multiuser diversity available for InterCI mitigation.

6.7 Performance Results

In this section, we provide a range of simulation results, in order to demonstrate and compare the achievable error rate performance and spectrum-efficiency performance of the multicell downlink MC DS-CDMA systems employing various subcarrier-allocation in Chapter 4 and the code-allocation algorithms proposed in this chapter. In all the simulations for error rate performance, we assume that quadrature phase-shift keying (QPSK) is employed for baseband modulation. For both error rate and spectrum-efficiency, we assume that all subcarriers experience independent flat Rayleigh fading. Furthermore, we assume that, in each of the three cells, the number of users supported by the MC DS-CDMA is $K = M \times N$, with M being the number of subcarriers and N

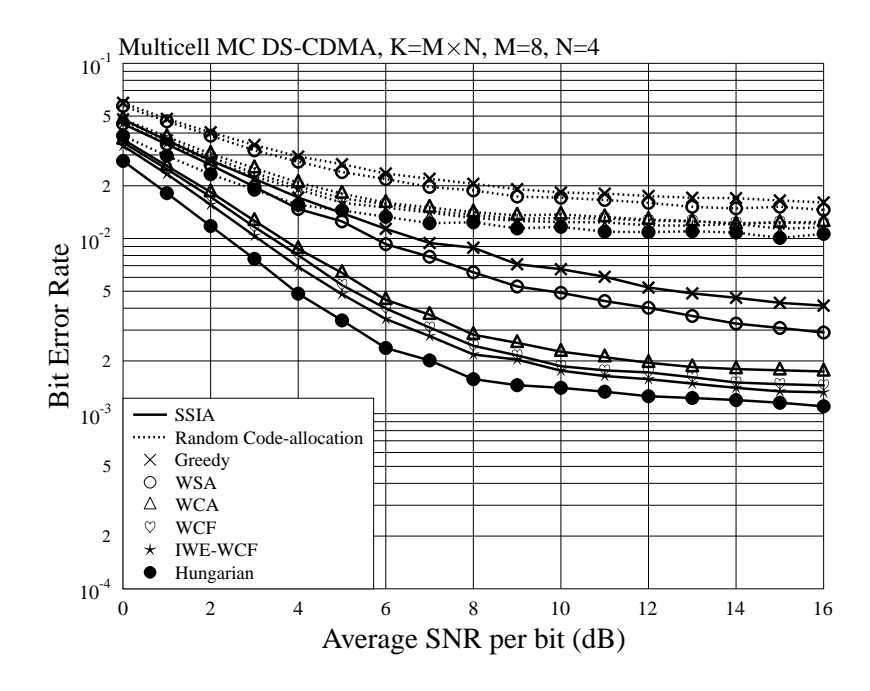


Figure 6.4: BER performance of the multicell downlink MC DS-CDMA systems employing various of subcarrier-allocation algorithms and the SSIA code-allocation algorithm.

being the length of the orthogonal DS spreading codes. Signals received at all users are assumed to experience the AWGN with the same noise variance. For modelling of large-scale fading, we assume that the pathloss exponent is $\mu = 4.0$, while the standard deviation for the shadowing effect is $Y = 8\,$ dB. Additionally, When the ESIA algorithm is employed, we assume that the number of bins for the IS method is $N_b + 2 = 6$.

Figure 6.4 demonstrates the BER performance of the multicell downlink MC DS-CDMA systems employing various subcarrier-allocation algorithms and the SSIA code-allocation algorithm. In the figure, the subcarrier-allocation algorithms considered are the WCA, WCF and the IWE-WCF algorithms, which were proposed in [208] and Chapter 4. The solid curves in Figure 6.4 give the BER performance of the multicell MC DS-CDMA systems employing the SSIA codeallocation algorithm, while the dashed curves are that, when the multicell MC DS-CDMA employs the random code-allocation algorithm. Here, the random code-allocation means that codes are randomly assigned to the users after subcarrier-allocation, which we sometimes refer to as "non code-allocation". From the results shown in the figure, we observe that the proposed SSIA algorithm is capable of achieving significant SNR gains over the random code-allocation, when considering different subcarrier-allocation algorithms. As shown in Figure 6.4, regardless of the code-allocation algorithms employed, the best BER performance is always achieved, when the multicell MC DS-CDMA systems use the Hungarian subcarrier-allocation algorithm, while the worst BER performance given by the systems employing the Greedy algorithm. When the random code-allocation algorithm is employed, the BER results of the multicell MC DS-CDMA systems employing different subcarrier-allocation algorithms are close to each other. This is because, in

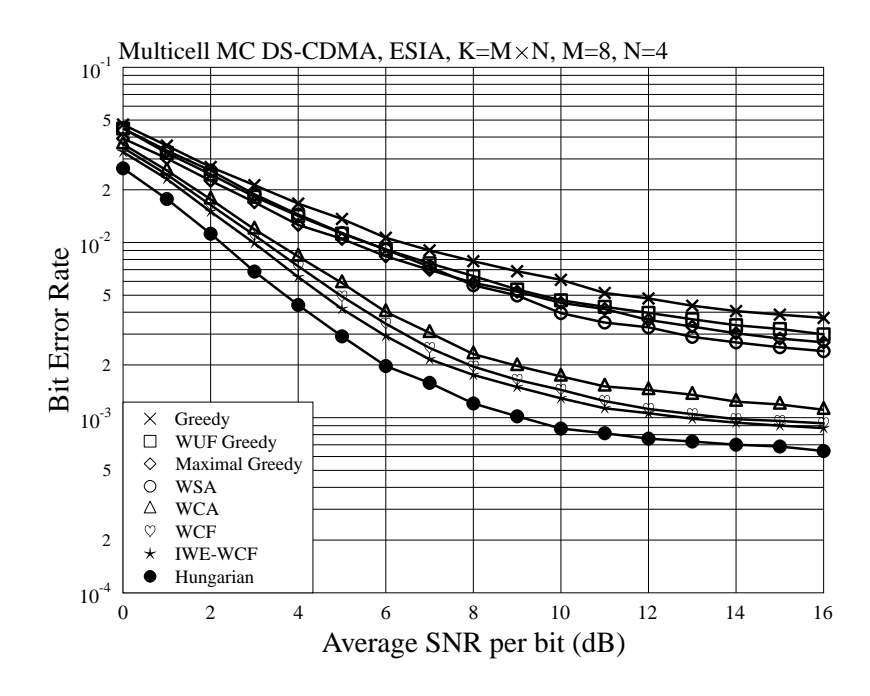


Figure 6.5: BER performance of the multicell downlink MC DS-CDMA systems employing various subcarrier-allocation algorithms and the ESIA code-allocation algorithm.

these cases, the BER performance difference between any two subcarrier-allocation algorithms is overwhelmed by strong InterCI, as the result of no code-allocation. By contrast, when the SSIA code-allocation algorithm is used, the subcarrier-allocation algorithms proposed in Chapter 4, including the WCA, WCF and the IWE-WCF algorithms, significantly outperform the other two sub-optimum subcarrier-allocation algorithms, namely, the greedy and WSA algorithms, owing to the InterCI mitigation capability of the SSIA algorithm. The performance difference between any two subcarrier-allocation algorithms considered agrees with that observed in Chapter 4.

Figure 6.5 shows the BER performance of the downlink multicell MC DS-CDMA systems employing various subcarrier-allocation algorithms and the ESIA code-allocation algorithm. The results can provide us some important observations. First, in comparison with the BER of the system using the random code-allocation algorithm, which is shown in Figures 6.4, the BER performance achieved by using either the ESIA or the SSIA code-allocation is clearly improved. Second, by comparing Figures 6.5 with Figure 6.4, we can find that the ESIA algorithm outperforms the SSIA algorithm, in terms of the BER performance. Furthermore, when the WSA subcarrier-allocation algorithm is employed, the ESIA algorithm slightly outperforms the SSIA algorithm. By contrast, when the three subcarrier-allocation algorithms, including the WCA, the WCF and the IWE-WCF algorithms proposed in Chapter 4, are employed, the ESIA algorithm significantly outperforms the SSIA algorithm, typically the SNR gain is about 2-4 dB. This observation implies that, in the multicell MC DS-CDMA systems, both subcarrier-allocation and code-allocation have a strong impact on the achievable BER performance.

199

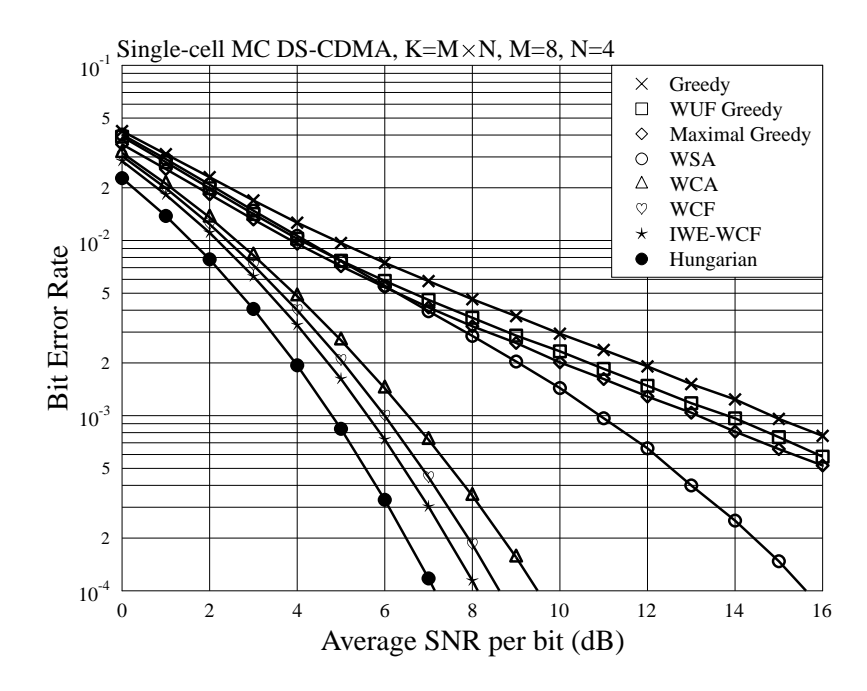


Figure 6.6: BER performance of the downlink single-cell MC DS-CDMA systems employing various subcarrier-allocation algorithms.

For the sake of comparison, Figure 6.6 gives the BER versus SNR performance of the downlink single-cell MC DS-CDMA systems employing various subcarrier-allocation algorithms, which can be viewed and thought of as the lower bounds of BER of the multicell scenarios in Figures 6.4 and 6.5. By comparing Figure 6.6 with Figures 6.4 and 6.5, we can see that the relationship between the BER of two subcarrier-allocation algorithms is the same. However, the BER performance of the multicell downlink MC DS-CDMA systems shown in Figures 6.4 and 6.5 is worse than the corresponding ones of the single-cell systems. Furthermore, in the multicell MC DS-CDMA systems, error floors appear in the high SNR region. This is because, although the proposed code-allocation algorithm is capable of reducing the InterCI, they are unable to fully remove the InterCI. This residual InterCI yields the observed error floors. Additionally, when comparing Figure 6.5 with Figure 6.4, we can see that the BER floors generated by the ESIA algorithm is lower than the corresponding ones given by the SSIA algorithm.

In Figure 6.7, we compare the BER performance of the ESIA and SSIA algorithms, when the multicell MC DS-CDMA systems employ the WCF subcarrier-allocation algorithm. First, when either the ESIA or the SSIA algorithm is employed, the BER performance of the multicell MC DS-CDMA systems becomes better as the number of subcarriers M increases, or as the DS spreading factor N increases. This is because the diversity order increases, as M and/or N increases. Second, for all the cases considered, the ESIA algorithm outperforms the SSIA algorithm, and the BER performance gap becomes larger, as the result that the ESIA algorithm exploits higher diversity from three cells than the SSIA algorithm, which only makes use of the diversity from two cells. Furthermore, it is worthy of noting that a better BER performance is achieved in the case of M=8

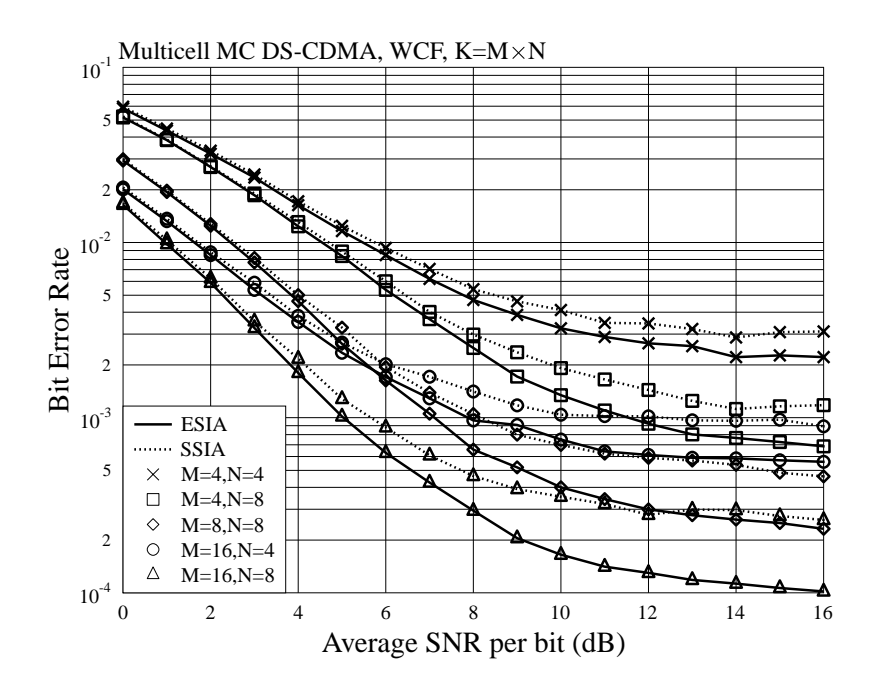


Figure 6.7: Comparison of BER performance of the multicell downlink MC DS-CDMA systems employing the ESIA and SSIA code-allocation algorithms, and the WCF subcarrier-allocation algorithm.

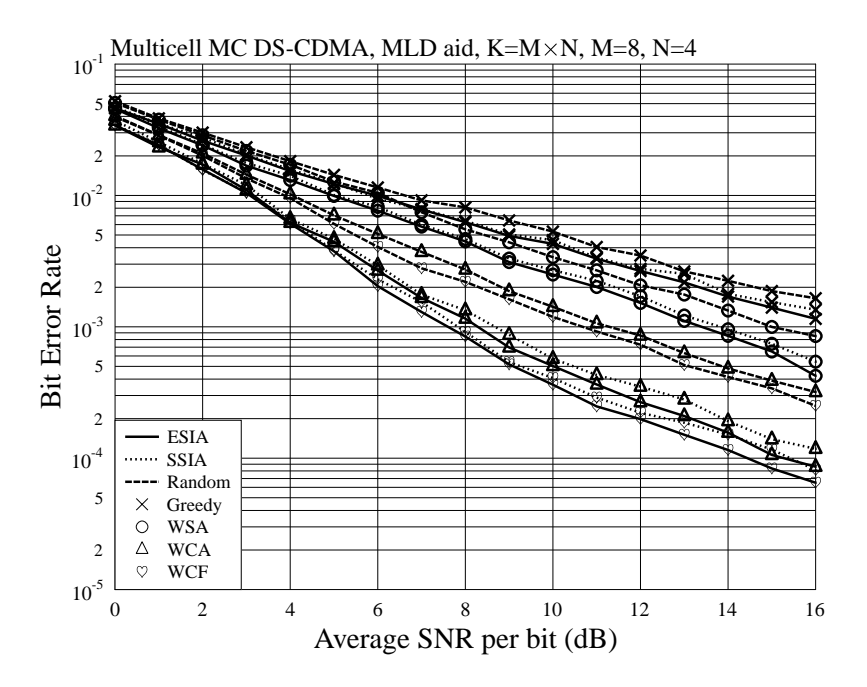


Figure 6.8: BER performance of the multicell downlink MC DS-CDMA systems employing various subcarrier- and code-allocation algorithms.

and N=8 than the case of M=16 and N=4. This observation implies that, the InterCI imposes a big impact on the error performance of the multicell MC DS-CDMA systems and, when N is larger, code-allocation is capable of making more contribution to suppress the InterCI.

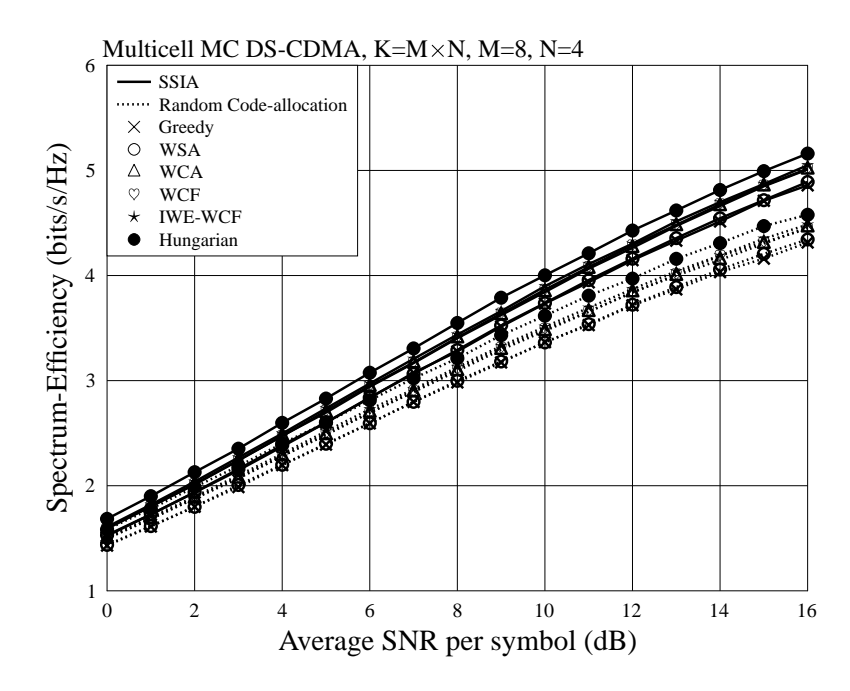


Figure 6.9: Spectrum-efficiency performance of the multicell downlink MC DS-CDMA systems employing the SSIA or random code-allocation, and various subcarrier-allocation algorithms.

In the considered multicell downlink MC DS-CDMA systems, a user receives the InterCI only from two users, which are allocated the same subcarrier and the same spreading code as the considered user, as shown in (6.6). In order to further mitigate the InterCI, a mobile user may employ the advanced detectors, such as the maximum likelihood detector (MLD). Explicitly, doing this does not impose much added complexity on the receiver, as there are just three users to consider, when we only consider three cells. Therefore, in Figure 6.8 we show the BER performance of the multicell downlink MC DS-CDMA systems employing various subcarrier- and code-allocation algorithms, where the MLD is used. Explicitly, the MLD efficiently suppresses the InterCI, and, as shown in the figure, there are no error floors anymore. However, we still see that the SSIA and ESIA code-allocation algorithms outperform the random code-allocation, with a typical gain of about 2-4 dB. In comparison with the results shown in Figures 6.4 and 6.5, all the corresponding BER performance shown in Figure 6.8 becomes better. However, the BER performance gap between the ESIA and the SSIA algorithms becomes smaller, owing to the contribution made by the MLD. In addition to employing MLD at the users side, the error floors in Figures 6.4, 6.5 and 6.7 may be reduced by using a class of good spreading codes for downlink transmission.

In Figures 6.9 and 6.10, we study the spectrum-efficiency performance of the multicell down-link MC DS-CDMA systems employing the proposed code-allocation algorithms, and various subcarrier-allocation algorithms. The results show that the ESIA and the SSIA code-allocation algorithms are capable of achieving better spectrum-efficiency performance than the random code-allocation. However, when comparing Figure 6.9 with Figure 6.10, the ESIA algorithm only has

6.8. Conclusions 202

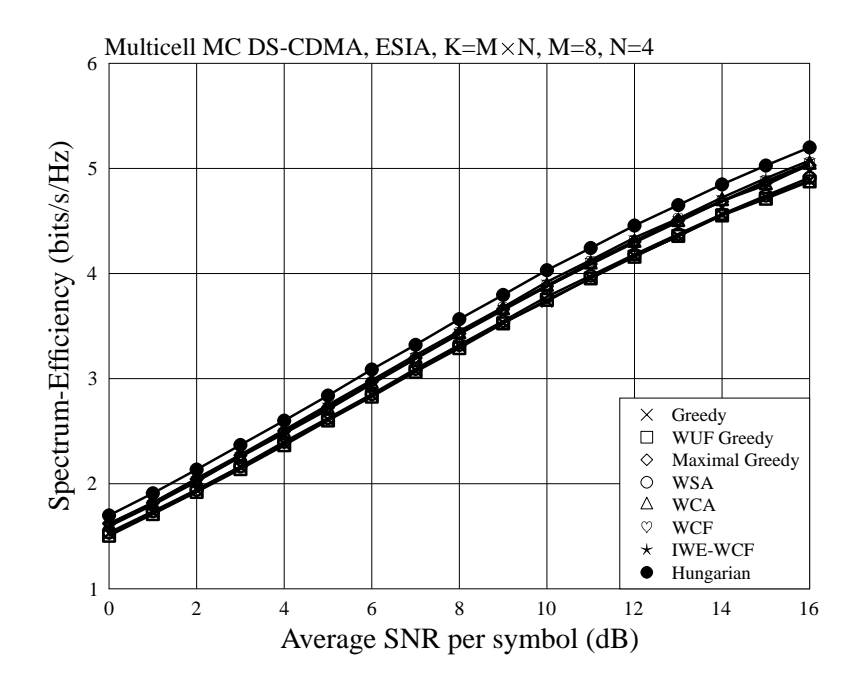


Figure 6.10: Spectrum-efficiency performance of the multicell downlink MC DS-CDMA systems employing the ELSA code-allocation, and various subcarrier-allocation algorithms.

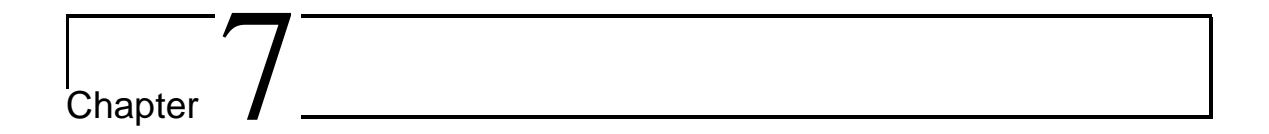
a very small spectrum-efficiency gain over the SSIA algorithm. Considering both the error rate and spectrum-efficiency, we can conclude that our proposed code-allocation algorithms cannot only achieve better BER performance, but also yield higher spectrum-efficiency. Furthermore, Figures 6.9 and 6.10 once again demonstrate that the three proposed subcarrier-allocation algorithms outperform the other considered sub-optimum subcarrier-allocation algorithms in terms of the spectrum-efficiency.

6.8 Conclusions

In this chapter, we have studied the resource allocation in the multicell downlink MC DS-CDMA systems. Motivating to minimize the complexity for resource allocation in the multicell downlink MC DS-CDMA systems, we have proposed a novel resource allocation scheme. In this resource allocation scheme, each BS first independently carries out the subcarrier-allocation, based on a subcarrier-allocation algorithm considered in Chapter 4. Then, spreading codes are jointly allocated on the basis of the subcarrier-allocation. In this chapter, we have proposed two low-complexity and high-efficiency code-allocation algorithms, namely, the SSIA and the ESIA algorithms, respectively, by making use of only the information about large-scale fading, i.e., propagation pathloss shadowing effect. To be more specific, both code-allocation algorithms are motivated to minimize the maximum InterCI factor of the users sharing the same subcarrier and the same spreading code, when assuming that only the InterCI factors are shared among the BSs. Specifically, the ESIA al-

6.8. Conclusions 203

gorithm operates the code-allocation for each of the users based on the full knowledge of the three InterCI factor matrices. By contrast, the SSIA algorithm allocates each of the users a code by considering only one InterCI factor matrix. Therefore, the SSIA algorithm enjoys a lower complexity than the ESIA algorithm. However, the ESIA algorithm can exploit a higher diversity for code-allocation than the SSIA algorithm. Therefore, the ESIA algorithm is capable of achieving a better error performance than the SSIA algorithm, although its spectrum-efficiency performance is only slightly higher than that of the SSIA algorithm. Furthermore, our BER and spectrum-efficiency performance results show that the proposed subcarrier-allocation algorithms proposed in Chapter 4 outperform all the other existing sub-optimum algorithms, when they are operated in the multicell MC DS-CDMA systems, in general, and, they retain all the characteristics as shown in the context of the single-cell MC DS-CDMA systems. Additionally, our studies show that both the SSIA and the ESIA code-allocation algorithms significantly outperform the random code-allocation algorithm. Therefore, considering the multicell communication environments, if the number of users per cell is relatively high, and if the backhaul resources are limited, our proposed code-allocation algorithms can be very promising candidates, which are efficient for practical implementation.



Conclusions and Future Work

In this chapter, a summary of the thesis and main conclusions are first provided in Section 7.1. Then, some recommendations for future research are provided and discussed in Section 7.2.

7.1 Summary and Conclusions

In this thesis, we have investigated the cooperation and resource allocation issues in relay and multicarrier communication systems. In detail, we have proposed a novel relay aided cooperative system, namely the THCL system, and analyzed its error performance, when the system employs various relay processing schemes. In contrast to the most existing references on relay communications, which typically assume that relay cooperation does not consume energy, in our studies, we have put the emphasis on analyzing the cost of carrying out the cooperation among the relays by studying the effect of the power-allocation to the different hops on the achievable performance of the THCL system. In the context of the resource allocation in multicarrier communications, we have first considered the single-cell downlink OFDMA and MC DS-CDMA systems, and designed and investigated various power- and subcarrier-allocation algorithms. A range of sub-optimum subcarrier-allocation algorithms have been designed, with the objectives to attain the near-optimum performance, but not to make a performance trade-off between reliability and spectrum-efficiency. Then, we have designed and studied the high-efficiency low-complexity resource allocation algorithms for the multicell downlink OFDMA and MC DS-CDMA systems. Typically, in our considered multicell systems, subcarriers are allocated in a distributed way, while InterCI is mitigated with our proposed approaches. Specifically, two high-efficiency low backhaul cost InterCI mitigation algorithms have been proposed for the multicell OFDMA systems, and two novel low-complexity code-allocation algorithms have been designed for the multicell MC DS-CDMA systems.

In more detail, the studies and contributions of the thesis can be summarized as follows, chapter by chapter.

In Chapter 2, we have introduced and studied a so-called THCL system, which aims to accomplish a communication between a source node and a destination node with the aid of a cluster of relays. Using this two-hop relay link, we motivate to demonstrate the cost for relay cooperation and the challenges for error performance analysis of this type of systems. As shown in Chapter 2, we have studied three main RP schemes as detailed in Section 2.3, which include the distributed RP, ideal cooperative RP and the cooperative RP. When the distributed RP is employed, the relays simply forward their received signals to the destination. In the context of the ideal cooperative RP, we assume that information exchange among relays can be accomplished without energy consumption, which is also a typical assumption used in many existing reference, e.g., [46–49]. For the sake of investigating the cost of cooperation among relays, we have studied a more practical cooperative RP scheme, i.e., the cooperative RP, which assumes energy consumption for information exchange among relays. In the cooperative RP, information exchange among relays is implemented with the aid of MA and BC transmissions by invoking an IECU. In Section 2.4, we have provided the analyses for the BER of the THCL systems employing various RP schemes over Nakagmi-m fading channels, when BPSK baseband modulation is assumed. A range of closed-form BER expressions have been obtained for the systems employing the ideal cooperative RP schemes. Two novel approximation approaches, namely, the Nakagami-TAp and the Nakagami-SAp, have been proposed for obtaining the PDF of the sum of Nakagami-m variables. With the aid of these two approaches, we have obtained the approximated average BER expressions of the THCL systems employing the TEGC-DRP and the CMVC-TEGC-RP, when the first and second hops are assumed to experience flat Nakagami-m fading, while the communications for information exchange among relays suffer from the flat Nakagami-m fading or only AWGN. Furthermore, when the CMRC scheme is used at the IECU, we have proposed the Gamma-Ap approach for finding the approximate PDF of the instantaneous SNR of the detection at the IECU, and derived the average BER of the THCL systems employing the CMRC-TEGC-RP scheme. From our studies in Chapter 2, we can have the following observations. When the distributed RP or the cooperative RP is employed, as shown in Section 2.5, the approximated average BER of the THCL systems has some small deviations from that obtained by simulations, when the fading of communication channels is severe, whereas, they agree with each other very well, as the channel conditions become better. As shown in Figures 2.16-2.19, we have studied the impact of power-allocation on the error performance of the THCL systems employing various RP schemes. Clearly, we have observed that, the cooperation among the relays for information exchange requires $30\% \sim 70\%$ of the total system transmission power, in order to achieve the best BER performance. Our performance results in Section 2.5 have shown that using the ideal cooperative RP assumption always overestimates the BER performance of the THCL system. In practice, the cooperative RP scheme may even achieve worse BER performance than the distributed RP, when the MA/BC links for information exchange experience flat Rayleigh fading. By considering both the BER performance and complexity, we may conclude that the TEGC-DRP constitutes a desirable and practical RP scheme, which demands the lowest complexity for implementation, but is capable of achieving the required BER performance, especially, when the number of relays is relatively high.

In Chapter 3, we have studied and investigated the resource allocation in the single-cell downlink OFDMA systems, where various subcarrier- and power-allocation algorithms are considered. As discussed in Section 3.3, our resource allocation aims to minimize the average BER of the downlink OFDMA systems without making the trade-off with the spectrum-efficiency (or throughput). We aim to design the subcarrier- and power-allocation algorithms that can be carried out separately with low-complexity but without loss of much performance [83, 84]. In this chapter, we have designed two low-complexity subcarrier-allocation algorithms for downlink OFDMA systems, namely, the BWSA and BSS algorithms, which, respectively, motivate to avoid assigning users the worst subchannels as many as possible, or to assign users the best possible subchannels. As detailed in Section 3.6, the BWSA algorithm represents a two-dimensional extension of the existing one-dimensional WSA algorithm. The BWSA algorithm can avoid the worst subchannels and allocate the best subcarriers in both subcarrier-oriented mode and user-oriented mode. In contrast to the BWSA algorithm considering the subcarrier-allocation starting from the worst subchannels, the BSS algorithm starts its operations from the best subchannels. Specifically, the BSS algorithm is operated in two stages: 1) a search stage to find the best possible candidate subchannels, and 2) an allocation stage to assign users the subchannels chosen from the candidate subchannels. Our studies illustrate that the search stage can usually be completed within a relatively small number of iterations, especially, when large OFDMA systems supporting a big number of users are considered. This property guarantees the BSS to have low-complexity. We have analyzed the upperand lower-bound of error rate for the subcarrier-allocation in the downlink OFDMA systems in Section 3.9, when assuming square QAM baseband modulation. Furthermore, we have summarized and compared the complexity of the proposed BWSA and BSS algorithms and some other subcarrier-allocation algorithms in Table 3.3. Our simulation results have shown that, as the communication channels become more frequency-selective, the BSS algorithm's performance becomes closer to that of the optimum Hungarian algorithm. As the number of users involved increases, the achievable BER and spectrum-efficiency performance move close to that achieved by the Hungarian algorithm. However, the BSS algorithm may be outperformed by the BWSA or WSA algorithm, when the OFDMA systems are very small, such as, of using M=4 subcarriers to support K=4users, which are usually not the cases in practice. In practice, the OFDMA systems are usually large, using e.g., 64 - 2048 subcarriers, in the LTE/LTE-A OFDMA systems. By contrast, the BWSA algorithm is efficient, regardless of the size of the OFDMA systems. In Figure 3.15, the PDFs of the spectrum-efficiency show that our proposed BWSA and BSS algorithms are capable of providing users fairer data rates than the other sub-optimum algorithms, in addition to providing the relatively higher throughput.

In Chapter 4, we have investigated the resource allocation, including both power- and subcarrierallocation, in the single-cell downlink MC DS-CDMA systems. Similar to Chapter 3, the resource allocation in the MC DS-CDMA system aims to maximize the system reliability without mak-

ing the trade-off with the spectrum-efficiency. We also seek the low-complexity schemes, and, hence, the power- and subcarrier-allocation have been assumed to be operated separately. In this chapter, a range of subcarrier-allocation algorithms have been proposed, which include the parallel Hungarian algorithm, WCA, WCF and the IWE algorithms. Specifically, in comparison with the optimum Hungarian algorithm, the parallel Hungarian algorithm is capable of reducing the complexity from $\mathcal{O}(M^3N^3)$ to $\mathcal{O}(NM^3)$, by processing N number of $(M \times M)$ cost matrices in the principles of the Hungarian algorithm, instead of operating on a $(MN \times MN)$ matrix. Besides the parallel Hungarian algorithm, all the other sub-optimum subcarrier-allocation algorithms proposed in Section 4.4 motivate to avoid assigning users the worst subchannels as many as possible. We have generalized the WSA algorithm to the WCA algorithm, which is suitable for operation in any multicarrier systems and is capable of achieving better BER performance and higher spectrumefficiency than the WSA algorithm. We have proposed the WCF algorithm, which can be operated more efficiently and reliably than the WCA algorithm, while retains all the advantages of the WCA algorithm. Finally, in Section 4.5, we have proposed a low-complexity iterative algorithm, namely the IWE algorithm, for further improving the performance of the WSA, WCA and the WCF algorithms, resulting in the IWE-WSA, IWE-WCA and the IWE-WCF algorithms, respectively. In this chapter, we have also analyzed and compared the complexity of the proposed subcarrier-allocation algorithms and some existing subcarrier-allocation algorithms considered, which are summarized in Table 4.3. The results show that all our proposed subcarrier-allocation algorithms have the merit of low-complexity. Our simulation results have shown that the proposed subcarrier-allocation algorithms are capable of attaining better BER and spectrum-efficiency performance than the other existing sub-optimum algorithms considered. They do not make a trade-off between the achievable BER and the spectrum-efficiency of the downlink MC DS-CDMA systems. Furthermore, invoking an IWE-assisted algorithm always improves the reliability and spectrum-efficiency of the original subcarrier-allocation algorithm. Additionally, our results have also demonstrated that the reliability attained by the IWE-WCF algorithm is close to that achieved by the high-complexity optimum Hungarian algorithm.

In Chapter 5, we have studied the subcarrier-allocation in multicell downlink OFDMA systems, which aims to maximize the spectrum-efficiency of the system, while does not make a trade-off with the reliability. Our subcarrier-allocation procedure is described in Figure 5.2, showing that the BSs first independently carry out the subcarrier-allocation and, then, InterCI mitigation is attempted with the aid of minimum BS cooperation, in order to guarantee that all users attain the required communication quality. In this chapter, the subcarrier-allocation algorithms are assumed the same as those in previous chapters. By contrast, we have proposed two efficient InterCI mitigation algorithms, namely the DDMC and the CDMC algorithms, in order to maximize the spectrum-efficiency of the cell-edge users whose SIRs are lower than the SIR threshold η_t , which is determined by the required quality of communication. Our DDMC algorithm is a distributed decision-making algorithm, in which the BSs individually make their InterCI mitigation decisions. After the decisions, a

BS may ask help from another BS to set up a STBC-aided cooperative transmission to a user with poor SIR. This is in contrast to the existing OOP algorithm, which simply turns off the transmission to a user with poor SIR. By introducing this light BS cooperation, our studies show that the proposed DDMC algorithm outperforms the OOP algorithm. With the motivation to maximize the pay-off from the cooperation while simultaneously at the minimum cost caused, in this chapter, we have proposed the CDMC algorithm, which makes the InterCI mitigation decisions in a centralized approach via sharing limited InterCI information among the BSs. As our studies show, the CDMC algorithm cannot only attempt to maximize the spectrum-efficiency of the system, but also improve the frequency reuse factor of the subcarriers. Specifically, the CDMC algorithm makes the decisions for the users sharing a subcarrier based on a (3×3) dimensional matrix with its elements taking only three values determined by the corresponding InterCI. From this we can know that, in our CDMC algorithm, BSs only share very limited information for decision making. The principles of the CDMC algorithm have been detailed associated with the three cases in Figures 5.3-5.5. Specifically, in Case 1, the CDMC algorithm sets up a cooperation for a user with poor SIR; In Case 2, it may establish a cooperation for a poor user; Finally, in Case 3, the CDMC algorithm simply switches off the transmission to one or more users with poor SIRs, in order to benefit system's overall performance. In Section 5.7, we have shown that both the proposed DDMC and CDMC algorithms achieve higher spectrum-efficiency than the OOP algorithm, and than the case without employing any InterCI mitigation. In comparison with the DDMC algorithm, the CDMC algorithm can always find a better joint InterCI mitigation strategy, which results in better performance than that attained by the DDMC algorithm. Furthermore, the spectrum-efficiency performance gain of the CDMC over the DDMC becomes bigger, as the SIR threshold η_t increases. Moreover, we have shown that the CDMC algorithm always attains the highest frequency reuse factor, while the DDMC algorithm can obtain a higher frequency reuse factor than the OOP algorithm.

Finally, in Chapter 6, we have extended the resource allocation problems studied in Chapter 4 in the context of the single-cell downlink MC DS-CDMA systems to the multicell scenarios. Again, our motivation is to minimize the average BER of the multicell downlink MC DS-CDMA system, while remembering to make the cost for resource allocation and BS cooperation as low as possible. Specifically, in this chapter, we have proposed a novel resource allocation scheme, in which each BS first independently carries out the subcarrier-allocation. Then, the DS spreading codes are jointly allocated on the basis of the subcarrier-allocation with the aid of information exchange among the BSs. We have proposed two low-complexity and high-efficiency code-allocation algorithms, namely the SSIA and the ESIA algorithms, by making use of only the information about the large-scale fading, i.e., propagation pathloss and shadowing effect, experienced by the users. The principles of the SSIA and ESIA algorithms have been detailed in Sections 6.4 and 6.5, respectively. To be more specific, both the SSIA and the ESIA algorithms are motivated to minimize the maximum InterCI factor of the users sharing the same subcarrier and the same spreading code, when assuming that only the InterCI factors, which are determined by the large-scale fading, are shared

among the BSs. Specifically, the SSIA algorithm allocates each of the users a code by considering only one InterCI factor matrix at a time, while the ESIA algorithm allocates a code to three users in three cells by simultaneously considering three InterCI factor matrices. Hence, the ESIA algorithm achieves better performance than the SSIA algorithm, but has the cost of slightly increased complexity. According to our simulation results shown in Section 6.7, both the SSIA and the ESIA code-allocation algorithms significantly outperform the random code-allocation algorithm in terms of both the error rate and the spectrum-efficiency performance. The ESIA algorithm is capable of achieving a better error performance than the SSIA algorithm, although its spectrum-efficiency performance is only slightly higher than that of the SSIA algorithm. Furthermore, our BER and spectrum-efficiency performance results show that the proposed subcarrier-allocation algorithms proposed in Chapter 4 also outperform all the other existing sub-optimum algorithms, when they are operated in the multicell MC DS-CDMA systems. In general, when operated in the multicell scenarios, our proposed subcarrier-allocation algorithms retain all the characteristics observed in the context of the single-cell MC DS-CDMA systems.

7.2 Recommendations for Future Research

In this thesis, we have mainly focused our attention on the resource allocation and cooperation, as well as on the various multicarrier communication systems. In this section, we provide some suggestions for potential future research.

- In this thesis, we have studied and analyzed the error performance of the relay aided cooperative system, i.e., the THCL, which only considers the two-hop transmission. We may extend our THCL system to the multihop scenarios, where a source node transmits to a destination node via several hops with the aid of multiple relays. During a hop, the information-carrying signal is forwarded by a portion of the relays, and information exchange among these relays can be carried out in the principles of multiway relay. In this multihop relay aided cooperative system, energy consumption by the cooperation among relays may be investigated via error performance or spectrum-efficiency. Studying this type of multihop transmission systems may give us the observation whether the cooperation among relays is desirable.
- Joint resource allocation in the multicell multicarrier systems constitutes one of the important future research areas. In this thesis, the resource allocation algorithms proposed in multicell systems are carried out in a separate way, due to our motivation of low-complexity implementation. When increased complexity is available, we may design the joint resource allocation algorithms, and simultaneously consider the power- and subcarrier-allocation, as well as InterCI mitigation.
- In Chapter 6, we have proposed the code-allocation algorithms in the multicell MC DS-CDMA systems, when assuming that all the subcarriers and spreading codes have to be allo-

cated to the users in each of the cells. In our future work, we may design the code-allocation algorithms by assuming that not all the subcarriers and spreading codes have to be allocated to the users in one cell, which is actually a practical assumption. In this case, some users may not be assigned subcarriers and/or codes and, hence, these users do not transmit, forming the OOP scheme studied in Chapter 5. Furthermore, for the sake of mitigating InterCI, as the InterCI mitigation algorithms suggested in Chapter 5, our code-allocation algorithms may be jointly designed with the InterCI mitigation algorithms, so that cooperative transmissions can be set up for the users suffering from strong InterCI.

- In this thesis, when we consider the multicell systems, only three-cell scenarios have been considered. In our future research, we may extend our resource allocation to the scenarios that more than three cells are considered. In this case, our resource allocation algorithms can still be motivated to maximize the system throughput as well as minimize the complexity. Certainly, it is more promising for us to design the high-efficiency distributed resource allocation algorithms, which do not require to share the InterCI information among BSs. In addition, the DDMC and CDMC algorithms proposed in Chapter 5 may be revised and extended to the multicell scenarios having more than three cells.
- Our algorithms proposed in this thesis may be extended for both the user association and resource allocation in downlink multi-tier heterogeneous wireless networks (HetNets), which have emerged as a competitive technology to achieve high-rate, high-quality and diverse communication demands in the future fifth generation (5G) wireless cellular networks. Aiming at obtaining the best trade-off between energy- and spectrum-efficiency, we may first focus on the user association and, then, implementation the resource allocation on the basis of the derived user association. Furthermore, the joint design of user association and resource allocation is another very interesting research area.

As an interesting future research area, in the following part of this section, we provide some deeper discussion about the user association and resource allocation in the downlink HetNets, and explain how high-efficiency algorithms may be designed for the purposes.

In contrast to the resource allocation in the homogeneous cellular networks, as what considered in this thesis, resource allocation in HetNets is much more challenging, due to their infrastructure configurations. In literature, a range of centralized resource allocation schemes for downlink HetNets have been investigated [209–215]. To be a little more specific, the authors of [209] have studied the centralized resource allocation in the context of the HetNets without considering fairness among users, which first distributes the radio frequency resources and, then, allocates the power. By contrast, the authors in [210, 211] have investigated the centralized resource allocation in HetNets with considering the proportional fairness, and the resource allocation in [211] assumes InterCI-free. Furthermore, Lertwiram *et al.* [212] have studied the trade-off between resource allocation and interference alignment in a two-tier HetNet, when assuming that InterCI only exists

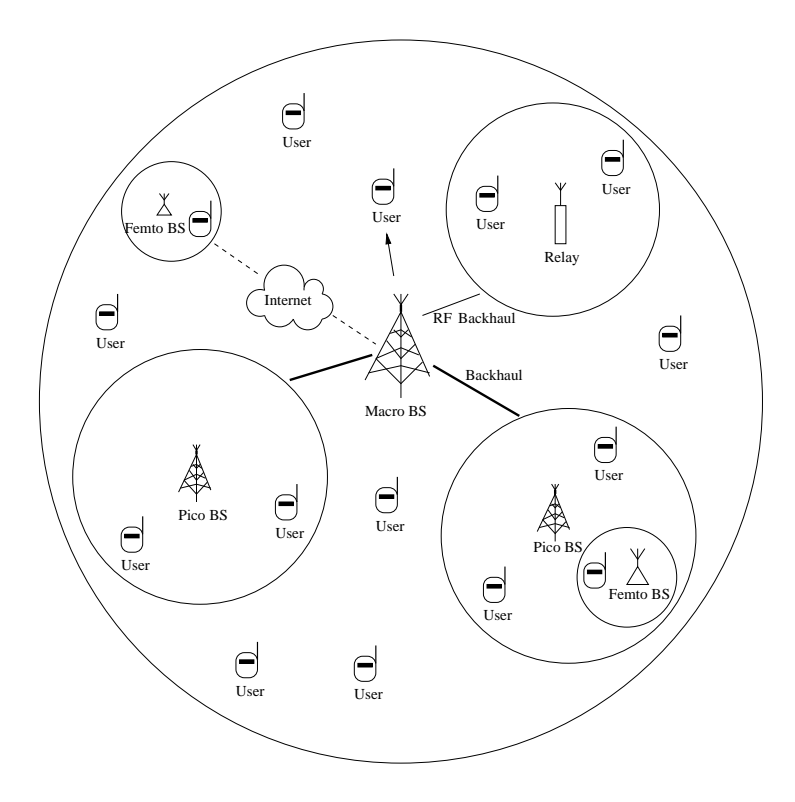


Figure 7.1: System model of a downlink three-tier HetNet, where the Macro cell is overlaid with relay, pico and femto cells.

between macro and femto BSs. To the best of our knowledge, in HetNets, all the references have focused on the resource allocation in the two-tier HetNets. Resource allocation in multi-tier (\geq 3 tiers) HetNets has rarely been studied. Due to the limits of complexity and backhaul resources, we can expect that distributed resource allocation algorithms will become more attractive in the future HetNets, as distributed algorithms have the characteristics of low-complexity, robustness, quick response to fast-varying wireless channels, etc. However, in HetNets, distributed resource allocation has not received sufficient emphasis and only a very few researches, such as [216, 217], can be found in this area.

Besides the resource allocation, in HetNets, user association is another important research aspect in HetNets. It can be shown that user association enjoys a lot of similarities with resource allocation, if we view BSs and other access points (APs) as a type of resources. In user association, the major challenge is that, maximizing the overall network throughput, while making a good trade-off between load balancing and InterCI. Furthermore, we also need to consider the fairness. So far, a range of references have investigated the user association in HetNets [215,218–221], with the objective to maximize the spectrum-efficiency without the constraint on quality-of-services. As suggested in [222, 223], it is highly desirable to design the energy-efficient user association algorithms, so as to make a compromise among received signal strength of mobile users, battery life of users and uplink interference levels, etc. Correspondingly, energy-efficient resource allocation has also been an important research branch, as shown by our overview in Chapter 1.

Against the research background in HetNets, one important future research area is the user association and distributed resource allocation in downlink multi-tier HetNets. Specifically, Figure 7.1 shows on a HetNet system consisting of one macro BS, multiple pico and femto BSs, and some relays acting as APs. In this HetNet, we may assume that pico BSs are connected with the macro BS via backhaul links, femto BSs connect with the core network via broadband (such as ADSL), while radio frequency (RF) backhaul links are assumed for the communication between the macro BS and the APs. With the objective to obtain the best possible trade-off between energy- and spectrum-efficiency, we may first focus on the user association and, then, implement the distributed resource allocation on the basis of the derived user association. Furthermore, high-efficiency joint user association and distributed resource allocation algorithm is another important research topic.

For example and more specifically, in contrast to the existing studies, according to our studies in this thesis, user association algorithms may be designed by considering both the downlink signal strength and the InterCI level, in association with diverse QoS requirements for different wireless links. As in the future HetNets, dense deployments of low-power BSs will be popular, low complexity and low energy consumption will be two critical factors for design of communication schemes. For this sake, user association decisions may be made mainly based on the CSI about the large-scale fading and on a small amount of CSI about the InterCI that can be obtained locally. Furthermore, while guaranteeing the required spectrum-efficiency, high energy-efficiency user association algorithms are highly desirable.

Following the study of user association, distributed resource allocation algorithms will be designed for the multi-tier HetNet. Following our studies, in order to reduce the complexity and enhance the robustness, resource allocation algorithms can be operated in a distributed way, so that each BS is capable of efficiently distributing the resources, including transmission time slots, radio frequency, power, etc., as well as performing precoding for signal transmission to its own users. When considering these issues, there is a major challenge from the InterCIs in the HetNet, which exists among the cells of the same tiers and also among the cells from different tiers. Hence, in the distributed resource allocation, each BS may allocate the resources either in a joint approach or in a separate way based on the limited CSI. The optimization objectives may include maximizing the utility of its own resources and minimizing the InterCI to the other cells. Moreover, after the distributed resource allocation, InterCI may be handled with the aid of high-efficiency InterCI mitigation schemes. For example, the algorithms proposed in Chapter 5, may be extended to to mitigate the InterCI in the HetNets. A BS may set up a cooperative transmission or stop transmission to the users suffering strong InterCI. Additionally, in the HetNets scenario, in addition to the OFDMA, we may consider the different multicarrier multiple access schemes for the downlink transmissions. For instance, the macro BS may employ the MC DS-CDMA scheme or pure DS-CDMA scheme, so as to avoid problems generated from synchronization, frequency offset, Doppler frequency-shift, etc. By contrast, OFDMA may be used for communication in small cells to provide high-rate. Furthermore, we may investigate the inter-impact between user association and resource allocation

with the aim to design the joint user association and distributed resource allocation algorithms, in order to further improve the spectrum- and energy-efficiency of the HetNets, but at the cost of complexity.

Bibliography

- [1] L. L. Yang, Multicarrier Communications. John Wiley, 2009.
- [2] E. C. V. der Meulen, "Three-terminal communication channels," *Advanced Applied Probability*, vol. 3, pp. 120 154, 1971.
- [3] T. M. Cover and A. A. E. Gamal, "Capacity theorems for the relay channel," *IEEE Transactions on Information Theory*, vol. 25, pp. 572 584, Sep. 1979.
- [4] J. N. Laneman and G. W. Wornell, "Distributed space-time-coded protocols for exploiting cooperative diversity in wireless networks," *IEEE Transactions on Information Theory*, vol. 49, pp. 2415 2425, Oct. 2003.
- [5] J. N. Laneman, D. N. C. Tse, and G. W. Wornell, "Cooperative diversity in wireless networks: Efficient protocols and outage behavior," *IEEE Transactions on Information Theory*, vol. 50, pp. 3062 3080, Dec. 2004.
- [6] A. Sendonaris, E. Erkip, and B. Aazhang, "User cooperation diversity. part I. system description," *IEEE Transactions on Communications*, vol. 51, pp. 1927 1938, Nov. 2003.
- [7] A. Sendonaris, E. Erkip, and B. Aazhang, "User cooperation diversity. part II. implementation aspects and performance analysis," *IEEE Transactions on Communications*, vol. 51, pp. 1939 1948, Nov. 2003.
- [8] K. Azarian, H. El-Gamal, and P. Schniter, "On the achievable diversity-multiplexing tradeoff in half-duplex cooperative channels," *IEEE Transactions on Information Theory*, vol. 51, pp. 4152 4172, Dec. 2005.
- [9] S. Wei, "Diversity-multiplexing tradeoff of asynchronous cooperative diversity in wireless networks," *IEEE Transactions on Information Theory*, vol. 53, pp. 4150 4172, Nov. 2007.
- [10] A. A. Haghighi and K. Navaie, "Outage analysis and diversity-multiplexing tradeoff bounds for opportunistic relaying coded cooperation and distributed space-time coding coded cooperation."

- eration," *IEEE Transactions on Wireless Communications*, vol. 9, pp. 1198 1206, March 2010.
- [11] A. Bletsas, A. Khisti, D. P. Reed, and A. Lippman, "A simple cooperative diversity method based on network path selection," *IEEE Journal on Selected Areas in Communications*, vol. 24, pp. 659 672, March 2006.
- [12] A. Bletsas, S. Hyundong, and M. Z. Win, "Cooperative communications with outage-optimal opportunistic relaying," *IEEE Transactions on Wireless Communications*, vol. 6, pp. 3450 3460, Sept. 2007.
- [13] D. S. Michalopoulos and G. K. Karagiannidis, "Performance analysis of single relay selection in Rayleigh fading," *IEEE Transactions on Wireless Communications*, vol. 7, pp. 3718 3724, Oct. 2008.
- [14] W. Su and X. Liu, "On optimum selection relaying protocols in cooperative wireless networks," *IEEE Transactions on Communications*, vol. 58, pp. 52 57, Jan. 2010.
- [15] B. Rankov and A. Wittneben, "Spectral efficient protocols for half-duplex fading relay channels," *IEEE Journal on Selected Areas in Communications*, vol. 25, pp. 379 389, Feb. 2007.
- [16] Y. Fan, C. Wang, J. Thompson, and H. V. Poor, "Recovering multiplexing loss through successive relaying using repetition coding," *IEEE Transactions on Wireless Communications*, vol. 6, pp. 4484 4493, Dec. 2007.
- [17] C. Luo, Y. Gong, and F.-C. Zheng, "Interference cancellation in two-path successive relay system with network coding," in *Proceedings of IEEE International Symposium on Personal Indoor and Mobile Radio Communications (PIMRC)*, pp. 465 469, Sept. 2010.
- [18] C. Luo, Y. Gong, and F. Zheng, "Full interference cancellation for two-path relay cooperative networks," *IEEE Transactions on Vehicular Technology*, vol. 60, pp. 343 347, Jan. 2011.
- [19] K. J. R. Liu, A. K. Sadek, W. F. Su, and A. Kwasinski, *Cooperative Communications and Networking*. U.K.: Cambridge University Press, 2009.
- [20] T. C. Y. Ng and W. Yu, "Joint optimization of relay strategies and resource allocations in cooperative cellular networks," *IEEE Journal on Selected Areas in Communications*, vol. 25, pp. 328–339, February 2007.
- [21] M. M. Fareed and M. Uysal, "BER-optimized power allocation for fading relay channels," *IEEE Transactions on Wireless Communications*, vol. 7, pp. 2350–2359, June 2008.
- [22] F. A. Onat, A. Adinoyi, Y. Fan, H. Yanikomeroglu, J. S. Thompson, and I. D. Marsland, "Threshold selection for SNR-based selective digital relaying in cooperative wireless networks," *IEEE Transactions on Wireless Communications*, vol. 7, pp. 4226–4237, Nov. 2008.

[23] S. Lee, W. Su, S. Batalama, and J. D. Matyjas, "Cooperative decode-and-forward ARQ relaying: Performance analysis and power optimization," *IEEE Transactions on Wireless Communications*, vol. 9, pp. 2632–2642, Aug. 2010.

- [24] G. A. Ropokis, A. A. Rontogiannis, and K. Berberidis, "BER performance analysis of cooperative DaF relay networks and a new optimal DaF strategy," *IEEE Transactions on Wireless Communications*, vol. 10, pp. 1044–1049, April 2011.
- [25] Y. Zhao, R. Adve, and T. J. Lim, "Improving amplify-and-forward relay networks: Optimal power allocation versus selection," in *Proceedings of IEEE International Symposium on Information Theory (ISIT)*, pp. 1234–1238, July 2006.
- [26] Y. Zhao, R. Adve, and T. J. Lim, "Symbol error rate of selection amplify-and-forward relay systems," *IEEE Communications Letters*, vol. 10, pp. 757–759, Nov. 2006.
- [27] N. C. Beaulieu and J. Hu, "A closed-form expression for the outage probability of decodeand-forward relaying in dissimilar Rayleigh fading channels," *IEEE Communications Letters*, vol. 10, pp. 813–815, Dec. 2006.
- [28] I.-H. Lee and D. Kim, "BER analysis for decode-and-forward relaying in dissimilar Rayleigh fading channels," *IEEE Communications Letters*, vol. 11, pp. 52–54, Jan. 2007.
- [29] A. Adinoyi and H. Yanikomeroglu, "Cooperative relaying in multi-antenna fixed relay networks," *IEEE Transactions on Wireless Communications*, vol. 6, pp. 533–544, Feb. 2007.
- [30] S. Ikki and M. H. Ahmed, "Performance analysis of cooperative diversity wireless networks over Nakagami-*m* fading channel," *IEEE Communications Letters*, vol. 11, pp. 334–336, April 2007.
- [31] E. van der Meulen, "A survey of multi-way channels in information theory: 1961-1976," *IEEE Transactions on Information Theory*, vol. 23, pp. 1 37, Jan. 1977.
- [32] D. Gunduz, A. Yener, A. Goldsmith, and H. V. Poor, "The multi-way relay channel," in *Proceedings of IEEE International Symposium on Information Theory (ISIT)*, pp. 339 343, July 2009.
- [33] A. U. T. Amah and A. Klein, "Non-regenerative multi-way relaying with linear beamforming," in *Proceedings of IEEE International Symposium on Personal, Indoor and Mobile Radio Communications (PIMRC)*, pp. 1843 1847, Sept. 2009.
- [34] A. U. T. Amah and A. Klein, "A transceive strategy for regenerative multi-antenna multi-way relaying," in *Proceedings of IEEE International Workshop on Computational Advances in Multi-Sensor Adaptive Processing*, pp. 352 355, Dec. 2009.
- [35] L. Ong, S. J. Johnson, and C. M. Kellett, "An optimal coding strategy for the binary multi-way relay channel," *IEEE Communications Letters*, vol. 14, pp. 330 332, April 2010.

[36] J. Cao, L.-L. Yang, and Z. Zhong, "Noncoherent multi-way relay based on fast frequency-hopping M-ary frequency-shift keying," in *Proceedings of International Symposium on Wireless Communication Systems (ISWCS)*, pp. 250 – 254, Sept. 2010.

- [37] M. O. Hasna and M. S. Alouini, "Outage probability of multihop transmission over Nakagami fading channels," *IEEE Communications Letters*, vol. 7, no. 5, pp. 216–218, 2003.
- [38] M. O. Hasna and M. S. Alouini, "End-to-end performance of transmission systems with relays over Rayleigh-fading channels," *IEEE Transactions on Wireless Communications*, vol. 2, pp. 1126–1131, Nov. 2003.
- [39] M. O. Hasna and M. S. Alouini, "Harmonic mean and end-to-end performance of transmission systems with relays," *IEEE Transactions on Communications*, vol. 52, pp. 130–135, Jan. 2004.
- [40] M. O. Hasna and M. S. Alouini, "Optimal power allocation for relayed transmissions over Rayleigh-fading channels," *IEEE Transactions on Wireless Communications*, vol. 3, pp. 1999–2004, Nov. 2004.
- [41] I. Trigui, S. Affes, and A. Stephenne, "A useful integral for wireless communication theory and its application in amplify-and-forward multihop relaying," in *Proceedings of IEEE Global Telecommunications Conference (GLOBECOM-2010)*, pp. 1–5, Dec. 2010.
- [42] S. Borade, L. Zheng, and R. Gallager, "Amplify-and-forward in wireless relay networks: Rate, diversity, and network size," *IEEE Transactions on Information Theory*, vol. 53, pp. 3302–3318, Oct. 2007.
- [43] D. Wubben, "High quality end-to-end-link performance," *IEEE Vehicular Technology Magazine*, vol. 4, pp. 26–32, Sept. 2009.
- [44] P. Liu and I.-M. Kim, "Optimum/sub-optimum detectors for multi-branch dual-hop amplify-and-forward cooperative diversity networks with limited CSI," *IEEE Transactions on Wireless Communications*, vol. 9, pp. 78–85, Jan. 2010.
- [45] G. Pan, E. Ekici, and Q. Feng, "Performance analysis of multi-branch multi-hop wireless relay systems over log-normal channels," *IEEE Transactions on Wireless Communications*, vol. 13, pp. 223–233, Jan. 2014.
- [46] B. Barua, H. Ngo, and H. Shin, "On the SEP of cooperative diversity with opportunistic relaying," *IEEE Communications Letters*, vol. 12, pp. 727 729, Oct. 2008.
- [47] A. Bletsas, H. Shin, and M. Z. Win, "Outage optimality of opportunistic amplify-and-forward relaying," *IEEE Communications Letters*, vol. 11, pp. 261 263, March 2007.

[48] Y. Chen, S. Kishore, and J. Li, "Wireless diversity through network coding," in *Proceedings of IEEE Wireless Communications and Networking Conference (WCNC-2006)*, vol. 3, pp. 1681 – 1686, April 2006.

- [49] J. N. Laneman and W. Gregory, "Distributed space-time-coded protocols for exploiting cooperative diversity in wireless networks," *IEEE Transactions on Information Theory*, vol. 49, pp. 2415 2425, Oct. 2003.
- [50] J. A. C. Bingham, "Multicarrier modulation for data transmission: an idea whose time has come," *IEEE Communications Magazine*, pp. 5–14, May 1990.
- [51] I. Kalet, "The multitone channel," *IEEE Transactions on Communications*, vol. 37, pp. 119–124, May 1989.
- [52] N. Benvenuto and S. Tomasin, "On the comparison between OFDM and single carrier modulation with a DFE using a frequency-domain feedforward filter," *IEEE Transactions on Communications*, vol. 50, pp. 947–955, June 2002.
- [53] H. G. Myung, J. Lim, and D. Goodman, "Single carrier FDMA for uplink wireless transmission," *IEEE Vehicular Technology Magazine*, vol. 1, pp. 30–38, Sept. 2006.
- [54] L.-L. Yang, "Time-hopping multicarrier code-division multiple-access: System outline and performance," in *IEEE International Symposium on Personal, Indoor and Mobile Radio Communications (PIMRC-2006)*, pp. 1–5, Sept. 2006.
- [55] L.-L. Yang, "Time-hopping multicarrier code-division multiple access," *IEEE Transactions on Vehicular Technology*, vol. 56, pp. 731–741, March 2007.
- [56] A. Chouly, A. Brajal, and S. Jourdan, "Orthogonal multicarrier techniques applied to direct sequence spread spectrum CDMA systems," in *Proceedings of IEEE Global Telecommunications Conference (GLOBECOM-1993)*, pp. 1723–1728, Nov. 1993.
- [57] B. M. Popovic, "Spreading sequences for multicarrier CDMA systems," *IEEE Transactions on Communications*, vol. 47, pp. 918–926, June 1999.
- [58] X. Gui and T. S. Ng, "Performance of asynchronous orthogonal multicarrier CDMA system in frequency selective fading channel," *IEEE Transactions on Communications*, vol. 47, pp. 1084–1091, July 1999.
- [59] V. M. DaSilva and E. S. Sousa, "Multicarrier orthogonal CDMA signals for quasi-synchronous communication systems," *IEEE Journal on Selected Areas in Communications*, vol. 12, pp. 842–852, June 1994.
- [60] E. A. Sourour and M. Nakagawa, "Performance of orthogonal multicarrier CDMA in a multipath fading channel," *IEEE Transactions on Communications*, vol. 44, pp. 356–367, March 1996.

[61] L.-L. Yang and L. Hanzo, "Multicarrier DS-CDMA: a multiple access scheme for ubiquitous broadband wireless communications," *IEEE Communications Magazine*, vol. 41, pp. 116 – 124, Oct. 2003.

- [62] C. Y. Wong, R. S. Cheng, K. B. Lataief, and R. D. Murch, "Multiuser OFDM with adaptive subcarrier, bit, and power allocation," *IEEE Journal on Selected Areas in Communications*, vol. 17, pp. 1747 1758, Oct. 1999.
- [63] Y.-F. Chen and J.-W. Chen, "A fast subcarrier, bit, and power allocation algorithm for multiuser OFDM-based systems," *IEEE Transactions on Vehicular Technology*, vol. 57, pp. 873 881, March 2008.
- [64] D. Kivanc, G. Li, and H. Liu, "Computationally efficient bandwidth allocation and power control for OFDMA," *IEEE Transactions on Wireless Communications*, vol. 2, pp. 1150– 1158, Nov. 2003.
- [65] Y. K. K. Han and S. L. Kim, "Joint subcarrier and power allocation in uplink OFDM systems," *IEEE on Communications Letters*, vol. 21, pp. 526 528, June 2005.
- [66] G. Kulkarni, S. Adlakha, and M. Srivastava, "subcarrier allocation and bit loading algorithms for OFDMA-based wireless networks," *IEEE Transactions on Mobile Computing*, vol. 4, pp. 652 662, Nov. 2005.
- [67] C. Mohanram and S. Bhashyam, "A sub-optimal joint subcarrier and power allocation algorithm for multiuser OFDM," *IEEE Communications Letters*, vol. 9, pp. 685 687, Aug. 2005.
- [68] N. Y. Ermolova and B. Makarevitch, "Low complexity adaptive power and subcarrier allocation for OFDMA," *IEEE Transactions on Wireless Communications*, vol. 6, pp. 433 437, Feb. 2007.
- [69] G. Song and Y. Li, "Cross-layer optimization for OFDM wireless networks-part I: theoretical framework," *IEEE Transactions on Wireless Communications*, vol. 4, pp. 614 624, March 2005.
- [70] G. Song and Y. Li, "Cross-layer optimization for OFDM wireless networks-part II: algorithm development," *IEEE Transactions on Wireless Communications*, vol. 4, pp. 625 634, March 2005.
- [71] T. Wang and L. Vandendorpe, "Iterative resource allocation for maximizing weighted sum min-rate in downlink cellular OFDMA systems," *IEEE Transactions on Signal Processing*, vol. 59, pp. 223 234, Jan. 2011.

[72] D. W. K. Ng and R. Schober, "Energy-efficient resource allocation in OFDMA systems with large numbers of base station antennas," *IEEE Transactions on Wireless Communications*, vol. 11, pp. 3292 – 3304, Sept. 2012.

- [73] H. Zhu and J. Wang, "Chunk-based resource allocation in OFDMA systemspart I: Chunk allocation," *IEEE Transactions on Communications*, vol. 57, pp. 2734 2744, Sept. 2009.
- [74] H. Zhu and J. Wang, "Chunk-based resource allocation in OFDMA systemspart II: Joint chunk, power and bit allocation," *IEEE Transactions on Communications*, vol. 60, pp. 499 509, Feb. 2012.
- [75] C. Y. Ng and C. W. Sung, "Low complexity subcarrier and power allocation for utility maximization in uplink OFDMA systems," *IEEE Transactions on Wireless Communications*, vol. 7, pp. 1667 1675, May 2008.
- [76] D. Dardari, "Ordered subcarrier selection algorithm for OFDM-based high-speed WLANs," *IEEE Transactions on Wireless Communications*, vol. 3, pp. 1425 1458, Sept. 2004.
- [77] K. B. Letaief and Y. J. Zhang, "Dynamic multiuser resource allocation and adaptation for wireless systems," *IEEE Transactions on Wireless Communications*, vol. 13, pp. 38 – 47, Aug. 2006.
- [78] J. Jang and K. B. Lee, "Transmit power adaptation for multiuser OFDM systems," *IEEE Journal on Selected Areas in Communications*, vol. 21, pp. 171 178, Feb. 2003.
- [79] W. Rhee and J. M. Cioffi, "Increase in capacity of multiuser OFDM system using dynamic subchannel allocation," in *Proceedings of IEEE Vehicular Technology Conference* (VTC2000-Spring), vol. 2, pp. 1085 1089, May 2000.
- [80] K. Kim and J. Kim, "A 2-D subcarrier allocation scheme for capacity enhancement in a clustered OFDM system," *EICE Transactions on Communications*, vol. E90-B, pp. 1880 – 1883, July 2007.
- [81] L. Gao and S. Cui, "Efficient subcarrier, power, and rate allocation with fairness consideration for OFDMA uplink," *IEEE Transactions on Wireless Communications*, vol. 7, pp. 1507 1511, May 2008.
- [82] K. A. D. Teo, Y. Otani, and S. Ohno, "Adaptive subcarrier allocation for multi-user OFDM system," *EICE Transactions on Communications*, vol. E89-A, pp. 3131 3137, July 2006.
- [83] T. Liu, C. Yang, and L.-L. Yang, "A low-complexity subcarrier-power allocation scheme for frequency-division multiple-access systems," *IEEE Transactions on Wireless Communications*, vol. 9, pp. 1564 1570, May 2010.

[84] D. Palomar, J. Cioffi, and M. Lagunas, "Joint Tx-Rx beamforming design for multicarrier MIMO channels: a unified framework for convex optimization," *IEEE Transactions on Signal Processing*, vol. 52, pp. 2381 – 2401, Sept. 2003.

- [85] N. Y. Ermolova and B. Makarevitch, "Performance of practical subcarrier allocation schemes for OFDM," *Proceedings of IEEE International Symposium on Personal, Indoor and Mobile Radio Communications (PIMRC)*, pp. 1 4, Sept. 2007.
- [86] O. Nwamadi, X. Zhu, and A. Nandi, "Dynamic subcarrier allocation for single carrier FDMA systems," in *Proceedings of EUSIPCO-2008*, Aug. 2008.
- [87] A. Biagioni, R. Fantacci, D. Marabissi, and D. Tarchi, "Adaptive subcarrier allocation schemes for wireless OFDMA systems in WiMAX networks," *IEEE Journal on Selected Areas in Communications*, vol. 27, pp. 217 225, Feb. 2009.
- [88] D. W. K. Ng, E. S. Lo, and R. Schober, "Energy-efficient resource allocation in multi-cell OFDMA systems with limited backhaul capacity," *IEEE Wireless Communications and Networking Conference (WCNC-2012)*, pp. 1146 1151, April 2012.
- [89] T. Wang, Y. Fang, and L. Vandendorpe, "Novel subcarrier-pair based opportunistic DF protocol for cooperative downlink OFDMA," in *Proceedings of IEEE Wireless Communications and Networking Conference (WCNC-2013)*, pp. 3282 3287, April 2013.
- [90] J. Jang and K. B. Lee, "Transmit power adaptation for multiuser OFDM systems," *IEEE Journal on Selected Areas in Communications*, vol. 21, pp. 171–178, Feb. 2003.
- [91] D. Kivanc, G. Li, and H. Liu, "Computationally efficient bandwidth allocation and power control for OFDMA," *IEEE Transactions on Wireless Communications*, vol. 2, pp. 1150– 1158, Nov. 2003.
- [92] Z. Shen, J. G. Andrews, and B. L. Evans, "Adaptive resource allocation in multiuser OFDM systems with proportional rate constraints," *IEEE Transactions on Wireless Communications*, vol. 4, pp. 2726–2737, Nov. 2005.
- [93] K. Seong, M. Mohseni, and J. M. Cioffi, "Optimal resource allocation for OFDMA downlink systems," in *Proceedings of IEEE International Symposium on Information Theory (ISIT)*, pp. 1394–1398, July 2006.
- [94] I. Hammerstrom and A. Wittneben, "Power allocation schemes for amplify-and-forward MIMO-OFDM relay links," *IEEE Transactions on Wireless Communications*, vol. 6, pp. 2798–2802, Aug. 2007.
- [95] G. Bansal, J. Hossain, and V. K. Bhargava, "Optimal and suboptimal power allocation schemes for OFDM-based cognitive radio systems," *IEEE Transactions on Wireless Communications*, vol. 7, pp. 4710–4718, Nov. 2008.

[96] P. K. Sampath, H. Cam, and A. Natarajan, "Power and subcarrier allocation for multirate MC-CDMA system," in *Proceedings of IEEE Vehicular Technology Conference (VTC2003-Fall)*, vol. 3, pp. 1900–1902, Oct. 2003.

- [97] P.-W. Fu and K.-C. Chen, "Rate, sub-carrier, and power allocations for multi-carrier CDMA with LMMSE multiuser detection," *IEEE Transactions on Wireless Communications*, vol. 6, no. 5, pp. 1574 1580, 2007.
- [98] Y. Wang, G. Xie, Y. an Liu, and N. Li, "Feasible resource allocation with partial channel information for grouped MC-CDMA system," pp. 683 688, 2007.
- [99] E. S. Lo, P. W. C. Chan, V. K. N. Lau, R. S. Cheng, K. B. Letaief, R. D. Murch, and W.-H. Mow, "Adaptive resource allocation and capacity comparison of downlink multiuser MIMO-MC-CDMA and MIMO-OFDMA," *IEEE Transactions on Wireless Communications*, vol. 6, pp. 1083 1093, March 2007.
- [100] P. W. C. Chan, E. S. Lo, V. K. N. Lau, R. S. Cheng, K. B. Letaief, R. D. Murch, and W.-H. Mow, "Performance comparison of downlink multiuser MIMO-OFDMA and MIMO-MC-CDMA with transmit side information multi-cell analysis," *IEEE Transactions on Wireless Communications*, vol. 6, pp. 2193 2203, June 2007.
- [101] Y.-W. Kuo, C.-K. Yang, and J.-H. Lin, "Joint bit loading and power allocation for downlink minimum mean square error combining based multi-carrier code division multiple access systems," *IET Communications*, vol. 7, pp. 1015–1023, July 2013.
- [102] Y. Wang, P. Zhang, Y. an Liu, and J. Liu, "A novel criterion of subcarrier allocation for grouped MC-CDMA systems," in *Proceedings of International Conference on Communica*tions and Networking in China, pp. 1090–1095, Aug. 2007.
- [103] J. Huang and Z. Niu, "WLC08-4: a fairness-based and adaptive user grouping and subcarrier allocation algorithm for grouped MC-CDMA systems," in *Proceedings of IEEE Global Telecommunications Conference (GLOBECOM-2006)*, pp. 1–5, Nov. 2006.
- [104] P.-W. Fu and K.-C. Chen, "Rate, sub-carrier, and power allocations for multi-carrier CDMA with LMMSE multiuser detections," in *Proceedings of IEEE International Symposium on Personal, Indoor and Mobile Radio Communications (PIMRC)*, vol. 2, pp. 1034–1038, Sept. 2005.
- [105] T. Jia and A. Duel-Hallen, "Improved channel allocation for multicarrier CDMA with adaptive frequency hopping and multiuser detection," *IEEE Transactions on Communications*, vol. 57, no. 11, pp. 3389 3396, 2009.
- [106] Y. Zhu and E. Gunawan, "Performance of MC-CDMA system using controlled MRC with power control in Rayleigh fading channel," *Electronics Letters*, vol. 36, pp. 752 753, 2000.

[107] J. Zhu and Y. Bar-Ness, "Power allocation algorithm in MC-CDMA," in *Proceedings of IEEE International Conference on Communications (ICC-2002)*, vol. 2, pp. 931 – 935, 2002.

- [108] L. Loyola and T. Miki, "Speed-aware multicarrier transmission and resource allocation scheme for the uplink channel of highly mobile networks," in *Proceedings of IEEE Topical Conference on Wireless Communication Technology*, pp. 117–118, Oct. 2003.
- [109] Z. Zhang, Y. Zhao, and Y. Ya, "Adaptive modulation and power allocation for multicarrier DS/CDMA," in *Proceedings of IEEE International Conference on Communications, Circuits and Systems and West Sino Expositions*, vol. 1, pp. 243–246, June 2002.
- [110] C.-W. Chang and L.-C. Wang, "WLC03-3: A joint subcarrier power allocation and interference avoidance code assignment strategy for multi-rate MC-DS-CDMA with TF-domain spreading," in *Proceedings of IEEE Global Telecommunications Conference (GLOBECOM-2006)*, pp. 1–5, Nov. 2006.
- [111] Q. Qu, L. B. Milstein, and D. R. Vaman, "Distributed spectrum and power control in cognitive radio based wireless ad hoc networks," in *Proceedings of IEEE Sarnoff Symposium*, pp. 1–6, April 2007.
- [112] C.-W. Chang and L.-C. Wang, "Effects of subcarrier power allocation on an interference avoidance code assignment strategy for multirate MC-DS-CDMA systems," *IEEE Transactions on Vehicular Technology*, vol. 57, pp. 1513–1526, May 2008.
- [113] C.-W. Chang and C.-C. Kuo, "A low interference time-slicing code assignment for the 2D-Spread MC-DS-CDMA systems," in *Proceedings of IEEE Vehicular Technology Conference* (VTC2009-Spring), pp. 1–5, April 2009.
- [114] C.-W. Chang and C.-C. Kuo, "A novel interference-avoidance code reassignment for down-link two-dimensional-spread MC-DS-CDMA systems with power control," *IEEE Transactions on Vehicular Technology*, vol. 59, pp. 3104–3108, July 2010.
- [115] Q. Qu, L. B. Milstein, and D. R. Vaman, "Cognitive radio based multi-user resource allocation in mobile ad hoc networks using multi-carrier CDMA modulation," *IEEE Journal on Selected Areas in Communications*, vol. 26, pp. 70–82, Jan. 2008.
- [116] D. Gesbert, S. G. Kiani, A. Gjendemsjo, and G. E. Oien, "Adaptation, coordination, and distributed resource allocation in interference-limited wireless networks," *Proceedings of the IEEE*, vol. 95, pp. 2393–2409, Dec. 2007.
- [117] Z. Liang, Y. H. Chew, and C. C. Ko, "A linear programming solution to subcarrier, bit and power allocation for multicell OFDMA systems," in *Proceedings of IEEE Wireless Communications and Networking Conference (WCNC-2008)*, pp. 1273 1278, March 2008.

[118] Y. Hua, Q. Zhang, and Z. Niu, "Resource allocation in multi-cell OFDMA-based relay networks," pp. 1 - 9, 2010.

- [119] M. Pischella and J. C. Belfiore, "Weighted sum throughput maximization in multicell OFDMA networks," *IEEE Transactions on Vehicular Technology*, vol. 59, pp. 896 905, Feb. 2010.
- [120] S. M. H. Andargoli and K. Mohamed-Pour, "Weighted sum throughput maximisation for downlink multicell orthogonal frequency-division multiple access systems by intercell interference limitation," *IET Communications*, vol. 6, pp. 628 637, April 2012.
- [121] M. Abaii, Y. Liu, and R. Tafazolli, "An efficient resource allocation strategy for future wireless cellular systems," *IEEE Transactions on Wireless Communications*, vol. 7, pp. 2940 – 2949, Aug. 2008.
- [122] B. Da and R. Zhang, "Exploiting interference alignment in multi-cell cooperative OFDMA resource allocation," in *Proceedings of IEEE Global Telecommunications Conference* (GLOBECOM-2011), pp. 1 5, 2011.
- [123] D. W. K. Ng, E. S. Lo, and R. Schober, "Energy-efficient resource allocation in multi-cell OFDMA systems with limited backhaul capacity," *IEEE Transactions on Wireless Communications*, vol. 11, pp. 3618 3631, Oct. 2012.
- [124] Z. Wang, Q. Peng, and L. B. Milstein, "Multi-user resource allocation for downlink multicluster multicarrier DS CDMA system," *IEEE Transactions on Wireless Communications*, vol. 10, pp. 2534–2542, Aug. 2011.
- [125] Z. Wang, D. Yang, and L. B. Milstein, "Multi-user resource allocation for a distributed multi-carrier DS-CDMA network," *IEEE Transactions on Communications*, vol. 60, no. 1, pp. 143 152, 2012.
- [126] G. Y. Li, Z. Xu, C. Xiong, C. Yang, S. Zhang, Y. Chen, and S. Xu, "Energy-efficient wireless communications: tutorial, survey, and open issues," *IEEE Wireless Communications*, vol. 18, pp. 28–35, Dec. 2011.
- [127] K. Vardhe, D. Reynolds, and B. D. Woerner, "Joint power allocation and relay selection for multiuser cooperative communication," *IEEE Transactions on Wireless Communications*, vol. 9, pp. 1255–1260, April 2010.
- [128] S. Mallick, R. Devarajan, M. M. Rashid, and V. K. Bhargava, "Resource allocation for selective relaying based cellular wireless system with imperfect CSI," *IEEE Transactions on Communications*, vol. 61, pp. 1822–1834, May 2013.

[129] K. T. K. Cheung, S. Yang, and L. Hanzo, "Achieving maximum energy-efficiency in multirelay OFDMA cellular networks: A fractional programming approach," *IEEE Transactions* on Communications, vol. 61, pp. 2746–2757, July 2013.

- [130] R. A. Loodaricheh, S. Mallick, and V. K. Bhargava, "Energy-efficient resource allocation for OFDMA cellular networks with user cooperation and QoS provisioning," *IEEE Transactions* on Wireless Communications, vol. 13, pp. 6132–6146, Nov. 2014.
- [131] G. Miao, N. Himayat, Y. Li, and D. Bormann, "Energy efficient design in wireless OFDMA," in *Proceedings of IEEE International Conference on Communications (ICC-2008)*, pp. 3307–3312, May 2008.
- [132] Z. Hasan, G. Bansal, E. Hossain, and V. K. Bhargava, "Energy-efficient power allocation in OFDM-based cognitive radio systems: A risk-return model," *IEEE Transactions on Wireless Communications*, vol. 8, pp. 6078–6088, Dec. 2009.
- [133] G. Miao, N. Himayat, and G. Y. Li, "Energy-efficient link adaptation in frequency-selective channels," *IEEE Transactions on Communications*, vol. 58, pp. 545–554, February 2010.
- [134] D. W. K. Ng, E. S. Lo, and R. Schober, "Wireless information and power transfer: Energy efficiency optimization in OFDMA systems," *IEEE Transactions on Wireless Communications*, vol. 12, pp. 6352–6370, Dec. 2013.
- [135] M. Fathi and E. Karipidis, "Distributed resource optimization in multicell OFDMA networks," in *Proceedings of IEEE Wireless Communications and Networking Conference* (WCNC-2012), pp. 1316 1320, April 2012.
- [136] K. W. Choi, E. Hossain, and D. I. Kim, "Downlink subchannel and power allocation in multicell OFDMA cognitive radio networks," *IEEE Transactions on Wireless Communications*, vol. 10, pp. 2259–2271, July 2011.
- [137] B. Ozbek, D. L. Ruyet, and M. Pischella, "Adaptive reduced feedback links for distributed power allocation in multicell MISO-OFDMA networks," *IEEE Wireless Communications Letters*, vol. 3, pp. 141–144, April 2014.
- [138] D. W. K. Ng and R. Schober, "Resource allocation and scheduling in multi-cell OFDMA systems with decode-and-forward relaying," *IEEE Transactions on Wireless Communications*, vol. 10, pp. 2246 2258, July 2011.
- [139] M. Moretti, A. Todini, A. Baiocchi, and G. Dainelli, "A layered architecture for fair resource allocation in multicellular multicarrier systems," *IEEE Transactions on Vehicular Technol*ogy, vol. 60, pp. 1788–1798, May 2011.

[140] Y. Yu, E. Dutkiewicz, X. Huang, and M. Mueck, "Downlink resource allocation for next generation wireless networks with inter-cell interference," *IEEE Transactions on Wireless Communications*, vol. 12, pp. 1783–1793, April 2013.

- [141] N. Odeh, M. Abolhasan, and F. Safaei, "Low complexity interference aware distributed resource allocation for multi-cell OFDMA cooperative relay networks," in *Proceedings of IEEE Wireless Communications and Networking Conference (WCNC-2010)*, pp. 1–6, April 2010.
- [142] K. Yang, N. Prasad, and X. Wang, "A message-passing approach to distributed resource allocation in uplink DFT-Spread-OFDMA systems," *IEEE Transactions on Communications*, vol. 59, pp. 1099–1113, April 2011.
- [143] A. Gjendemsjo, D. Gesbert, G. E. Oien, and S. G. Kiani, "Optimal power allocation and scheduling for two-cell capacity maximization," in *Proceedings of International Symposium on Modeling and Optimization in Mobile, Ad Hoc and Wireless Networks*, pp. 1–6, April 2006.
- [144] S. G. Kiani, G. E. Oien, and D. Gesbert, "Maximizing multicell capacity using distributed power allocation and scheduling," in *Proceedings of IEEE Wireless Communications and Networking Conference (WCNC-2007)*, pp. 1690 1694, March 2007.
- [145] I. G. Fraimis, V. D. Papoutsis, and S. A. Kotsopoulos, "A decentralized subchannel allocation scheme with inter-cell interference coordination (ICIC) for multi-cell OFDMA systems," in Proceedings of IEEE Global Telecommunications Conference (GLOBECOM-2010), pp. 1–5, Dec. 2010.
- [146] H. Zhang, Q. Yang, F. Gao, and K. S. Kwak, "Distributed adaptive subchannel and power allocation for downlink OFDMA with inter-cell interference coordination," in *Proceedings* of IEEE Global Telecommunications Conference (GLOBECOM-2010), pp. 1–5, Dec. 2010.
- [147] S. Liu, Y. Chang, G. Wang, and D. Yang, "Distributed resource allocation with inter-cell interference coordination in OFDMA uplink," in *Proceedings of IEEE Vehicular Technology Conference (VTC2012-Fall)*, pp. 1–5, Sept. 2012.
- [148] D. Goodman and N. Mandayam, "Power control for wireless data," *IEEE Personal Communications*, vol. 7, pp. 48–54, April 2000.
- [149] Z. Han, Z. Ji, and K. J. R. Liu, "Power minimization for multi-cell OFDM networks using distributed non-cooperative game approach," in *Proceedings of IEEE Global Telecommunications Conference (GLOBECOM-2004)*, vol. 6, pp. 3742–3747, Nov. 2004.
- [150] Z. Han, Z. Ji, and K. J. R. Liu, "Non-cooperative resource competition game by virtual referee in multi-cell OFDMA networks," *IEEE Journal on Selected Areas in Communications*, vol. 25, pp. 1079–1090, Aug. 2007.

[151] H. Kwon and B. G. Lee, "Distributed resource allocation through noncooperative game approach in multi-cell OFDMA systems," in *Proceedings of IEEE International Conference on Communications (ICC-2006)*, vol. 9, pp. 4345–4350, June 2006.

- [152] Z. Liang, Y. H. Chew, and C. C. Ko, "Decentralized bit, subcarrier and power allocation with interference avoidance in multicell OFDMA systems using game theoretic approach," in *Proceedings of IEEE Military Communications Conference (MILCOM)*, pp. 1 7, 2008.
- [153] L. Wang and Z. Niu, "Adaptive power control in multi-cell OFDM systems: A noncooperative game with power unit based utility," *IEICE Transactions on Communications*, vol. E89-B, pp. 1951–1954, June 2006.
- [154] X. Yu, T. Wu, J. Huang, and Y. Wang, "A non-cooperative game approach for distributed power allocation in multi-cell OFDMA-relay networks," in *Proceedings of IEEE Vehicular Technology Conference (VTC2008-Spring)*, pp. 1920–1924, May 2008.
- [155] W. S. Jeon, J. A. Han, and D. G. Jeong, "Distributed resource allocation for multi-cell relay-aided OFDMA systems," *IEEE Transactions on Mobile Computing*, vol. 13, pp. 2003–2015, Sept. 2014.
- [156] S. Berger, M. Kuhn, A. Wittneben, T. Unger, and A. Klein, "Recent advances in amplify-and-forward two-hop relaying," *IEEE Communications Magazine*, vol. 47, pp. 50 56, July 2009.
- [157] C. Zhang, H. Yin, W. Wang, and G. Wei, "Selective partial decode-and-forward schemes for distributed space-time coded relaying networks," in *Proceedings of IEEE Vehicular Technology Conference (VTC2009-Spring)*, pp. 1 5, April 2009.
- [158] A. H. Bastami and A. Olfat, "Optimal SNR-based selection relaying scheme in multi-relay cooperative networks with distributed space-time coding," *IET Communications*, vol. 4, pp. 619 630, April 2010.
- [159] Z. Bai, Y. Xu, B. Shen, K. Kwak, and D. Yuan, "Performance analysis of dual-hop UWB system with non-regenerative relaying scheme," in *Proceedings of International Conference on Advanced Communication Technology*, pp. 1221 1225, Feb. 2011.
- [160] A. Sendonaris, E. Erkip, and B. Aazhang, "Increasing uplink capacity via user cooperation diversity," in *Proceedings of IEEE International Symposium on Information Theory (ISIT)*, p. 156, Aug. 1998.
- [161] J. N. Laneman and G. W. Wornell, "Energy-efficient antenna sharing and relaying for wireless networks," in *Proceedings of IEEE Wireless Communications and Networking Confernce (WCNC-2000)*, vol. 1, pp. 7 12, Aug. 2000.

[162] A. Nosratinia, T. E. Hunter, and A. Hedayat, "Cooperative communication in wireless networks," *IEEE Communications Magazine*, vol. 42, pp. 74 – 80, Oct. 2004.

- [163] O. Amin, S. S. Ikki, and M. Uysal, "On the performance analysis of multirelay cooperative diversity systems with channel estimation errors," *IEEE Transactions on Vehicular Technology*, vol. 60, pp. 2050 2059, June 2011.
- [164] C. Dong, L.-L. Yang, and L. Hanzo, "Performance analysis of multihop-diversity-aided multihop links," *IEEE Transactions on Vehicular Technology*, vol. 61, pp. 2504 2516, July 2012.
- [165] P. A. Anghel and M. Kaveh, "Exact symbol error probability of a cooperative network in a Rayleigh-fading environment," *IEEE Transactions on Wireless Communications*, vol. 3, pp. 1416 1421, Sept. 2004.
- [166] A. Ribeiro, X. Cai, and G. B. Giannakis, "Symbol error probabilities for general cooperative links," *IEEE Transactions on Wireless Communications*, vol. 4, pp. 1264 1273, May 2005.
- [167] L.-L. Yang and H.-H. Chen, "Error probability of digital communications using relay diversity over Nakagami-*m* fading channels," *IEEE Transactions on Wireless Communications*, vol. 7, pp. 1806 1811, May 2008.
- [168] T. Himsoon, W. P. Siriwongpairat, W. Su, and K. J. R. Liu, "Differential modulations for multinode cooperative communications," *IEEE Transactions on Signal Processing*, vol. 56, pp. 2941 – 2956, July 2008.
- [169] J. Boyer, D. D. Falconer, and H. Yanikomeroglu, "Multihop diversity in wireless relaying channels," *IEEE Transactions on Communications*, vol. 52, pp. 1820 1830, Sept. 2004.
- [170] Y. Zhao, R. Adve, and T. J. Lim, "Outage probability at arbitrary SNR with cooperative diversity," *IEEE Communications Letters*, vol. 9, pp. 700 702, Aug. 2005.
- [171] H. A. Suraweera, P. J. Smith, and J. Armstrong, "Outage probability of cooperative relay networks in Nakagami-*m* fading channels," *IEEE Communications Letters*, vol. 10, pp. 834 836, Dec. 2006.
- [172] N. C. Sagias, F. I. Lazarakis, G. S. Tombras, and C. K. Datsikas, "Outage analysis of decode-and-forward relaying over Nakagami-*m* fading channels," *IEEE Signal Processing Letters*, vol. 15, pp. 41 44, Jan. 2008.
- [173] G. Kramer, M. Gastpar, and P. Gupta, "Cooperative strategies and capacity theorems for relay networks," *IEEE Transactions on Information Theory*, vol. 51, pp. 3037 – 3063, Sept. 2005.
- [174] A. Host-Madsen and J. Zhang, "Capacity bounds and power allocation for wireless relay channels," *IEEE Transactions on Information Theory*, vol. 51, pp. 2020 2040, June 2005.

[175] A. Host-Madsen, "Capacity bounds for cooperative diversity," *IEEE Transactions on Information Theory*, vol. 52, pp. 1522 – 1544, April 2006.

- [176] J. Shi and L.-L. Yang, "Performance of multiway relay DS-CDMA systems over Nakagamim fading channels," in *Proceedings of IEEE Vehicular Technology Conference (VTC2011-Spring)*, pp. 1 – 5, May 2011.
- [177] L.-L. Yang and L. Hanzo, "Performance of generalized multicarrier DS-CDMA over Nakagami-*m* fading channels," *IEEE Transactions on Communications*, vol. 50, pp. 956 966, June 2002.
- [178] L.-L. Yang, "Receiver multiuser diversity aided multi-stage MMSE multiuser detection: A low-complexity detector fast-converging to the optimum," in *Proceedings of IEEE Vehicular Technology Conference (VTC2010-Spring)*, pp. 1 5, May 2010.
- [179] L.-L. Yang, "Receiver multiuser diversity aided multi-stage MMSE multiuser detection for DS-CDMA and SDMA systems employing I-Q modulation," in *Proceedings of IEEE Vehicular Technology Conference Fall (VTC2010-Fall)*, pp. 1 5, Sept. 2010.
- [180] M. K. Simon and M.-S. Alouini, *Digital Communication Over Fading Channels: A Unified Approach to Performance Analysis*. New York, USA: Wiley, 2000.
- [181] T. Eng and L. B. Milstein, "Coherent DS-CDMA performance in Nakagami multipath fading," *IEEE Transactions on Communications*, vol. 43, pp. 1134 1143, Feb. 1995.
- [182] I. S. Gradshteyn and I. M. Ryzhik, *Table of Integrals, Series, and Products*. Singapore: Elsevier Pte Ltd., 7th ed., 2007.
- [183] V. Rotar, *Probability and Stochastic Modeling*. Florida, USA: Chapman and Hall/CRC, 2012.
- [184] M. Nakagami, "The *m*-distribution, a general formula of intensity of rapid fading," *Statistical Methods in Radio Wave Propagation:Proceeding of a Symposium*, June 1958.
- [185] H. W. Kuhn, "The Hungarian method for the assignment problem," *Naval Research Logistics Quarterly*, vol. 2, pp. 83 97, 1995.
- [186] H. Wang, Q. Cui, X. Tao, M. Valkama, and Y. Guo, "Optimal cooperative water-filling power allocation for OFDM system," in *Proceedings of IEEE Wireless Communications and Networking Conference (WCNC-2013)*, pp. 3742 3747, April 2013.
- [187] H. Moon, "Waterfilling power allocation at high SNR regimes," *IEEE Communications Letters*, vol. 59, pp. 708 715, March 2011.

[188] Y. Liang, V. V. Veeravalli, and H. V. Poor, "Resource allocation for wireless fading relay channels: Max-Min solution," *IEEE Transactions on Information Theory*, vol. 53, pp. 3432 – 3453, Oct. 2007.

- [189] C. Zeng, L. M. C. Hoo, and J. M. Cioff, "Efficient water-filling algorithms for a Gaussian multiaccess channel with ISI," in *Proceedings of IEEE Vehicular Technology Conference Fall (VTC2000-Fall)*, vol. 3, pp. 1072 1077, Sept. 2000.
- [190] A. Goldsmith, Wireless Communications. U.K.: Cambridge University Press, 2005.
- [191] J. Munkres, "Algorithms for the assignment and transportation problems," *Society for Industrial and Applied Mathematics*, vol. 5, pp. 32 38, March 1957.
- [192] W. H. Press, S. A. Teukolsky, W. T. Vetterling, and B. P. Flannery, *Numerical recipes in C: the art of scientific computing*. Cambridge, U.K.: Cambridge University Press, 3rd ed., 1992.
- [193] M. O. Fitz and J. P. Seymour, "On the bit error probability of QAM modulation," *Int. J. Wireless Inform. Networks*, vol. 1, no. 2, pp. 131 139, 1994.
- [194] K. Cho, D. Yoon, W. Jeong, and M. Kavehrad, "Ber analysis of arbitrary rectangular QAM," vol. 2, pp. 1056 1059, 2001.
- [195] D. Yoon, K. Cho, and J. Lee, "Bit error probability of M-ary quadrature amplitude modulation," in *Proceedings of IEEE Vehicular Technology Conference (VTC200-Fall)*, vol. 5, pp. 2422–2427, 2000.
- [196] C. Tellambura, M. Soysa, and D. Senaratne, "Performance analysis of wireless systems from the MGF of the reciprocal of the signal-to-noise ratio," *IEEE Communications Letters*, vol. 15, no. 1, pp. 55 57, 2011.
- [197] M. Abramowitz and I. Stegun, *Handbook of Mathematical Funcations*. New York, USA: Dover Publications, Inc., 1970.
- [198] J. Shi, C. Dong, and L.-L. Yang, "Performance comparison of cooperative relay links with different relay processing strategies: Nakagami/Gamma-Approximation approaches," *EURASIP Journal on Wireless Communications and Networking*, vol. 53, pp. doi:10.1186/1687–1499–2014–53, April 2014.
- [199] G. Li and H. Liu, "Downlink radio resource allocation for multi-cell OFDMA system," *IEEE Transactions on Wireless Communications*, vol. 5, pp. 3451–3459, Dec. 2006.
- [200] L. Venturino, N. Prasad, and X. Wang, "Coordinated scheduling and power allocation in downlink multicell OFDMA networks," *IEEE Transactions on Vehicular Technology*, vol. 58, pp. 2835–2848, July 2009.

[201] H. Zhang, L. Venturino, N. Prasad, P. Li, S. Rangarajan, and X. Wang, "Weighted sum-rate maximization in multi-cell networks via coordinated scheduling and discrete power control," *IEEE Journal on Selected Areas in Communications*, vol. 29, pp. 1214–1224, June 2011.

- [202] S. H. Ali and V. C. M. Leung, "Dynamic frequency allocation in fractional frequency reused OFDMA networks," *IEEE Transactions on Wireless Communications*, vol. 8, pp. 4286 4295, Aug. 2009.
- [203] H. Galeana-Zapien and R. Ferrus, "Design and evaluation of a backhaul-aware base station assignment algorithm for OFDMA-based cellular networks," *IEEE Transactions on Wireless Communications*, vol. 9, pp. 3226–3237, Oct. 2010.
- [204] A. Chowdhery, W. Yu, and J. M. Cioffi, "Cooperative wireless multicell OFDMA network with backhaul capacity constraints," in *Proceedings of IEEE International Conference on Communications (ICC-2011)*, pp. 1–6, June 2011.
- [205] X. Xiao, X. Tao, Y. Jia, and J. Lu, "An energy-efficient hybrid structure with resource allocation in OFDMA networks," in *Proceedings of IEEE Wireless Communications and Networking Conference (WCNC-2011)*, pp. 1466–1470, March 2011.
- [206] A. J. Viterbi, A. M. Viterbi, and E. Zehavi, "Other-cell interference in cellular power-controlled CDMA," *IEEE Transactions on Communications*, vol. 42, pp. 1501 1504, Feb. 1994.
- [207] S. Alamouti, "A simple transmit diversity technique for wireless communications," *IEEE Journal on Selected Areas in Communications*, vol. 16, pp. 1451 1458, Oct. 1998.
- [208] J. Shi and L.-L. Yang, "Novel subcarrier-allocation schemes for downlink MC DS-CDMA systems," *IEEE Transactions on Wireless Communications*, vol. 13, pp. 5716–5728, Oct. 2014.
- [209] J. Xiang, Y. Zhang, T. Skeie, and L. Xie, "Downlink spectrum sharing for cognitive radio femtocell networks," *IEEE Systems Journal*, vol. 4, pp. 524 534, Dec. 2010.
- [210] K. Lee, O. Jo, and D.-H. Cho, "Cooperative resource allocation for guaranteeing intercell fairness in femtocell networks," *IEEE Communications Letters*, vol. 15, pp. 214 216, Feb. 2011.
- [211] D. Calabuig, J. F. Monserrat, and N. Cardona, "Fairness-driven fast resource allocation for interference-free heterogeneous networks," *IEEE Communications Letters*, vol. 16, pp. 1092 – 1095, July 2012.
- [212] N. Lertwiram, P. Popovski, and K. Sakaguchi, "A study of trade-off between opportunistic resource allocation and interference alignment in femtocell scenarios," *IEEE Wireless Communications Letters*, vol. 1, pp. 356 359, Aug. 2012.

[213] Q. Kuang, J. Speidel, and H. Droste, "Joint base-station association, channel assignment, beamforming and power control in heterogeneous networks," in *Proceedings of IEEE Vehicular Technology Conference (VTC2012-Spring)*, pp. 1 – 5, May 2012.

- [214] D. Fooladivanda, A. A. Daoud, and C. Rosenberg, "Joint channel allocation and user association for heterogeneous wireless cellular networks," in *Proceedings of IEEE International Symposium on Personal Indoor and Mobile Radio Communications (PIMRC)*, pp. 384 390, Sept. 2011.
- [215] D. Fooladivanda and C. Rosenberg, "Joint resource allocation and user association for heterogeneous wireless cellular networks," *IEEE Transactions on Wireless Communications*, vol. 12, pp. 248 257, Jan. 2013.
- [216] A. Ladanyi, D. Lopez-Perez, A. Juttner, X. Chu, and J. Zhang, "Distributed resource allocation for femtocell interference coordination via power minimisation," in *Proceedings of IEEE GLOBECOM Workshops (GC Wkshps)*, pp. 744 749, Dec. 2011.
- [217] M. Ismail and W. Zhuang, "A distributed multi-service resource allocation algorithm in heterogeneous wireless access medium," *IEEE Journal on Selected Areas in Communications*, vol. 30, pp. 425 432, Feb. 2012.
- [218] N. D. R1-103264, "Performance of eICIC with control channel coverage limitation," *3GPP Std., Montreal, Canada*, May 2010.
- [219] A. Khandekar, N. Bhushan, J. Tingfang, and V. Vanghi, "LTE-Advanced: Heterogeneous networks," in *Proceedings of European Wireless Conference*, 2010.
- [220] S. Corroy, L. Falconetti, and R. Mathar, "Dynamic cell association for downlink sum rate maximization in multi-cell heterogeneous networks," in *Proceedings of IEEE International Conference on Communications (ICC-2012)*, vol. 1, pp. 2457 2461, June 2012.
- [221] R. Q. Hu and Y. Qian, resource management for heterogeneous networks in LTE systems. New York, USA: Springer, 2014.
- [222] R. Q. Hu and Y. Qian, "An energy efficient and spectrum efficient wireless heterogeneous network framework for 5G systems," *IEEE Communications Magazine*, vol. 52, pp. 94 101, May 2014.
- [223] A. Mesodiakaki, F. Adelantado, L. Alonso, and C. Verikoukis, "Energy-efficient user association in cognitive heterogeneous networks," *IEEE Communications Magazine*, vol. 52, pp. 22–29, July 2014.

Subject Index

Symbols	CSI12, 14, 24, 29
<i>R</i> -QAM95	D
4G142	DDMC
5G210	
•	DF
A	DMT 2
AF	DS
APs	DS-CDMA
AWGN25, 26, 72	E
В	E2E5
BC24	EGC25
BER 4, 17, 36	ESIA181, 187
BPSK 22, 36	F
BS71, 109	
BSS 86	F-domain8
BWSA82	FFH
C	FFT
CDE	G
CDF	Gamma-Ap48
CDMC	***
CF	H
CMRC	HetNets
CMRC-TEGC-RP	I
CMRC-TMRC-RP30	ICMRC-TEGC-RP29, 47, 55
CMVC21, 25, 32	ICMRC-TMRC-RP29
CMVC-TEGC-RP30	ICMVC-TEGC-RP29, 54, 55
CMVC-TMRC-RP30	ICMVC-TMRC-RP
CMVC/MMSE	IECU
CMVC/MUD25	IMD
CMVC/RMD25	InterCI
	1101 01 12, 13

SUBJECT INDEX 234

IntraCI	PDF 24, 36, 66, 95, 139
IS193	PMF124
ISI	0
IWE109, 120, 121	Q
IWE-WCA	QAM17, 94
IWE-WCF121, 123	QoS
IWE-WSA123, 126	QPSK
•	R
L	R-D21, 24
LTE	RF 212
LTE-A	RMD/MS-MMSE
M	RP21, 24, 28
MA 24, 47	
MAI11	S
MAP	S-R
MC DS-CDMA	SER
MC-CDMA 6	SIC143
MGF	SINR 148, 150, 151, 156
MIMO14	SIR 144, 149
MISO143	SISO6
ML143	SNR 25, 45, 49, 57, 72, 98
MLD	SOPA61
MMSE 25, 65	SSIA181, 187
MRC	STBC144
MUD	T
MUI25	T-domain9
MVC	TDD72, 110
N.	TEGC
N	TEGC-DRP
Nakagami-SAp	THCL21–23, 65
Nakagami-TAp	TMRC 22, 25
0	TMRC-DRP27
OFDM6	
OFDMA	\mathbf{W}
OOP144	WCA 109, 117
OPA58, 59	WCF109, 118, 119, 122
_	WE
P	WSA 69
PAPR 7	WUF 69, 79, 94

Author Index

A	Andrews, J.G. [92]
Aazhang, B. [160]20	Anghel, P.A. [165]20, 21
Aazhang, B. [6]	Asoke Nandi, [86] . 10, 69, 80, 93, 107, 108,
Aazhang, B. [7]	114, 127, 130, 167, 187
Abaii, M. [121]13, 143	Azarian, K. [8]2
Abolhasan, M. [141]	В
Abramowitz, M. [197]	Baiocchi, A. [139]
Adelantado, F. [223] 211	Bansal, G. [95]
Adinoyi, A. [29] 5	Bansal, G. [132]
Adinoyi, A. [22] 4	Bar-Ness, Y. [107]
Adlakha, S. [66]	Barua, B. [46] 6, 20, 21, 28, 66, 205
Adve, R. [26]4, 5	Bastami, A.H. [158]
Adve, R. [25]4, 5	Batalama, S. [23]
Affes, S. [41]5	Beaulieu, N.C. [27]
Ahmed, M.H. [30] 5	Belfiore, J.C. [119]
Al Daoud, A. [214]	Benvenuto, N. [52]
Alamouti, S. [207]151, 155	Berberidis, K. [24]
Ali, S.H. [202]144	Berger, S. [156]
Alonso, L. [223]	Bhargava, V.K. [128]
Alouini, MS. [180] 37, 48, 49, 96, 97	Bhargava, V.K. [95]
Alouini, MS. [37]	Bhargava, V.K. [132]
Alouini, MS. [39] 5	Bhargava, V.K. [130]
Alouini, MS. [38] 5	Bhashyam, S. [67]
Alouini, MS. [40] 5	Bhushan, N. [219]
Amah, A.U.T. [33] 5	Biagioni, A. [87]
Amah, A.U.T. [34] 5	Bin Da, [122]
Amin, O. [163] 20	Bin Shen, [159]
Andargoli, S.M.H. [120] 13, 143	Bingham, J.A.C. [50]
Andrea Goldsmith, [190]75, 77, 180	Bletsas, A. [47] 6, 21, 28, 66, 205
Andrew Lippman, [11]2	Bletsas, A. [11]

Bletsas, A. [12]	Cho Yiu Ng, [75]10, 68, 74, 148, 185
Borade, S. [42]6	Chouly, A. [56] 8
Boris Makarevitch, [68]10, 68, 69, 73	Chowdhery, A. [204]
Bormann, D. [131]	Chunbo Luo, [17]3
Boyer, J. [169]20	Chunbo Luo, [18]3
Brajal, A. [56] 8	Cioff, J.M. [189]
Byeong Gi Lee, [151]16	Cioffi, J.M. [204]
C	Cioffi, J.M. [93]11
Colobuia D [211]	Cioffi, J.M. [84] 10, 69, 70, 73–75, 107, 148,
Calabuig, D. [211]	185, 187, 206
Cam, H. [96]	Cioffi, J.M. [79]
Cardona, N. [211]	Cong Xiong, [126]14
Chan, P.W.C. [99]	Cover, T.M. [3]
Chan, P.W.C. [100]	D
Chao Wang, [16]	
Chan Dong [108]	Dacheng Yang, [125] 14, 108, 181 Dacheng Yang, [147]
Chen Dong, [198]	
	Dainelli, G. [139]
Chen-Kao Yang, [101]	Dardari, D. [76]
Cheng, R.S. [62]	DaSilva, V.M. [59]
Cheng, R.S. [99]	Datsikas, C.K. [172]
Cheng, R.S. [100]	der Meulen, E.C.V. [2]
Chenyang Yang, [83] . 10, 11, 69, 70, 74, 75,	Devarajan, R. [128]
81, 82, 93, 105, 107, 108, 113, 114,	Dong Geun Jeong, [155]
117, 125, 148, 167, 185, 187, 206 Chanyang Yang, [126]	Dong In Kim, [136]
Chenyang Yang, [126]	
Cheong Yui Wong, [62]	Dongfeng Yuan, [159]
Cheung, K.T.K. [129]	Dongweon Yoon, [195]
Chew, Y.H. [117]	Dongwoo Kim, [28] 5
Chi Chung Ko, [152]	Droste, H. [213]
Chi Chung Ko, [132]	Duel-Hallen, A. [105]
Chi Wan Sung, [75] 10, 68, 74, 148, 185	Dutkiewicz, E. [140]
Chien-Cheng Kuo, [114]	Dutklewicz, E. [140]
Chien-Cheng Kuo, [113]	E
Chih-Wen Chang, [110]	Ekici, E. [45] 6
Chih-Wen Chang, [112]	EL Gamal, A.A. [3] 2, 3
Chih-Wen Chang, [114]	El-Gamal, H. [8]
Chih-Wen Chang, [113]	Eng, T. [181]
	Erkip, E. [160]20

Erkip, E. [6]	Gradshteyn, I.S. [182]
Erkip, E. [7]	Gregory, W. [49] 6, 21, 28, 66, 205
Ermolova, N.Y. [85] 10, 69, 79, 93, 107, 130,	Guangde Wang, [147]
187	Gunawan, E. [106]
Ermolova, Natalia Y. [68] 10, 68, 69, 73	Gunduz, D. [32] 5, 24
Evans, B.L. [92]	Guo, Y.J. [186]
T.	Guo Wei, [157]20
F DD HAOL	Guoqing Li, [91]
Falconer, D.D. [169]	Guoqing Li, [64]
Fantacci, R. [87]	Guoqing Li, [199]142
Fareed, M.M. [21]	Guowang Miao, [131]14
Fathi, M. [135]	Guowang Miao, [133]14
Feifei Gao, [146]	Gupta, P. [173]21
Feng, Q. [45]	11
Ferrus, R. [203]	H
Fitz, M.O. [193]	Haghighi, A.A. [10]
Flannery, B.P. [192]	Haichao Zhang, [146]
Fooladivanda, D. [214]	Hammerstrom, I. [94]
Fooladivanda, D. [215]210, 211	Hanzo, L. [177]
Fraimis, I.G. [145]	Hanzo, L. [129]
Fu-Chun Zheng, [17]3	Hanzo, L. [164]20
Fuchun Zheng, [18]	Hasan, Z. [132]
G	Hasna, M.O. [37]
Galeana-Zapien, H. [203]144	Hasna, M.O. [39]
Gallager, R. [42] 6	Hasna, M.O. [38] 5
Gang Xie, [98]	Hasna, M.O. [40] 5
Gaofeng Pan, [45] 6	Hedayat, A. [162]20
Gastpar, M. [173]	Hichan Moon, [187]73
Gesbert, D. [143]	Hien Ngo, [46]6, 20, 21, 28, 66, 205
Gesbert, D. [116]12, 13, 15, 16, 143, 144,	Himayat, N. [131]14
151, 152	Himayat, N. [133]14
Gesbert, D. [144]	Himsoon, T. [168]20
Giannakis, G.B. [166]20, 21	Hojoong Kwon, [151]16
Gjendemsjo, A. [143]	Honghai Zhang, [201]
Gjendemsjo, A. [116] 12, 13, 15, 16, 143,	Hoo, L.M.C. [189]
144, 151, 152	Hossain, E. [132]
Goldsmith, A. [32] 5, 24	Hossain, E. [136]
Goodman, D. [148]	Hossain, J. [95]
Goodman, D. [53]	Host-Madsen, A. [174] 21

Host-Madsen, A. [175] 21	Jinri Huang, [103]11
Hsiao-Hwa Chen, [167]20	Johnson, S.J. [35] 5
Hu, J. [27]5	Jourdan, S. [56]
Hu, R.Q. [221]	Junshi Liu, [102]11
Hu, R.Q. [222]	Junsung Lim, [53]8
Huarui Yin, [157]20	Juttner, A. [216]
Hui Liu, [91]11	17
Hui Liu, [64]	K
Hui Liu, [199]	Kae Won Choi, [136]14, 143
Hui Wang, [186]	Kai Yang, [142]
Huiling Zhu, [73]	Kalet, I. [51]
Huiling Zhu, [74]	Karagiannidis, G.K. [13]
Hunter, T.E. [162]20	Karipidis, E. [135]
Hyundong Shin, [46] . 6, 20, 21, 28, 66, 205	Kaveh, M. [165]
T	Kellett, C.M. [35]
I	Khandekar, A. [219]
Ikki, S.S. [163]	Khisti, A. [11]
Ikki, S. [30]	Kiani, S.G. [143]
II-Min Kim, [44]	Kiani, S.G. [116] 12, 13, 15, 16, 143, 144,
In-Ho Lee, [28]	151, 152
Ismail, M. [217]	Kiani, S.G. [144]
J	Kibeom Seong, [93]
Jean Armstrong, [171]	Kim, J. [80] 10, 69, 78, 80, 93, 107, 112, 187
Jean-Wei Chen, [63]	Kim, K. [80]10, 69, 78, 80, 93, 107, 112, 187
Jeong Ae Han, [155]16	Kim, S.L. [65]
Jia Shi, [198]	Kim Han, Y.K. [65]
Jia Shi, [176]24	Kishore, S. [48]
Jia Shi, [208]	Kisong Lee, [210]
Jia-Hong Lin, [101]11	Kivanc, D. [91]
Jianfei Cao, [36]5	Kivanc, D. [64]
Jiangzhou Wang, [73] 10, 69	Klein, A. [156]
Jiangzhou Wang, [74] 10, 69	Klein, A. [33]
Jianhua Lu, [205]144	Klein, A. [34]
Jie Xiang, [209]210	Kotsopoulos, S.A. [145]
Jie Zhang, [216]211	Kramer, G. [173]
Jiho Jang, [90]	Kuhn, H.W. [185] . 70, 76, 93, 108, 114, 115,
Jiho Jang, [78] 10, 69, 70, 107, 187	126, 127, 129 Vuba M [156] 20
Jing Huang, [154]	Kuhn, M. [156]
Jing Li, [48]6, 21, 28, 66, 205	Kulkarni, G. [66]

Kwang Bok Lee, [90]11	Lie-Liang Yang, [167]
Kwang Bok Lee, [78]10, 69, 70, 107, 187	Lie-Liang Yang, [198]96, 97
Kwang-Cheng Chen, [104]	Lie-Liang Yang, [36]5
Kwang-Cheng Chen, [97] 11, 108, 181	Lie-Liang Yang, [178]25, 34–36
Kwasinski, A. [19]	Lie-Liang Yang, [179]25, 34–36
Kyongkuk Cho, [194]95	Lie-Liang Yang, [177]24
Kyongkuk Cho, [195]95	Lie-Liang Yang, [54]8
Kyung Sup Kwak, [146]	Lie-Liang Yang, [176]
Kyungsup Kwak, [159] 20	Lie-Liang Yang, [55]8
T	Lie-Liang Yang, [164]
L	Lie-Liang Yang, [83]. 10, 11, 69, 70, 74, 75,
Ladanyi, A. [216]	81, 82, 93, 105, 107, 108, 113, 114,
Laetitia Falconetti, [220]	117, 125, 148, 167, 185, 187, 206
Lagunas, M.A. [84] 10, 69, 70, 73–75, 107,	Lie-Liang Yang, [208] 181, 186, 197
148, 185, 187, 206	Liu, K.J.R. [19]
Lajos Hanzo, [61]	Liu, K.J.R. [168]20
Laneman, J.N. [161]	Liu, K.J.R. [149]16
Laneman, J.N. [5]	Liu, K.J.R. [150]
Laneman, J.N. [4]	Lizhong Zheng, [42]6
Laneman, J.N. [49] 6, 21, 28, 66, 205	Lo, E.S. [99]
Lang Xie, [209]	Lo, E.S. [100]
Lataief, K.B. [62]	Lo, E.S. [123]
Lau, V.K.N. [99]	Lo, E.S. [134]
Lau, V.K.N. [100]	Lo, E.S. [88]
Lazarakis, F.I. [172]	Long Gao, [81]
Le Ruyet, D. [137]14, 143	Loodaricheh, R.A. [130]
Lee, J. [195]	Lopez-Perez, D. [216]211
Lertwiram, N. [212]	Loyola, L. [108]11, 12
Letaief, K.B. [77] 10, 69, 107, 180, 187	Luc Vandendorpe, [89] 10, 69
Letaief, K.B. [99]	
Letaief, K.B. [100]	M
Leung, V.C.M. [202]	Makarevitch, B. [85]10, 69, 79, 93, 107, 130,
Li, G.Y. [133]14	187
Li, G.Y. [126]	Mallick, S. [128]
Li-Chun Wang, [110]	Mallick, S. [130]
Li-Chun Wang, [112]	Mandayam, N. [148]
Lie Liang Yang, [1] . 1, 7–10, 25, 33, 34, 37,	Marabissi, D. [87]
97, 107–109, 146, 180–182	Marsland, I.D. [22]
Lie-Liang Yang, [61]9, 68, 107	Matyjas, J.D. [23] 4

Mesodiakaki, A. [223]211	Odeh, N. [141]
Michalopoulos, D.S. [13] 2	Ohno, S. [82] 10, 69, 107, 187
Miki, T. [108]	Ohyun Jo, [210]210
Milstein, L.B. [181]	Oien, G.E. [143]15, 152
Milstein, L.B. [115]	Oien, G.E. [116] 12, 13, 15, 16, 143, 144,
Milstein, L.B. [111]11, 12	151, 152
Milstein, L.B. [125] 14, 108, 181	Oien, G.E. [144]15, 152
Milstein, L.B. [124]	Olfat, A. [158]20
Mohamed-Pour, K. [120]13, 143	Onat, F.A. [22]
Mohanram, C. [67]	Ong, L. [35]
Mohsen Kavehrad, [194]95	Otani, Y. [82] 10, 69, 107, 187
Mohseni, M. [93]	Ozbek, B. [137]
Monserrat, J.F. [211]	P
Moretti, M. [139]	
Mueck, M. [140]	Palomar, D.P. [84] 10, 69, 70, 73–75, 107,
Munkres, J. [191] 76, 93, 114, 127	148, 185, 187, 206 Percutais VD [145] 15
Murch, R.D. [62]	Papoutsis, V.D. [145]
Murch, R.D. [99]	Peilong Li, [201]
Murch, R.D. [100]	Peng Liu, [44]
Myung, H.G. [53] 8	Peng Zhang, [102]
N	Pischella, M. [119]
Na Li, [98]11, 108, 181	Po-Wei Fu, [104]
Nakagami, M. [184]	Po-Wei Fu, [97]
Nakagawa, M. [60]	Poor, H.V. [32] 5, 24
Natarajan, A. [96]	Poor, H.V. [188]
Navaie, K. [10]	Poor, H.V. [16]
Ng, D.W.K. [138]14, 15, 143, 144	Popovic, B.M. [57]
Ng, D.W.K. [123]13, 14, 143, 144	Popovski, P. [212]210
Ng, D.W.K. [72]	Prasad, N. [201]
Ng, D.W.K. [134]	Prasad, N. [142]
Ng, D.W.K. [88]	Prasad, N. [200]
Ng, T.C.Y. [20] 4	Press, W.H. [192]
Niu, Z. [153]	,
Nosratinia, A. [162]	Q
NTT DOCOMO R1-103264, [218]211	Qi Qu, [115]
	Qi Qu, [111]11, 12
0	Qian, Y. [221]
Obilor Nwamadi, [86] 10, 69, 80, 93, 107,	Qian Zhang, [118]
108, 114, 127, 130, 167, 187	Qihang Peng, [124]14

Qimei Cui, [186]	Shin Hyundong, [12]
Qinghai Yang, [146]	Shuangqing Wei, [9]
Quan Kuang, [213]210	Shugong Xu, [126]
R	Shuguang Cui, [81] 10, 69
	Shuhui Liu, [147]
Rangarajan, S. [201]	Shunqing Zhang, [126]14
Rankov, B. [15]	Simon, M.K. [180] 37, 48, 49, 96, 97
Rashid, M.M. [128]	Siriwongpairat, W.P. [168] 20
Raviraj Adve, [170]	Skeie, T. [209]210
Reed, D.P. [11]	Smith, Peter J. [171]21
Reynolds, D. [127]	Song, G. [69] 10, 68, 69
Ribeiro, A. [166]	Song, G. [70] 10, 68, 69
Rontogiannis, A.A. [24] 4	Sourour, E.A. [60]9
Ropokis, G.A. [24] 4	Sousa, E.S. [59]
Rosenberg, C. [214]210	Soysa, M. [196]
Rosenberg, C. [215] 210, 211	Speidel, J. [213]
Rudolf Mathar, [220]	Srivastava, M. [66]10, 68
Rui Zhang, [122]	Stegun, I. [197]
Ryzhik, I.M. [182]	Stephenne, A. [41] 5
S	Steven Corroy, [220]211
Sadek, A.K. [19]	Su, W.F. [19]
Safaei, F. [141]	Su, W. [14]
Sagias, N.C. [172]	Su, W. [23]
Sakaguchi, K. [212]	Suraweera, Himal A. [171]21
Sampath, P.K. [96]	T
Sangkook Lee, [23]4	
Schniter, P. [8]	Tafazolli, R. [121]
Schober, R. [138]14, 15, 143, 144	Tao Jia, [105]
Schober, R. [123]13, 14, 143, 144	Tao Wang, [71]
Schober, R. [72]	Tao Wang, [89]
Schober, R. [134]	Tarchi, D. [87]
Schober, R. [88]	Tellambura, C. [196]
Senaratne, D. [196]	Teng Joon Lim, [26]
Sendonaris, A. [160] 20	Teng Joon Lim, [25]
Sendonaris, A. [6]	-
Sendonaris, A. [7]	Teo, K.A.D. [82]
Seymour, J.P. [193]95	Teukolsky, S.A. [192]
Shaoshi Yang, [129]	Thompson, J. [16]
Shin, H. [47] 6, 21, 28, 66, 205	Thompson, J. [10]

Tingfang, J. [219]	Weidong Wang, [157]20
Tingting Liu, [83]10, 11, 69, 70, 74, 75,	Weifeng Su, [168]20
81, 82, 93, 105, 107, 108, 113, 114,	Weihua Zhuang, [217]211
117, 125, 148, 167, 185, 187, 206	Wha Sook Jeon, [155]
Todini, A. [139]	Win, M.Z. [47] 6, 21, 28, 66, 205
Tomasin, S. [52] 8	Win, M.Z. [12]
Tombras, G.S. [172]21	Wittneben, A. [156] 20
Tong Wu, [154]	Wittneben, A. [15]
Trigui, I. [41]	Wittneben, A. [94]
Tse, D.N.C. [5] 2, 20	Woerner, B.D. [127]14
Tung Sang Ng, [58]9	Wonjong Rhee, [79]10, 69
TI	Wornell, G.W. [161]20
U	Wornell, G.W. [5]
Unger, T. [156]	Wornell, G.W. [4] 2
Uysal, M. [163]	Wubben, D. [43] 6
Uysal, M. [21] 4	WunCheol Jeong, [194]95
\mathbf{V}	X
Valkama, M. [186]	Xiang Gui, [58] 9
Vaman, D.R. [115]	Xiao Xiao, [205]
Vaman, D.R. [111]11, 12	Xiaodong Cai, [166]20, 21
van der Meulen, E. [31] 5, 20	
Vandendorpe, L. [71] 10, 69	Xiaodong Wang, [201]
Vanghi, V. [219]	Xiaodong Wang, [200]144
Vardhe, K. [127]	Xiaofeng Tao, [186]
Veeravalli, V.V. [188]74, 148, 185	Xiaojing Huang, [140]
Venturino, L. [201]144	Xiaoli Chu, [216]211
Venturino, L. [200]	Xiaoming Tao, [205]144
Verikoukis, C. [223]211	Xin Liu, [14]
Vetterling, W.T. [192]	Xinmin Yu, [154]
Viterbi, A.J. [206]146, 147, 184	Xu Zhu, [86] . 10, 69, 80, 93, 107, 108, 114,
Viterbi, A.M. [206] 146, 147, 184	127, 130, 167, 187
Vladimir Rotar, [183]38	127, 130, 107, 107
\mathbf{W}	Y
	Yachen Wang, [102]
Wai-Ho Mow, [99]	Yachen Wang, [98] 11, 108, 181
Wang, L. [153]	Yahong Zhao, [109]
Wei Yu, [204]144	Yajian Liu, [121]
Wei Yu, [20]	Yan Chen, [126]14
ποι τ u , [Δυ]4	Yan Ya, [109]11

Yan Zhang, [209]210	Zhiquan Bai, [159] 20
Yanikomeroglu, H. [169] 20	Zhisheng Niu, [103]
Yanikomeroglu, H. [29]5	Zhisheng Niu, [118]13, 143
Yanikomeroglu, H. [22]4	Zhongpei Zhang, [109]11
Yao Hua, [118]	Zhu, J. [107]
Yaw-Wen Kuo, [101]	Zhu, Y. [106]
Ye Li, [131]14	Zhu Han, [149]16
Ye Li, [69]	Zhu Han, [150]16
Ye Li, [70]	Zhu Ji, [149]16
Yener, A. [32] 5, 24	Zhu Ji, [150]16
Yi Qian, [222]	Zhuwei Wang, [125]14, 108, 181
Yi Zhao, [170]	Zhuwei Wang, [124]14
Yi Zhao, [26] 4, 5	Zukang Shen, [92]11
Yi Zhao, [25] 4, 5	
Yijia Fan, [16]3	
Yijia Fan, [22]4	
Ying Jun Zhang, [77] . 10, 69, 107, 180, 187	
Ying Wang, [154]	
Yingbin Liang, [188] 74, 148, 185	
Yingda Chen, [48] 6, 21, 28, 66, 205	
Yiwei Yu, [140]	
Yizhen Jia, [205]	
Yong Fang, [89]10, 69	
Yongjie Xu, [159]	
Yongyu Chang, [147]15, 16	
Yu Gong, [17]3	
Yu Gong, [18]3	
Yuan an Liu, [102]11	
Yuan an Liu, [98]11, 108, 181	
Yung-Fang Chen, [63]10, 68	
Z	
Zehavi, E. [206]	
Zeng, C. [189]	
Zhang, J. [174]	
Zhangdui Zhong, [36]5	
Zhenyu Liang, [152]	
Zhenyu Liang, [117]13	
Zhikun Xu, [126]14	